LUT
Lappeenranta
University of Technology

Salimzhan Gafurov

THEORETICAL AND EXPERIMENTAL ANALYSIS OF DYNAMIC LOADING OF A TWO-STAGE AIRCRAFT ENGINE FUEL PUMP AND METHODS FOR ITS DECREASING

Thesis for the degree of Doctor of Science (Technology) to be presented with due permission for public examination and criticism in the Auditorium 2310 at Lappeenranta University of Technology, Lappeenranta, Finland on the 10th of November, 2017, at 1 p.m.

Acta Universitatis
Lappeenrantaensis 775

Supervisors Professor Heikki Handroos
LUT School of Engineering Science
Lappeenranta University of Technology
Finland

Professor Evgeniy Shakhmatov
Automatic Systems of Power Plants
Samara National Research University
Russian Federation

Reviewers Full Professor Jaroslaw Stryczek
Wroclaw University of Science and Technology
Poland

Professor Takao Nishiumi
National Defense Academy
Japan

Opponents Full Professor Jaroslaw Stryczek
Wroclaw University of Science and Technology
Poland

Professor Takao Nishiumi
National Defense Academy
Japan

ISBN 978-952-335-169-1
ISBN 978-952-335-170-7 (PDF)
ISSN-L 1456-4491
ISSN 1456-4491

Lappeenrannan teknillinen yliopisto
Yliopistopaino 2017

Abstract

Salimzhan Gafurov
Theoretical and Experimental Analysis of Dynamic Loading of a Two-stage Aircraft Engine Fuel Pump and Methods for Its Decreasing
Lappeenranta 2017
185 pages
Acta Universitatis Lappeenrantaensis 775
Diss. Lappeenranta University of Technology
ISBN 978-952-335-169-1, ISBN 978-952-335-170-7 (PDF), ISSN-L 1456-4491,
ISSN 1456-4491

Aircraft fuel pumps are known to be the most loaded units of the gas turbine engines. Primary engine fuel pump is the key component limiting the reliability and endurance of the fuel system, and, as a result, the durability of the whole engine.
This dissertation is devoted to development of the mathematical model allowing to describe the working processes inside of the two-stage aircraft engine fuel pump consisting of screw-centrifugal and gear stages. A finite-volume discretization method was realized in a commercial code ANSYS CFX and subsequently used for the Navier-Stokes equations solution. Developed mathematical model was verified and showed to produce good accuracy of pump performance estimation. Developed approach was used for CFD simulations of the ingestion process of free gas into the first stage of the pump. The CFD analysis has been used to calculate an unsteady three-dimensional viscous flow of multi-component fluid in the screw-centrifugal pump. Calculations have been made to determine unsteady loads of fuel pump in different operating modes. To examine the efficiency of the CFD analysis, a series of experiments have been conducted. The experimental results proved the accuracy of the numerical model. The results allowed to develop design modifications of the considered pump for reduction of its dynamic loads. The main focus in this study was addressing the reduction of dynamic loading of the two-stage fuel pumps. It had to be done without any changes in operation modes of engine fuel system. Design modifications have been proposed to decrease the two-stage aircraft engine pump loading. This loading includes both pressure pulsation and the vibrational load. This dissertation describes theoretically and experimentally the efficiency of the proposed pump design modifications entering re-designs. The results illustrate how the proposed redesigns reduce the flow unsteadiness in the two-stage pump at its different operating regimes. Proposed construction changes enhance the reliability and endurance of aircraft engine fuel pumps.

In addition, this dissertation describes the developed semi-natural test bench and measurement techniques which were applied for investigations of considered pump dynamic loading. The semi-natural test bench contains the mathematical model of the gas-turbine engine for research the fuel supply and control systems characteristics. A number of semi-natural and hardware-in-loop (HIL) test benches for investigation of both gas turbine engine's fuel and control systems are shown. An aggregate composition of

hydro-mechanical system and the methodology of the used testing technique are also presented. Some aspects of controlled object mathematical simulation and the basic approaches for its implementation are described. Developed bench allows to simulate and define the performances of the whole fuel system and its aggregates in steady-state and transient operating regimes in the closed and open loop circuits. Additionally, it allows to perform the analysis of available control system stability margins, to carry out the interaction of separate circuits and aggregates or to study influence the perturbations and external factors on control system fail safety.

Finally, the theory of vortex resonance inside screw-centrifugal stage of the pump induced by its gear stage elements vibrations and trailing vortices is presented. The main idea of this theory is the coincidence of frequencies of trailing vortices, stalling from the screw and centrifugal wheels, and frequencies of leakages from the gear stage that are poured out into the chamber between stages. Obtained experimental results confirm this theory and allow better understanding of the flow processes inside the pump.

Keywords: aircraft engine, fuel system, axial flow pump, centrifugal pump, gear pump, bearing, destruction, reliability, dynamic loading, flow instabilities, cavitation, mixing flow, turbulence, back eddies, numerical simulations, semi-natural test bench, experimental investigations, improvements

Acknowledgements

This dissertation was carried out in the department of Automatic Systems of Power Plants at Samara National Research University, Russia, and at the Laboratory of Intelligent Machines in the Department of Mechanical Engineering of Lappeenranta University of Technologies, Finland during between 2015 and 2017.

I would like to express my deepest thanks to all the people who were nearby me and support me. Without you this work won't be possible. First of all, I would like to express my appreciation for supervisor, Professor Heikki Handroos, who believed in me and gave such a great opportunity to work together and made this research possible. It is an honour to work with you. I also would like to thank another supervisor, Professor Evgeniy Shakhmatov from Samara National Research Unviersity, who supported me at the earliest stage of this research, guided me from the moment when I graduated. Your valuable advices helped me to realize my dream to get a scientific degree.

I thank the dissertation reviewers, Professor Jaroslaw Stryczek from Wroclaw University of Science and Technology (Poland) and Professor Takao Nishiumi from National Defense Academy (Japan), for their time, passion and advice. Yours valuable remarks and suggestions allow me to significantly improve my research.

I would like to express my gratitude to the personnel of the Automatic Systems of Power Plants. Many thanks to Professor Georgy Makaryants. You brought me into the university and allowed to think differently., Thanks also to Leonid Rodionov for his collaboration in research and especially for his technical help. Thanks to Alexander Igolkin, Alexander Kryuchov, Viktor Sverbilov and Vera Salmina for your support and collaboration. Thanks also to all of the administrators and staff members in Lappeenranta University of Technology and Samara National Research University who have helped me over the years.

My special thanks to my Finnish friends Mikhail Sokolov and Anna Unt for your care and guiding me. You helped me a lot to settle in Finland. A great thank to Hamid Roozbahani. You have invited me to this trip, supported me. I will never forget our first talk at the lake Saimaa.

Most of all, I wish to thank my mother Elena, father Azat and sister Anna for you love, support and for your believing in me. I feel your support every moment. My deepest kowtow to my grandmother Veronika. You have inspired and gave the feeling that I could do more. My wife Maria and my children Marianna and Tamerlan, thank you for support, love, devotion, inspiration and encouragement throughout of my life. Without you I would never have finished it.

Salimzhan Gafurov
November 2017
Lappeenranta, Finland

To Maria, Marianna and Tamerlan

Content

List of publications

This thesis contains material from the following papers. The reprints of the articles are not included in the thesis.

I. Gafurov, S., Rodionov, L., Kryuchkov, A., Handroos, H. (2016). Conference article. HIL test bench for engine's fuel control systems investigation. *Proceedings of the 30th Congress of the International Council of the Aeronautical Sciences, ICAS 2016*. South Korea.

II. Gafurov, S.A., Rodionov, L.V., Zharkov, A.V. (2016). Conference article. Experimental Vibroacoustic Research of the Gear Pump from Different Materials. *Proceedings of the 3rd International Scientific Conference on Dynamics and Vibroacoustics of Machines, DVM2016,* pp. 41. Samara: Samara National Research University

III. Gafurov, S.A., Rodionov, L.V., Zharkov, A.V. (2016). Conference article. Modelirovaniye shuma shesterennogo nasosa [Simulation of Gear Pump Noise]. *Proceedings of the 3rd International Scientific Conference on Dynamics and Vibroacoustics of Machines, DVM 2016,* pp. 43. Samara: Samara National Research University (in Russian)

IV. Gafurov, S.A., Rodionov, L.V., Makaryants, G.M. (2016). Conference article. Simulation of gear pump noise generation. *Proceedings of the 9th FPNI Ph.D. Symposium on Fluid Power, FPNI 2016.* Lappeenranta: Taylor

V. Gafurov, S.A., Rodionov, L.V. (2014). Conference article. Acoustic Visualization of Cavitation in Fuel Combination Pump. *Proceedings of the 21st International Congress on Sound and Vibration (ICSV21), Beijing, China.* International Institute of Acoustics and Vibration, pp. 3916 – 3923

VI. Gafurov, S.A., Rodionov, L.V. (2014). Conference article. Roof Mounted Boiler House Noise Reduction. *Proceedings of the 21st International Congress on Sound and Vibration (ICSV21), Beijing, China*. International Institute of Acoustics and Vibration, pp. 3196-3203

VII. Gafurov, S.A., Rodionov, L.V., Gimadiev, A.G. (2016). Conference article. Combined air supply at fuel pump entrance. *Proceedings of the 8th FPNI Ph.D Symposium on Fluid Power, FPNI 2014, 2014*

VIII. Gafurov, S.A., Prokofiev, A.B., Shakhmatov, E.V. (2014). Conference article. Reduction of vibroacoustic loads in aviation combined pumps. *Proceedings of the 29th Congress of the International Council of the Aeronautical Sciences, ICAS 2014.* St. Petersburg: International Council of the Aeronautical Sciences

IX. Makaryants, G.M., Gafurov, S.A., Zubrilin, I.A., Kryuchkov, A.N. Shakhmatov, E.V., Berestovitskiy, E.G., Gladilin, Yu.A. (2014). Raschot gidrodinamicheskogo shuma diffuzora protochnogo kanala gasitelya pul'satsiy [Calculation of Fluid Born Noise of a Diffuser Inside a Pressure Pulsation Dampener]. *Vestnik Samarskogo Gosudarstvennogo Aerokosmicheskogo Universiteta imeni akademika S.P. Koroleva (nacionalnogo isledovatelskogo universiteta)*, 1(43), pp. 131-143 (in Russian)

X. Makaryants, G.M., Kryuchkov, A.N., Prokofiev, A.B., Gafurov, S.A. (2014). CFD modelling of hydrodynamic noise silencer. *Transport. Przemyslowy I maszyny robocze*, 2(24), pp. 52-56

XI. Gafurov, S.A., Rodionov, L.V. (2014). Conference article. Acoustic visualization of cavitation in fuel combination pump. Proceedings of the 21st International Congress on Sound and Vibration 2014, ICSV 2014,. vol. 5, pp. 3916-3923

XII. Gafurov, S.A., Blyumin K.V., Gimadiev, A.G. (2014). The semi-natural test bench with virtual gas turbine engine model for fuel supply and control system characteristics investigation. *Research Journal of Applied Sciences,* 9(11), pp. 806-811

XIII. Makaryants, G.M., Gafurov, S.A., Blyumin K.V., Kryuchkov, A.N. Shakhmatov, E.V. (2013). Metodika proyektirovaniya gasitelya gidrodinamicheskogo shuma [Design Methodology for Fluid Born Dampener]. Vektor nauki Tolyatinskogo universiteta, 2, pp. 103-107 (in Russian).

XIV. Makaryants, G.M., Zubrilin, I.A., Gafurov, S.A., Kryuchkov, A.N., Prokofiev, A.B., Shakhmatov, E.V. (2013). Conference article. Design Methodology of Hydrodynamic Noise Silencer. Proceedings of the 20th International Congress on Sound and Vibration (ICSV20). 7-11 July 2013. PP. 2531-2536

XV. Makaryants, G.M., Prokofiev, A.B., Makaryants, M.V, Shakhmatov, E.V., Gafurov, S.A., Kryuchkov, A.N., Prokofiev, A.B., (2013). Conference article. Vibration mitigation in pipe system of hydraulic drive. Proceedings of the Fifth International Conference on Experimental Vibration Analysis for Civil Engineering Structures EVACES13. pp. 282-286

XVI. Gafurov, S.A., Shakhmatov, E.V. (2012). Conference article. Chislennoye issledovaniye gidrodinamicheskikh protsessov, proiskhodyashchikh v sisteme smazki podshipnikovogo uzla. Международный научно-технический форум, посвященный 100-летию ОАО «Кузнецов» и 70-летию СГАУ. Международная научно-техническая конференция с участием молодых ученых «Динамика и виброакустика машин»., Vol. 2, pp. 109-110. Samara. ООО «Самбр принт».

XVII. Gafurov, S.A., Rodionov, L.V., Kryuchkov, A.N, Makaryants, G.M., Shakhmatov, E.V. (2012). Issledovaniye prichin razrusheniya podshipnikovoy opory shnekotsentrobezhnoy stupeni kombinirovannogo nasosnogo agregata [Investigation of the causes of the auger-centrifugal pump bearing destruction]. *Vestnik Samarskogo Gosudarstvennogo Aerokosmicheskogo Universiteta imeni akademika S.P. Koroleva (nacionalnogo isledovatelskogo universiteta)*, 2(33), pp. 164-171

Author's contribution

Author Salimzhan Gafurov is the principle author and investigator in papers I – VIII, XI, XII, XVI, XVII. Author Zharkov, A.V. in papers II and III conducted numerical investigations in Actran software and post processed obtained results. Author Makaryants G.M. done a part of literature overview relative to fluid borne noise in paper IV.

Additionally, Makaryants G.M. was the corresponding author in papers IX, X and XIII – XV and conducted the solutions of developed mathematical model for fluid borne noise silencer design. Author Rodionov L.V. helped to conduct the experiments and gathered the results obtained in paper V and VI. Authors Zubrilin I.A., Kryuchkov A.N., Shakhmatov E.V., Berestovitskiy E.G. and Gladilin, Yu. A. in paper IX helped to verify the numerical code. In paper XII author Blyumin K.V. developed a software for Hardware-In-the-Loop test bench by means of LabView commercial software.

Nomenclature

In the present work, variables and constants are denoted using *slanted style*, vectors are denoted using **bold regular style**, and abbreviations are denoted using regular style.

Latin alphabet

A	volume	m^3
B	equation term responsible for vortex generation	-
b	surface tension constant	
C	volume fraction	-
c	specific heat capacity	$J \cdot kg^{-1} \cdot K^{-1}$
D	dispersion	-
E	potential energy	J
e	error	-
$\mathbf{F}$	force	N
f	rotation frequency	Hz
G	mass flow rate	kg/s
g	acceleration of gravity	m/s^2
H	net positive suction head (NPSH) of a pump	Pa
h	enthalpy	$J \cdot mol^{-1}$
I	inertia	$kg \cdot m^2$
i	unit vector in the coordinate direction	-
j	unit vector in the coordinate direction	-
K	kinetic energy	J
k	kinetic energy of turbulence	J
L	length	m
l	shape function	-
M	torque	N·m
m	mass	kg
N	speed of rotation	min^{-1}
n	time intervals per signal sampling time	s
O	cavitation resistance of the pump flow channel including the back eddies zone	-
P	power	W
p	pressure	Pa
Q	volume flow rate	m^3/s
$\mathbf{R}$	thrust	N
r	radius	m
S	source term	-
s	area	m^2
t	time or time response	S
T	temperature	K

u	significance level for Fisher ratio test	-
$\mathbf{V}$	vibration acceleration	m/s^2
W	work done by the pressure inside the bubble	J
w	velocity relative to the rotating blades	m/s^2
X	compliance of the lumped elasticity at pump inlet	m
x	grid element size	m
Y	total elasticity of cavitation cavities of the pump flow channel	m
y	first layer thickness	m

Greek alphabet

α	incidence angle	rad
β	flow angle	deg
β_b	blade angle	deg
δ	deviation angle	deg
ε	kinetic energy dissipation	
ζ	ratio of the cavities volume before a screw to back eddies zone volume	-
η	efficiency	-
κ	Kronecker's delta (tensor unity)	-
λ	thermal conduction	$W \cdot m^{-1} \cdot K^{-1}$
μ	dynamic viscosity	Pa·s
ν	kinematic viscosity	m^2/s
ν_T	turbulent viscosity	m^2/s
ν_C	calculated value	-
ξ	angle of attack	deg
π^*	pressure ratio (ratio of oulet pressure to inlet pressure)	-
ρ	density	kg/m^3
σ	tensile stress	Pa
τ	stress tensor	Pa
τ_{ij}	denotes the sub-grid-scale stress and includes the effect of small scales	Pa
τ_w	tangent stress	Pa
v	fluid velocity in a non-rotating coordinate system	m/s^2
φ	given variable	-
χ	angle of inclination of discharge channel to the axial of rotation	deg
ψ	mixture phase	-
ω	turbulence frequency	Hz

Dimensionless numbers

Cp	pressure coefficient
Cur	Courant number
J	Fishers' criteria
K_{cav}	cavitation number
Num	number of mixture components
R	coefficient of the linearized hydraulic resistance
Re	Reynolds number
Ru	Rudnev critical coefficient for liquid-gas mixture
Sh	Strouhal number
q	regime parameter
ζ	ratio of the cavities volume in front of a screw to the total volume of back eddies

Superscripts

S	screw
C	centrifugal
G	gear
T	total
i	flow parameter of a component in Cartesian reference system along its y axis
j	flow parameter of a component in Cartesian reference system along its x axis
SCS	screw-centrifugal stage

Subscripts

A	air
a	axial direction
B	bubble
BE	back eddies
C	calculated value
crit	critical
E	energy
F	fuel
H	hub
in	inlet
K	kerosene
k	cavitation cavity
M	momentum
m	mixture
md	circumferential directions

max	maximum
mid	middle
min	minimum
mix	mixing chamber
N	nozzle
out	outlet
r	radial direction
SP	supply pipeline
s	saturated vapor
stab	stability region
T	tip
T	target value
V	vapor
x	Cartesian axis. Coincide with the pump longitudinal axis
y	Cartesian axis. Coincide with the pump lateral axis. Aligned with the horizon plane
z	Cartesian axis. Coincide with the pump lateral axis. Perpendicular to the horizon plane
α	phase term
θ	meridional direction
ψ	phase

Abbreviations

2D	two dimensional
3D	three dimensional
CFD	computational fluid dynamics
GS	gear stage
GTE	gas-turbine engine
HIL	hardware-in-the-loop
LES	large eddy scale
SCS	screw-centrifugal stage
SST	shear stress turbulence model

1 Introduction

Aviation engines' reliability is defined by their fuel systems. As a rule, pump units are the most loaded aggregates in such systems. Generally, pumps durability is 2-3 times shorter than the engine's. The latter has a durability equal to 15-20 thousand hours. A number of aircraft accidents are known to be caused by fuel pump failures. This problem is especially actual for afterburner engines operating in abnormal operating conditions. Operating conditions of such engines vary in a wide range of flow rates and revolution speeds, resulting in increased dynamic loading of main fuel pump. Typically, fuel pumps of afterburner engine are two-stage pumps consisting of a booster and primary stages. Usually the booster stage is a screw-centrifugal pump and the primary stage is external gear pump. Such pumps are subjected to invisible intense cavitation processes caused by operational process and gas bubbles. Invisible cavitation does not lead to breakdown of the pump head but leads to significant dynamic loading of the elements of the pump. Cavitation in such pumps is caused by a wide range of flow rates into combustion chamber and afterburner. Thereon, all fuel consumed by the engine is pumped through a booster pump, which leads to off-design behaviour during this stage.

Distinctive feature of aviation fuel systems is being known to consist of a number of functionally related hydro-mechanical elements and aggregates. Each of these elements can be a source of pressure oscillations, flow oscillations and noise, in addition their interference can lead to self-oscillations in the system. All these processes have effect on the fuel pumps. Complex built of aviation fuel aggregates, interference and a number of factors that influence their operating conditions determine a number of causes for uncertain processes inside the pumps. Fuel pumps both generate instabilities inside the system and simultaneously take on the loads from it. Consequently, theoretical and experimental analysis of flow phenomena and processes in aircraft engine fuel pumps is an actual and extremely important research topic for increasing the reliability of aviation fuel systems.

The **motivation** of this study is to solve the problem of destruction of journal-and-thrust bearing of the fuel pump of the aircraft engine NK-36. Given turbofan engine has been designed and produced at JSC "Kuznetsov" (Russian Federation). The destruction of the bearing leads to failure of the whole fuel system and causes the failure of the engine. The exact reasons of pump failures have not been determined for the last 20 years.

1.1 Purpose and objectives of the research

Main purpose of this dissertation is to develop the methods for decreasing the dynamic loads in two-stage pump of aircraft engine. These loads include both flow pulsation and vibration loadings of pump's elements. Reduction of pump loading had to be done without any changes in operating regimes of aviation fuel system.

The subject of this thesis is the flow phenomena and operational processes inside a two-stage fuel pump ND-32 of aircraft engine NK-36. Rather than attempt a general treatise

on aviation pumps, the attention is focused on the special challenges and design issues associated with the flow of liquid through fuel pumps consisting of a screw-centrifugal stage and a gear stage. Dynamic loading of aviation pump is caused by the potential for cavitation and turbulence, and by the considerable amount of hydraulic aggregates that are attached to pumps. These factors determine the set of problems and possible outcomes.

Two-stage pump ND-32 was chosen as **an object** for investigations. Stages of this pump cannot be considered separately, as they interact and mutually influence one another. Therefore, afterburner engine fuel pumps should be considered in an integrated manner. Pump ND-32 is mounted in the fuel system of the aircraft engine NK-36. This fuel system represents a complex hydro-mechanical system. The field experience and a number of previous investigations show that the component limiting the reliability of the aviation engine fuel pump is a journal-and-thrust bearing of the booster pump. Previous research has not succeeded to identify unambiguously the reasons for the bearing destructions. This current fuel system consists of a number of sources of induced oscillations which are connected to each other.

The conducted literature overview shows that there are no thorough studies concerning the screw-centrifugal stage of aircraft engine pump which take into account the interaction between its stages. There are no existing methods allowing to determine cavitation and energetic properties of screw-centrifugal pumps as well as its dynamic loading. There is still a lack of information about unsteady pressure pulsations inside centrifugal and axial flow pumps as well as about unsteady loading of pump blades. Additionally, pump design has achieved a level when only detail description of working processes allows increasing their exploitation characteristics. Therefore, investigation of the sources of increased loading of aircraft engine two-stage pumps is a state of the art problem.

The main objectives of this dissertation are:

- analysis of the interaction of the screw-centrifugal and gear stages;
- determination of the main causes that lead to dynamic loading of the pump elements;
- analysis of the methods for forecasting the performance of the two-stage pumps;
- analysis of the methods and mechanisms for decreasing of the dynamic loads of aviation pumps;
- development of the simulation model for investigation of the phenomena inside the screw-centrifugal stage and its operational processes by taking into account the influence of the gear stage, operational conditions, mixture flow, cavitation and turbulence. Developed model should be realized numerically to obtain screw-centrifugal cavitation- and energetic properties as well as its efficiency and local

sources of dynamic loading in case of one-component and multi-component flows. The model is to be verified experimentally;
- development of a semi-natural test bench for experimental investigations of aircraft engine fuel systems in a real-scale operational conditions;
- development of novel pump designs for decreasing its dynamic loading;
- experimental investigation of the two-stage pump flow phenomena.

For this reason, only detail investigation of flow inside a two-stage fuel pump with taking into account external fuel supply system makes possible determining the reasons of pump failures. This mechanism should be based on theoretical and experimental methods through developing of the mathematical model of hydrodynamic processes inside the booster stage of the pump while considering cavitation, turbulence and mixed flows.

1.2 Contribution of the work

- A simulation model of fluid flow inside a screw-centrifugal stage of an aircraft engine fuel pump has been developed. The model takes into account the influence of the gear stage and the working conditions. The model allows to estimate the cavitation performances, energetic parameters and dynamic loading. The modified Reyleigh-Plesset model is used for simulation of the cavitation. The modification takes into account the dependence of the density and viscosity of the fluid on its temperature and pressure.
- An approach for CFD simulation of the multi-component fluid flow inside a screw-centrifugal stage has been developed. Multi-component fluid consists of fuel and dissolved gas. The verification of the model has been provided.
- A model of the flow induced screw-centrifugal stage elements vibrations is developed. Proposed model allows to determine the local sources of dynamics loading.
- An experimental test bench for hybrid-in-the-loop simulations of the aviation fuel system has been developed.
- Construction designs for decreasing the dynamic loading of the screw-centrifugal stage have been developed. These measures focus on the elimination of the back eddies at the pump entrance and dividing the streams from drain to bypass pipelines into a series of small streams.

1.2.1 Theoretical significance

- Obtained simulation model of multicomponent fluid flows inside a screw-centrifugal stage of an aircraft engine fuel pump allows to determine output performances of the stage.

- The model of the flow induced vibrations has been developed. It allows to estimate the sources of the high frequency loading of the stage.

These considerations help to reduce the cost of the physical experiments and optimize the pump characteristics.

1.2.2 **Practical significance**

- The newly developed pump designs provide a decrease in the dynamic loading of the two-stage fuel pump. Pump's inlet redesigns have been proposed and experimental results of their efficiency described. The results illustrate how the proposed redesigns reduce the flow unsteadiness in a booster stage of the pump during different operating regimes. The results help to enhance the reliability and endurance of aviation fuel pumps.
- The main factors of failures of the fuel pump radial-and-thrust journal bearing have been established. The most important factor was found to be the dissolved gas.
- An approach of developing of novel semi-natural test bench for aircraft engine fuel pumps investigation has been proposed. Developed test bench takes into account real-scale working conditions of the pump and allows to simulate real-scale behavior of the fuel system.
- The influence of various volume fractions of dissolved gas on aircraft engine fuel system has been investigated. The influence of different factors has been determined. Small volume fractions led to significant increase of dynamic loading of the pump, larger values led to reduction of dynamic loading of the pump.

2 Reliability of Two-stage Aircraft Engine Fuel Pump

2.1 Reliability analysis of aircraft engine

In comparison with modern engines, prospective aviation engines will have to have in 1.5 - 2 times higher durability, in 2 times lower mass and serviceability, by 10-15 % improved efficiency, decreased by 20…30 EPN dB noise and decreased up to 3 times hazardous emission (Olifirov, 2011). Such significant improvement of the engine performance requires solving a number of scientific and engineering problems. One of the most important challenges is development of more efficient and reliable systems of aircraft engines.

Numerous approaches and models have been proposed to describe, predict and prevent failures:

- models that are based on classical probability principles (Narmada, 1996);
- faults tree analysis (Geymayr, 1995);
- failure modes and effect analysis (Gilchrist, 1993), (Stamatis, 2003.);
- models that are based on Markov theory (Papazoglou, 2000);
- poisson based models (Saldanha, 2001);
- Bayesian theory based models (Percy, 2001);
- Monte Carlo based models (Marseguerra, 2002);
- hybrid models (Rosqvist, 2000)

In spite of large number of possible approaches, their implementations for practical issues has oftentimes only a limited range (Liu, 2014). As a rule, these methods require the information about object failures such as faults statistics, probabilities and failure effects. Oftentimes this kind of information is either expensive to obtain or altogether absent. The most significant of the models listed above is the hypothesis about independence of failures. The modern aviation systems are extremely complex, research of Moore et al., Holme et al., Motter et al., and Zongxiang et al. (Moore, 2000), (Holme, 2002), (Motter, 2002), (Zongxiang, 2004) show that in a real-world system the failure of a single element leads to a cascading failures, which results in a failure of the entire system. Thus, failure of one component leads to consequential failures of other components and, as a result, to cascading failure. The approach of dependent failures was proposed in studies of (Shorin, 1996) and (Liu, 2014). Article (Liua, 2013) proposed an approach of engine components representation as a node system. Node structure of aircraft engine NK-36 is represented in Figure 2.1. The description of the nodes is given in Table 2.1.

The relation between nodes and edges allows to estimate the reliability of the system. Developed node structure shows that control system of aircraft engine is the key system, defining the reliability of the whole engine. However regardless of ongoing smooth transition to digital control systems in propulsion engineering, the hydro-mechanical

control systems are still widespread. These are used not only as primary systems but also as standby systems. Moreover, hydraulic pumps and valves are applied even in fully digital control systems for control of engine geometry, fuel supply and distribution. Such hydraulic systems are known to contain a large number of functionally related hydro-mechanical components, each of which can be a source of vibration, pressure, flow and noise (Gafurov, 2014). Increased vibrations and pressure oscillations in aviation fuel supply systems are known to have adverse effects on combustion chamber operating stability, regulating system accuracy, elements' fatigue strength and dynamic loading of rotors and bearings. Consequently, the increase of fuel system performance leads to increase of aircraft performance.

The statistics of aircraft failures also show that aviation engine fuel pumps are the key components limiting durability and reliability of the whole engine (Bazovsky, 2013) as they are subjected to significant vibration load (Gafurov, 2011), (Gasparov, 2007). Therefore, the reliability analysis of the fuel system has justified motivation.

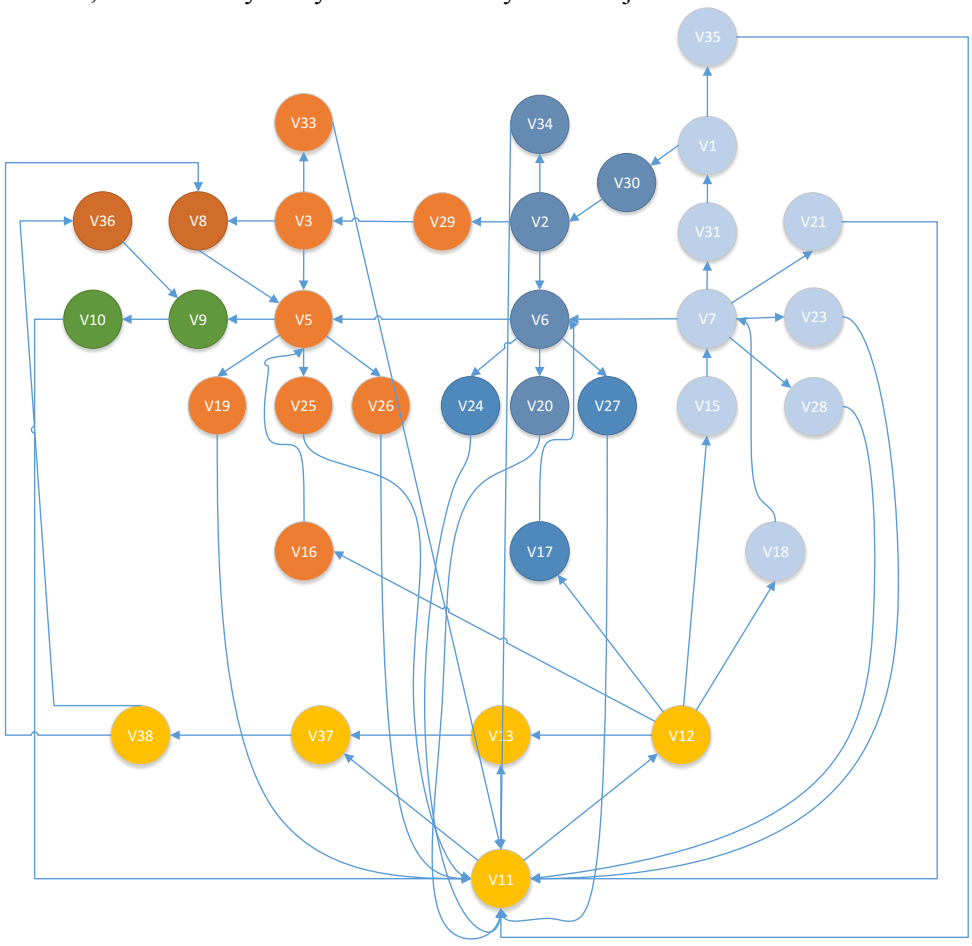

Figure 2.1: Node structure of the NK-36 aircraft engine

Table 2.1: Node structure of the aircraft engine NK-36

Node	Name	Node	Name	Node	Name
V1	Low pressure compressor	V13	Fuel metering unit	V26	Sensor of high pressure turbine outlet pressure
V2	Middle pressure compressor	V14	Variable stator vane	V27	Sensor of middle pressure turbine outlet pressure
V3	High pressure compressor	V15	Variable bleed valve	V28	Sensor of low pressure turbine outlet pressure
V4	Combustor	V16	High pressure turbine active clearance control valve	V29	Position sensor of high pressure compressor stator vane
V5	High pressure turbine	V17	Middle pressure turbine active clearance control valve	V30	Position sensor of middle pressure compressor stator vane
V6	Middle pressure turbine	V18	Low pressure turbine active clearance control valve	V31	Position sensor of low pressure compressor stator vane
V7	Low pressure turbine	V19	Rotary variable differential transformer of high pressure rotor speed	V32	Sensor of fan outlet temperature
V8	Combustor chamber	V20	Rotary variable differential transformer of middle pressure rotor speed	V33	Position sensor of high pressure compressor bleed valve
V9	Nozzle	V21	Rotary variable differential transformer of low pressure rotor speed	V34	Position sensor of middle pressure compressor bleed valve
V10	Thrust level	V23	Sensor of low pressure turbine outlet temperature	V35	Position sensor of low pressure compressor bleed valve
V11	Full authority digital engine controller	V24	Sensor of middle pressure turbine outlet temperature	V36	Afterburner
V12	Hydro mechanical unit for nozzle and afterburner control	V25	Sensor of high pressure turbine outlet temperature	V37	Fuel pump
				V38	Flow directional valve

2.2 Reliability analysis of aircraft engine fuel system

Aviation fuel systems are known to be extremely complex. Flow phenomena and operational processes are described in Appendix A. Developed node structure of considered fuel system of engine NK-36 is represented in Figure 2.3. Two-stage fuel pump ND-32 consisting of a screw-centrifugal stage and a gear stage is intended for fuel supply to the main combustion chamber and to the afterburner of the engine.

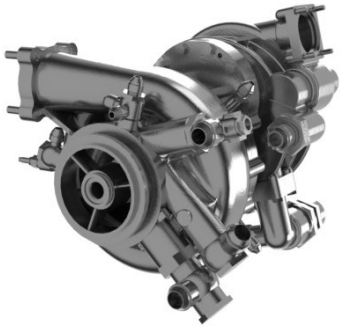

Figure 2.2: External view of the two-stage pump ND-32

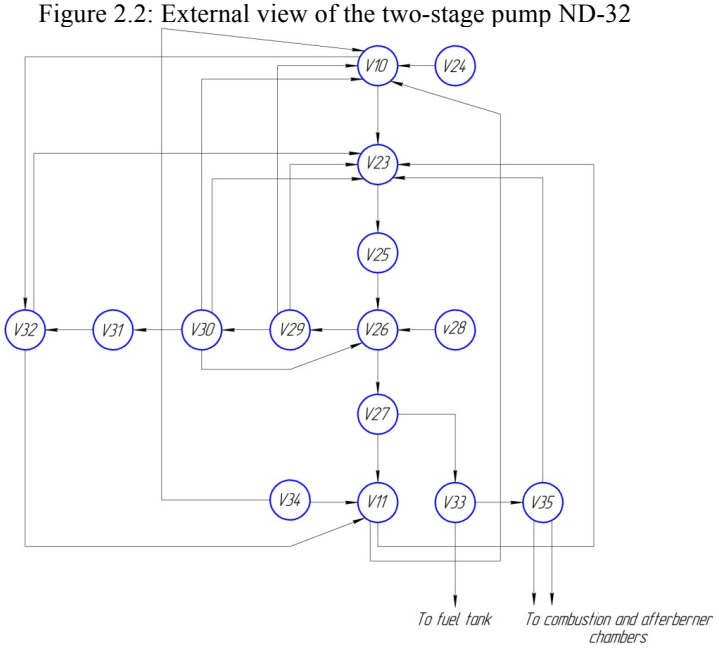

Figure 2.3: Node structure of the fuel system of NK-36 aircraft engine

Considerable number of previous researches (Kruchkov, 2000), (Igolkin, 2002), (Gasparov, 2006), (Stryczek, 1991), (Slodczyk, 2011) has shown that two-stage pumps are the most loaded units of the gas turbine engines. According to study of Shakhmatov (Shakhmatov, 1993), fuel pumps are the sources of the vibrations and pulsations in the fuel systems, but at the same time they are suffering from high dynamic loads. Considered

fuel system failure statistics has shown that the key components, limiting its reliability and as a result the reliability of the whole engine, are two-stage pumps failures. There are two main pumps that are used in such systems – ND-25 and ND-32. The only difference between them is in the diameters of inlet supply lines – 0.076 and 0.092 m correspondingly. These failures occur due to increased wear of the journal-and-thrust bearing. Increasing wear leads to the contact between the blades of impeller and casing volute (Gasparov, 2006).

Table 2.2: Node structure of the aircraft engine fuel system

Node	Name	Node	Name	Node	Name
V10	Full authority digital engine controller	V26	Valve	V31	Actuator of turbine cooling band
V11	Hydro mechanical unit for nozzle and afterburner control	V27	Gear stage	V32	Rev limiter
V23	Fuel metering unit	V28	Fuel-oil heat exchanger	V33	Aggregate of fuel bypassing
V24	Aggregate for nozzle control	V29	Centrifugal pump	V34	Heat probe
V25	Filter	V30	Aggregate for bypassing control	V35	Fuel directional valve

The exploitation data of two-stage pumps ND-25 and ND-32 allowed to build their failure functions – failure density, intensity and probability (Figures 2.3 – 2.5). The statistics of pump exploitation have shown that:

- design service life of the pumps is 1000 hours;
- pump failures occur in time period of 15 to 900 hours;
- the mean time between failures is equal to 150 - 300 hours for the majority of the failed pumps;
- the average clearances between the bearing and impeller ranges from 0.0018 to 0.0025 m.

Generally, hydraulic pump wear is difficult to quantify. Models for pump wear can be explored in work of (Frith, 1996). Measuring the actual material lost due to wear is impossible in practical conditions. Available simulation procedure is the contaminated sensitivity performance test, which measures flow degradation with increasing amounts of contamination in the fluid. Wear can be related to flow degradation and knowing the mass of contamination causing wear, critical contamination can be determined.

The data of the axial clearance between centrifugal wheel and bearing in the beginning of the exploitation and after failures allowed to calculate the wear rate of the bearing. The natural wear and tear are:

- for ND-25 - 0.000049...0.001 m;
- for ND-32 - 0.0001...0.054 m.

Consequently, the wears are not equal despite the very similar structure of the fuel systems and structure of the pumps. This is caused by the fact that the wear depends mostly on the operational conditions. For this reason, design and operational principles of the two-stage fuel pump should be investigated for determining the reasons of its failures.

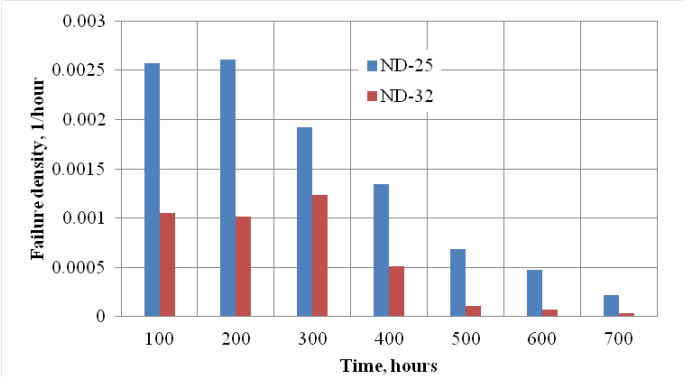

Figure 2.4: Failure density functions for pumps ND-25 and ND-32

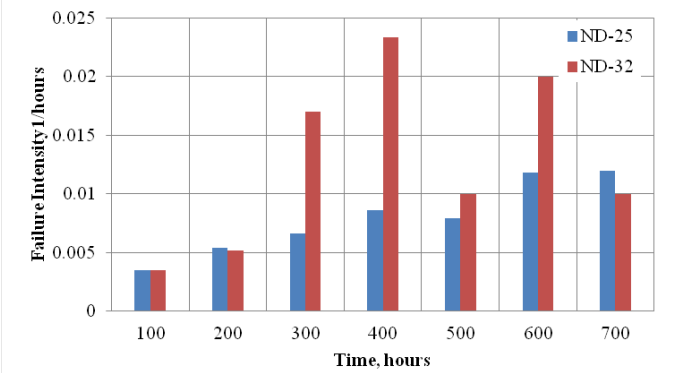

Figure 2.5: Failures intensity of the pumps ND-25 and ND-32

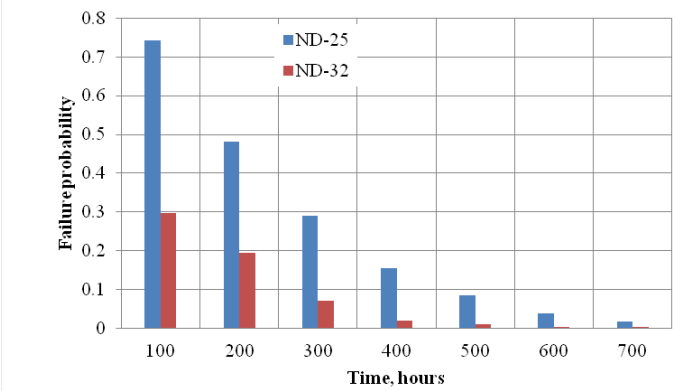

Figure 2.6: Failure probability of the pumps ND-25 and ND-32

3 Principle of Two-stage Aircraft Engine Pump

3.1 Pump Geometry

Generally, aviation fuel pumps combine booster and primary pumps and bearings. As a rule, they include screw and centrifugal wheels and a gear stage. They are manufactured in one common case with one shaft for driving the wheels. This allows to save up to 35 % of the accessory gearbox mass and total mass of the fuel aggregates due to decreased number of bearing assemblies and connection elements between aggregates.

Two-stage pump ND-32 (Figure 3.1 and Figure 3.2) consists of a screw-centrifugal stage (booster pump) and a gear stage (primary stage). Screw-centrifugal stage has an open type impeller with 11 straight blades (Figure 3.3, a) and double-lead screw. It also has a single unvaned volute casing. The shape of the volute casing was designed according to the theory of a constant average velocity for all sections (Figure 3.1, b). The second stage is a gear stage. Gears as well as centrifugal wheel have 11 teeth. Stages have a common shaft and case. Their connections are provided by means of a flange, splines and elastic clutch. Shaft is driven by a shaft of the engine's high-pressure spool through the reduction gearbox. An inlet pipe of a screw-centrifugal stage has numerous fittings for drain and bypass pipes connections. The inlet pipe of the screw-centrifugal stage also has 3 guide vanes. They are installed before the screw for flow stabilization and loss reduction.

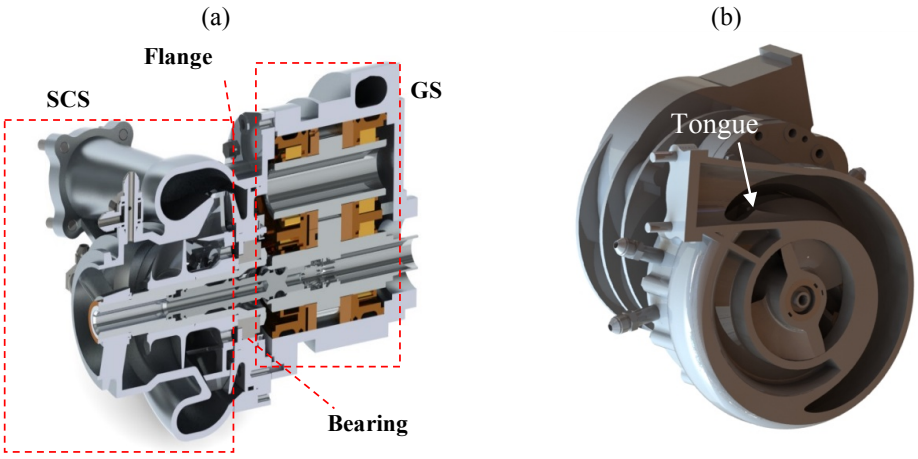

Figure 3.1: Two-stage pump ND-32
a - longitudinal cross-section; b - transverse section of the volute

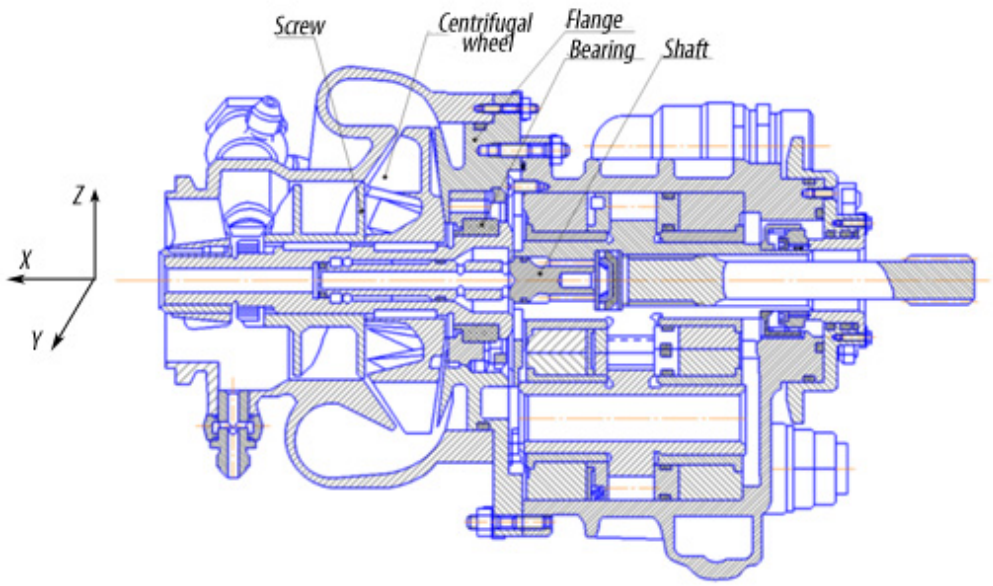

Figure 3.2: Construction of the two-stage pump ND-25

Figure 3.3: Rotor of the screw-centrifugal stage with the bearing assembly (a) and its journal-and-thrust bearing (b)

3.2 Analysis of two-stage pumps operation

Considered aircraft fuel system is schematically drawn in Figure 3.4. This figure demonstrates that main tanks ejector pumps do not switch off when fuel supply to feeder tanks is terminated. In this case tank pressurization gas is mixed with fuel. Aircraft evolutions are accompanied by variation of a tank charging pressure and this, eventually, leads to gas liberation before a fuel pump. Liberated gas is known to accumulate in stagnant zones at low mass flow rates. In this case the gas is periodically extracted from these zones and penetrating the pump. This process can be spontaneous and be defined

by a variety of factors such as external conditions, operating regimes, pipes geometry, aircraft evolutions.

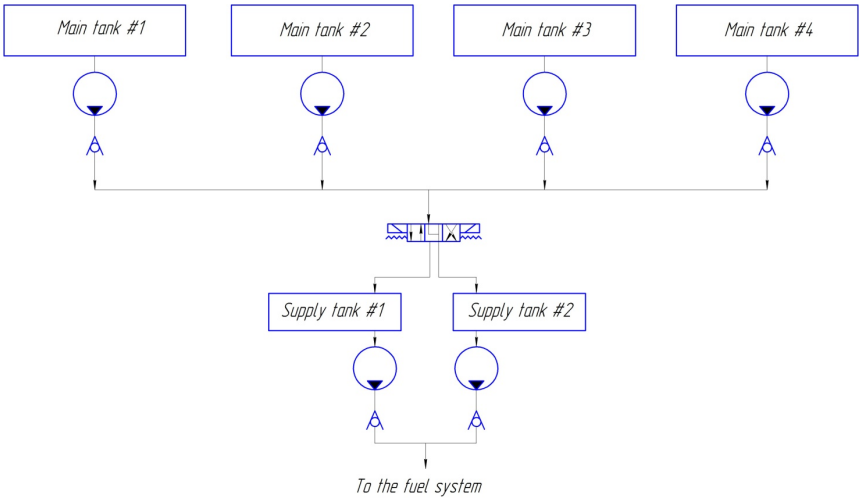

Figure 3.4: The fragment of the aircraft fuel supply system

During an aircraft altitude changing its engines work in a flight-idle regime. This regime is attended with decreased fuel consumption which is 40 times lower compared to fuel consumption during take-off regime. Moreover, rotation frequency and pump discharge pressure at a flight-idle regime reach 30% and 20% correspondingly from the values on a take-off regime. The considered fuel system requires the two-stage pump for supplying all the fuel needed for wide range of operation modes of the aircraft. It means that the pump should provide a wide range of flow rates in the combustion chamber and afterburner. Therefore, it needs bypass lines that are connected with the booster stage entrance. In such a manner, hydraulic scheme of the considered pump consists of 4 hydraulic parts: supply, delivery, bypass and drain. Drain and bypass lines at the pump entrance produce a circumferential distortion of the flow parameters. Circumferential nonuniformity of pressure fields results in unbalances of radial and axial forces.

A scheme of the pump stages vibration and hydrodynamic interaction is proposed to determine the sources of the dynamic loads inside the two-stage pump (Figure 3.5). Subscripts 1, 2...11 denote particular values of corresponding flow parameters at specific pump cross-sections.
The screw-centrifugal stage has a volute diffuser. It has an irregular form and so-called “tongue” (Figure 3.1, b). These factors result in circumferential distortion of flow parameters at the centrifugal wheel outlet. Additionally, there is a non-stationary interaction between delivery pipeline and screw, as well as between screw and centrifugal wheel and between centrifugal wheel and volute. This interaction occurs due to relative motion of its components and induces pressure pulsations, leading to occurrence of non-stationary forces. These forces increase the vibrations of the pump elements and induce

noise. Developed scheme also shows that the leakages from the gear stage can influence the working capacity of the bearing.

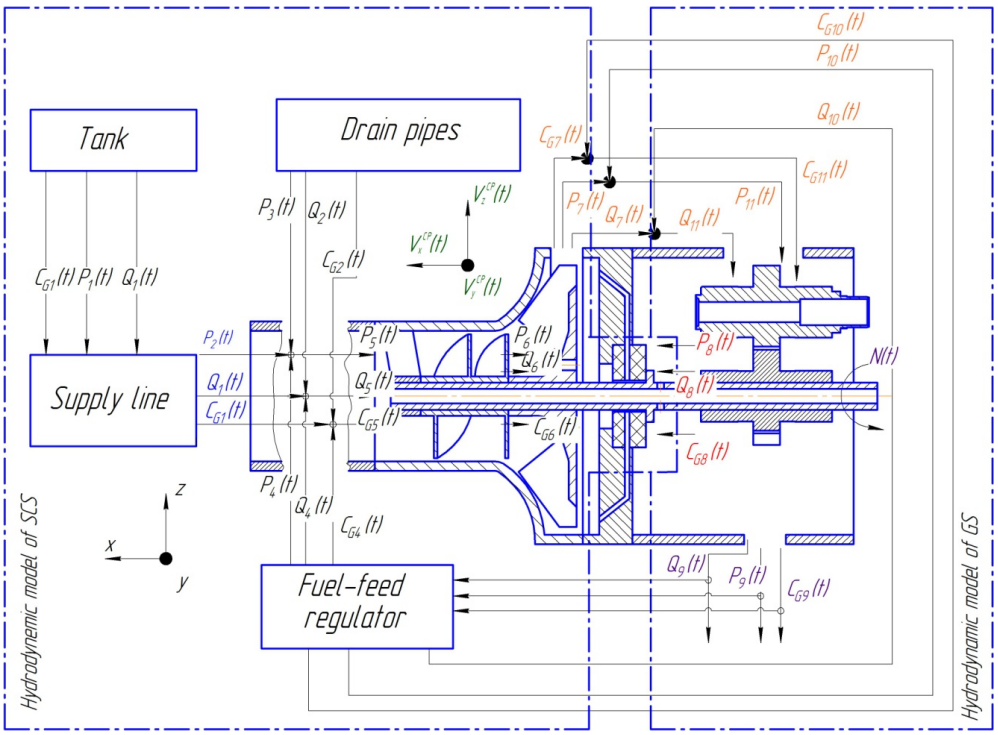

Figure 3.5: A scheme of mechanical and hydrodynamic interaction of pump stages

Oscillations generated by the gear stage can propagate in two directions according to the Figure 3.2 and Figure 3.5:

- from the gear stage to the fuel metering unit and further to the screw-centrifugal stage inlet;
- from the gear stage to the backup valve and low-pressure filter and further to the screw-centrifugal stage.

If we assume that blade channels of the screw-centrifugal stage do not prevent the high frequency oscillations propagation from its outlet to inlet, then these high-amplitude pressure oscillations with impeller blade frequency can penetrate though blade channels from the stage outlet to its inlet and further. Mounting a relief valve at the stage inlet leads to standing wave formation. Changing the rotation frequency of the shaft must change the amplitude of this standing wave. Eventually, this should lead to leap of the pressure amplitude of this high frequency oscillations due to resonance. Adverse combination of

oscillations phases at the stage inlet and outlet lead to significant pressure drop on the rotor. This can induce the rotor oscillations and straightforward shock impact on the bearing.

However, experimental results obtained by Kalnin et al. (Kalnin, 1980) did not confirm the version about presence of high-frequency oscillations at screw-centrifugal stage of the ND-25 and ND-32 pumps. Obtained results show no oscillations with impeller blade frequencies at pumps' entrances in spite of their presence at the outlet. Moreover, such oscillations with impeller blade frequencies prevailed over other frequencies at the outlets. Thus, high-frequencies pressure pulsations at the screw-centrifugal stage outlet can be assumed not to affect the pressure pulsations at the stage inlet.

Adverse pressure distribution in the two-stage pump canal can also be a source of bearing fault. Pressure field distribution in the pump hydraulic canal was embedded in such a manner that it should have provided a screw-centrifugal stage shaft in a fixed position by means by the bearing at least on the nominal regime. However, simulation results obtained in research (OJSC "Samara construction bureau of engines design", 1998) showed that axial force amplitude acting on the rotor can overcome its mean value on the transient regime from idle to 0.4 nominal. It can induce sharp loads on the bearing.

The developed scheme of fuel pump stages interaction tells us that there are a number of possible loading factors, each of which can be a source of increased pressure pulsations, vibrations and noise. Interaction of these factors can lead to additional self-oscillations inside the fuel system. Developed scheme also allowed us to understand that the screw-centrifugal stage directly determines the working conditions of the journal-and-thrust bearing. This fact leads to necessity to investigate flow phenomena inside screw-centrifugal pumps and their operational principles. In such a manner, only screw-centrifugal stage should be thoroughly considered in further investigation.

3.3 Geometric Notation

The geometry of a generalized two-stage pump is represented schematically in (Figure 3.2 and Figure 3.3). Generally, it consists of a number of stages. Screw-centrifugal stage can be represented as a set of rotor blades attached to a hub and operating inside a stationary case (Figure 3.6). The characteristic radii of screw and centrifugal inlet and discharged blades are $r_{T1}^{S}, r_{H1}^{S}, r_{T2}^{S}, r_{H2}^{S}$ and $r_{T1}^{C}, r_{H1}^{C}, r_{T2}^{C}, r_{H2}^{C}$ respectively. Subscripts 1 and 2 are used in this thesis to denote flow parameters at the inlet and the discharge correspondingly.

Discharge channel is inclined to the axial of rotation at an angle χ. This angle is varied in a range $0 < \chi < 90$. Angle is close to 0 degrees in a screw area and to 90 degrees in a centrifugal wheel area.

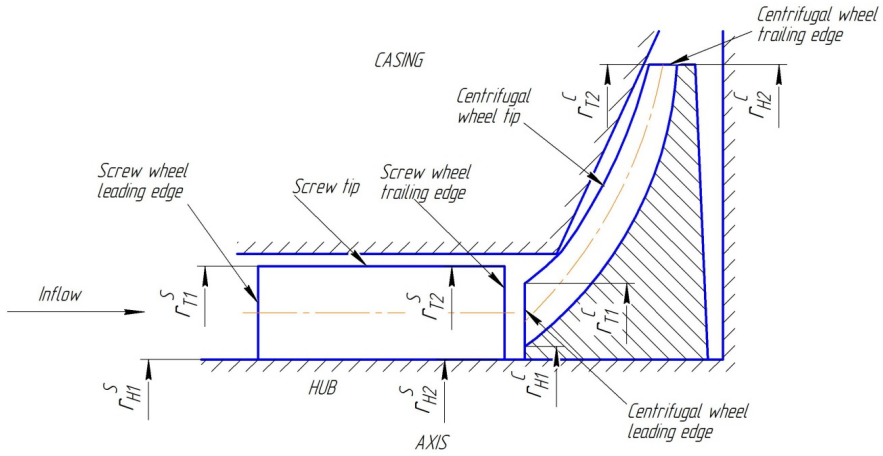

Figure 3.6: Cross-sectional view through the axis of a pump wheels

The flow through the kinetic pumps is usually visualized by means of meridional surface (Figure 3.7). Two coordinate frames are normally used: inertial frame and rotating frame. Fluid has a velocity *v(r)* in an inertial coordinate system and velocity *w(r)* relative to rotating blades. These velocities have corresponding components in circumferential and meridional directions - v_θ, w_θ and v_m, w_m respectively. Blade speed of rotation is equal to $N \cdot r$.

β is the flow angle. It is defined as the angle between the relative velocity vector in the meridional plane and a plane perpendicular to the axis of rotation;

β_b is the blade angle. It is the inclination of the tangent to the blade in the meridional plane and the plane perpendicular to the axis of rotation.

The difference between blade angle and the flow angle at the pump inlet defines the incidence angle, α (Figure 3.8). Another important angle is the angle of attack. This an angle between the incoming relative flow direction and the chord line of the blades. The difference between the blade angle and the flow angle at the trailing edge defines the deviation angle $\delta(r)$.

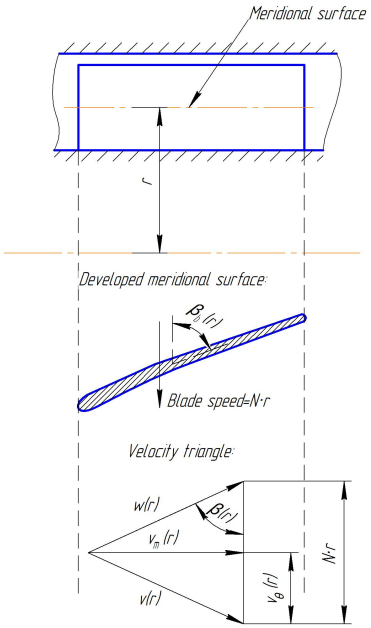

Figure 3.7: Developed meridional surface and velocity triangle

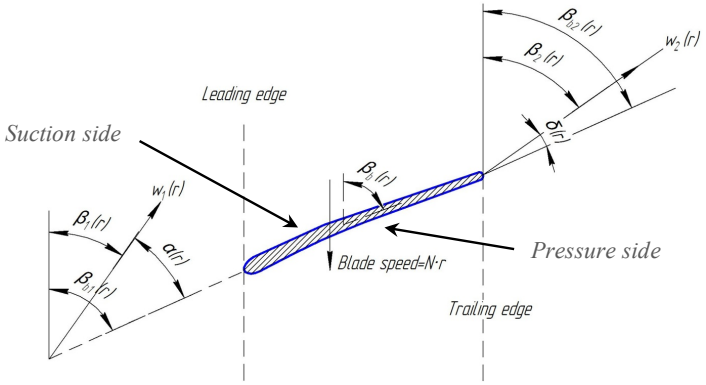

Figure 3.8: Definition of blade angles

Screw geometrical parameters and pump operating regimes are known to be the vital parameters in flow structure at the screw-centrifugal stage entrance. Both these factors can be combined into a common factor – regime parameter, q, which can be determined as a ratio of a current flow rate to the flow rate corresponding to impeller blade angles of attack equal to zero ($\xi = 0$):

$$q = \frac{Q}{Q_0} \tag{3.1}$$

4 Simulation Model for Investigation the Flow Phenomena and Operational Processes inside Screw-centrifugal Stage of Aircraft Engine Fuel Pump

4.1 Two-dimensional analysis of flow inside centrifugal and axial flow pumps

The relation between small linear pressure and mass flow pulsations at pump inlet and outlet was investigated in paper (Brennen, 1978). C. Brennen conducted a series of experiments in a variety of pump operating regimes, with cavitation and without. He presented results by means of dynamic transfer matrices. Results were obtained from direct pressure pulsations measurement. The data gathered by means of this approach did not converge with the results obtained by means of theoretical pump models.

A physical model of cavitating screw-centrifugal pump was obtained in paper (Kinelev, 1976). This model is based on the representation of flow structure inside a pump. Vortex structures are considered as sources of periodical hydrodynamic excitation. Studies of Belousov and Ovsyannikov (Belousov, 1974) and (Ovsyannikov, 1979) describe approaches for determination of stresses that may occur in axial and centrifugal pump. Static and dynamic components of loading from static pressure are considered in these papers. However, in practice it very difficult to determine dynamical forces on pump elements caused by moving fluid by means of equation of momentum. Meanwhile, the distribution of working parameters along pump channel should be known. The presence of constructive features of screw, impeller and volute makes this issue extremely challenging.

The flow pattern created inside a screw-centrifugal pump by the motion of impellers and two gears rotating in opposite directions is deceptively complex despite the simple geometry of the pumps. The flow cannot be analyzed, based on a steady-state assumption that is usually employed to analyze turbo-machinery despite the fact that the flow is essentially steady. Only the time-dependent, unsteady, dynamic meshing can predict the motion of the fluid flow against the very high adverse pressure distribution. Although the complexity of analysis is inherent in all hydraulic pumps, kinetic pumps pose an exceptional challenge due to the fact that there are a number of physical phenomena as cavitation, turbulence and non-stationary flow and rotating components housed within a stationary three-dimensional-casing. The study and analysis presented in this thesis will deal with those problems to make an acceptable preliminary investigation on the screw-centrifugal pump flow.

4.2 Three-dimensional analysis of flow inside centrifugal and axial flow pumps

Nowadays CFD simulation is a powerful tool for investigations of working processes inside hydraulic pumps. It allows to estimate their energetic and cavitation characteristics, understand the distribution of working parameters along pump channel. It has become a reality due to developing of numerical algorithms as well as computational capabilities.

During the recent decade, many researchers have carried out investigations with the aid of this method. The capability for simulation of flows has significantly affected recent developments in designing parameters (Zhang, 2008). Works (Zhang, 2002), (Gonza´lez J., 2001), (Hagelstein, 2000) describe numerical simulations of the turbomachinery unsteady work processes. Energetic and cavitation properties of axial and centrifugal pump, having a wide range of geometric sizes and power-speed coefficients, were investigated in papers (Goto, 2001) and (Amone, 2001). The obtained RMS of accuracy was 2.5%. Papers (Zhang, 2002), (Gonza´lez, 2001), (Gonza´lez, 2002) and (Hillewaert, 2000), (Hillewaert, 1999), (Longatte, 1999), (Zhang, 2002), (Majidi, 2003), (Majidi, 2000), (Majidi, 2004), (Han, 2000), (Zixiang, 2000), (Kurokawa, 2000), (Kurokawa, 2000), (Tatebayashi, 2001), (Tatebayashi, 2002), (Tatebayashi, 2003), (Kim, 2000), (Goto, 2002) are devoted to transient analysis of pump performances. Cavitation still remains very important and interesting phenomenon that should be taken into account during pump CFD simulation. A number of papers describe the two-phase flow in rotodynamic pumps and calculates cavitation performances (Kelecy, 2003), (Medvitz, 2002), (Yong, 2009). There are a number of cavitation model that can be implemented for pumps simulations. Several of them are described in papers (Wang, 2009), (Singhal, 2002), (Frobenius, 2002), (Hosangadi, 2001). All of them are based on Rayleigh-Plesset model. Paper (Kelecy, 2003) describes a simulation of cavitation origination in a screw-centrifugal pump by means of commercial software ANSYS Fluent. In paper (Frosina, 2013) a tridimensional CFD analysis of the lubrication circuit oil pump of a modern high-performance engine manufactured by Aprilia was shown. The model was built up with PumpLinx®, a commercial CFD 3D code by Simerics Inc.®, taking into account all the phenomena associated to the fluid cavitation. The model was validated by data of an experimental campaign performed on a hydraulic test bench.
Computational fluid dynamics can help to optimize the design of the pump and improve the efficiency of pumps and entire hydraulic systems. Results obtained by Demeulenaere (Demeulenaere, 2002) show that full-size model of a kinetic pump is needed to get more accurate data as such computational domain allows to better understand unsteady processes inside a pump. This investigation used a commercial code Fine/Turbo of Numeca to investigate transient interaction of rotor and stator of the first stage of the rocket centrifugal turbopump LH2. Results derived from full-size showed more accurate results in comparison with one-six domain.

The results obtained by Page (Page, 2001) show that the commercial finite volume solver ANSYS CFX can be used for accurate numerical solution of flows inside kinetic pumps. This paper includes the comparison of commercial packages CFX-TASCflow

(Technology, 2010), FIDAP (FLUENT) (Incorporated, 2009) and FINE/Turbo (NUMECA) (International, 2010) for calculation the characteristics of an axial pump. Reynolds-averaged Navier-Stokes equations with the $k-\varepsilon$ turbulence model (Wilcox, 2006) under the same boundary conditions were solved. All three packages showed almost identical results and a strong convergence of the experimental results. At that, the mean- square calculation error of basic energy parameters of the pumps is 2.5%.

Despite its long history of usage and numerous researches on kinetic pumps flow analysis (Iaccarino, 2004), (Murthy, 2004), no work has been reported in the literature that examined the numerical turbulent flow analysis of screw-centrifugal pump taking into account a gear pump, unsteady flows, cavitation phenomena and turbulence to describe three-dimensional flow inside a pump. Therefore, this research has been initiated using ANSYS CFX, a commercial finite volume CFD software package, to investigate tree-dimensional spatial turbulent flow analysis of a screw-centrifugal stage of aircraft engine pump. This investigation is expected to provide important information for defining of the causes of the journal-and-thrust bearing failures.

4.3 Developed model description

4.3.1 **Model**

Investigation of pressure and velocity fields distribution is very challenging due to spatial flow around screw and centrifugal blades as well as circumferential distortions at pump inlet and outlet. Momentum variation, heat and mass transferring in working fluid can be described by means of Navier-Stokes equations. These equations should be solved numerically over all screw-centrifugal pump computational domain including the bearing. The gear stage should be also considered. Its influence should be considered in form of leakages.

Developing model of flow inside screw-centrifugal stage of the pump should involve unsteady, turbulent, multiphase flow of a mixture of viscous liquid through rotating pump elements. Multiphase flow is caused by the presence of additive gas. The additive is fed at a relatively low mass concentration to the pump intake as individual streams of pure additive. The sequence of numerical simulation is shown in Figure 4.1. Setting boundary conditions, defining fluid properties, executing the solution, refining the grid, and viewing and post-processing the results are generally performed within the chosen CFD software. For this research, Solid Works was used for geometric model development, ICEM CFD was used for pre-processing and grid generation. ANSYS CFX was used for model solution and post-processing.

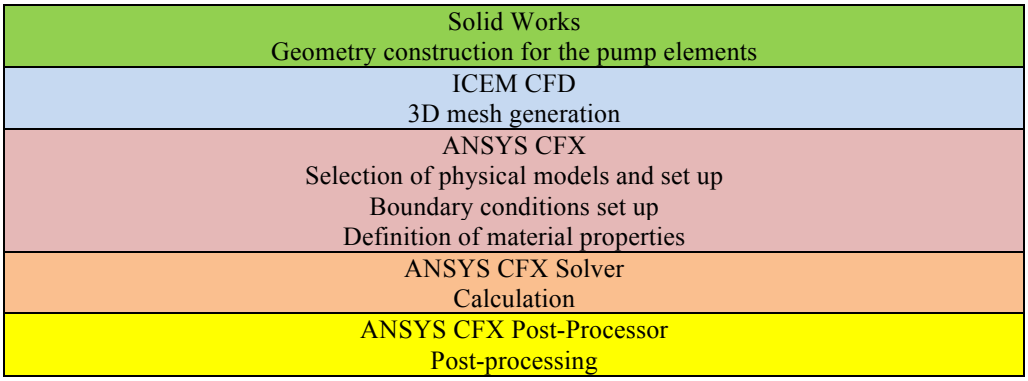

Figure 4.1: Basic program structure in numerical simulation

The problem involves all three spatial dimensions. Hence it is necessary to develop the full three-dimensional geometric model of flow channel of the pump to precisely simulate three-dimensional flows inside it. General data of the screw-centrifugal stage of the pump ND-32 is shown in Table 4.1.

Table 4.1 - General data of screw-centrifugal stage

Pump Type	Kinetic pump
Solid material:	Aluminum for stage housing and pump rotor
Hydraulic fluid:	Kerosene
Rotor drives	Counterclockwise
Speed range	From 0 to 10 000 min^{-1}
Pump inlet pressure	From 0 Pa up to 0.24 MPa at operating temperature
Supply pipeline diameter	0.076 m
Outlet Pressure Range SCS: GS	 Up to 1.8 MPa Up to 8 MPa
Fluid Temperature	Up to 243 K
Total no. of screw blades:	2
Total no. of centrifugal wheel blades:	11
Axial length of screw:	0.043 m
Axial length of centrifugal wheel:	0.036 m
r_{T1}^{S},	0.092 m
r_{H1}^{S}	0.042 m
Pitch of screw	0.0315 m
r_{T1}^{C}	0.094 m
r_{H1}^{C}	0.042 m
r_{T2}^{C}	0.144 m

Developed computational domain of screw-centrifugal stage ND-32 takes into account the drains into the pump (drain from aggregates for nozzle control, drain from actuator of turbine cooling, drain from the, drain from rev limiter, aggregate of fuel bypassing, drain from the fuel metering unit), main components: inducer, centrifugal wheel, volute, intake pipeline, journal-and-thrust bearing (Figure 4.2). The length of the supply pipe of the input area L_{in} should be six calibers $L_{in}=6D_{in}$ for accurate modeling of back vortex flow at the pump inlet. The length of the drain regions L_{drain} is equal to five caliber $L_{drain}=5D_{drain}$.

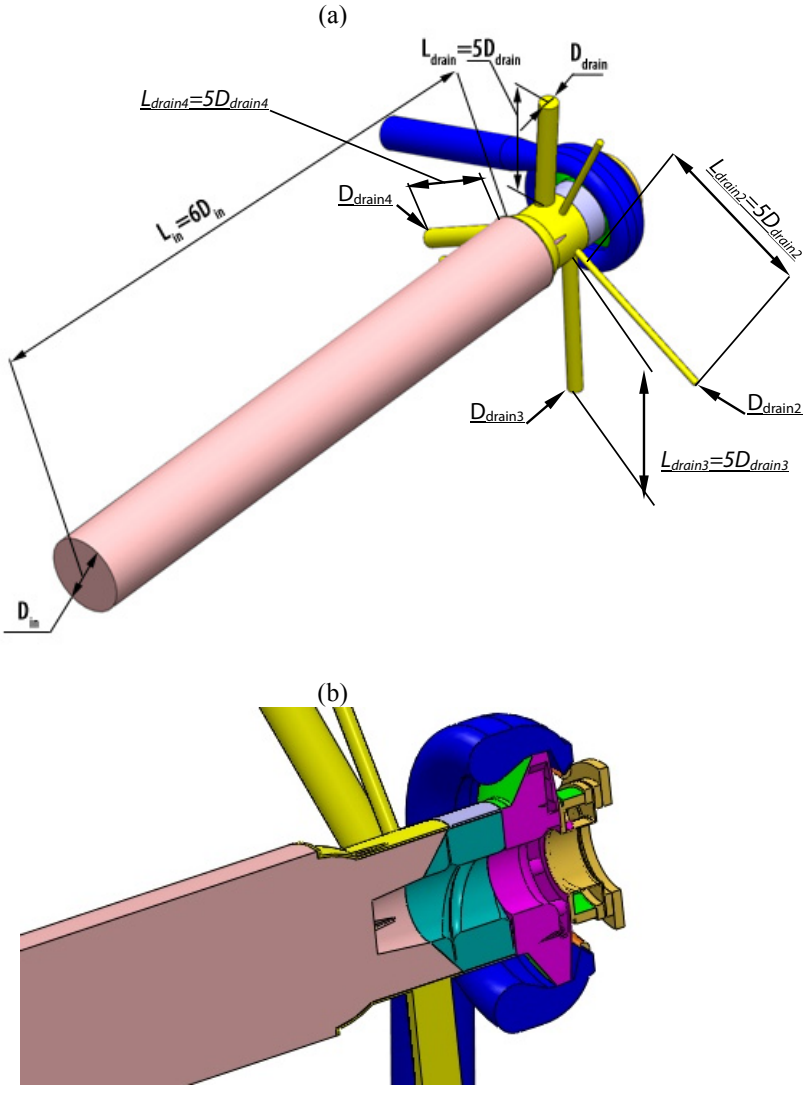

Figure 4.2: Physical configuration of SCS geometric model
a- physical configuration; b - cut away side view along axis of rotation

The main design features of the computational domain of the screw-centrifugal pump were taken into account: the radial clearance between the pump case and the blades; discharge blades, built on the back face of the centrifugal wheel; discharge holes; spirally profile of the volute; design features on the journal-and-thrust bearing (helical grooves over the internal cylindrical surface, radial grooves on the end face, fuel inlet channel for bearing lubrication, axial and radial clearances between the shaft and the bearing). Peculiarities of interaction of flows through drain pipelines and primary flow coming from the supply pipeline are also taken into account. It worth to note, that liquid from drain pipelines flows directly to the screw leading edge and leads to significant circumferential distortion at the entrance of the screw. The coordinate system is chosen such that the origin of the Cartesian coordinate is at the center of the centrifugal wheel.

The following assumptions were made for simulation model development:

1. The fluid is a Newtonian;
2. The fluid is originally stationary;
3. Body forces are negligible;
4. The walls are modeled using a log-law wall function;
5. The influence of the gear stage was taken into account using the model developed by Rodionov L.V. (Rodionov, 2009).

4.3.2 **Physics**

The aspects of operational processes of the aircraft engine pumps, considered in Chapter 1, have to be taken into account. One of the most important is the multiphase flow inside the pump. When undissolved gas gets into the supply pipe of engine pump, the working fluid represents a multi-component fluid containing the gas and liquid phases of kerosene and gas in a free state. The properties of the working fluid components used in present simulation of unsteady flows in the screw-centrifugal stage are shown in the Table 4.2.

Table 4.2: Working fluid properties at a temperature of 20 ^{0}C (T=20 ^{0}C)

Parameter	Kerosene Jet-A	Kerosene vapor	Air
Mole weight, kg/kmol	167.3	167.3	28.96
Density, kg/m^3	780	7.1	1.185
Specific heat capacity, J/kg·K	2090	1710	1004.4
Dynamic Viscosity, Pa·s	0,0024	$7\cdot10^{-6}$	$1.831\cdot10^{-5}$
Specific heat conductivity, W/m·K	0.149	0.0178	0.0261
Thermal coefficient of linear expansion, K^{-1}	-	0.003356	0.003356

Nowadays two main approaches for the numerical calculation of multiphase flows are known: the Euler-Lagrange approach and the Euler-Euler approach. Euler-Lagrange approach allows to model the discrete phase. In this case, time-averaged Navier-Stokes

equations are solved for continuous liquid phase while the dispersed phase is modelled by means of tracking a large number of bubbles though the calculation flow field. This approach requires the assumption of negligibility of gas phase volume fraction. In case of aircraft engine fuel system such approach can result in low accuracy of calculations. The second approach is the Euler-Euler approach model of working mixture as an interpenetrating continuum. In this approach, the volume of phase fraction cannot be occupied by the other phase. These volume fractions are assumed to be continuous functions of space and time and their sum is equal to one. In the developed mathematical model of pump's stages interaction, the Euler-Euler approach is used. The same approach was used in papers (Singhal, 2002), (Sauer, 2000), (Zwart, 2004) for flow simulations inside centrifugal and axial flow pumps. Obtained numerical results of cavitation flows showed a good convergence with the experimental data. Thus, a set of n momentum and continuity equations for each phase should be solved.

The flow inside the screw-centrifugal stage is described by means of the non-stationary Navier-Stokes equations in the form of conservation. Navier – Stokes equations are the equations that describe variation of momentum, heat and mass exchange. Equations describing other effects, such as cavitation and turbulence can be also solved in combination with the Navier-Stokes equations.

Fluid motion and transport characteristics are governed not only by three conservation equations, but also by additional equations for turbulent and cavitation describing. Conservation equations are derived for each phase to obtain a set of equations, which have similar structure for all phases.

4.3.3 **Governing equations for one-component flow**

Transport equations:

Continuity equation

$$\frac{\partial \rho}{\partial t} + \nabla(\rho \upsilon) = 0 \tag{4.1}$$

Equation (4.1) is equivalent to equation (4.2):

$$\frac{\partial \rho}{\partial t} + \upsilon grad\rho + \rho div\upsilon = 0 \tag{4.2}$$

Addend $\frac{\partial \rho}{\partial t}$ describes local variation in time of mass environmental density. Addend $\upsilon grad\rho$ characterizes density variation which is caused by convection diffusion (molecular and eddy diffusion) of fluid particle in a nonuniform environment. Addend is $\rho divU$ a divergent equation member.

Therefore, the sum of local and convectional densities variations is the density total time variation. Physically its explained be the addend $\rho div\upsilon$. Density variation is caused by expansion and contraction of a fluid particle. It is obvious that if $div\upsilon > 0$,then the expansion is attended with density decrease $\frac{\partial\rho}{\partial t} < 0$ and conversely, if $\mathrm{div}\upsilon < 0$, then the contraction is attended with density increase $\frac{\partial\rho}{\partial t} > 0$.
Therefore, equations (4.1) and (4.2) are equal to zero in accordance with the law of mass conversation.

Momentum equation

$$\frac{\partial(\rho\upsilon)}{\partial t} + \nabla(\rho\upsilon\otimes\upsilon) = -\nabla p + \nabla\tau + S_M, \qquad (4.3)$$

where stress tensor is determined by the Stokes' law and showing the relation between stress and deformation of the system:

$$\tau = \mu\left(\nabla\upsilon + (\nabla\upsilon)^T - \frac{2}{3}\kappa\nabla\cdot\upsilon\right) \qquad (4.4)$$

Total energy equation

$$\frac{\partial(\rho\rho_{tot})}{\partial t}\cdot\frac{\partial p}{\partial t} + \nabla(\rho\cdot\upsilon\cdot h_{tot}) = \nabla(\lambda\nabla T) + \nabla(\upsilon\cdot\tau) + \upsilon\cdot S_M + S_E, \qquad (4.5)$$

where

$$h_{tot} = h + \frac{1}{2}\upsilon^2. \qquad (4.6)$$

Component $\nabla(\upsilon\cdot\tau)$ in the equation (4.5) expresses the work done by external forces – work done by viscosity force. This component also shows internal heating due to the presence of viscosity.

Component $\upsilon\cdot S_M$ expresses the work done by the external source of momentum.

State equations:

The above transfer equations have to be supplemented by state equations for the density and enthalpy to form a closed system of equations. In general, these equations have the following forms:

$$\rho = f(p,T) \qquad (4.7)$$

$$dh = \frac{\partial h}{\partial t}|_P \; dT + \frac{\partial h}{\partial p}|_T \; dp = c_P dT + \frac{\partial h}{\partial p}|_T \; dp, \tag{4.8}$$

where heat capacity at constant pressure can be found as

$$c_p = f(p,T) \tag{4.9}$$

Thermal energy equation

Kinetic energy equation

$$K = \frac{1}{2}\upsilon^2 \tag{4.10}$$

Mechanical energy equation can be obtained by scalar product of velocity υ and momentum equation:

$$\frac{\partial(\rho_m \cdot K)}{\partial t} + \nabla(\rho_m \cdot \upsilon \cdot K) = -\upsilon \cdot \nabla p + \upsilon \cdot (\nabla \tau) + \upsilon \cdot S_M \tag{4.11}$$

The thermal energy equation is obtained by subtraction this equation (4.11) from the total-energy equation (4.5):

$$\frac{\partial(\rho \cdot h)}{\partial t} - \frac{\partial \rho}{\partial t} + \nabla(\rho \cdot \upsilon \cdot h) = \nabla(\lambda \nabla T) + \upsilon \cdot \nabla p + \cdot \frac{\tau}{\nabla \upsilon + S_E} \tag{4.12}$$

Component $\frac{\tau}{\nabla \upsilon + S_E}$ is always positive and is called viscous dissipation. It describes the internal heating of the liquid due to the presence of viscosity.

4.3.4 **Governing equations for multi-component flow**

As it is shown in Appendix A, the flow in a screw-centrifugal stage is multi-phase and can be accompanied by undissolved gas which intensifies cavitation processes. Therefore, the flow consists of liquid and gaseous phases, ψ, of the kerosene and the gas component. Sum of each of the volume fractions should be:

$$C_K + C_V + C_A = 1 \tag{4.13}$$

As a result, the Navier-Stokes equations (transport and state) as well as the equation of cavitation and turbulence are given for the case of multicomponent viscous flow. In this case the continuity and momentum equations become:

-continuity equation for each mixture phase

$$\frac{\partial(C_\psi \rho_\psi)}{\partial t} + \frac{\partial(C_\psi \rho_\psi \upsilon^i)}{\partial x^i} = \dot{S}_\psi \tag{4.14}$$

- momentum conservation for each mixture phase

$$\frac{\partial(\rho_m \upsilon^i)}{\partial t} + \frac{\partial(\rho_m \upsilon^j \upsilon^i)}{\partial x^i} = -\frac{\partial p}{\partial x^i} + \frac{\partial(\tau^{ij})}{\partial x^j} + \rho_m C_\psi g^i \tag{4.15}$$

The stress tensor is determined from the Stokes' law, which is as follows:

$$\tau^{ij} = \mu_m \left(\frac{\partial \upsilon^i}{\partial x^j} + \frac{\partial \upsilon^j}{\partial x^i} \right) \tag{4.16}$$

Mass source is supposed to occur from the interphase transfer and it should satisfy the condition:

$$\sum_{\alpha=1}^{Num} \dot{S}_\psi = 0 \tag{4.17}$$

There is also a condition that the mixture phases fill the entire considered volume of the mixture:

$$\sum_{\psi=1}^{Num} C_\psi = 1 \tag{4.18}$$

Equations (4.14), (4.15) and (4.18) build a closed equation system, including *(Num+4)* known equations and (*Num+4*) unknown equations.

4.3.5 **Turbulence model**

Flow inside the screw-centrifugal stage is turbulent. To model it, the additional stress components in the momentum equation (4.15) are necessary as the velocities in the considered equation are averaged. These stresses are modeled using the eddy viscosity, calculated using turbulence models, for example, $k - \varepsilon$ or Shear Stress Transport (SST) (Menter, 2000). The exact prediction of turbulent flow behavior is not possible, but it is possible to try to design a numerical model that reproduces several of the statistical characteristics of turbulent motion. There are three basic principles for numerical turbulence simulation:

- Direct Numerical Simulation, DNS
- Large Eddy Simulation, LES
- Reynolds averaged Navier-Stokes equation systems, RANS

DNS method is the most reasonable and accurate, but it requires a detailed space-time resolution and yields to large computational costs.

Turbulence models used in engineering calculations are usually based on RANS turbulence models. The statistical approach to the study of turbulence, realized in this method, involves motion equations averaging. All movement parameters are divided into average and turbulent components. The averaging used in RANS is the ensemble averaging. The Reynolds stresses, appearing in the momentum equation in form of the Navier-Stokes equations, have to be closed. The Reynolds equations closure (turbulent stresses definition $\tau^{ij} = \rho\overline{\upsilon_i' \upsilon_j'}$) is performed using semi-empirical turbulence models. RANS turbulence models are split into two classes:

- models, using the Boussinesq hypothesis (algebraic models; models with a single equation (Spalart-Allmares SA model, Sekundov model); models with two equations ($k-\varepsilon$ model, $k-\omega$ model, Menter SST model, based on the $k-\omega$ model, etc.);
- models of Reynolds stresses (differential models of Reynolds stresses (DRSM); algebraic model of Reynolds stresses (ARSM); decisive algebraic model of Reynolds stresses (EARSM)).

It also may be noted that there is an intensive development in recent years of the so-called detached eddy simulation (DES). This method is a "hybrid" approach that combines the high accuracy of the existing semi-empirical statistical models (RANS) (in the areas of attached boundary layer) and acceptable computational costs of large vortex simulation of separated-flow regions.

To create the numerical model of working processes in this dissertation the RANS turbulence model was used. The comparison of different turbulence models was also carried out: $k-\varepsilon$ and Shear Stress Transport (SST) model (Menter, 1994). Based on the results of this comparison, SST model, using the automatic face function, was chosen as the main model. This model is based on two equations: the equations for the kinetic energy of turbulence *k* and its frequency ω. In the near-wall flow region $k-\omega$ turbulence model is used, in the external flow - $k-\varepsilon$ model. ε is a kinetic energy dissipation. The equation for the turbulent kinetic energy and its frequency are:

$$\frac{dk}{dt} = \nabla\cdot((\nu+\sigma_k\nu_T)\nabla k) + P_k - \beta^*\omega k, \tag{4.19}$$

$$\frac{d\omega}{dt} = \nabla\cdot((\nu+\sigma_\omega\nu_T)\nabla\omega) + \frac{\gamma}{\nu_T}P_k - \beta\omega^2 + (1-F_1)\frac{2\sigma_{\omega 2}}{\omega}(\nabla k)\cdot(\nabla\omega), \tag{4.20}$$

Constants of the equations (4.19) and (4.20) are shown in Table 4.3.

Table 4.3: Parameters of SST turbulence model

Parameter	Value	Parameter	Value
β_1^*	0.09	β_2^*	0.09
β_1	0.055	β_2	0.0928
α_1	0.25	γ	$\frac{\beta}{\beta^*} - \frac{\sigma_\omega k^2}{\sqrt{\beta^*}}$
σ_{k1}	0.85	σ_{k2}	1.0
$\sigma_{\omega 1}$	0.5	$\sigma_{\omega 2}$	0.81

Turbulence for all fluid components is calculated by the same equations. This is physically valid for fluids having a layered flow.

4.3.6 **Cavitation model**

Cavitation has to be taken into account for accurate simulation of flow inside the screw-centrifugal stage. Different modeling concepts, embodying qualitatively similar source terms with alternate numerical techniques, have been proposed by various researches (Kubota, 1992), (Merkle, 1998), (Kunz, 2000), (Singhal, 2002), (Senocak, 2003). Although all considered models provide qualitatively comparable wall pressure distributions in agreement with the experimental data, quantitative differences are observed in the closure region of the cavity, due to different compressibility characteristics of each cavitation model.

In this study, modeling concept proposed in (Singhal, 2002) has been used. The pressure in the cavitation cavity is constant and equal to the saturated vapour pressure at the corresponding liquid temperature in the free-stream flow. Functional relationship between kerosene TS-1 vapour pressure and temperature is shown in Figure 4.3.

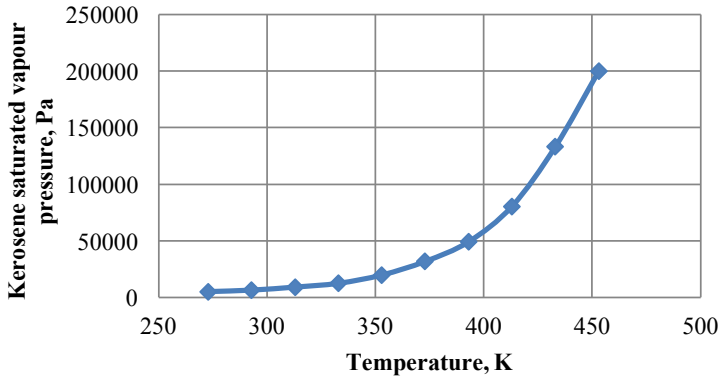

Figure 4.3: Functional relationship between kerosene TS-1 vapor pressure and temperature

A number of CFD models, developed for cavitation estimation, use state equations for a barotropic fluid. Such models are supposed the mixture density to be expressed in terms of local pressure. Such methods of obtaining of spatial heterogeneity of density field is based on including of state equation in Navier-Stokes equation systems. This approach is quite attractive, because it does not require considerable effort for using in any CFD code. This assumption implies thermodynamic equilibrium between phases. In such a manner, the two-phase mixture is assumed to immediately reach thermodynamic equilibrium, when mixture flow conditions are changed. The inconsistency of this approach is shown in paper (Senocak, 2004). This inconsistency stems from the fact that the barotropic density dependence on pressure causes the barocline torque to equal to zero.

Objectively, the formation of vapor cavitation cavity is accompanied by heat consumption, fluid temperature in the evaporation zone is reduced. This reduces the saturated vapor pressure, increases the fluid viscosity and density in comparison with free-stream flow (Ovsyannikov, 1975). Due to the thermodynamic cavitation effect, the value of fluid saturated vapor pressure variation depends directly on the derivative $\frac{dp_V}{dT}$. However, experimental results obtained in papers (Grigoriev, 1985), (Iga, 2009) show that the value of $\frac{dp_V}{dT}$ is so small that the thermodynamic effect for a normal water at normal temperature (288 – 293 K) almost does not change the vapor pressure. This is especially obvious in the case of cryogenic liquids. In paper (Iga, 2009) influence of the thermodynamic effect of the working fluid flow on a set of flat plates was numerically investigated. Water or liquid nitrogen were used as a working fluid. The influence of thermodynamic effect for these fluids was not equal: for the same cavitation number, liquid nitrogen temperature decrease leads to an increase of cavitation cavities volume; water temperature decrease leads to a decrease of cavitation cavities volume.

Functional relationship between kerosene kinematic viscosity changing and its temperature is shown in

Figure 4.4. For moderate temperatures (243 – 413 K), the relationship can be described by the following equation:

$$\nu = 2.6101e^{-0.015T} \tag{4.21}$$

Functional relationship between kerosene density and its temperature is shown in Figure 4.5 and can be described by the equation:

$$\rho = -0.73T + 791.12 \tag{4.22}$$

Provided analysis allowed to make a conclusion that using of cavitation models, based on the barotropic mixture model is competent and proper. Consequently, the average mixture density ρ_m can be represented through its volume phases content r_α:

$$\rho_m = \sum_{\psi} C_\psi \rho_\psi \tag{4.23}$$

The total pressure of the components is derived from the equation:

$$p_{tot} = p_{stat} + \sum_{\psi} \frac{1}{2} C_\psi \rho_\psi \cdot \upsilon_\psi^2 \tag{4.24}$$

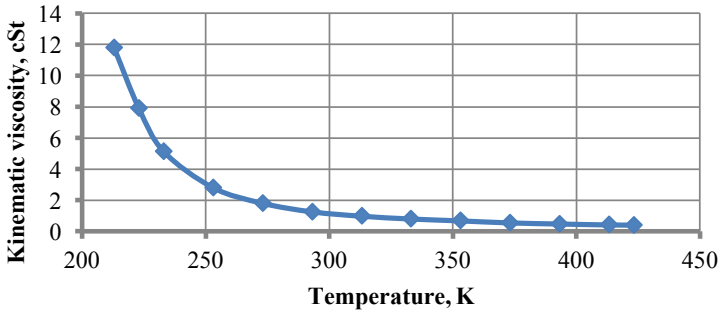

Figure 4.4: Functional relationship between kinematic kerosene TS - 1 viscosity and temperature

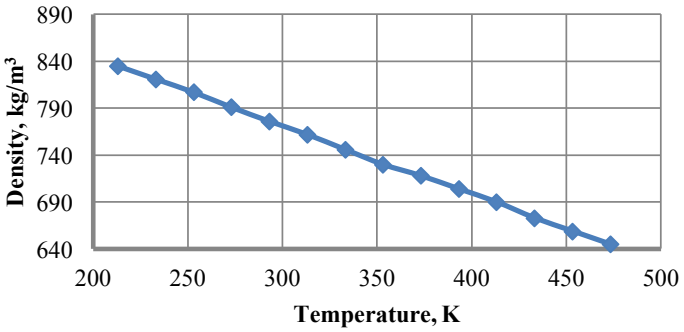

Figure 4.5: Functional relationship between kerosene TS-1 density and temperature

In fact, the final number of processes, taking place during the cavitation and based on the complex of physical processes, is very important. A number of attempts to create cavitation model that takes in account all the complex processes inside rotating machines have been made at present time. The most widespread approach to account non-equilibrium phenomena is the introduction into a mathematical model the source terms that control the interphase mass transfer into the transport equations. Most of these models are based on the Rayleigh-Plesset equation (Plesset, 1949), which describes the growth and collapse of a single bubble in the near-field pressure distribution. The examples of such models are given in papers (Schnerr, 2001), (Gerber, 2002) and (Senocak, 2002). The structure of these models is different, but all of them consider the steam formation

using the conservation equation, which has a source term defined by the Rayleigh-Plesset equation.

The model used in this dissertation is also based on the Rayleigh-Plesset equation. The Rayleigh-Plesset equation describes the dynamics of a vapor bubble in a fluid and has the following form:

$$r_B \frac{d^2 r_B}{dt^2} + \frac{3}{2}\left(\frac{dr_B}{dt}\right)^2 + \frac{2b}{r_B} = \frac{p_v\text{-}p}{\rho_m}, \tag{4.25}$$

where initial bubble radius is set to R_B=10^{-6} m.

The second-order term and surface tension coefficient in the equation (4.25) are often neglected during cavitation simulation. Then, the equation (4.25) becomes:

$$\frac{dr_B}{dt} = \sqrt{\frac{2}{3}\frac{p_v\text{-}p}{\rho_m}} \tag{4.26}$$

Mass variation of a single bubble is calculated from the expression:

$$\frac{dm_B}{dt} = 4\pi r_B^2 \rho_v \sqrt{\frac{2}{3}\frac{p_v\text{-}p}{\rho_V}} \tag{4.27}$$

If there are several bubbles N_B per unit volume, then the volume vapor ratio is expressed by the equation:

$$\mathrm{r}_v = A_B \cdot Num_B = \frac{4}{3} \cdot \pi r_B^2 \cdot Num_B \tag{4.28}$$

The partial gas pressure inside the bubble is assumed to obey the polytropic law. The effective viscosity is taken as a multiple of the dynamic viscosities to account for damping mechanisms in the form of viscous dissipation (Brennen, 2002).

After that, the total value of mass transfer between phases per unit volume is expressed as follows:

$$\dot{S}_{lv} = \begin{cases} W_{VAP} \cdot \dfrac{3 \cdot r_{NUC} \cdot (1 - r_V)\rho_V}{r_B} \cdot \sqrt{\dfrac{2}{3}\dfrac{p_V\text{-}p}{\rho_K}}, & p < p_V \\ W_{COND} \cdot \dfrac{3 \cdot r_V \cdot \rho_V}{r_B} \cdot \sqrt{\dfrac{2}{3}\dfrac{p_V\text{-}p}{\rho_K}}, & p > p_V \end{cases} \tag{4.29}$$

where W is the empirical tuning coefficient. Describing the vaporization processes

W_{vap} = 47, in the case of condensation processes - W_{cond} = 0.088; r_{NUC} is a volume ratio of evaporation center, $r_{NUC} = 5 \cdot 10^{-4}$

This model is good enough for both vapor condensation description and vaporization processes. According to this model, cavitation bubbles are not in contact with each other. This assumption is physically valid only at early stages of cavitation. Evaporation center density should decrease in accordance with the volume vapor fraction increase.

In general, the surface tension forces prevent the occurrence of cavitation. And in the case of cavitation these forces conduce to the rapid cavitation elimination. The influence of the surface tension on the growth rate of spherical cavitation bubble in viscous fluid is shown in Figure 4.6 (Chebayevskiy, 1973).
Fractional bubble radius, r, in Figure 4.6, can be obtained by means of the equation:

$$r = \frac{r_B}{r_0} \tag{4.30}$$

Dimensionless temporal factor, t_{dl}, should be found as follows:

$$t_{dl} = \frac{t}{R_0}\sqrt{\frac{p_V - p_K}{\rho}} \tag{4.31}$$

Dimensionless fluid viscosity, $\bar{\nu}$:

$$\bar{\nu} = \frac{4\mu}{r_0 \cdot \sqrt{\rho \cdot (p_K - p_V)}} \tag{4.32}$$

Dimensionless parameter, D_n:

$$D_n = \frac{\sigma}{r_0 \cdot (p_K - p_V)} \tag{4.33}$$

In paper (Chebayevskiy, 1973) the experimental results of surface tension quantity influence in the weight loss of a wall material is shown. It is apparent that the role of the surface tension is quite significant. However, such a strong influence only appears when the cavitation bubbles are small (less than 10^{-7}…10^{-6} m). Their size in their turn depends on cavitation zone size. Therefore, it is necessary to set the surface tension constant to properly describe the gas bubble diameter growth. For kerosene, this value is equal to 0.0263257 N/m.

The coupling of the Rayleigh-Plesset dynamics with the Navier-Stokes equations is achieved by using the Euler-Euler approach. Volume fraction is calculated to obtain the

main flow density distribution, which is then used to reiterate the continuity and momentum equations of the main flow. After the iteration, the aggressiveness of all collapses (including the collapses of the bubble fragments) is evaluated along the streamlines nearest to the solid surface.

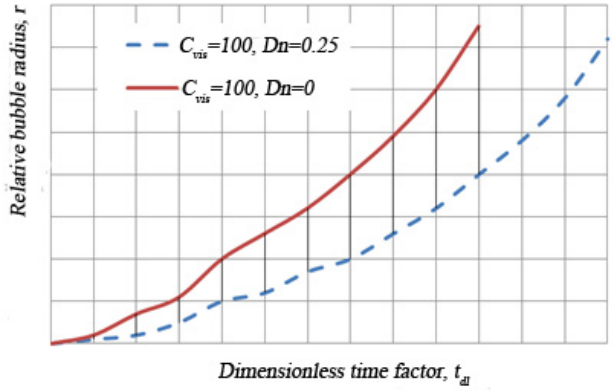

Figure 4.6: The surface tension coefficient influence on the growth rate of a spherical cavitation bubble in a viscous fluid

4.3.7 **Computational grid**

Numerical diffusion is extremely important for an accurate simulation of unsteady turbulent flow inside the pump. It should pay special attention to the quality of the grid models to adequately describe the flow in the computational domain. Artificial smearing of gradients would produce computational errors in estimation of pressure and velocity fields.

Several types of meshes are used for building grid models: structured, unstructured, and the combined grids. Using structured hexahedral mesh gives high solution accuracy within relative short space of time required for calculation. However, their generation can be quite time consuming compared to the process of generation of unstructured grids. Unstructured grids do not always reduce the solution accuracy, but their calculation takes longer than that for the calculation of a structured mesh. Using of combined grids for a calculation model allows to combine the advantages of both types of grids. In this case, a calculation model consists of both structured and unstructured grids.

Recommendations for grid model generation of kinetic pumps computational domain are:

1. It is necessary that the grid lines are perpendicular to the solid boundaries of the model. Angles elements have to lie in the range from 20^0 to 160^0. Note that for angles of less than 40^0 are significantly reduced both the solution accuracy and its convergence;
2. Cells with a negative volume are not allowed;

3. The best option - the grid lines are parallel to the supposed direction of flow;
4. The grid cell size change should be gradual. The optimum area ratio of neighboring cells is the range of 0.75 ... 1.5. Particular attention should be paid to this point in locations where there is a high gradient of flow velocities (leading and trailing blades edges; in clearances and next to the faces, etc.)

Block-structured meshes were built for inlet supply line (Figure 4.7), radial edges input area (Figure 4.9) as well as for the screw area (Figure 4.10). Unstructured tetra and hexa meshes with prismatic layers were used for drain channels (Figure 4.8); centrifugal wheel (Figure 4.11); volute (Figure 4.12) and the journal-and-thrust bearing (Figure 4.13). The computational grids were developed in ANSYS ICEM CFD and AUTOGRID 5 commercial software.

The radial clearance between the shaft full diameter and the bearing seat area, as well as the axial clearance between shaft and bearing ends are set to $5 \cdot 10^{-4}$m because of the ICEM CFD software restriction in which the bearing grid model was designed. Increased clearances in comparison with their nominal values are less significant for cavitation development.

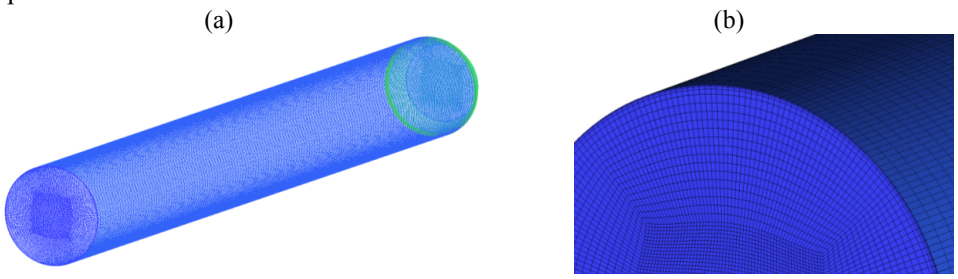

Figure 4.7: Inlet pipe grid model of the. Number of elements is 1 404 259:
a -grid model configuration; b – enlarged view of the pipe line inlet area

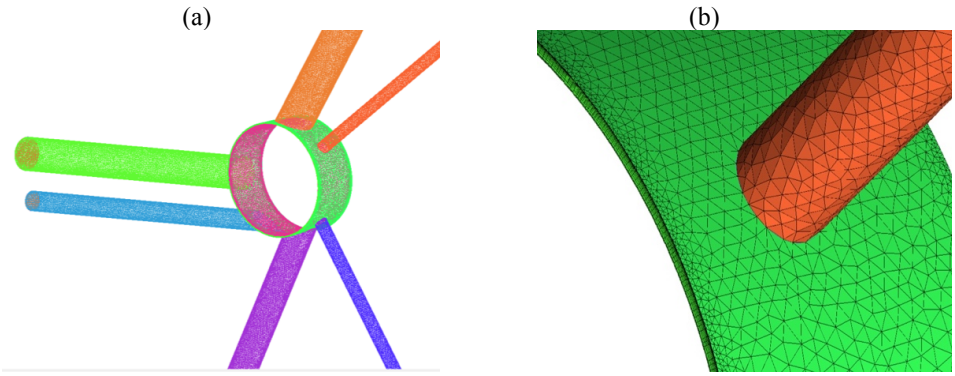

Figure 4.8: Drain channels grid model of. Number of elements is 1253808:
a - grid model configuration; b - enlarged view of near-wall area

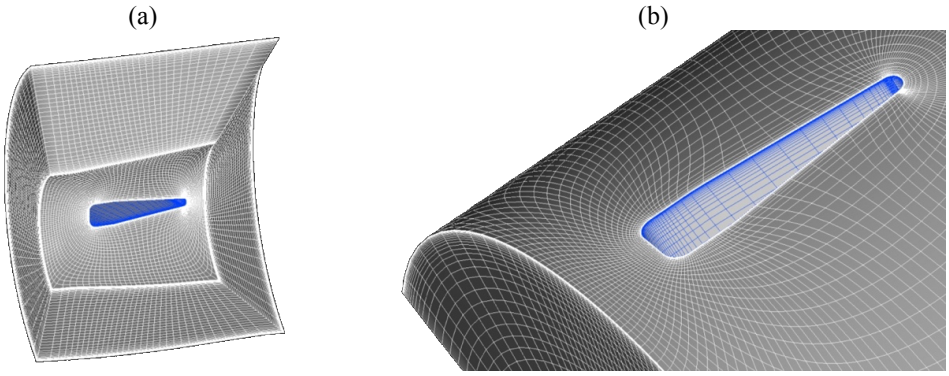

Figure 4.9: Radical edges grid model of. Number of elements is 860160:
a - grid model configuration; b - enlarged view of radical edge area

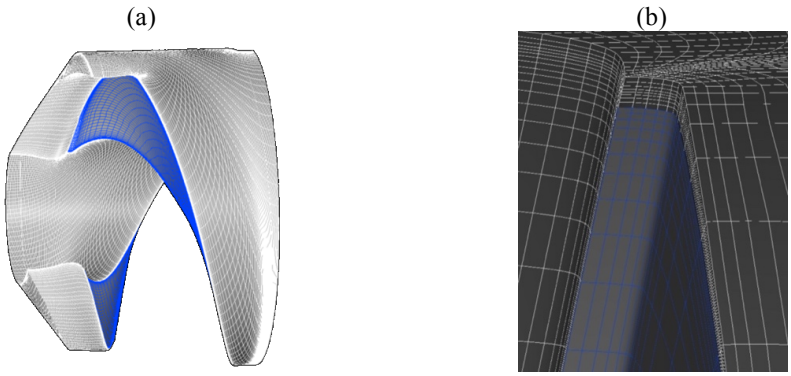

Figure 4.10: The screw grid model. Number of elements is 929466:
a - grid model configuration; b - enlarged view of pipe line inlet area

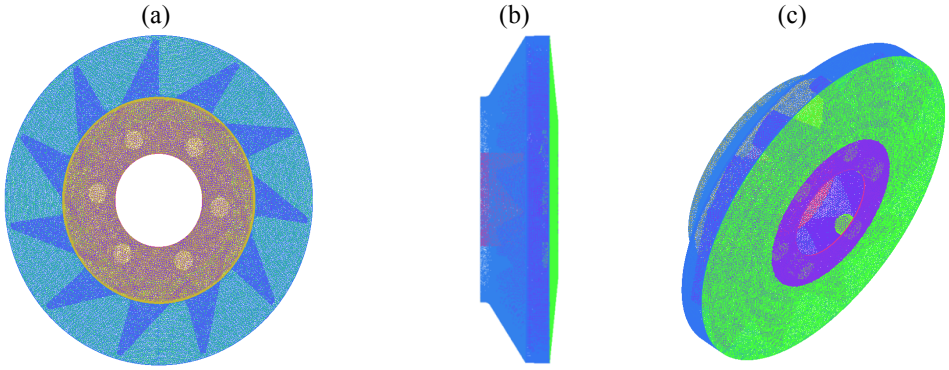

Figure 4.11: Centrifugal wheel grid model of the. Number of elements is 3115676

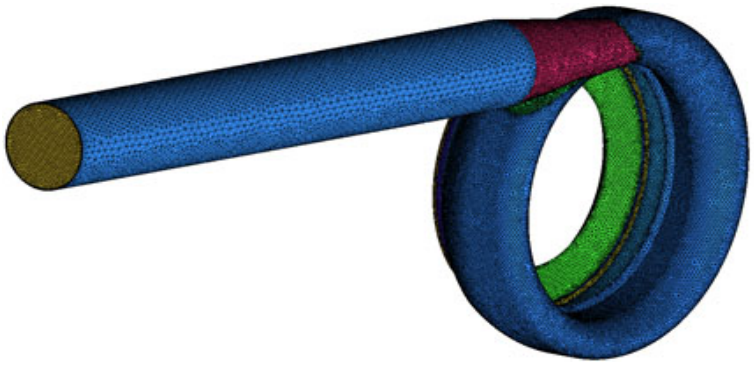

Figure 4.12: Volute grid model. Number of elements is 1881808

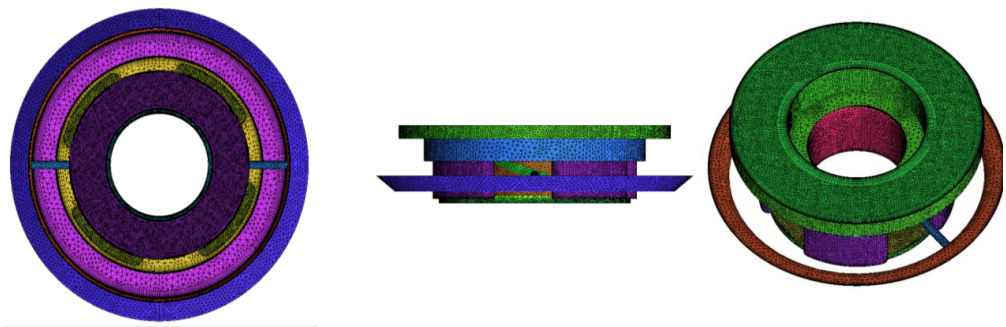

Figure 4.13: Different views of the journal-and-thrust bearing grid model of the. Number of elements is 3115676

The near-wall layers were designed to model the interface at the boundary of solid and fluid bodies (prismatic grid was used in unstructured grids). The first cell thickness was calculated as follows:

1. Reynolds number definition

$$Re = \frac{\rho \cdot \upsilon \cdot d}{\mu}, \tag{4.34}$$

where d is a characteristic cross-section size in different sections of the pump flow channel.

2. Definition of the internal friction coefficient at the boundary layer

$$C_f = \frac{0.078}{Re^{1/4}} \tag{4.35}$$

3. Tangent stress definition on the faces

$$\tau_w = \frac{1}{2} C_f \rho \cdot \upsilon^2 \tag{4.36}$$

4. Definition of the velocity tangent to a face

$$\upsilon_\tau = \sqrt{\frac{\tau_w}{\rho}} \tag{4.37}$$

The first layer thickness y_p is defined by

$$y_p = \frac{y_p^+ \nu}{\upsilon_\tau} \tag{4.38}$$

The first layer thickness based on required y^+ value.

4.3.8 **Model of collapse aggressiveness**

The model of bubble collapse used in this paper is based on the model described in (Zima, 2012). By neglecting liquid surface tension, viscosity and compressibility the work done by the pressure inside the bubble p_B against the ambient liquid pressure p_K to expand the bubble from the minimum (or initial) radius $r_{B\min}$ to the maximum radius r_{Bmax} can be expressed by:

$$W = \int_{rB\,min}^{rB\,max} 4\pi r^2 (p_K - p_B) dr \tag{4.39}$$

The energy, dissipated during the *i*-th collapse of a bubble, can be then estimated by subtracting the values of W for two successive maximums of the bubble radius. The two pressures p_K and p_B and the radius of the bubble, r, are determined from the numerical solution of the turbulent flow. To estimate the energy that is dissipated during the first collapse, the work of expansion from the initial radius r_{B0} (= r_{min1}) to the first maximum r_{Bmax1} and the work of expansion from the first collapse radius r_{Bmin2} to the second maximum r_{Bmax2} are subtracted. The energy, dissipated during the *i*-th collapse is then given by:

$$E_{ii+1} = W\Big\|_{rB\,mini}^{rB\,maxi} - W\Big\|_{rB\,mini+1}^{rB\,maxi+1} \tag{4.40}$$

A part of this energy, denoted as an E_{EP}, is an erosive potential defined by:

$$E_{EP} = 0.5 E_{ii+1} \tag{4.41}$$

The values of E_{EP} are calculated for each bubble collapse, summed up for all bubbles along each streamline and expressed as the power per unit area (or E_{EP} per unit area and time, based on the local flow velocity).

4.3.9 Model of rotor-stator interaction

Interaction of different domains is made on the surfaces marked in the Figure 4.14. The model «General Connecting» provided by ANSYS CFX was used for domains interaction without averaging at the domain boundaries. The model «Frozen Rotor» was used for stationary calculations for the interaction of static and dynamic domains. «Transient Rotor Stator» model was used during transient calculations.

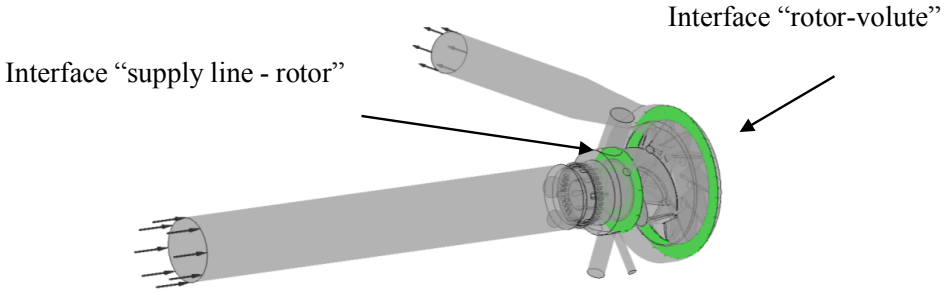

Figure 4.14: Surfaces used for interface coincidence

The numerical calculations were carried out with a multiple reference frames, whereby the rotor flow field is solved in a rotating frame and the stator is in a fixed one.

During the numerical simulations, the sample time interval was chosen based on conditions for Courant number providing equal to unity:

$$Cur = \frac{\upsilon \Delta t}{dx} \tag{4.42}$$

4.3.10 Discretization

The analytical solution of the Navier-Stokes equations exists only for the simplest models of fluid flow under ideal conditions. An algebraic approximation can be used to describe real flows, which can be solved using CFD codes. At the present time, there are several numerical solutions that are used in CFD codes. The most common is the method of finite volumes. Therefore, the conservation equations described above are discretized using the finite volume method. ANSYS CFX uses a control volume technique to convert the governing equations into algebraic equations. The control volume technique is the integration of the governing equations in each control volume, yielding discrete equations which conserve each quantity on a control-volume basis.

The basic equations described above are integrated throughout. The volume integral is discretized inside of each element sector. The values of the corresponding parameters on the surfaces that limit the given volume can be derived from the Gauss Theorem (stating that the outward flux of a vector field through a closed surface is equal to the volume integral of the divergence over the region inside the surface). The surface integral is discretized at the integration points which situated at each segment surface center (Figure 4.15). Thus, the volume integrals determine variable source or increment while the surface integrals determine direction of the flow. For example, the continuity equation for the control volume has a discrete analog as follows:

$$\frac{V}{\delta t}\left(\left(\rho_\psi r_\psi\right)^{n+1}-\left(\rho_\psi r_\psi\right)^{n}\right)+\sum_{ip}\left(\rho_\psi u^i s^i\right)_{ip}^{n+1}\left(r_{\psi,ip}\right)^{n+1}=0 \tag{4.43}$$

The phase momentum equations sampling can be in the form of the equation of velocity field propagation for phase:

$$\begin{aligned}&\frac{V}{\delta t}\left(\left(\rho_\psi u^i\right)^{n+1}-\left(\rho_\psi u^i\right)^{n}\right)+\sum_{ip}\left(\rho_\psi u^j s^j\right)^{n}\left(u^i\right)^{n+1}=\\&=-\sum_{ip}P_{ip}^{n+1}s^i+\rho_\psi^{n+1}g^iV+\sum_{ip}\left(\left(\tau^{ij}\right)^{n+1}s^j\right)_{ip}\end{aligned} \tag{4.44}$$

This method allows to discretize a space domain using a grid. A grid (Figure 4.15) is used for plotting of finite elements. These elements in turn are used for calculating the above variables such as mass, momentum, energy, etc., because all the original variables and fluid properties are in the nodes (grid points). In general, the grid can comprise of tetrahedrons, prisms, pyramids and hexahedral elements. A control volume is formed by the average lines between mesh nodes. The control element is created around each nodal point, shown in Figure 4.15. Integration point is the point at which the flow sampling is made. The values of pressure and velocity gradients calculated at the integration points are obtained from the nodal values using the finite element shape function. The exceptions are the variables responsible for advection. These variables are obtained using the upwind-based sampling.

The finite element shape function for *i*-th node describes the variable φ change using the following expression:

$$\varphi=\sum_{i=1}^{l_{node}}l_i\varphi_i \tag{4.45}$$

$$\sum_{i=1}^{l_{node}}l_i=1 \tag{4.46}$$

The shape function used by ANSYS CFX is linear in parametric coordinates (the coordinates are the integration points and the normal vector to a surface).

All flow variables were interpolated by high-resolution scheme for all grid cells.

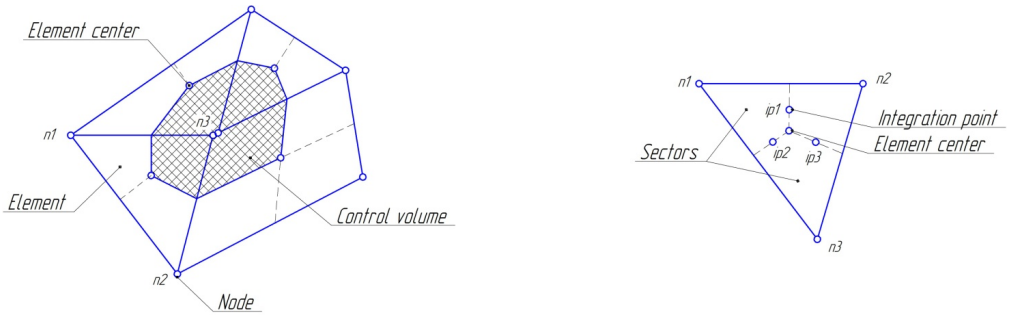

Figure 4.15: Calculation cells

4.3.11 **Convergence**

Crude initial conditions for mean and pulsating values can lead to inaccurate solution. Solution is started from the inlet boundary condition. First order discretization yields better convergence than the second-order scheme. At that, it leads to less accurate results. Thus, second-order discretization scheme was used in this study.

The time step of the unsteady calculations is related to the rotational speed of the rotor and is chosen in such a way that one complete rotor revolution is performed after each 180 time steps.

The chosen time step is small enough to get the necessary time resolution. Twenty sub-iterations were set up per time for the “flattering” of residuals. Certain underrelaxation factors were increased to values higher than the default in order to promote residual reduction. Residual RMS values are typically three orders of magnitude each time step, with the maximum RMS value at the end of a time step being of order 10^{-6}.

4.3.12 **Linearization**

The linear equations system is solved in ANSYS CFX using the Algebraic Coupled Multigrid method in each cell. This method was developed by Raw (Raw, 1996). This approach uses an implicit scheme to solve the linearized equations system. At that, the solution depends linearly on computational grid volume.

During the solution of the described equations system, the solver ANSYS CFX produces at each time step:

1. Coefficients generation. The nonlinear equations are linearized and grouped into a matrix.

2. The equations solution. For providing the convergence rate the initial grid is split into the several coarser grids.
3. A single variable field is solved by considering all cells at once. Then the method continues to solve for the next variable field again by considering all cells at once, and so on.

4.4 Verification of developed simulation model

Verification should be performed to test the developed approach. Numerical diffusion cannot completely be avoided although every reasonable attempt to avoid it was made.

The inlet and outlet grid topology, shape, and size matched the real pump CFD cases exactly. In steady-state mode there were no moving parts in implicit form. Besides the fact that the test case was run in steady-state mode, all other solver settings were exactly the same as those discussed in the previous sections.

Testing and verification of the developed numerical model are based on comparison of energy and cavitation characteristics of the screw-centrifugal stage obtained by calculation and experimental ways. Ten operating regimes were selected to obtain the screw-centrifugal stage energy performance and to identify the axial load trends on the rotor and the bearing (Table 4.4).

Table 4.4: Operating conditions for energy characteristic rating.

Speed of rotation, min^{-1}	Regime number	Flow rate, m^3/s	Total pressure at the pump inlet, Pa
4000; 5000; 6000; 7000; 8000; 8200	1	0.2184	202670
	2	2.1684	202852
	3	4.3368	203053
	4	6.4974	203255
	5	8.6658	203456
	6	10.8342	203658
	7	13.0026	203860
	8	15.1632	204061
	9	17.3316	204263
	10	19.5	204465

Boundary conditions for the stationary calculations are selected based on the actual operating conditions of air pump agregate. To select the most appropriate boundary conditions for high accuracy of calculation as well as a stable solution to a series of numerical experiments of one of the modes of operation of the pump unit were conducted (Table 4.5).

The most appropriate boundary conditions are the conditions, where the total pressure is given at the pump inlet, and at the pump outlet –flow rate. The boundary condition types

at the inlet and outlet are «inlet» and «outlet» respectively. All stream velocity components are equal to zero on the wall faces (no-slip condition of a power fluid); rate of rotation is given for the rotating parts of a screw-centrifugal stage; along with the total pressure turbulence intensity is also given at the inlet of the supply and drain pipelines. It is expected that the absolute velocity vectors are along the pipe lines and perpendicular to the mesh of corresponding surfaces. Mass flow rate was given at the outlet. Finding the head-capacity curve of a screw-centrifugal stage using a numerical method based on experimental conditions, total pressure at the pump inlet is defined as equal under all conditions. In general, the variables given at the pump inlet and outlet may present time functions.

Comparison of experimental head-capasity curve and calculated characteristics obtained by using different turbulence variants are shown in Figure 4.17 and Figure 4.18. The comparison shows that the use of SST model gives more accurate results. There is the acceptable convergence of both numerical simulation results and experimental results. Computation error reaches not more than 4%.

The optical spacer (Figure 4.19) was specially designed to observe the fluid flow in the screw-centrifugal pump. It was developed according to preservation of the cylindricity of the flow channel surface to avoid vortex formation and the local hydraulic losses.

To visualize the flow, the laser knife method was used (Zazhigayev, 1978). At that, the stream was illuminated by different light sources: incandescent lamp, stroboscopic flash lamp, and a flat laser beam. Special laser illuminator based on "laser knife" shaper was developed and manufactured to visualize the light-diffusing inclusions that are present in a thin flat layer of kerosene flow. In the capacity of a light source in the "laser knife" was used He-Ne continuous-wave laser LGN-125. The output power of which is 50 mW and operating wavelength 0.63 μm. The beam diameter equals to 0.003 m at the laser output. The flow area that is available for monitoring is limited by the width of a window (equals to 0.028 m). The optical scheme with a light "knife" for illuminating of a thin vertical layer of the considered flow is shown in Figure 4.16. Flat light beam, generated by an optical lens on a laser 1, deviates to the vertical plane by means of a rotary mirror 2, and passing through the upper and lower windows of the spacer 3 illuminates a thin vertical layer of the kerosene flow.

The experimental results of the real-scale flow structure investigation at the screw-centrifugal stage inlet, obtained by both laser and high-speed video visualizations, are in agreement with numerical simulations. The experimental observations and the developed numerical model demonstrate the presence of vortex flows that expand from in the upward flow direction. All the vortex lines are rotated in the same direction as the rotor of the screw-centrifugal stage. A comparison of numerical and experimental results of the flow structures on the same operating regimes (Figure 4.22), proves the efficiency of turbulence model as well as boundary conditions, and also the accuracy of developed grid models of the computational domain.

Table 4.5: Obtained values of mass flow at the inlet and outlet of the screw-centrifugal stage. Errors of screw-centrifugal head calculation

Boundary condition type at the inlet	Parameter	Boundary condition type at the outlet «OUTLET»											
		$P_{stat}^{C.out}$			$P_{tot}^{C.out}$			G_{out}^{C}			υ_{out}^{C}		
		G_{in}^{S}	G_{out}^{C}	e_H	G_{in}^{S}	G_{out}^{C}	e_H	G_{in}^{S}	G_{out}^{C}	e_H	G_{in}^{S}	G_{out}^{C}	e_H
Inlet	Static pressure, $P_{stat}^{S.in}$	0	5313.40	708424	-	-	-	12.92	13.00	-1.68	12.82	12.77	0.87
	Total pressure, $P_{tot}^{S.in}$	8.51	8.46	0.00	-	-	-	13.00	13.00	0.02	12.78	12.77	0.21
	Mass flow, $G^{S.in}$	13.00	12.99	0.17	-	-	-	Fall	Fall	Fall	Fall	Fall	Fall
	Velocity, $\upsilon^{S.in}$	12.67	12.65	0.16	-	-	-	Fall	Fall	Fall	12.66	0.12	1.01
Inlet		Boundary condition type at the outlet «OPENING»											
	Static pressure, $P_{stat}^{S.in}$	9.07	9.10	0.00	8.41	8.41	0.03	-	-	-	12.78	12.77	0.21
	Total pressure, $P_{tot}^{S.in}$	9.35	9.30	0.00	8.25	8.21	0.02	-	-	-	12.78	12.77	0.21
	Mass flow, $G^{S.in}$	13.00	12.99	0.18				-	-	-	13.00	12.99	0.17
	Velocity, $\upsilon^{S.in}$				12.66	12.65	0.15	-	-	-	Fall	Fall	Fall
Opening		Boundary condition type at the outlet «OUTLET»											
	Static pressure, $P_{stat}^{S.in}$	8.25	8.22	0.00	-	-	-	13.02	13.00	0.80	Fall	Fall	Fall
	Total pressure, $P_{tot}^{S.in}$	8.77	8.77	0.00	-	-	-	12.76	13.00	0.94	Fall	Fall	Fall
	Mass flow, $G^{S.in}$	-	-	-	-	-	-	-	-	-	-	-	-
	Velocity, $\upsilon^{S.in}$	12.66	12.65	0.15	-	-	-	12.66	13.00	1.03	Fall	Fall	Fall
Opening		Boundary condition type at the outlet «OPENING»											
	Static pressure, $P_{stat}^{S.in}$	6.81	6.81	0.00	8.48	8.46	0.03	13.08	13.00	0.71	Fall	Fall	Fall
	Total pressure, $P_{tot}^{S.in}$	6.98	6.98	0.00	8.48	8.48	0.02	13.1	13.00	1.02	Fall	Fall	Fall
	Mass flow, $G^{S.in}$	-	-	-	-	-	-	-	-	-	-	-	-
	Velocity, $\upsilon^{S.in}$	12.66	12.65	0.15	12.66	12.65	0.15	12.97	13.00	1.25	12.66	-0.12	1.01

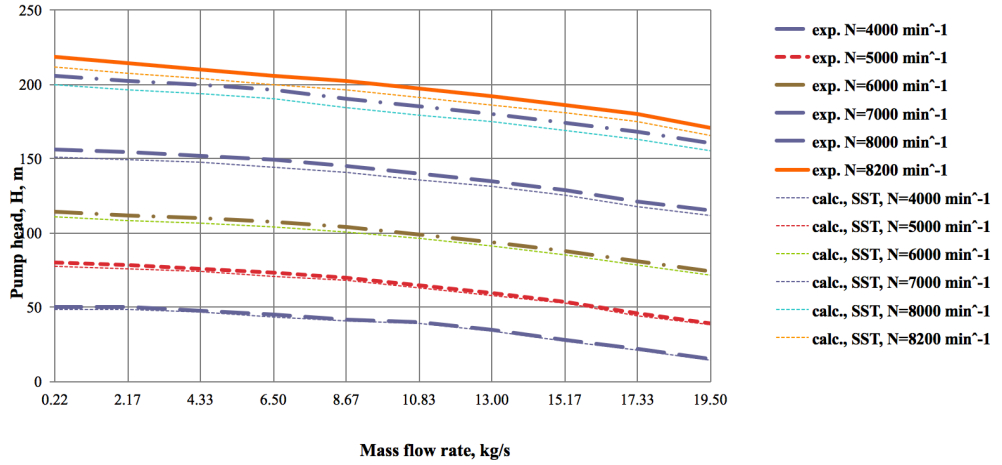

Figure 4.17: Calculated and experimental head-capacity curves of the screw-centrifugal stage of pump ND-25. STT tubulence model

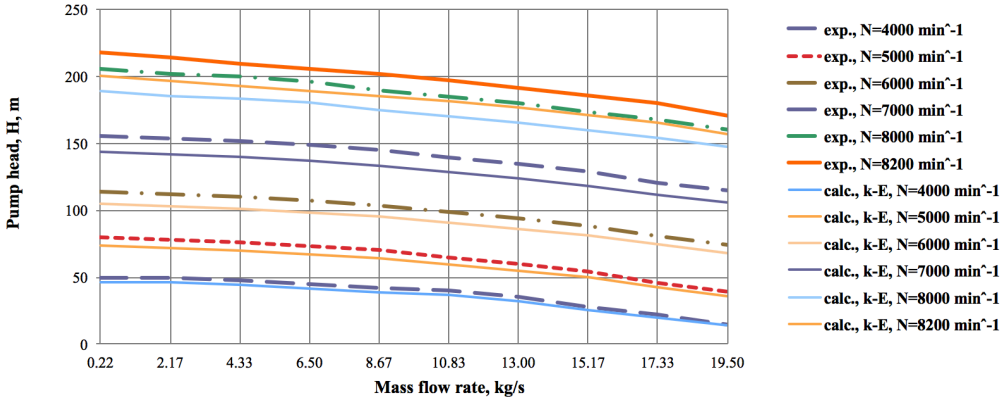

Figure 4.18: Calculated and experimental head-capacity curves of the screw-centrifugal stage of pump ND-32. $k-\varepsilon$ turbulence model

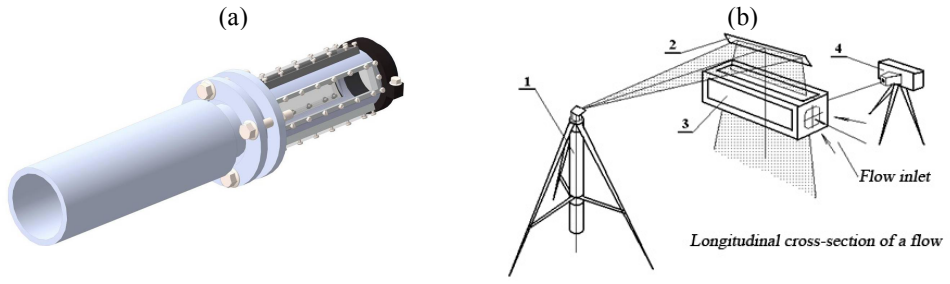

Figure 4.19: 3D-model of the transparent spacer (a) and laser knife layout (b)

Video recording of a flow structure at the pump inlet through the optical spacer was realized using instrumentation for high-speed digital video recording (Figure 4.20):

- high-speed video camera Photron SA-3 with two lenses;
- notebook with software;
- two spotlights to provide the required illumination in the area of interest.

Figure 4.20: Instrumentation for high-speed digital video recording

(a)

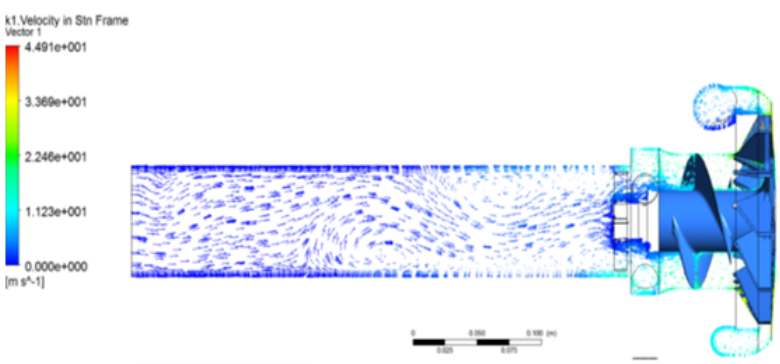

(b)

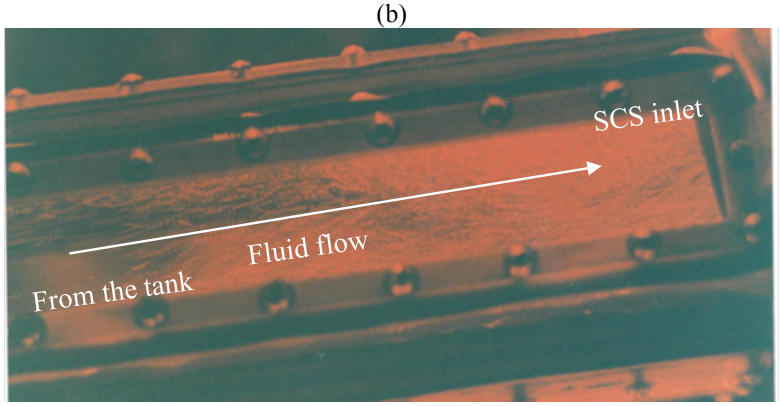

Figure 4.21: Flow structure in the screw-centrifugal stage on the regime G=0.82 kg/s, N=5750 min^{-1}, Pin=0.2 MPa, $Pout$=1.1 MPa:
a is calculated flow structure at cross section; b is a flow structure, obtained by laser knife method (kerosene flows from left to right (to the screw))

Obtained results allowed to conclude that back eddies at the pump entrance are induced by radial movement of the flow separation zone along the screw blade's sucking surface. This movement continues until the contact with the pump case occurs. Then this zone is turned by 90 degrees and further spread over a blade channel forming a source of the back eddies. The fluid, incoming from the source into this channel, divides into two streams, one of which flows to the outlet while the second one flows to the inlet. The latter forms back eddies. The circulation in the undisturbed flow can be described by $\upsilon \cdot r = const$. This results in to increasing of the circumferential stream velocity by approaching the centre of the vortex flow. At that, pressure decreases. Based on the observations, it can be concluded that the centre of the vortex stream flows as a solid body. These results are also confirmed by works (Ershov, 1959) and (Stepanoff, 1960).

(a)

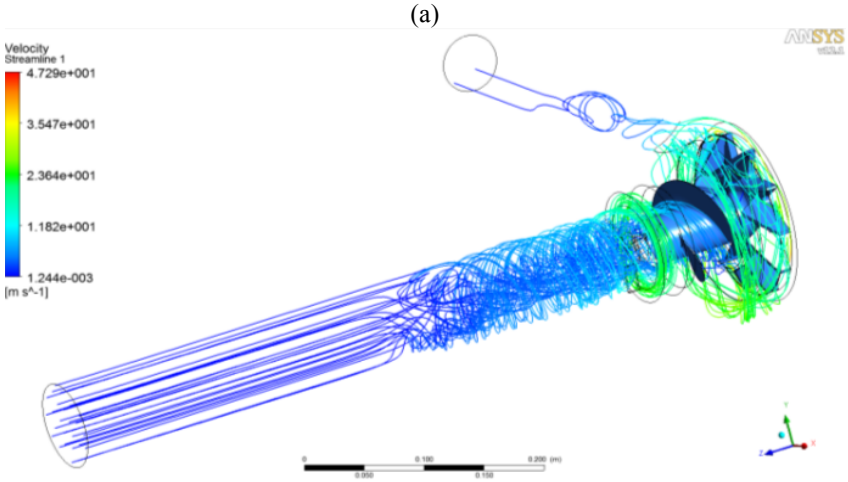

(b)

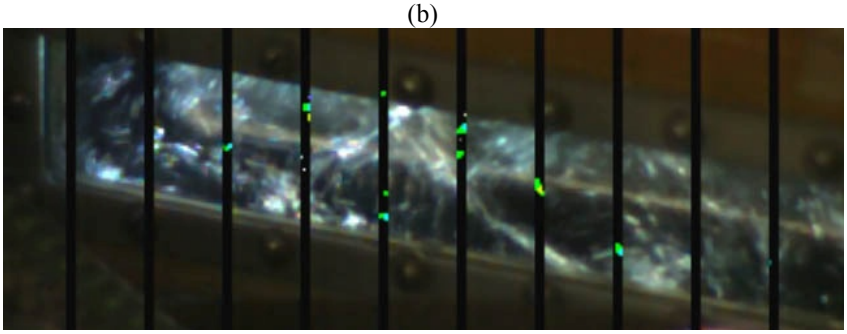

Figure 4.22: Flow structure in the screw-centrifugal stage on the regime G=0.82 kg/s, N=5750 min^{-1}, Pin=0.2 MPa, $Pout$=1.1 MPa.:
a is a calculated three-dimensional flow structure; b is a flow structure, obtained by high-speed video recording (kerosene flows from right to right (to the screw))

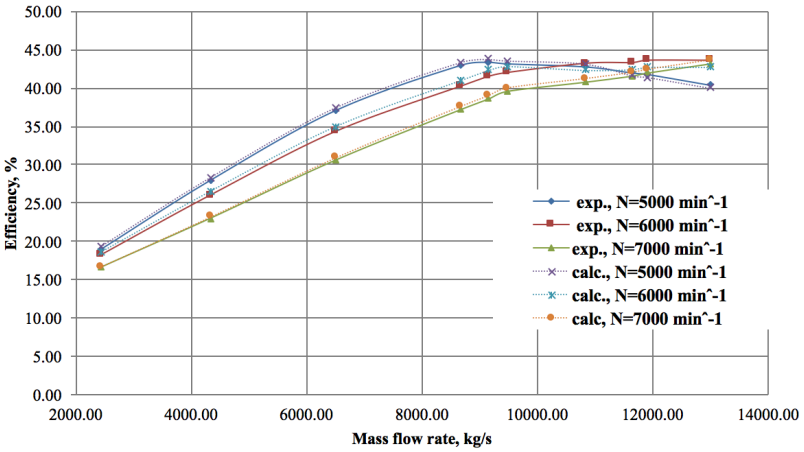

Figure 4.23 depicts the experimental and calculated efficiency characteristics. The comparison of calculated and experimental efficiency characteristics shows that the computation error is no more than 3%. Based on this, the numerical simulation results and their comparison with the experimental data let to draw the conclusion that the proposed mathematical model can accurate and proper predict the energy characteristics of the screw-centrifugal pump.

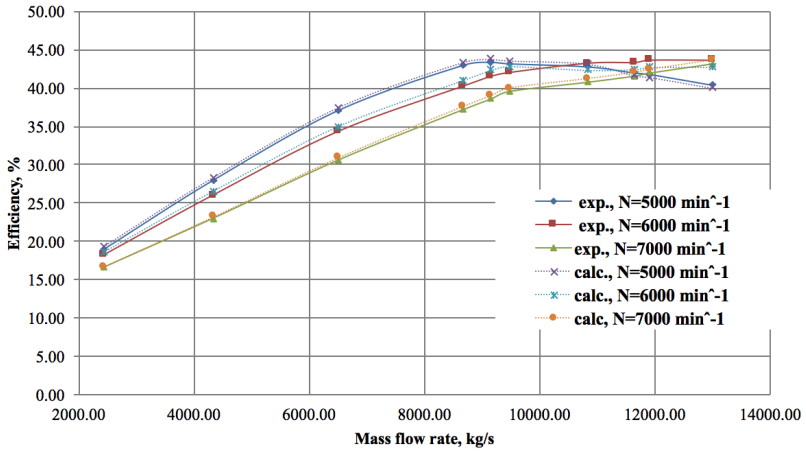

Figure 4.23: Efficiency change of the screw-centrifugal stage

Figure 4.24 illustrates the cavitation characteristics of the screw-centrifugal pump, which were obtained by calculations and experimentally. The comparison shows that the computation error is no more than 3%. In such a manner, the developed model is suitable for cavitation development description in the screw-cintrifugal pump. Cavitation breakdown of the screw-centrifugal pump on the third critical mode occurs when the input pressure is 0.057 MPa.

Developed model was sufficiency assessed on Fisher's ratio test (Zazhigayev, 1978):

$$J = \frac{s^2_{aq}}{s^2_y}, \tag{4.47}$$

where the dispersions of the corresponding variable, s^2_{aq} and s^2_y, can be found as:

$$s^2_{aq} = \frac{1}{n-1} \cdot \sum_{j=1}^{n} \left(\varphi_{Cj} - \overline{\varphi}_p\right)^2 \tag{4.48}$$

$$s^2_y = \frac{1}{n-1} \cdot \sum_{j=1}^{n} \left(\varphi_{Tj} - \overline{\varphi}\right)^2 \tag{4.49}$$

Average values of the calculated and target values can be found as follows:

$$\overline{\varphi}_C = \frac{\sum_{j=1}^{n} \varphi_{Cj}}{n} \tag{4.50}$$

$$\overline{\varphi}_T = \frac{\sum_{j=1}^{n} \varphi_{Tj}}{n} \tag{4.51}$$

Further, Fisher ratio test can be found from the Fisher table of *n-1* degrees of freedom setting the significance level *U* (*U* is typically chosen to be 0.05). If it is greater than calculated above, it can be associated with the experimental results. In the present case, the value of criteria *Ji*=1.25. For the significance level U_i=0.05 and *n*-1=32 J_C=1.91. J_C > *J*, therefore, the developed model is sufficient.

(a)

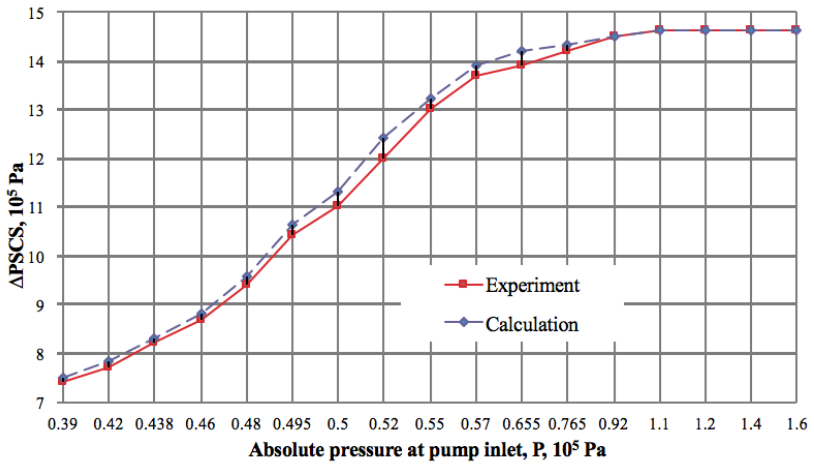

(b)

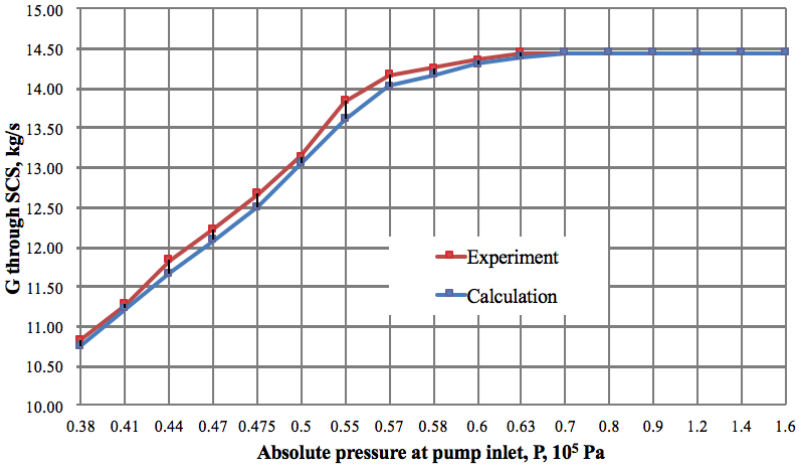

Figure 4.24: Calculated and experimental cavitation characteristics

5 Simulation of Flow Phenomena and Processes in Aircraft Engine Two-stage Pump

5.1 Initial conditions and assumptions

The following initial conditions were set up: at time $t \leq 0$, flow velocity inside the calculation domain is zero, $v = 0$; on casing wall $v = 0$.

For the steady-state calculations the following boundary conditions are assumed: at the inlet of the computational domain the mass flow rate, the turbulence intensity, the eddy length scale and a reference pressure at one grid point are specified. It is assumed, that the absolute velocity vectors at the inlet are perpendicular to the inlet grid surface and point into axial direction. The turbulent intensity was assumed to be 10 %. Furthermore, the eddy length scale was assumed to be 10% of the diameter at the inlet plane. At the outlet for all variables with exception of pressure a zero gradient condition was assumed. Both in the fixed frame and in the rotating frame the solid walls, i.e., the impeller blades, hub and shroud, the casing walls are modelled using a no-slip boundary condition.

For unsteady calculations fixed mass flow rate at the inlet of the computational domain is physically unsuitable for unsteady calculations and in particular for considering the rotor/stator interaction. Therefore, in the present study for unsteady calculations the following boundary conditions are used: instead of a fixed mass flow rate at the inlet the total absolute pressure, and at the outlet the static pressure in a single grid face are specified. The walls and solid surfaces were treated as adiabatic. Thus, there is no thermal exchange within the pump or externally.

Based on the above reasoning, the issue of cavitation flow in the screw-centrifugal stage is solved in a homogeneous formulation in case of stationary calculations. In this case, calculation is isothermal, fluid temperature is 298 K. For unsteady calculations, the variation of flow parameters such as density and viscosity were varied according to the equations 5.22 and 5.21 correspondingly.

All parameter settings, for example the time step and the number of iterations in each time step, have been retained unchanged for all test conditions. At each test condition at first a steady-state calculation is carried out and the result is used to initialize the unsteady calculation at this test point.

The calculating domain with characteristic boundaries is shown in Figure 5.1.

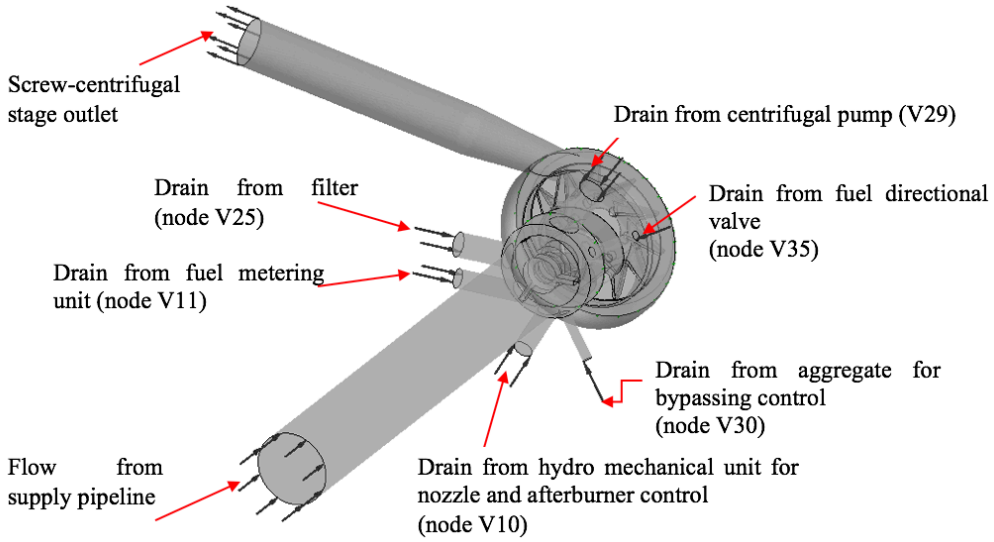

Figure 5.1: Geometrical model of the calculating domain of the screw-centrifugal stage

5.2 Radial and axial force estimation

The most important parameters for loading evaluation of the pump unit are forces, acting on the pump rotor and forces at the bearing. Two force components are considered: the static pressure forces and the dynamic components of the forces. Dynamic component is the working body reactions, occurring in the flow part of the pump unit.

Provided analysis of two-stage pumps ND-25 and ND-32 loading as well as experimental studies showed that the cause of its low reliability is a high level of the axial force fluctuations on the pump rotor. The main forces acting on the rotor stages are pressure forces, acting on the screw and centrifugal wheels, and the force acting on the rotor shank, located in the balance chamber of the pump unit. Thus, static axial force on the rotor is formed by the pressure forces at the screw inlet and outlet, p_{in}^{S} and p_{out}^{S}, at the centrifugal wheel outlet p_{out}^{C} and in the pump balance chamber, p_{ch}^{S}. The pressure in the rotor pocket behind the wheel and at its hub has a significant importance for axial loading of the rotor. This pressure is generated by radial cross-flows from the peripheral wheel part to its hub. Further, the liquid flow is divided into two directions. The first of them is connected to the cross-flow through the wheel discharge holes into the pocket behind the screw. The second flow passes through the holes in the bearing sleeve into the pump balance chamber. The loading schematic of the rotor is shown in Figure 5.2

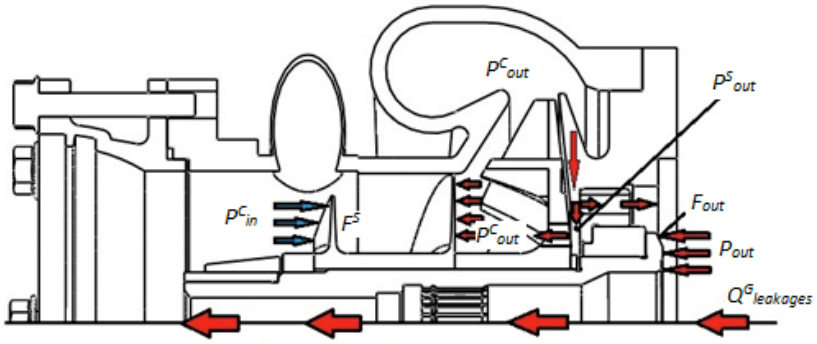

Figure 5.2: The schematic of pressure forces acting on the pump rotor

Figure 5.3 illustrates the calculation data of the axial force change on the rotor of the screw-centrifugal stage in accordance with its operating regime. The total axial force on the rotor is equal to the algebraic sum of the fluid pressure forces that are acting on blade wheel end faces and on the shaft ends. The positive direction of the resultant vector of the axial force is the direction towards the screw-centrifugal stage inlet.

Figure 5.3 - Figure 5.5 illustrate the results of variations of axial and radial forces, acting on the centrifugal wheel and on the screw. This allows to determine how each element affects the total force magnitude. The radial component of the hydrodynamic force emerges in the pump components where there are the radial components of flow velocity and there is no symmetry in the pressure distribution in a circumferential direction. Obtained results shows that axial force is generated mostly by the screw.

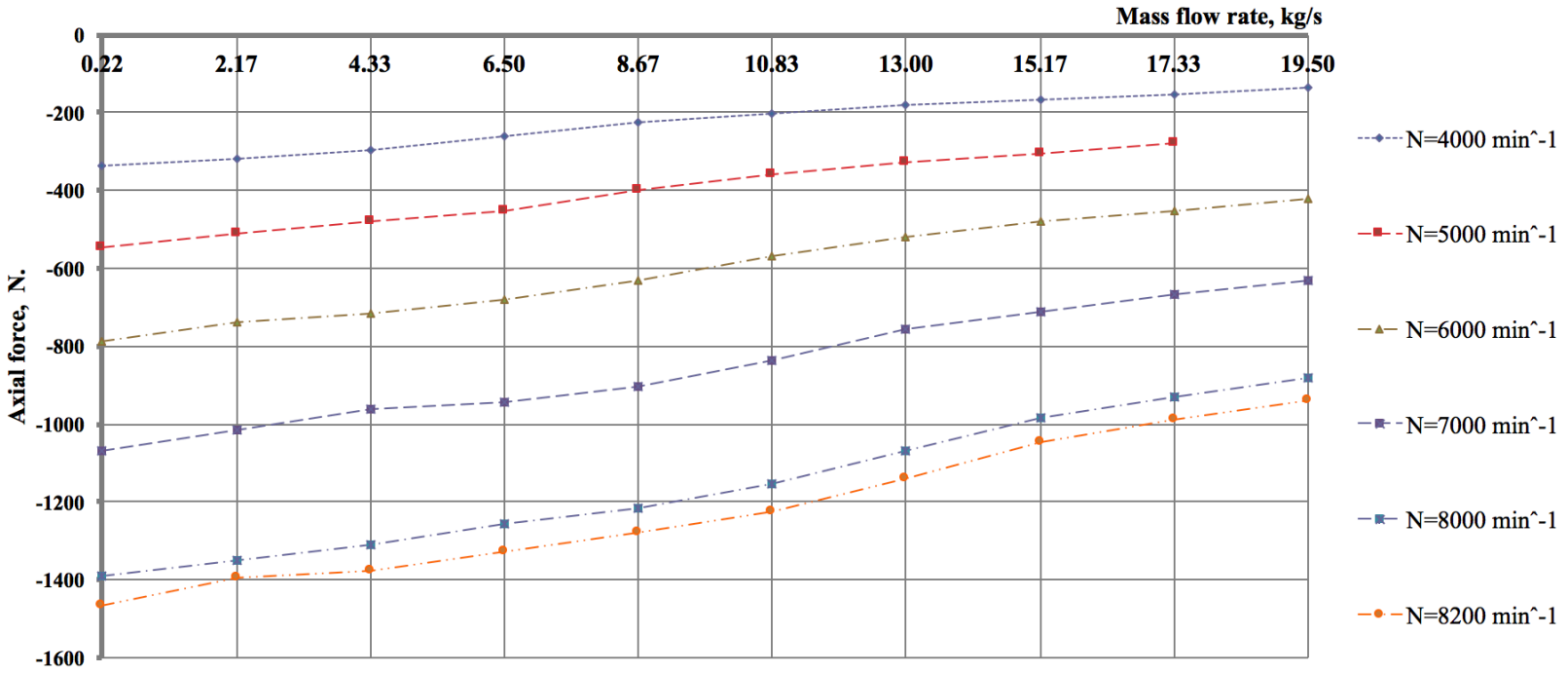

Figure 5.3: The total axial force change on the rotor according to the regime

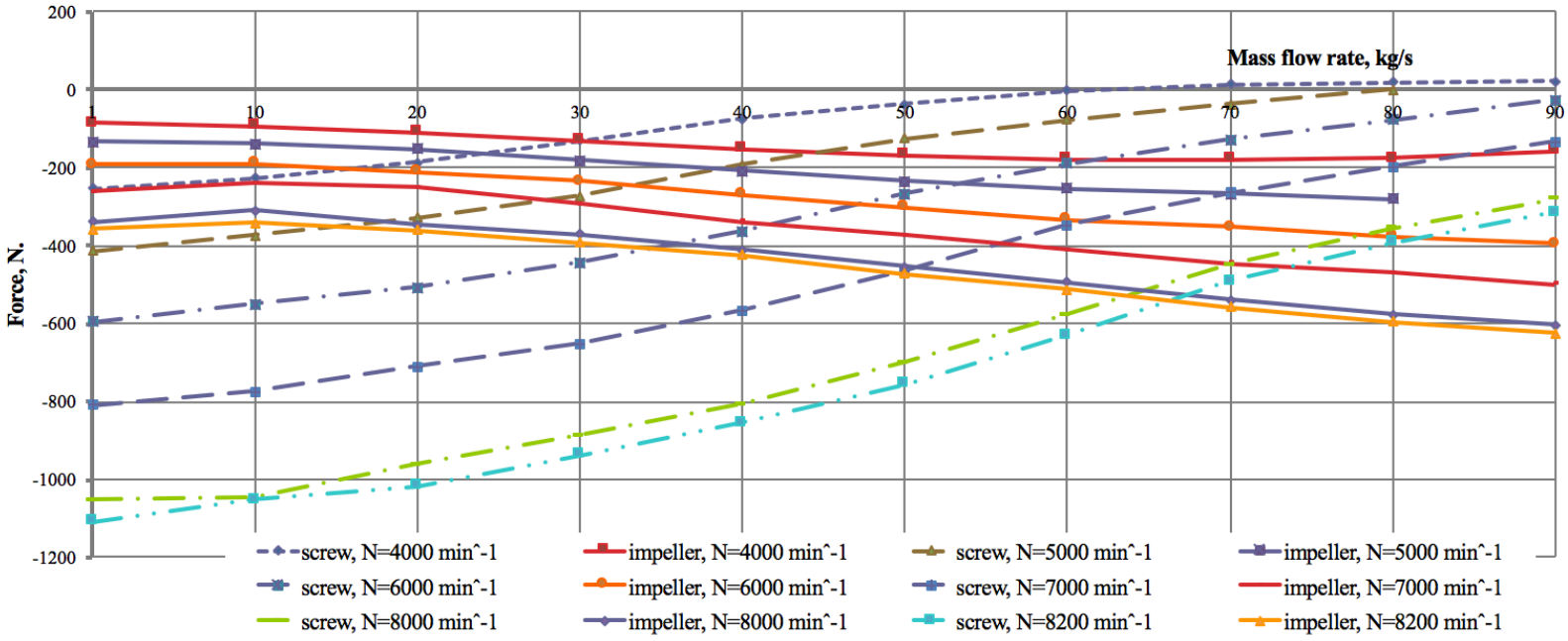

Figure 5.4: The axial force change on the screw and on the centrifugal wheels according to the operating regime

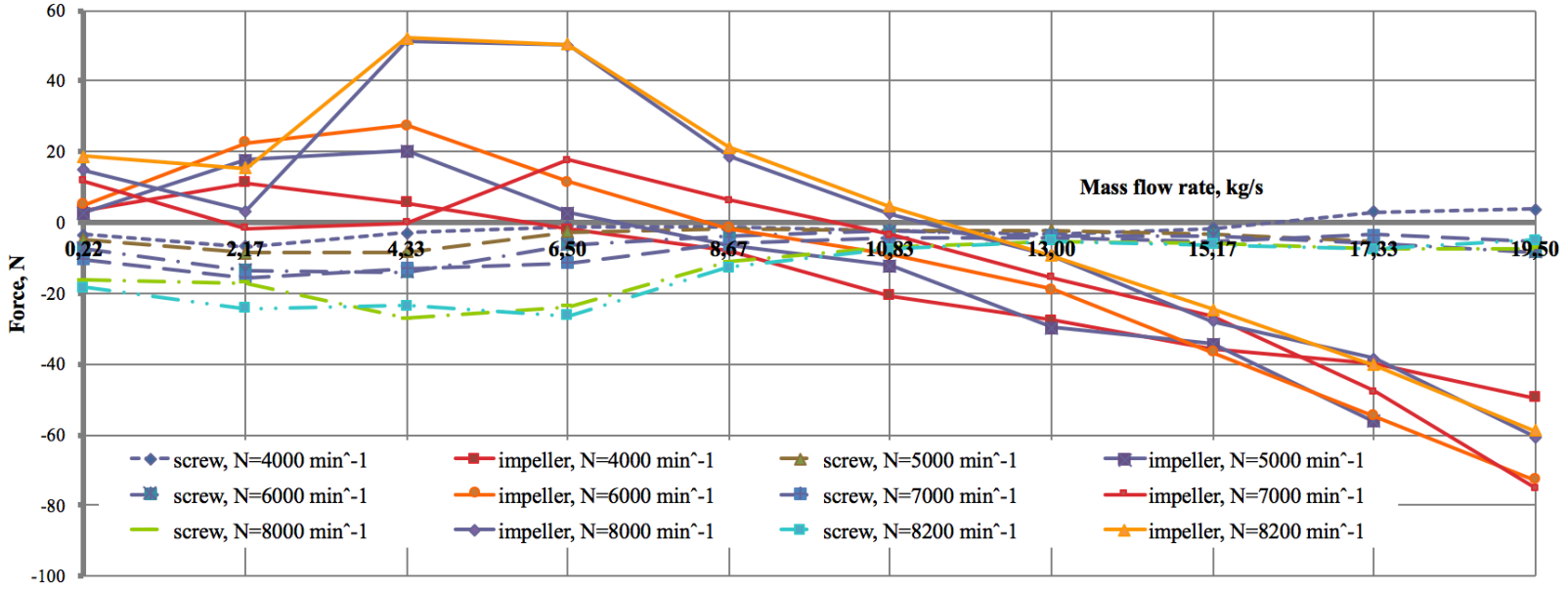

Figure 5.5: The radical force change on the screw and on the centrifugal wheels according to the operating regime

Figure 5.6 illustrates the pressure distribution on the bearing ends on the regimes G = 2.126 kg/s, N = 3500 min^{-1}, and G=6.75 kg/s, N=7500 min^{-1}. The figures depict the irregularity in the pressure distribution. This is especially expressed on the bearing rear face, where there is the pressure difference radially on the bearing reaches 0.1 MPa.

(a)

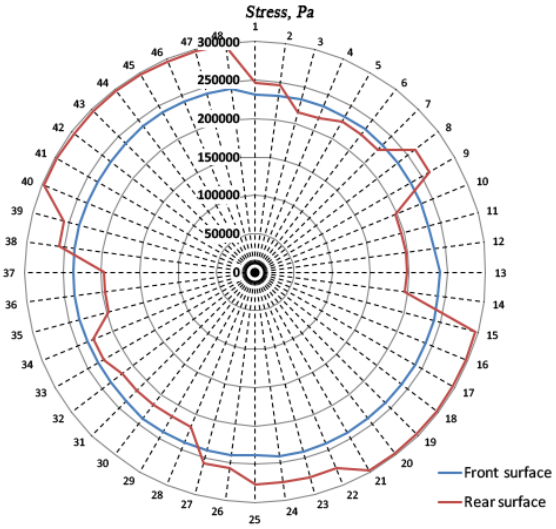

(b)

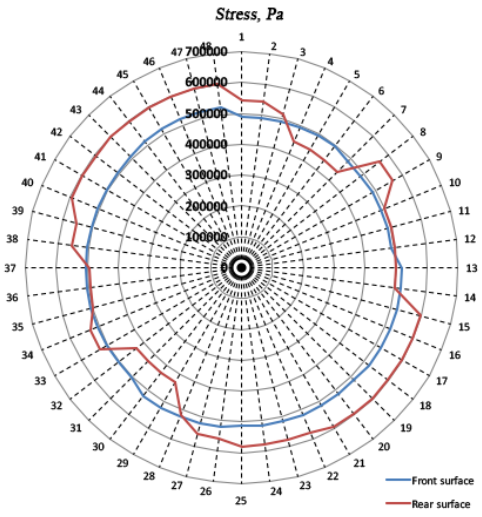

Figure 5.6: Pressure diagram on the bearing ends according to the volume flow rate a - operating regime G=2.126 kg/s, N=3500 min^{-1}; b – operating regime G=6.75 kg/s, N=7500 min^{-1}

5.3 Back vortex flow

As shown in the Chapter 1, the loading of the two-stage pump elements significantly depends on the vortex flow structure inside the pump. There is a number of papers considering the numerical modeling of back vortex currents in cyclone collectors, mixing chambers and other devices (Sharif, 1995), (Hogg, 1989), (Poroseva, 2001). However, there are no studies that describe the flow efflux from tangential drains into a screw-centrifugal stage.

The developed model has allowed to establish a significant influence of the drain pipelines on the back currents formation, resulting in the flow unsteadiness at the screw-centrifugal stage inlet (Figure 5.7). The vortex currents at the screw inlet are in the form of two "vortex cores". This leads to additional instability of vortex structure at the pump inlet. The simulation results allow to determine the boundary between the active and back currents. The results showed that the drain pipelines have a significant influence on the back eddies generation at the screw inlet.

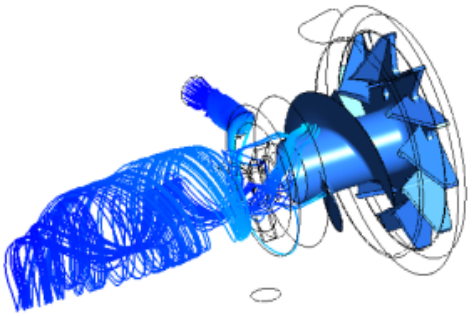

Figure 5.7: Streamlines of flow from drain pipelines $P_{tot}^{S} = 0.2$ MPa, G^{V11}=0.07 kg/s, G^{V10}=0.47 kg/s, $G_{tot}^{C} = 0.82$ kg/s, N=5750 min^{-1}

Specific flows, occurring at operating regimes with mass flow lower than 2.17 kg/s for different geometry of the supply pipeline, are shown in Figure 5.8. The flow analysis shows that the length of the back currents zone can be equal to six diameters of the supply pipe. The strongly twisted working fluid enters the volute. On some regimes, the pump entrance region is not completely filled with active fluid flow moving from the screw entrance to the blades. Part of the periphery section is filled with the back currents moving back from the screw to the inlet. The main flow core on the reduced operating regimes has a strong twist relative to the pipe axis. The operating regime parameter, q, was obtained to be equal 0.44.

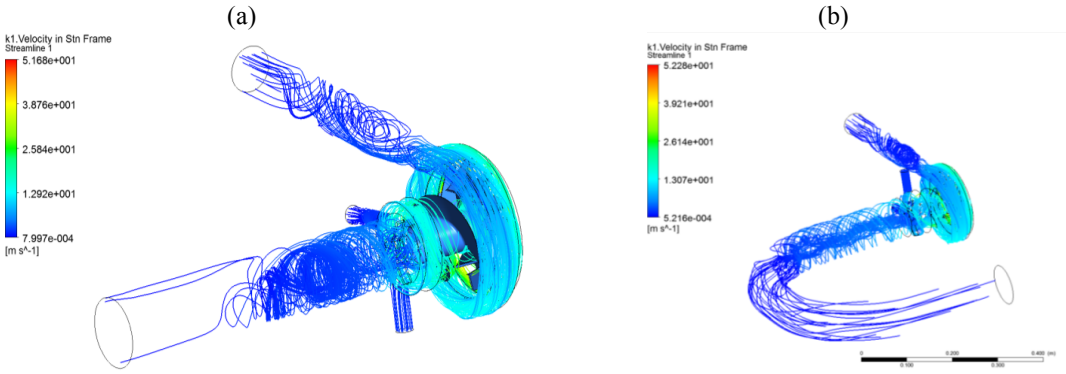

Figure 5.8: Fluid flow structure.
P_{tot}^{S} = 0.2 MPa, G^{V11}=0.07 kg/s, G^{V10}=0.47 kg/s, G_{tot}^{C} = 0.82 kg/s, N=5750 min^{-1}
a- straight-line pump inlet; b - curvilinear pump inlet

The characteristic pressure distribution patterns along the screw blade length on the screw nominal diameter are shown in Figure 5.9 - Figure 5.14. Pressure and suction sides of the blades are shown in Figure 3.8. Conducted results show that back vortices are formed when pressure on the suction side is more than pressure at pressure side of the blade. Obtained results shows that back vortices are generated on different lengths of the screw blade. For the same revolution speeds, increasing of the mass flow rate shifts the zone of back eddies origination to the leading edge. For the same mass flow rates, increasing of revolution speeds shifts the zone to trailing edge. Increasing of revolution speed yields to pressure drop on the suction side of the blade and to simultaneous increasing of pressure on the pressure side.

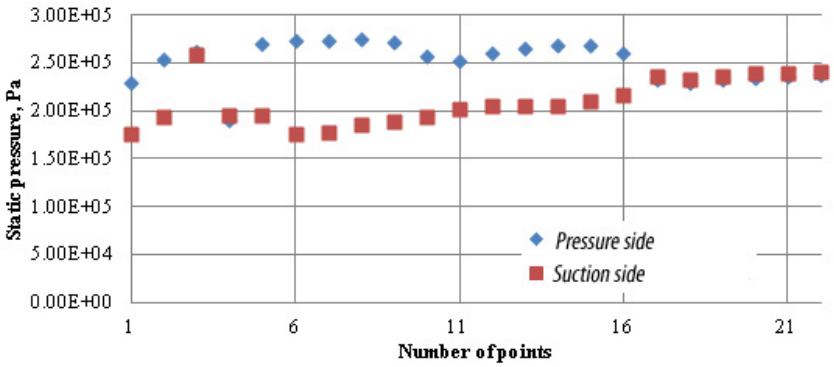

Figure 5.9: Pressure distribution along the length of the screw blade to its nominal diameter on regimes N=4000 min^{-1}, Q=0.22 kg/s

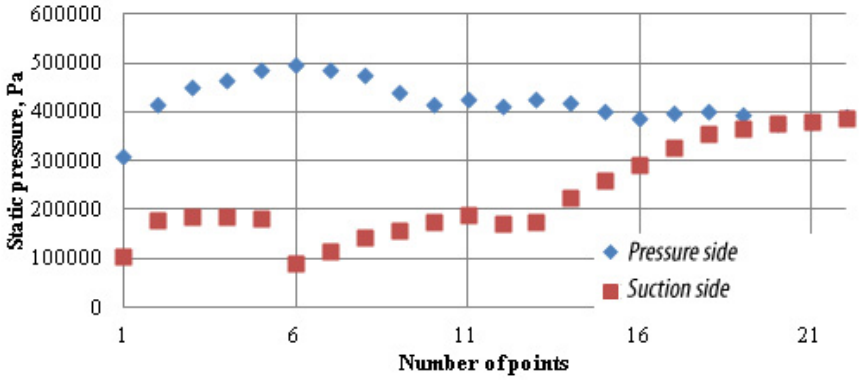

Figure 5.10: Pressure distribution along the length of the screw blade to its nominal diameter on regime N=8000 min^{-1}, Q=0.22 kg/s

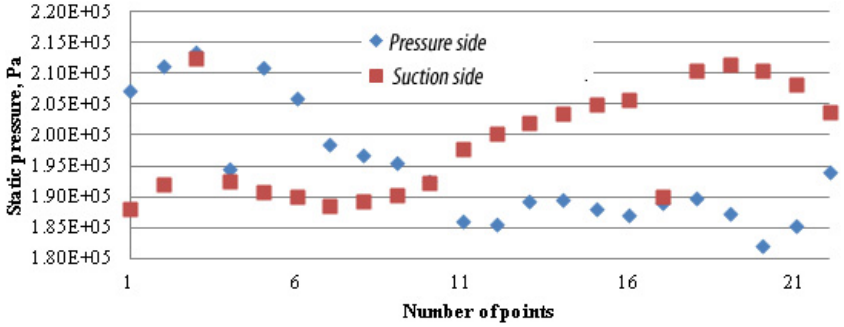

Figure 5.11: Pressure distribution along the length of the screw blade to its nominal diameter on regime N= 4000 min^{-1}, Q=10.83 kg/s

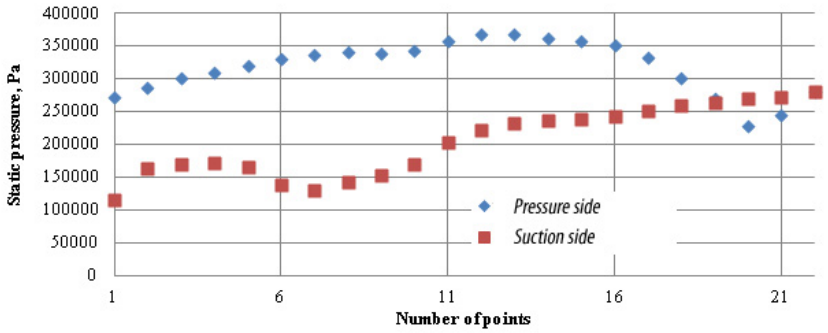

Figure 5.12: Pressure distribution along the length of the screw blade to its nominal diameter on regime N=8000 min^{-1}, Q=10.83 kg/s

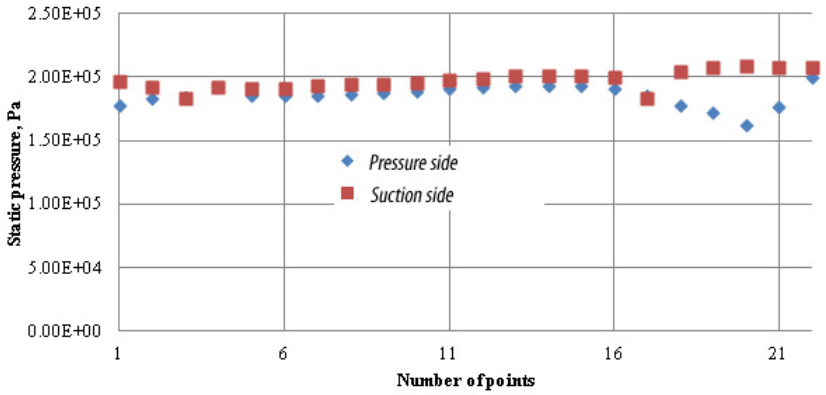

Figure 5.13: Pressure distribution along the length of the screw blade to its nominal diameter on regime N=4000 min^{-1}, Q=19.5 kg/s

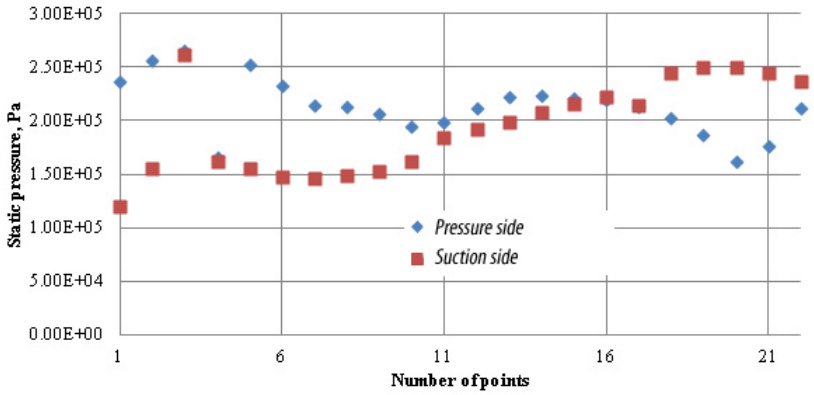

Figure 5.14: Pressure distribution along the length of the screw blade to its nominal diameter on regimes N=8200 min^{-1}, Q=19.5 kg/s

Obtained results are extremely useful for the understanding the pressure distribution inside the screw and for understanding the location of the zone of flow separation and back eddies formation. These results also show the contribution of the different parts of the screw to the total screw head.

5.4 Undissolved air hit at the pump entrance

During the numerical investigation for determining the main sources of screw-centrifugal dynamic loading, the focus was made on investigation the process of air ingress to the pump inlet. Multicomponent flow is realized in the pump in case when undissolved air hits into the supply line. To do this, the numerical model was developed to estimate the dynamics of the screw-centrifugal stage. This model provides the understanding of the reasons of pressure pulsations, occurring due to the air supply.

Boundary conditions which were used are shown in Table 5.1. Volume fractions of undissolved air were chosen based on operating conditions of the fuel system. Maximum gas volume fraction is 7% in real operating conditions.

Table 5.1: Boundary conditions

Mode	N, min^{-1}	p_{in}^{S}, MPa	p_{out}^{S}, MPa	G_{in}, kg/s	G^{V35}, kg/s	G^{V10}, kg/s	G^{V11}, kg/s	G^{V25}, kg/s	G^{V30}, kg/s	G^{V29}, kg/s	C_A, %
D287	6433	0.19	1.15	4.07	0.13	0.04	0.63	0.03	0.02	0.30	0.00
D288	6441	0.19	1.15	4.07	0.13	0.04	0.63	0.03	0.02	0.30	4.00
D289	6470	0.19	1.15	4.07	0.13	0.04	0.63	0.03	0.02	0.30	5.30
D290	6420	0.19	1.12	4.75	0.15	0.04	0.63	0.03	0.02	0.30	6.50

In a number of previous research, boundary conditions for transient analysis of centrifugal and axial flow pumps were the same as for stationary analysis. However, the assumption of the constant mass flow rate at inlet to the pump is not physically valid in case of transient analysis. Therefore, in this study, total pressure was used for inlet boundary condition and static pressure was used for a particular point on the outlet boundary condition.

Transient analysis of multicomponent fluid flow was based on stationary analysis of two-component fluid flow (kerosene and its vapor) which, in its turn, was based on the one-component fluid flow (only kerosene). Consequently, the calculation process has three steps. Such approach allows to achieve good convergence and high accuracy.

The sampling frequency for transient analysis was calculated based on corresponding rotational speeds. Blade frequencies were obtained by means the equation:

$$f = \frac{N}{60} \cdot Num \cdot i, \tag{5.1}$$

where i is a serial number of blade frequency.

Chosen sampling frequency should be enough to obtain the required time discretization. The number of iterations on each time interval was equal to 15. The fifth-order of accuracy was used. These parameters were constant for each calculation case.

The developed model was implemented for estimation of the dynamic of the axial force acting on the screw-centrifugal stage rotor. It allowed to understand its behavior in time. Figure 5.15 - Figure 5.18 show the results of the simulation of the axial force oscillations over time on the investigated operating regimes.

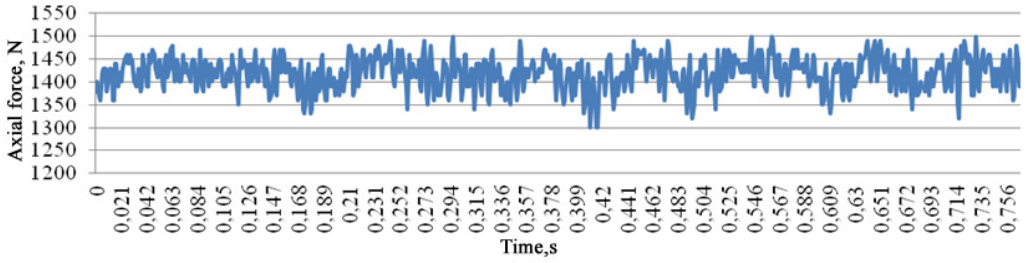

Figure 5.15: Oscillations of the axial force on the rotor. C_A= 0.00 %. Regime 287

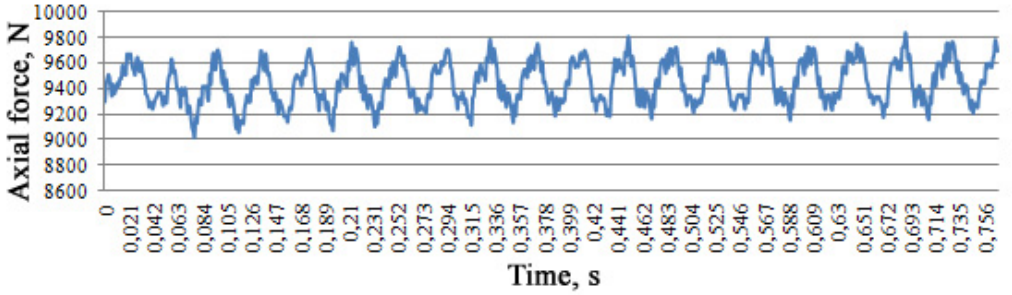

Figure 5.16: Oscillations of the axial force on the rotor. C_A=4.00 %. Regime 288

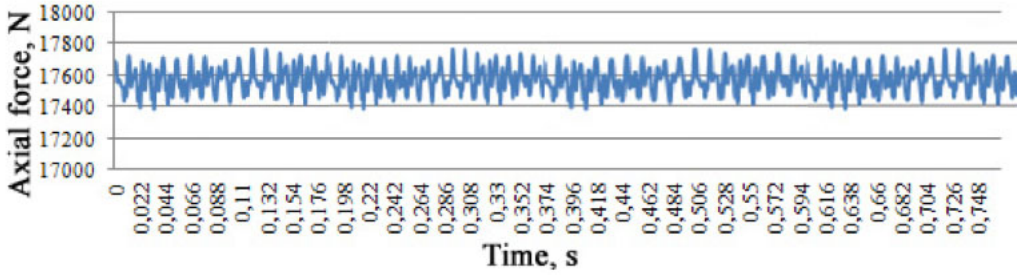

Figure 5.17: Oscillations of the axial force on the rotor. C_A=5.30 %. Regime 289

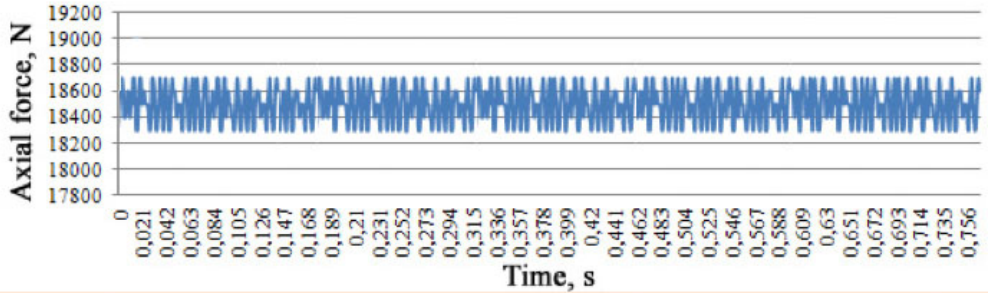

Figure 5.18 Oscillations of the axial force on the rotor. C_A=6.50 %. Regime 290

Numerical results show that undissolved air yields to increase both the average force value and its amplitude. Rise of average force value aligned with increased amplitude of pressure fluctuations and the initiation of pump rotor axial vibration. Flow around an air bubble similar to the flow around solid body. As a result, undissolved air at fuel entrance leads to the leap of local velocity which in its turn leads to local pressure breakdown.

The experimental investigation of the air influence on stress at the pump bearing was made by means of eight strain sensors which were mounted on the journal-and-thrust bearing casing (Figure 5.19).

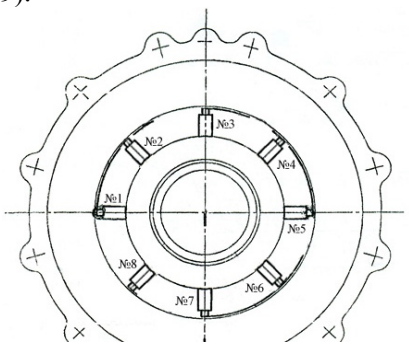

Figure 5.19: The installation scheme of strain sensors

Figure 5.20 shows the theoretical and experimental distributions of mean values of stresses on the bearing end face for a various air volume fractions. This figure shows a good accuracy of the obtained theoretical results and its good correlation with the experimental data. Calculation error does not exceed 5.00 %. In such a manner, the developed numerical approach allows to predict the loading state of the journal-and-thrust bearing of the two-stage pump in case of multicomponent fluid flow. Obtained results show that the loading of the bearing is unsymmetrical.

Additional air fractions were considered for more precise analysis of air influence on bearing loading. Consequently 6.5 %, 6.8%, 8.0%, 8.7%, 10.0% and 11.4% of volume air fractions were added for analysis. Figure 5.21 shows the significant increase of stresses on the bearing in case of air supply. The gas bubbles, due to the presence of the equalizing holes in the disc wheel (Figure 3.1 and Figure 5.2), penetrate into the axial gap between it and the bearing housing. The pressure in the gap is comparable with the pressure at the outlet of the screw. The gas bubble moves into an area of high pressure due to the centrifugal force where it collapses. This leads to a considerable (more than 18 times) increase of stresses on the surface of the bearing. Figure 5.21 also demonstrates by “bubbles” a description of air volume fraction.

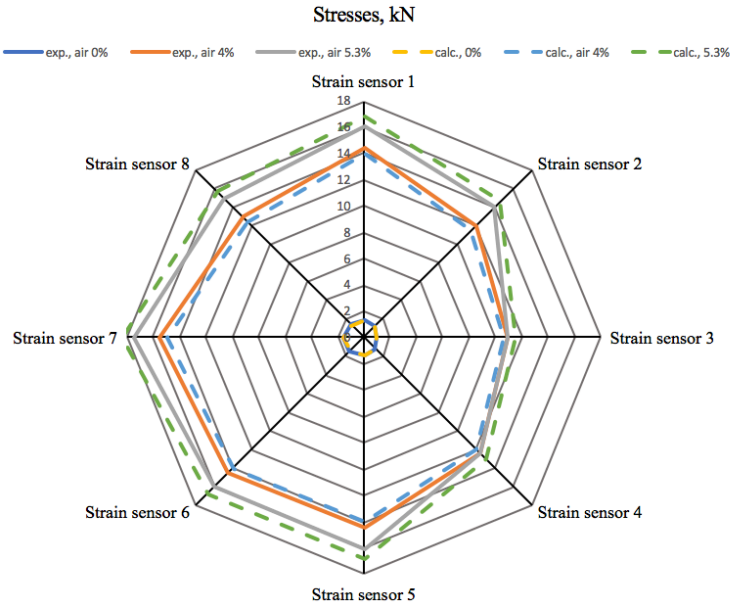

Figure 5.20: Variation of stresses mean values for various air fractions

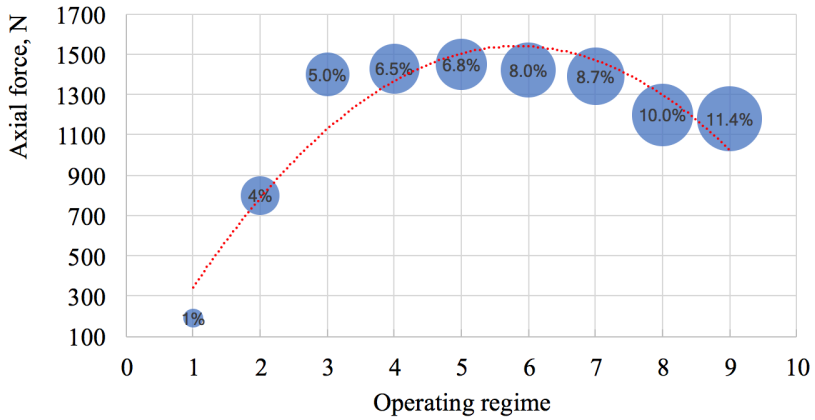

Figure 5.21: Numerical results of axial force acting on the bearing on the investigated pump operating regimes at different volume fraction of air

5.5 Cavitation

Developed cavitation upon the pump reduced operating regime D288 (see Table 5.1) was observed during the numerical study. The characteristic cavitation pattern is shown in Figure 5.22, a. The obtained results also showed that undissolved air supply results in occurring of cavitation in the bearing (Figure 5.22, b, c). Cavitation appears especially on

the bearing internal edge and on its end faces. The intensive cavity inside the bearing was observed and the bubble distribution was not symmetrical. The existence of the volute violates the axial symmetry of the pump, and is responsible for the asymmetry in the bubble distribution. Cavitation in this location is experimentally proved to lead to the erosion of the bearing (Figure 5.22, d). Even a small amount of non-condensable gas has a significant effect on the performance of the pump. The primary effect is due to the expansion of gas at low pressures, which can lead to significant values of gas local volume fraction, and thus have a considerable impact on density, velocity and pressure distributions. All described factors may lead to the violation of the lubrication conditions of the considered bearing and to problems with load lubricant layer capacity. Therefore, the numerical analysis conducted confirms cavitation character of the bearing end face damages.

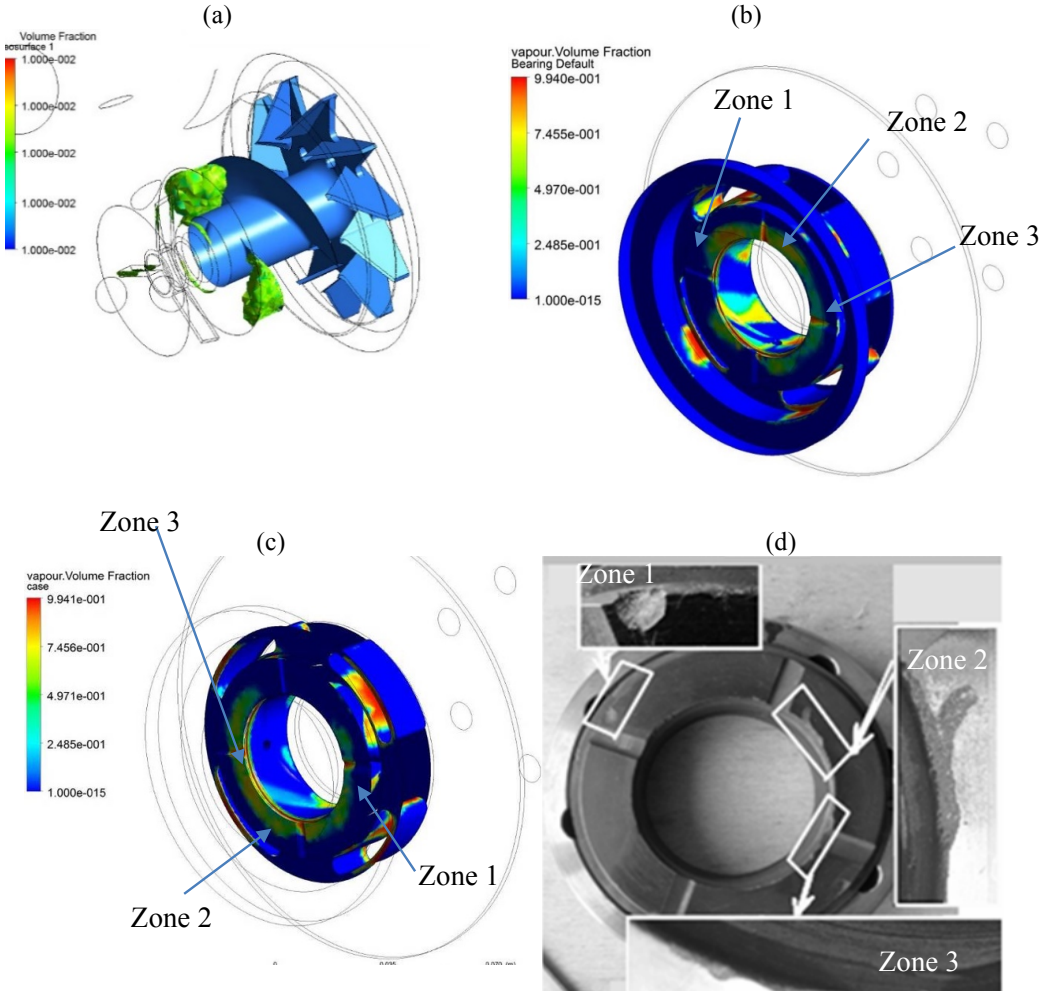

Figure 5.22: The distribution of kerosene vapor on the bearing surfaces (a - c) and bearing wear (d) obtained after pump operation: a – distribution of cavitation cavities on operating regime D288; b - operating regime 289; c - operating regime 290

5.6 Vortex resonance in two-stage pump

As it was shown in the Chapter 3, two-stage pump ND-32 also contains an external gear stage. Its three-dimensional model and a prototype pump are shown in Figure 2.2, Figure 3.1 and Figure 3.2. The stage parameters are shown in Table 5.2. It is worth to mention, that gears as well as centrifugal wheel have also 11 teeth.

Table 5.2: ND-32 gear stage characteristics

Gear pump type	External gear pump
Components materials	Aluminium, Bronze, Steel
Working medium	Kerosene
Gear rotation	Counter clockwise
Rotational frequency range	Up to 10000 min^{-1}
Pump inlet pressure	Up to 1.4 MPa
Pump outlet pressure	Up to 10 MPa
Pump dimensions	Gear rim width: 0.021 m Gear teeth number: 11 Distance between the gear centres: 0.067 m Gear outer diameter: 0.078 m Gear inner diameter: 0.030 m

The schematic diagram of the two-stage pump shows that its stages are hydraulically connected with each other not only by the way of fuel supply (Figure 2.3). There is another way of stage interaction. All leakages (edge and radial leakages as well as leakage through teeth contact of meshing gears) from the gear stage are poured out into the chamber between the stages. The path of leakage propagation in the considered pump is presented in Figure 5.23 by means of arrows. This chamber is also connected with the screw-centrifugal stage flow channel by means of the orifices in the bearing case (Figure 5.24, a) as well as by means of discharge holes in the impeller (Figure 5.24, b).

Gear pumps are well known to generate high frequency pressure ripples at the outlet pipeline as well as in pressure side of the supply chamber (Konami, 2017). According to articles (Tsniitastroymash, 1979) and (Zaguzov, 1994) the leakages from the gear pump also have high frequency oscillations due to its working principle. Consequently, leakages, having high frequency of pressure oscillations, move into the SCS and generate additional source of high-frequency oscillations of blades of the screw and centrifugal wheel. Herewith results obtained in papers (Kinelev, 1976), (Karelin, 1975), (Shapiro, 2004) show that the trailing vortices are the most important vibration sources in axial flow and centrifugal pumps. The coincidence of these frequencies in case of two-stage pumps lead to so-called “vortex resonance” inside the SCS.

A model of flow induced vibrations in the two-stage pump was firstly developed in study of Gasparov (Gasparov, 2006). The principle lies in trailing vortex stalling with a certain frequency (Figure 5.25). This trailing vortex is formed in a radial gap between the screw blades and a pump hull. At that, screw blades are loaded by high-frequency pressure

oscillations, spreading from a gear stage to screw-centrifugal stage inlet (Figure 5.23). These oscillations can coincide and lead to vibration loading of the pump rotor. The idea of vortex resonance was used in the article (Gasparov, 2006) to determine the sources of dynamic loading of the journal-and-thrust bearing inside pumps ND-25 and ND-32. Star-CD commercial software was used for CFD analysis to determine the frequency of tip vortices. However, low quality of the computational mesh, using of the standard $k-\varepsilon$ turbulence model for near-walls flows did not allow to get accurate results and to make final conclusions about the real causes of bearing damages. It is worth to note that some construction elements were not taken into account. Additionally, there is a lack of verification of obtained results. Herewith, experimental results, obtained in paper (OJSC "Scintific and production enterprice "Temp" named after F.Korotkov", 1990) did not confirm high-frequency pulsations at screw-centrifugal stage inlet. This discards the assumptions made by the authors.

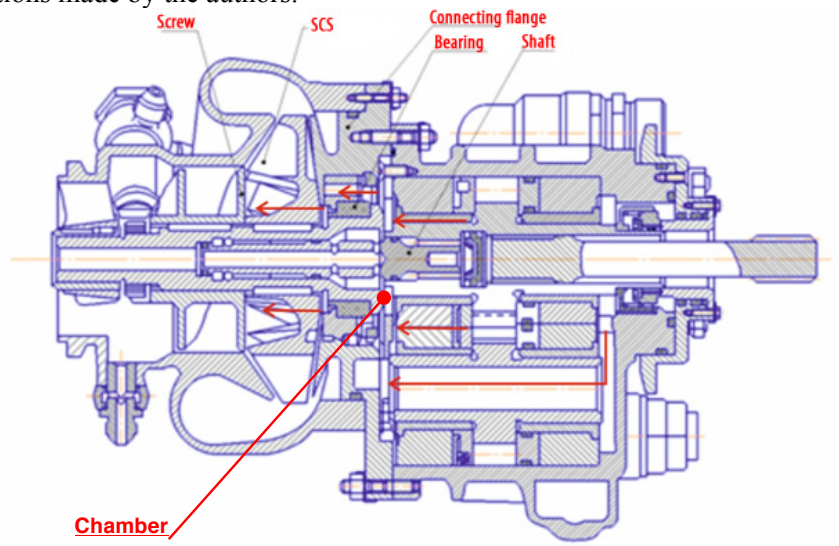

Figure 5.23: Leakages propagation path from the gear stage into the screw-centrifugal stage

Figure 5.24: Construction elements on the screw-centrifugal stage
a – bearing; b – centrifugal wheel

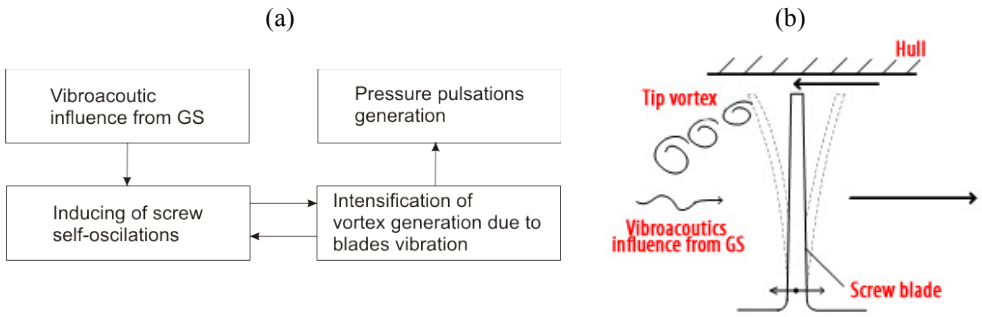

Figure 5.25: Scheme of pressure pulsations induced vibrations due to the trailing vortex stalling and gear stage influence

Therefore, in contrast to article of Gasparov, in this investigation not only screw blades are considered, but also the blades of the impeller are also taken into account. Consequently, the block diagram of the interaction of vortex disturbances in the SCS and screw and impeller blades, oscillating due to the hydrodynamic impact from the gear stage, is presented in Figure 5.26. The proposed model consists of the following sub-models:

- Hydrodynamic model of the screw-centrifugal stage. It was developed in the previous chapter. This model allows to estimate the structure of the flow inside the stage;
- Finite-elements models of the screw and impeller to estimate their natural frequencies;
- Model of leakages from the gear stage. They are represented as sources of oscillations. Their parameters can be obtained either theoretically or experimentally. There are a number of experimental and analytical approaches for leakage estimation. They are thoroughly described by Rundo in article (Rundo, 2017). In this dissertation, the mass flow ripples were estimated by means of model presented by Rodionov in an article (Rodionov, 2009). This model was validated and showed a good agreement with experimental data.

<table>
<tr><th>ANSYS CFX</th><th colspan="2">ANSYS Workbench</th><th>Theoretical data</th></tr>
<tr><td>3D geometric model of SCS</td><td>3D geometric model of screw</td><td>3D geometric model of centrifugal wheel</td><td rowspan="2">Leakages from GS</td></tr>
<tr><td>CFD model of SCS</td><td>FEM of screw</td><td>FEM of centrifugal wheel</td></tr>
<tr><td colspan="4">MODEL OF INTERACTION BETWEEN SCS IMPELLERS AND TIP VORTEX, TAKING INTO ACCOUNT GS</td></tr>
</table>

Figure 5.26: The block diagram of the interaction of vortex disturbances in the screw-centrifugal stage and oscillated screw and impeller blades

Boundary conditions for the general model are:

- The eddy frequency and its parameters such as its structure, pressure and velocity distribution inside the eddy;
- Amplitudes of pressure pulsations obtained by the numerical simulation of the screw-centrifugal stage;
- Natural frequencies of the screw and impeller;
- Hydrodynamic impact of the gear stage.

As it was shown in Chapter 5, the developed numerical model of the screw-centrifugal stage allows to estimate the separation of the flow inside a stage, which results in forming of eddy zone. An accuracy of these turbulence flows can be estimated by y^+ parameter distribution along the solid walls. This distribution is shown in Figure 5.27

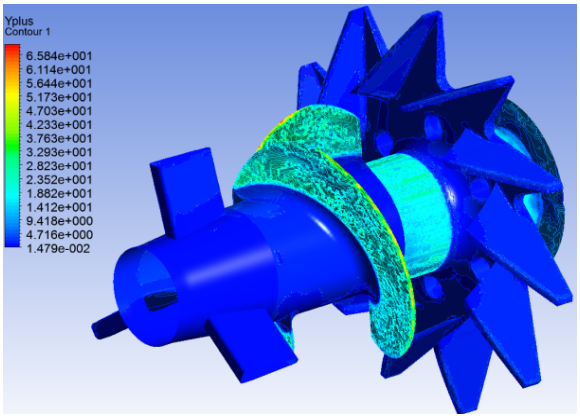

Figure 5.27: The distribution of y^+ parameter along the rotor walls

Figure 5.28 represents the pressure distribution along the solid walls of the screw-centrifugal stage rotor. There is a zone of flow separation on the suction side of the screw blade. The flow structure inside the screw is represented in Figure 5.29. Fluid flow passing the radial clearance between pump case and blades interacts with the main flow and radial flow from root sections to peripheral. This interaction occurs at the suction surfaces of the blades and results in rolling up of this flow into a vortex. Its radius and circulation depend on pump operating regime, its geometrical parameters and location of vortex appearance. Trailing vortex moves in the circumferential plane of the channel in a direction from the periphery of blades suction sides towards their pressure sides.

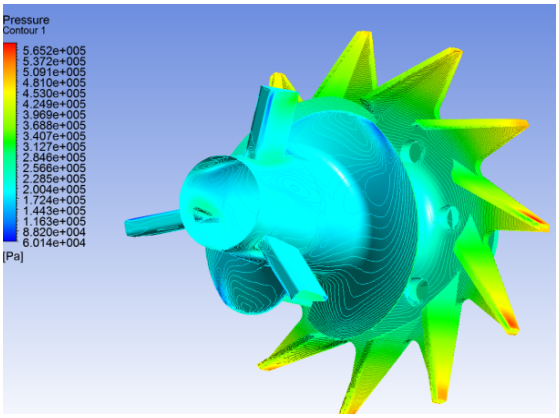

Figure 5.28: Pressure distribution along the solid walls of the screw-centrifugal stage rotor
N=4325 min^{-1}, G_{SCS}=2.41 kg/s, P_{in}=0.19 MPa, T=318 K

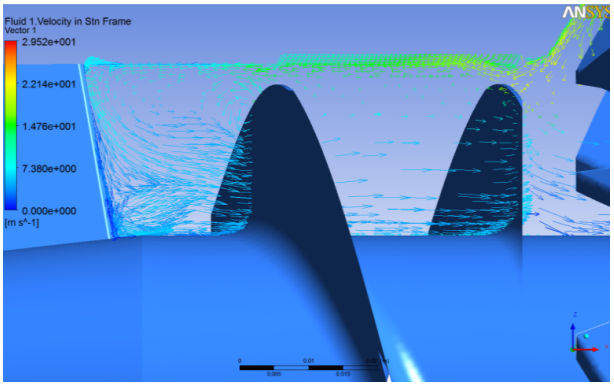

Figure 5.29: Flow structure on the operating regime
N=4325 min^{-1}, G_{SCS}=2.41 kg/s, P_{in}=0.19 MPa, T=318 K

Near-wall stream, occurring due to the radial flowing, is unsteady (Shapiro, 2004). Evolution of the disturbances leads to flow separation. Numerical simulation allows to estimate the parameters of the eddies and to determine its separation frequency by mean of Strouhal number:

$$f = \frac{\upsilon \cdot Sh}{l_{cavity}} = \frac{Sh\sqrt{2g \cdot \Delta H}}{l_{cavity}}, \tag{5.2}$$

where ΔH is pressure difference on the peripheral section of the blade; l_{cavity} is the maximum length of the cavity before the stall break.

Modal analysis of the screw and impeller was performed by ANSYS Workbench software. Finite-element meshes for the screw and impeller are shown in Figure 5.30. Size of the meshes does not exceed 0.003 m. The surrounding liquid was taken into account to consider the influence of added mass of the flow. To do this, a simple one-way fluid-structure interaction (FSI) analysis was provided. A partitioned approach was used. In this case the governing equations for the fluid flow and for the structure deformation are solved separately. The obtained data of flow parameters were considered as the boundary conditions for modal FEM-analysis. Conducted modal FEM-analysis has shown that natural frequencies of the screw and impeller are in the range of 3700-5000 Hz (Table 5.3). Natural frequencies of the screw and impeller were also obtained experimentally by means of knocking method. Wheels were hung up on a thread and excited by means of a hummer with a wooden tip. The changing of the sound pressure was being registered at the distance of 0.30 m. These measures were conducted in the air. To take into account the influence of the kerosene, the turning coefficient equal to 1.4 was assumed.

(a) (b)

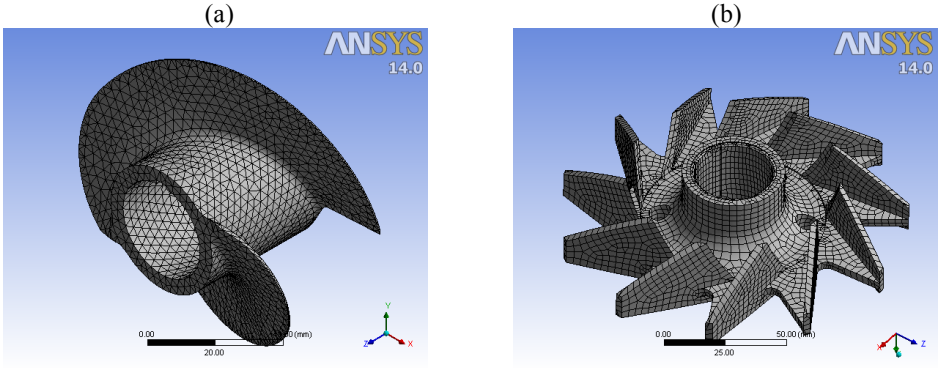

Figure 5.30: Finite-element meshes of the screw (a) and impeller (b)

Table 5.3: Natural frequencies of the screw and impeller

# of natural mode shape	Natural frequency of the screw, Hz	Natural frequency of the impeller, Hz.
1	3310.60	3769.60
2	3812.70	3846.6
3	4373.30	3901.00
4	4887.80	3964.90
5	5420.90	4155.60

Experimental spectrums of pressure pulsations are shown in Figure 5.31. Obtained results shows high-frequency pressure oscillations in the investigated range 3 – 4 kHz in the screw and centrifugal wheels zones. The origin of these oscillations is explained by the

coincidence of the eddy frequencies, separated from the wheels and their natural frequencies on several operating regimes. The influence of high-frequency pressure oscillations on two-stages fuel pumps ND-25 and ND-32 were investigated in paper (OJSC "Samara construction bureau of engines design", 1998). This paper shows that high-frequency pressure oscillations are the main contribution in total level of pumps. Note, that the paper did not determine the source of high-frequency pressure oscillations. Therefore, hydrodynamic disturbances inside the screw-centrifugal stage interact with hydrodynamic influence from the gear stage. This interaction results in oscillations of screw and impeller blades. Oscillations are significantly increased due to the coincidence of these frequencies and natural frequencies of the screw and impeller. Increasing of blades vibrations leads to intensification of pressure pulsations, caused by the hydrodynamic reasons and to increasing of vibration loading of the end face of the bearing.

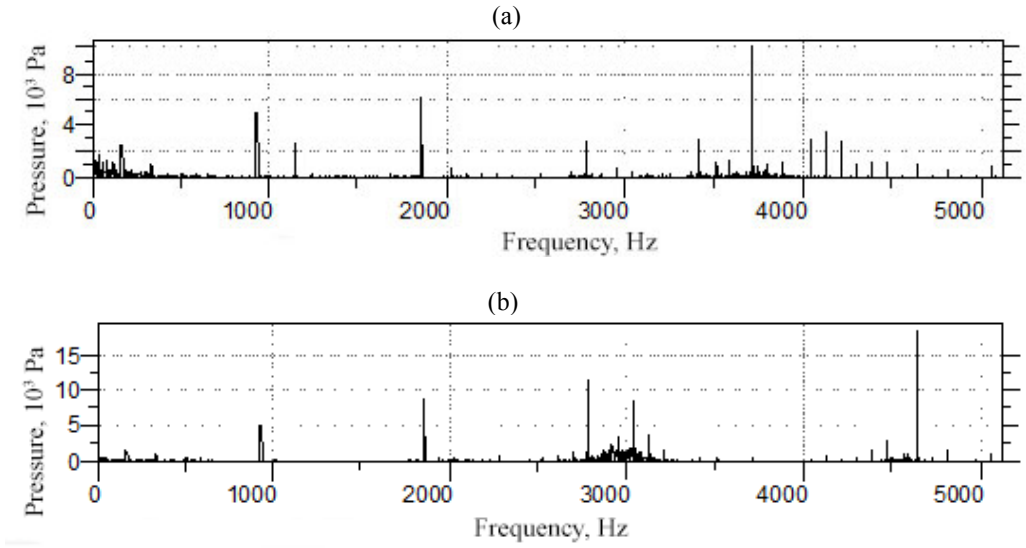

Figure 5.31: Spectrums of pressure pulsations, measured on the pump operating regime - N=4325 min^{-1}, G_{SCS}=2.41 kg/s, P_{in}=0.19 MPa, T=318 K
a – outlet of the centrifugal wheel; b – in the chamber between the stages, characterizing the gear stage influence

6 Development of Experimental Test Bench for Aircraft Engine Fuel Pumps Investigations

6.1 The description of the experimental test bench

Experimental research and theoretical simulations of GTE and their systems are one of the most significant and necessary stages in their design process, refinement, testing and certification. However, high cost and poor ecological indicators are severe disadvantages of the control systems (CS) full size refinement as a part of GTE. In case of full-scale tests, an engine operates under the off-nominal regimes. It yields to enormous error probability. Additional limiting factor is an increased fuel consumption in case of full-scale engine tests. As a result, the CS tests are usually reduced to inspection of its reliability and serviceability, verification of the characteristics of the aggregates and GTE systems prior to their installation on the full-scale engine.

Provided analysis of engineless test benches for experimental investigations of aircraft engine fuel pumps shows that the pump operating conditions as a part of the engine and as a part of engineless test bench are different. These mismatches are shown in Table 6.1: Fuel pump operating conditions mismatches.

Table 6.1: Fuel pump operating conditions mismatches

A part of the engine	A part of the test bench
Pump supply pressure is determined by the pressurization pressure, i.e. by the head of the booster pumps installed in the tank	Pump supply pressure does not vary a lot. It keeps constant in a range from 0.15 to 0.25 MPa if its reducing is not provided be the test program. This prevents the cavitation occurring and gas evolution in comparison with the full-scale configuration.
The fuel temperature in the supply pipelines is determined by the fuel temperature in tanks, environmental conditions, aircraft fuel-air heat exchangers. Fuel temperature varies from 216 K up to 383 K	The fuel temperature in the supply pipelines is determined by the temperature in the vessel of the fuel storage. Fuel systems of aircraft engine test benches have a closed-loop configuration. The temperature is maintained constant in a range of 288-323 K during operation. Such system configuration sustains to reduce the volume fraction of the dissolved gas into the fuel.

Additionally, full-scale pump operating conditions enable the free gas evolution from the fuel. The comparison of the two cases considered explains the absence of the journal-and-thrust bearing destructions during the laboratory investigations of the pump. Moreover, there have not been any failures or abnormal situations during such investigations. Consequently, the scheme of a laboratory test bench for aircraft engine two-stage pumps investigations as well as their operating conditions should be as close as possible to the

full-scale working conditions. The described problems are solved by HIL or semi-natural stands. They are thoroughly described in papers (Fatikov, 2005) and (Sheviakov, 1976). The necessity for application of such stands is justified when: the controlled object is at the stage of engineering while the control units already exist; the object cannot be tested in the laboratory conditions; the control units have nonlinear characteristics, frictions, and noise which could not be considered in their equations; carrying out full-scale experiments to configure the control unit is expensive or not acceptable.

The method of the integrated studies of GTE aggregates and its systems on HIL stands is described in works (Fatikov, 2005) and (Pogorelov, 2013). It consists of carrying out the whole complex of tests in real time by means of integration of full-scale control and diagnostic systems with GTE mathematical models.

Nowadays the information about a variety of stands and techniques providing the semi-natural test benches of GTE and its systems is a publicly available source. A variety of GTE HIL models and their systems processes development are described in articles (Zarubin, 2001), (Ryzhikov, 2004), (Godovanyuk, 2005), (Golberg, 2014) and (Golberg, 2010). The conception of hardware, algorithmic and software support for HIL simulations of GTE systems in all their life cycle stages are considered by Inozemtsev (Inozemtsev, 2008). Golberg (Golberg, 2014) describes a bench for the control laws development for GTE elements mechanizing system. This bench consists of the GTE model, engine housing (with the dismantled compressor's and turbine's rotors), fuel metering unit equipment and air intake mechanization devices. The HIL test benches in researches (Pogorelov, 2013), (Balashov, 2006), (Balashov, 2007) have a possibility of a comparative assessment of embedded real-time systems architectures at early development cycles. This feature set these benches apart from other existing solutions (Brouwer, 2000). Gurevich describes in article (Gurevich, 2010) the HIL test bench with demonstrational CS and electric executive devices. The HIL demonstrational GTE control and fuel supply systems with full-scale electric actuators is also described in article (Gurevich, 2010). The HIL approach was used for the airplane adaptive automatic control system development in article (Meikel, 2013). The HIL technology was used for the characteristics investigation of the GTE full-scale aggregates and its systems in researches (Sverbilov, 2013), (Shakhmatov, 2012), (Makaryants, 2012), (Makaryants, 2011), (Prokofiev, 2010).

Thus, the possibility of applying the complex mathematical models or the combination of both full-scale aggregates and aggregates' mathematical models is common for all described stands. Application of each particular approach depends on a degree of aggregates completion and tests type.

6.1.1 **Full-scale part of semi-natural test bench**

Developed semi-natural test bench consists of operator station with its own CS; data acquisition system; full-scale aggregates of the GTE fuel and control systems. The general views of the developed test bench are presented in Figure 6.1. Developed test bench

scheme is given in Figure 6.2. Top-of-the-range system is an operator station, which was organized on the basis of the industrial computer National Instrument PXIe and provides connection between computation system and operator. Operator station provides real-time displaying of the controlled object conditions; archiving and registration the information from transducers; calculating; components condition monitoring and real-time control. The lowest level of the semi-natural test bench is the data acquisition system. This is a computer system, which has a controller for direct connection with controlled object and transducers. The controller's functions are:

- collection and processing of the primary data from the transducers;
- direct automatic control of the controlled object;
- emergency situations debugging.

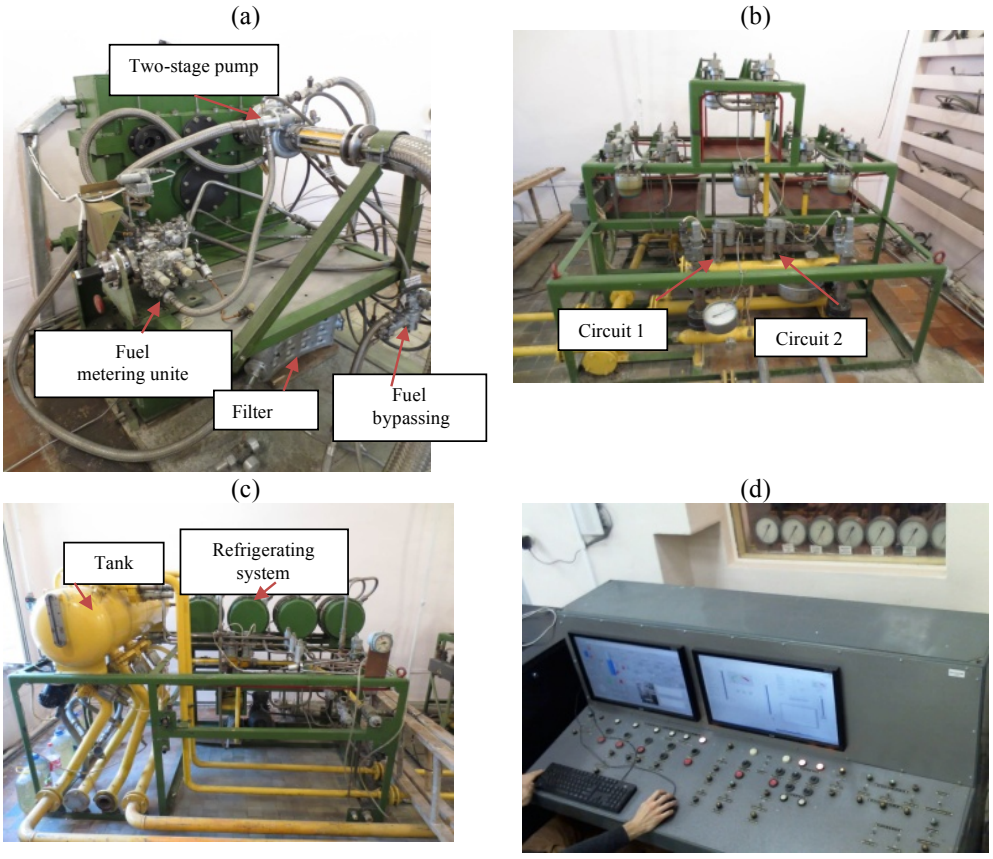

Figure 6.1: Developed semi-natural test bench
a – two-stage pump (gear stage and screw-centrifugal stage), hydro-mechanical fuel metering unite, fuel aggregates; b – system for combustion chamber simulation; c – fuel supply system and refrigerating system; d – operator station

The primary target parameter is an engine rotor rotational speed. The control factor is fuel flow through each circuit (they go to the GTE combustion chamber simulator). The mathematical model provides control of fuel aggregates by three main control parameters:

- rotational speed of the pump unit electromotor. It aligned with the GTE rotor rotational speed at a software level. The three-phase drive unit with a digital control is used as a electromotor;
- rotational speed of the hydro-mechanical fuel metering unit electromotor. It simulates rotational speed of the GTE rotor;
- an angle of the engine power control, located on the fuel metering unit. The angle is changed by the operator.

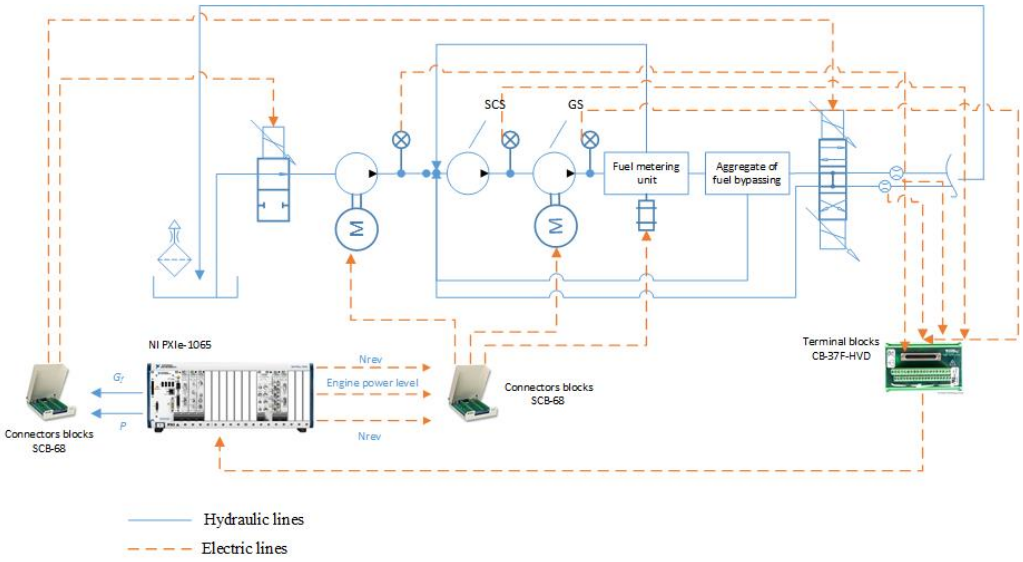

Figure 6.2: The Circuit diagram of developed semi-natural test bench

The mathematical model of the controlled object needs the values of system parameters, particularly pressure in key points and mass flows in imitators of circuits of combustion chamber, to accurate bench control during testing. Necessary values are taken by means of pressure or flow sensors as well as by feedbacks from actuators (for example an angle of engine power control). Signal converters are necessary for the hybrid bench control by means of GTE mathematical model. Consequently, the electric actuator of the engine power control, mounted on the fuel-metering unit, was installed in the system.

The hydraulic circuit diagram of the developed semi-natural bench is given in Figure 6.3.

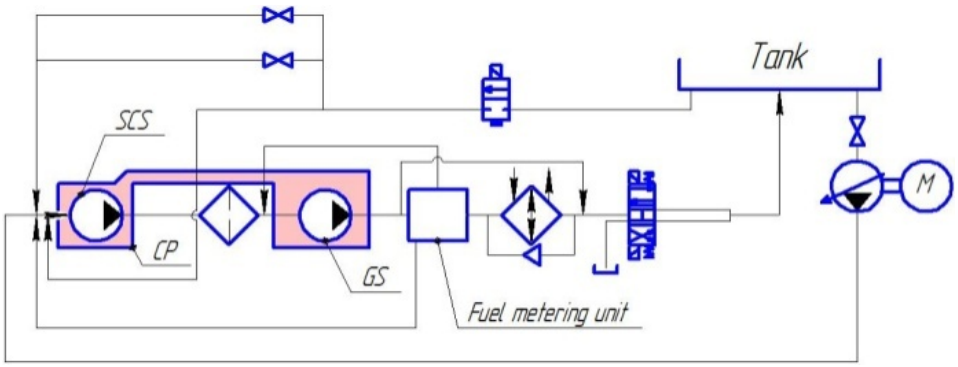

Figure 6.3: The hydraulic diagram of the fuel system

The hardware components of the bench (such as processors, memory, converters, distribution panels, etc.) were assembled from the standard industrial equipment focused on real-time operation. Mathematical models of the engine and its systems were created by means of visual simulation tools in LabView and MATLAB/Simulink.

Besides the fuel two-stage pump, a number of full-scale aggregates such as fuel-metering unit, low-pressure filter, fuel regulator and aggregate of fuel bypassing were also installed. Fuel flows to the cleaning station through the nozzle simulators and then pours into the tank though heat exchangers. The missing aggregates were simulated by means of the corresponding fuel-jets. Component connections were provided by means of full-scale pipelines instead of flexible pipes.

Operating conditions of full-scale fuel aggregates have been made maximally close to real operation conditions during tests. Therefore, they were mounted into altitude-temperature chamber and on shaking tables.

The developed semi-natural bench operates as a part of the distributed remote access network (Figure 6.4). It allows using global network Internet to perform experiments on the remote engine bench, or to perform tests using flight data directly from the airplane. Exterior participants are submitted a possibility to observe the tests, or meagerly participate in them by getting the remote access through a multidropping server. Test data are recorded in the special distributed database and stored there for the subsequent analysis and processing by means of a special server.

Developed test bench provides a reliable accident-protection system on both hardware and software levels. The protection system on bench's analog operating console objected on accidental pressing, restriction of aggregates working without preliminary oil and fuel supply and other are implemented on developed stand. The program utilizes a protection against accidental rupture data with the bench, which in its turn duplicated in analogue form on operating console.

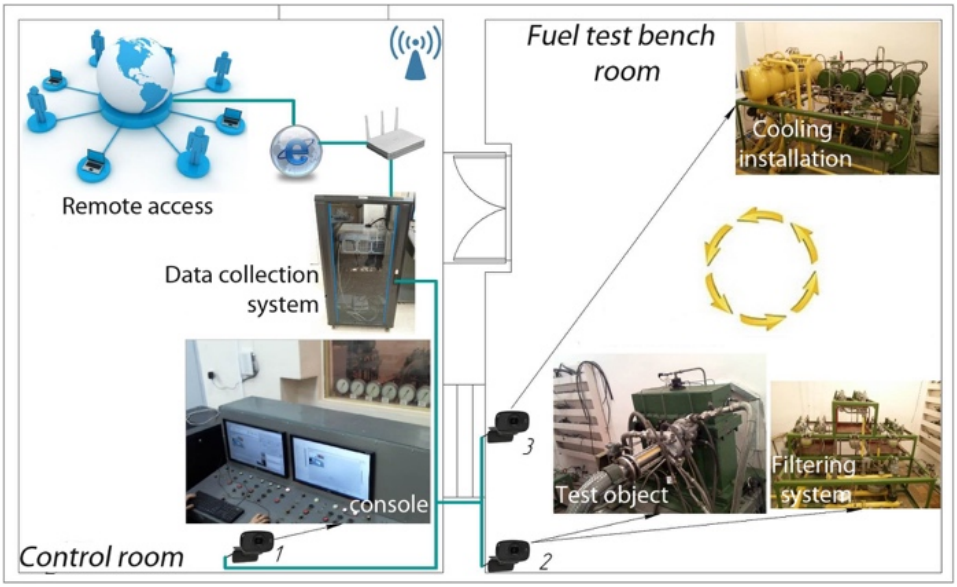

Figure 6.4: The distributed network circuit

6.1.2 **Virtual part of semi-natural test bench: GTE mathematical simulation**

The GTE mathematical models as a part of semi-natural stand should be adequate and provide the real-time interacting with the full-scale fuel aggregates for accurate investigation of the fuel system. GTE mathematical models, embedded into the full-scale CS, allow to execute not only adaptive control algorithms and controlling accuracy, but also to ensure reliable diagnostic of the engine and its systems.

The mathematical model of GTE has a subassembly structure, where output parameters of one block are input parameters for next one. The mathematical model consists of the following sections: inlet duct, fan, low and high-pressure compressors, combustion chamber, high and low-pressure turbines, mixing chamber and jet nozzle. The flowchart of the subassembly model is shown in Figure 6.5.

Following operation of the engine is generally simulated: input air behind the ventilator is divided into two flows – internal, G_{A1}, and external, G_{A2}. The whole internal flow is compressed by low and high-pressure compressors and enters a combustion chamber where fuel G_F is fed. The combustion chamber is simulated by the heat balance equation. The energy, gained from fuel combustion in the combustion chamber, is partially used up in the high-pressure turbine, and partially used up on the low-pressure turbine and eventually goes to rotors rotation. An internal and external gas flows are mixed in the mixing chamber creating pressure, temperature and a gas flow rate at a nozzle entry.

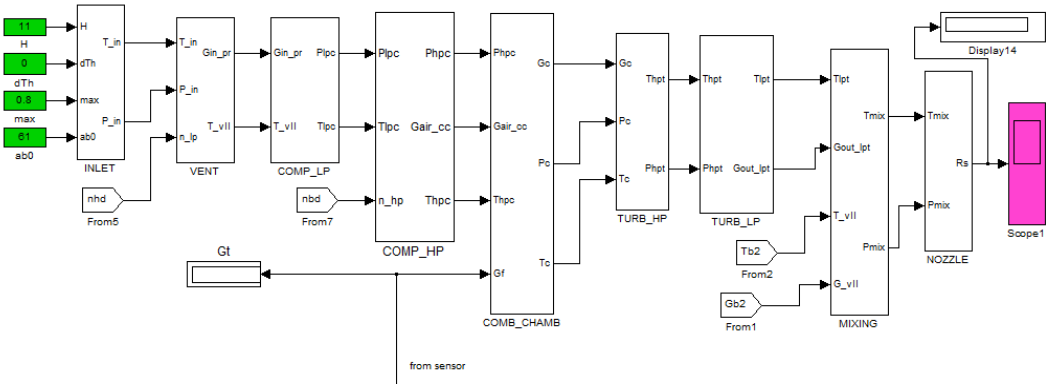

Figure 6.5: The subassembly mathematical model of turbofan engine (MATLAB Simulink)

The working parameters such as pressure, p, temperature, T, turbine power, P, torque, M, and pressure ratio, $\pi*$ at the corresponding node are calculated in corresponding block at each calculation time step. As far as the most important compressor parameter - a stall margin, it can be found in every compressor stage as well. The combustion chamber is simulated in simplified form and values $H_U, \eta_{comb}, c_p, c_v, \upsilon_{combchamb}$ are constant and chosen based on fuel type, air and air-gas mixture conditions. The rate of the fuel consumption, G_{fuel}, is received from the flow rate transducers.

The engine thrust, R_N, is the product of exhaust velocity and flow rate:

$$R_N = G_N \cdot \upsilon_N \tag{6.1}$$

The flow rate at predetermined parameters can be found by the following equation:

$$G_N = \frac{m_F \cdot q(\lambda) \cdot p_{mix} \cdot s_N}{\sqrt{T_{mix}}} \tag{6.2}$$

An outlet control parameter for the test bench is the rotational speed of the engine's shaft. The rotational speed of the engine's shaft can be found as a difference between turbine and compressor torques. The rotary accelerations are calculated in the block with derivatives with help of following equation:

$$\omega = \frac{M}{I} = 60\frac{M_{turbine} - M_{compressor}}{2\pi \cdot I} \tag{6.3}$$

Integrating these values results in getting rotational speed in terms of "min^{-1}".

The characteristics of the engine's fan, high and low-pressure compressors are simulated in their all frequency range of pressure and rotational speed to provide a possibility of engine testing in its all-range unsteady-state processes. It results in getting all numerical values of engine working parameters in its broadest working regimes apart from the

engine start mode. The diagram of engine main parameters changing (such as rotational speed of high-pressure and low-pressure shafts, fuel consumption, compressor delivery pressure and combustion outlet temperature) during tests are shown in Figure 6.6.

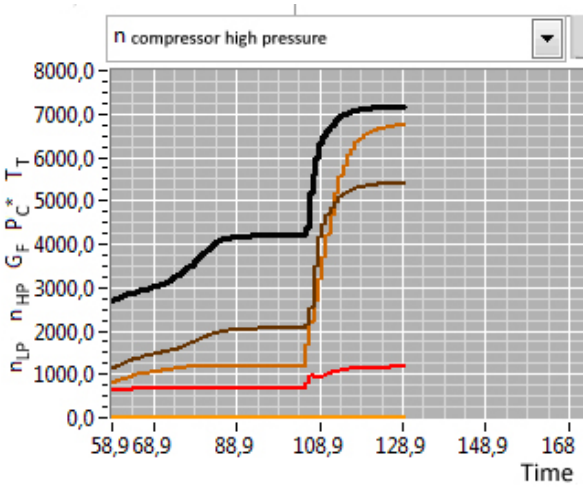

Figure 6.6: The diagram of engine parameters changing'

The mathematical simulation includes two reproducing techniques of the dynamic processes in an engine gas-generator. The first uses the piecewise linear approximation of throttles characteristics, obtained experimentally from the real engine. The second one is a full-sized part in terms of equations.

Mathematical model has been developed and debugged in MATLAB Simulink software. Further development has been made in NI LabVIEW software. Application of LabVIEW software as a programming language allows the end user to make changes in the mathematical model quickly. The mathematical model was converted from Simulink into NI LabVIEW for this purpose. It resulted in providing HIL test bench to operate with full-scale hydro-mechanical aggregates.

The control and measuring system of the semi-natural bench had been created by means of the commercial software LabVIEW (Figure 6.7 and Figure 6.8 correspondingly). The front panel of developed software displays in real time the full geometric model of all controlled objects, as an engine, its units and assemblies, as well as geometrical models of bench aggregates and components. In the same manner, the location of installed transducers can be shown in developed software, allowing to visualize the working processes. As far as remote control concerned, developed software is able to bring about it by getting the tests data to remote user.

A set of system possibilities includes: monitoring and processing parameters taken from flow, pressure sensors, rotational speed sensor of the pump rotor and incidence angle obtained by fuel metering unit actuator; controlling a rotational speed of the pump rotor

changing, both in a manual mode and in an automatic mode by means of engine power control; monitoring of alarm conditions.

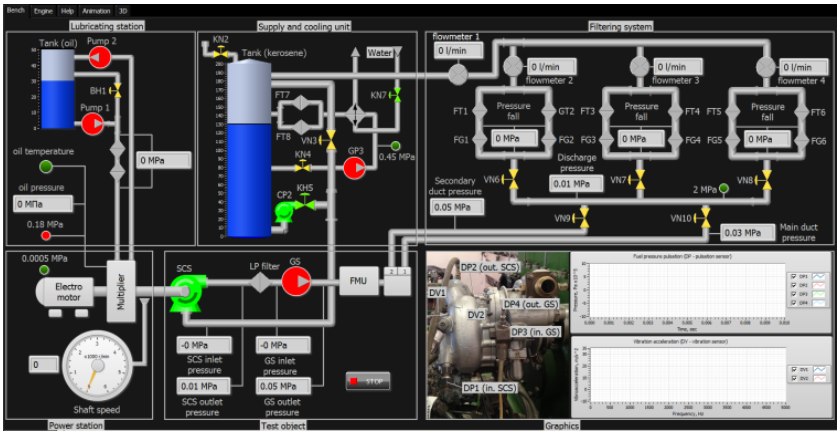

Figure 6.7: Measurement system front panel'

Figure 6.8: Control system front panel

Control Design and Simulation modules were used to realize the main equations. As to entering the turbine and compressor characteristics, MathScript module of LabView software was implemented, which works with MATLAB.

6.2 Description of the measurement methods and equipment

Parameters of the fuel system operation, obtaining during the experiments, are shown in Table 6.2 and Table 6.3. The circuit of transducers installation is represented in Figure 6.9.

Table 6.2: Work process-related parameters. Part 1

Symbol	Range	Appropriation and place for installation
N	0 - 8500 min^{-1}	Pump rotor frequency speed
p_{in}^{SP}	0 - 0.6 MPa	Static pressure in the supply pipeline. The transducer is installed at a distance of 600 mm away from the pump flange
p'^{SP}_{in}	*	Fuel pressure pulsations in the supply pipeline. The transducer is installed in the pump case near the screw.
p_{in1}^{S}	0 - 0.6 MPa	Upstream static pressure before the screw. The transducer is a probe represented in Figure 8.1.
p_{in2}^{S}	0 - 0.6 MPa	Downstream static pressure before the screw. The transducer is a probe represented in Figure 8.1.
p_{out}^{C}	0 - 2.5 MPa	Static pressure in the screw-centrifugal stage outlet
p'^{C}_{out}	*	Pressure pulsations in the screw-centrifugal stage outlet
p_{min}^{Cham}	0 - 1.6 MPa	Static pressure in the chamber formed by the centrifugal wheel and the pump case. The transducer is installed on the circle minimal radius of this chamber (Figure 8.4).
p_{mid}^{Cham}	0 - 1.6 MPa	Static pressure in the chamber formed by the centrifugal wheel and the pump case. The transducer is installed on the circle middle radius of this chamber (Figure 8.4).
p_{max}^{Cham}	0 - 1.6 MPa	Static pressure in the chamber formed by the centrifugal wheel and the pump case. The transducer is installed on the circle maximum radius of this chamber (Figure 8.4).
$p_{in}^{bearing}$	0 - 1.6 MPa	Static pressure at the inlet area of the bearing
p_{in}^{Chamb2}	0 - 1.6 MPa	Static pressure in the chamber between the screw-centrifugal stage and the gear stage**
$p'^{chamber}_{in}$	*	Pressure pulsations in the chamber between the screw-centrifugal stage and the gear stage**
p_{out}^{GS}	0…10 MPa	Static pressure after the gear stage
p'^{GS}_{out}	*	Pressure pulsations after the gear stage
p'^{S}_{mid}	*	Pressure pulsations at the middle of the screw length. The transducer is installed in the pump case
$G^{comb.}_{chamber}$	0.08 - 2.78 kg/s	Mass flow rate to the main combustion chamber. The DR1 transducer in Figure 8.4
G^{SCS}	0.28 - 8.33 kg/s	Mass flow rate through the screw-centrifugal stage. The DR1 transducer in Figure 8.4.
G^{V11}	0 - 1.25 kg/s	Mass flow rate through the regulator of the nozzle and afterburning. The DR3 transducer in Figure 8.4.
L	± 0.001 m	The displacement of the pump rotor. The inductive sensor is installed in the supply pipeline (Figure 8.4)

* - the expected pressure pulsations frequency was up to 4500 Hz. The pulsations amplitude is up to 100% from the middle value;
** - static pressure in the chamber between the pump stages. The leakages from the gear stage are pourn to this chamber. This chamber connects with both, the inlet of the screw-centrifugal stage though the channel inside the pump rotor shaft, and the chamber after the centrifugal wheel. The transducers are installed in the channels having the diameter 0.004 m and the length 0.015 m. These channels are made in the flange connecting the pump stages;

Table 6.3: Work process-related parameters. Part 2

St1, St2, St3… St16	Range	Strain sensors. They are installed in the case of the bearing***
V_{in}^{X}		Vibration transducer. It is installed on the flange that connects the pump stages. The direction of measurements is OX axis (Figure 8.4)
V_{in}^{Y}		Vibration transducer. It is installed on the supply pipeline flange ****. The direction of measurements is OY axis (Figure 8.4)
V_{in}^{Z}		Vibration transducer. It is installed on the supply pipeline flange ****. The direction of measurements is OZ axis (Figure 8.4)
V_{out}^{X}		Vibration transducer****. It is installed on the supply pipeline flange. The direction of measurements is OX axis (figure)
T_F^{SP}	0-473 K	Fuel temperature in the supply pipeline
T_F^{V33}	0-473 K	Fuel temperature in the inlet of the aggregate for fuel bypassing.

*** - the measurement of the axial force, acting on the journal and thrust bearing. This measurement is conducted by means of the stress transducers installed in the case of the bearing. This case at the same time is the flange that connects the pumps stages. Eight transducers were installed uniformly around the circumference of the case (Figure 6.10). The flange has a asymmetrical shape and for this reason its stiffness was estimated. This estimation had showed that such form did not effect on the flange stiffness in the transducers mounting zone. The calibration of the transducers was also provided by means of the static loading in the range 0…260 kg. This loading was applied to the wall of the flange;
**** - three-component vibration sensor

Static pressure was measured by means of manometers and inductive pressure transducers with a measurement range from 0 to 6 atm. The following transducers were used (Figure 6.11):

- pressure ICP transducers (with built-in electronic module) - PCB 101A06;
- vibration acceleration ICP transducer – PCB 353B16;
- three-component vibration acceleration ICP transducer – PCB 356B21.

(a) (b)

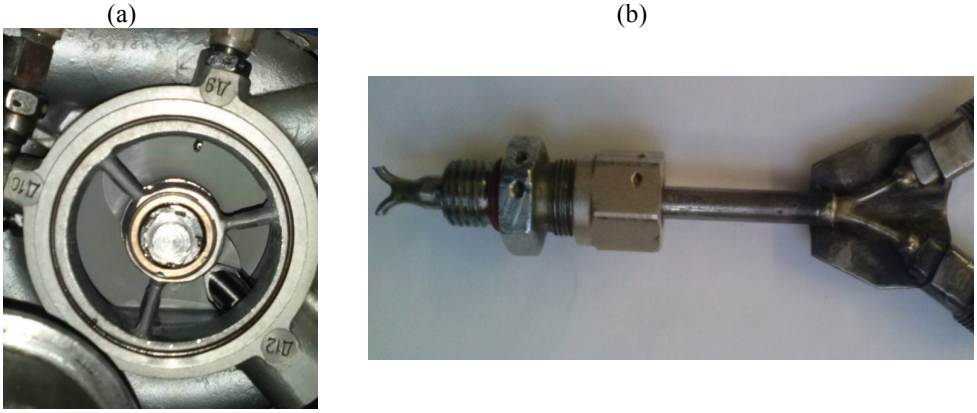

Figure 6.9: The probe for measuring the static pressure at the screw-centrifugal stage inlet
a – the probe near the wall; b –exterior of the probe

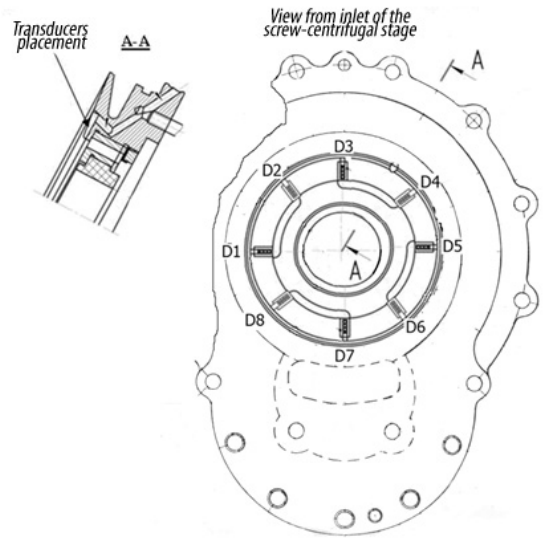

Figure 6.10: Plant layout of strain sensors

(a) (b) (c)

Figure 6.11: Exterior of the transducers
a - pressure ICP transducers; b - vibration acceleration ICP transducer; c - three-component vibration acceleration ICP transducer

The properties of the transducers are shown in the Table 6.4 -

Table 6.6.

Table 6.4: Main properties of the pressure ICP transducers 101A06

Characteristic	Value
Dynamic range	3450 kPa
Sensibility	1.45 mV/kPa
Maximum static pressure	34500 kPa
Resolution	0.07 kPa
Resonance frequency	≥400 kHz
Rise time	$<1.5 \cdot 10^{-6}$ s
Lower frequency	0.01 Hz
Temperature range	-73 up to +135 ^{0}C
Housing material	Stainless steel
Error of measurement	0.5 %

Table 6.5: Main characteristics of the vibration accelerations ICP transducer PCB 353B16

Characteristics	Value
Axial sensibility (±10%)	10 mV/g
Amplitude range	± 500 g
Maximum shock	±10 000 g
Bandwidth	1...10 kHz
Natural frequency (tie-down position)	>70 kHz
Temperature range	-54 up to +121 ^{0}C

Table 6.6: Main characteristics of the three-component vibration accelerations ICP transducer PCB 356B21

Characteristics	Value
Sensibility (±10%)	10 mV/g
Amplitude range	± 500 g
Maximum shock	±10 000 g
Bandwidth of the X axis	2...7 kHz
Bandwidth of the Y and Z axes	2...10 kHz
Natural frequency (tie-down position)	>55 kHz
Temperature range	-54 up to +121 ^{0}C

Table 6.2 shows that rotation frequency as well as flow rate and fuel temperature were estimated visually by means of instruments embedded in the test bench. Data acquisition, measurement and processing were done by means of multi-channel measurement system LMS SCADAS Mobile (Figure 6.13).

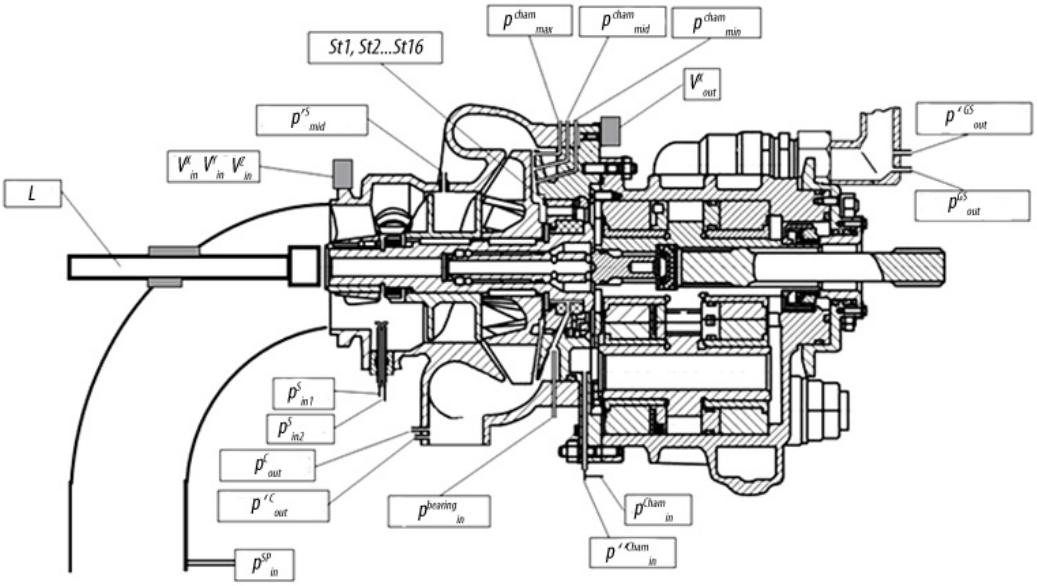

Figure 6.12: Transducers plant layout

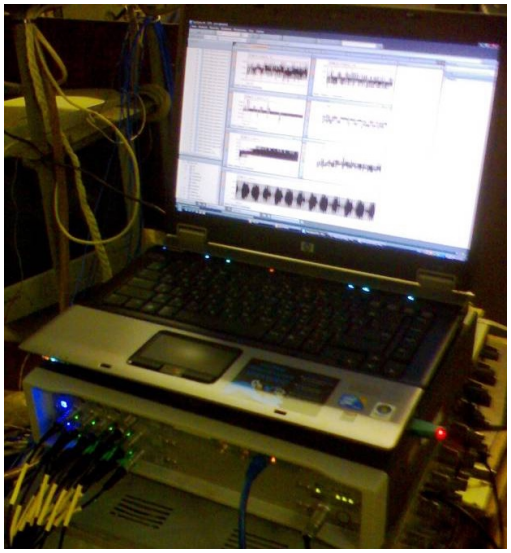

Figure 6.13: Exterior of the LMS SCADAS Mobile

LMS SCADAS Mobile is a unique module analyzer for dynamic signals measurement. It is compatible with different types of transducers. It is able to work with both, a personal computer and as a stand-alone measurement unit. It can be controlled by means of built

in software – LMS Test. Xpress. The main characteristics of LMS SCADAS Mobile are shown in Table 6.7

Table 6.7: Main characteristics of LMS SCADAS Mobile

Characteristics	Value
Channels	24
Maximum channels	40
Sampling frequency	up to 51.2 kHz
Error	±0,2% for 1 kHz
Temperature range	-10…+55 ^{0}C
Compliance to the requirements MIL-STD 810F:	
Vibration and shock	up to 60 g
Humidity	up to 95 %
Taco channels	2
Channels for signals generation (embedded)	2
Connection to personnel computer	Ethernet
Dynamic performances	
Signal-noise ratio	more than 105 dB
Idle dynamic band	more than 138 dB
Total dynamic band	min 170 dB

7 Experimental Investigations of Aircraft Engine Two-stage Pump Loading

7.1 Operational modes and conditions for experimental investigations

Benchmark tests of the pump ND-32 were carried out to investigate the causes of its dynamic loading and to determine the causes of the bearing destructions. The pumps operating conditions consisted of a variety of actual rotational speeds and mass flow rates. Experiments to estimate the loading state of the two-stage pump were conducted on 38 different operating regimes of fuel system. Conducted reliability analysis presented in Chapter 2 allowed to choose the regimes of engine fuel system operation. The operating regimes considered are represented in

Table 7.1. Operation regimes were changing by means of approach described in Chapter 7.1.2.

Table 7.1: Operational regimes

#	N, min^{-1}	G_{in}, kg/s	P_{in}, MPa	p_{out}^{SCS}, MPa	p_{out}^{GS}, MPa	T_F, K	#	N, min^{-1}	G_{in}, kg/s	P_{in}, MPa	p_{out}^{SCS}, MPa	p_{out}^{GS}, MPa	T_F, K
D1	1392	0.80	0.231	0.29	1.95	294	D20	6536	6.34	0.155	1.21	6.75	297
D2	1416	0.95	0.231	0.29	1.95	294	D21	6587	7.16	0.15	1.22	6.5	296
D3	2700	1.03	0.231	0.42	2.1	294	D22	6907	7.33	0.21	1.32	6.5	299
D4	3550	1.75	0.229	0.55	3.6	301	D23	7270	4.36	0.21	1.41	4.8	313
D5	4495	2.05	0.225	0.74	3.73	303	D24	7145	4.45	0.15	1.55	4.7	316
D6	4955	2.26	0.223	0.845	3.83	305	D25	7145	7.43	0.15	1.42	6.45	302
D7	5252	2.29	0.224	0.93	3.9	306	D26	7260	7.43	0.213	1.42	6.45	315
D8	5260	2.39	0.22	0.925	3.9	310	D27	7280	4.22	0.215	1.54	4.5	318
D9	5300	3.04	0.21	0.93	4.2	303	D28	7515	5.11	0.205	1.54	4.25	322
D10	5609	3.17	0.206	1.015	4.4	302	D29	7500	5.41	0.205	1.62	4.7	321
D11	5635	4.25	0.185	0.99	5	297	D30	7335	4.63	0.15	1.63	4.75	320
D12	6350	2.03	0.23	1.24	3.95	339	D31	7990	7.57	0.15	1.5	6.4	303
D13	6190	2.59	0.22	1.18	4.05	326	D32	6988	7.60	0.15	1.75	6.4	303
D14	6190	4.61	0.175	1.155	4.9	298	D33	4313	7.22	0.228	1.375	6.4	303
D15	6414	4.60	0.175	1.225	4.9	298	D34	4308	2.35	0.225	0.7	3.9	313
D16	6414	4.60	0.175	1.225	4.9	298	D35	5011	2.34	0.229	0.7	3.95	316
D17	This is an operational regime when the test bench is accelerating from 0 to N=3500 min^{-1}						D36	5015	2.54	0.229	0.86	3.7	323
D18	6404	4.60	0.222	1.225	4.9	298	D37	5166	2.53	0.229	0.86	3.65	326
D19	6470	2.58	0.15	1.26	4.4	321	D38	5308	2.57	0.229	0.9	3.65	330

7.2 Static and dynamic performances of the two-stage pump

Operation parameters variation during the tests are shown in Figure 7.1 and Figure 7.2. Regimes 1…9 correspond with the regimes of engine starting. Herewith rotational frequency of pump's rotor varied from 1400 to 5300 min^{-1} and the mass flow varied from 0.8 to 3.04 kg/s. Regimes 10…19 correspond with cruise rating of engine. Rotational speed and mass flow varied from 5200 to 6500 min^{-1} and from 2.58 to 4.61 kg/s accordingly. Regimes 20…32 correspond with engine ignition in-flight. Rotational speed and mass flow varied from 6600 to 7000 min^{-1} and from 4.36 to 7.6 kg/s accordingly. The regimes 33…38 are regimes with low flow rate while rotational speed is high.

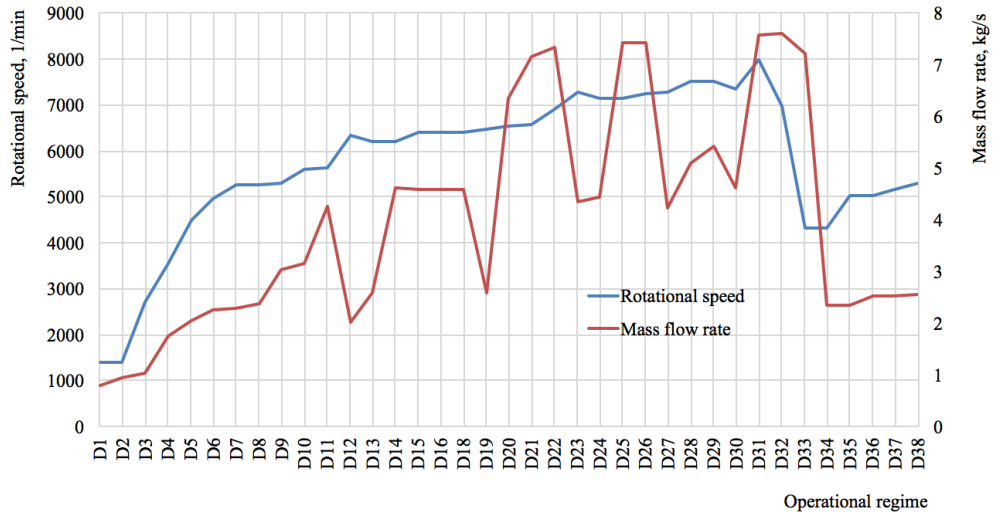

Figure 7.1: Variations of rotational speed and fuel flow rate through the screw-centrifugal stage

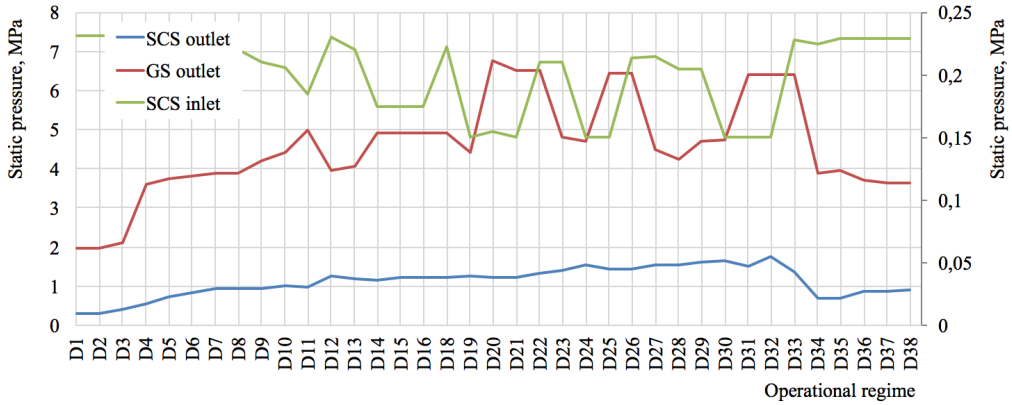

Figure 7.2: Variations of the inlet and outlet pressures at the screw-centrifugal stage and variation of pressure at the gear stage outlet

Figure 7.3 represents the variations of the static pressure distributions after the centrifugal wheel at its different radii: pressure at the wheel maximum radius, r_{max}, pressure at the wheel middle radius, r_{mid}, pressure at the wheel minimum radius, r_{min}. The static pressure in the channel for the bearing lubrication, $p_{in}^{bearing}$ is also represented. This channel is placed after the centrifugal wheel.

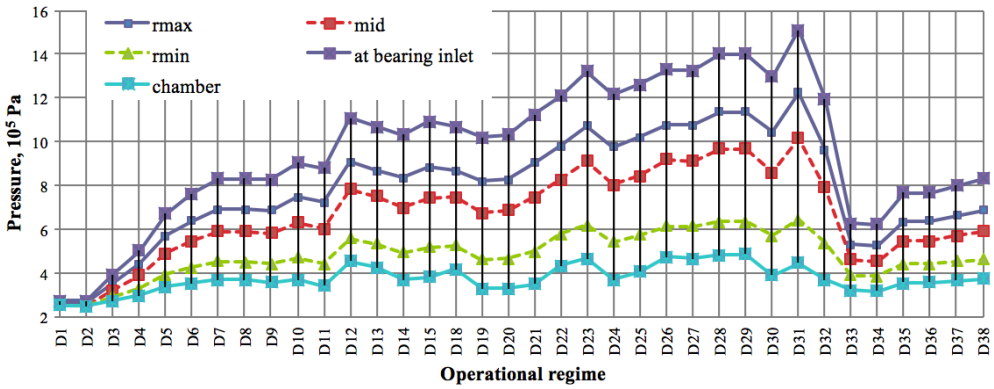

Figure 7.3: Static pressure variations

The pressure on the minimum radius is lower than pressure in the lubricant channel in all operational modes. Pressure in the cavity between the stages was changing insignificantly. Figure 7.3 shows that all fuel supplied for the bearing lubrication should pour out to this cavity.

The analysis of pressure pulsations inside the pump (Figure 7.4) shows that the maximum root-mean-square value of pressure pulsations are in the screw and on the gear stage outlet. These pressure pulsations are intensified with increasing pump rotational speed and can achieve more than 0.2 MPa and 7 MPa correspondingly. The intensity of pressure pulsations in the cavity has a resonant behavior and rose steeply on particular operating regimes up to 0.15 MPa. Figure 7.4 shows that pressure pulsations in the cavity are determined by pressure pulsations in the screw and pressure pulsations caused by the gear stage.

Pressure pulsation and vibration acceleration were estimated with help of RMS amplitude pressure and vibration acceleration fluctuation accordingly. RMS amplitude calculates by means of well-known equation:

$$RMS = \sqrt{\frac{1}{n}\sum_{j=0}^{n-1}\left(y_j\right)^2} \tag{7.1}$$

where n – time intervals per signal sampling time; y_j – value of the parameter's signal on a certain time interval.

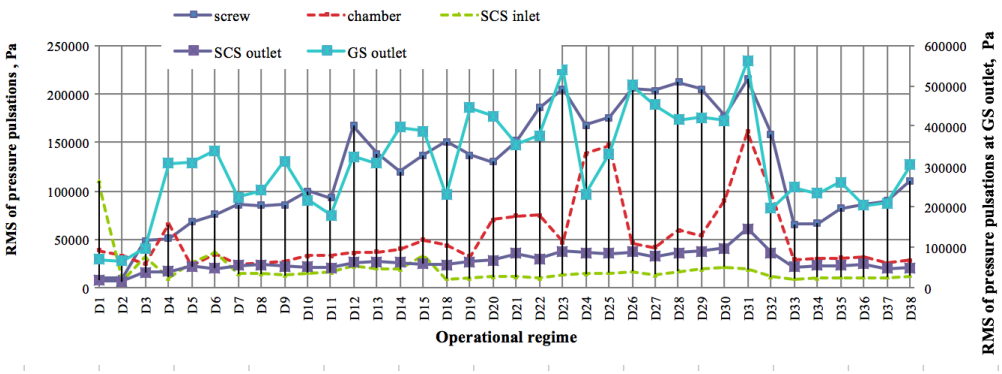

Figure 7.4: Variations of pressure pulsations root-mean-square values

Figure 7.5 represents the dependency graph of screw-centrifugal stage rotor displacement and the strains on the considered bearing on the regime parameter $\frac{G_{in}}{N}$. Positive direction of these variations is the direction to the bearing along to axis of rotation. Stresses were measured by means of 8 stress transducers. The mean value between them was taken to estimate the stress value. Figure 7.5 shows that the variations of bearing stress and rotor displacements variations coincide over the operating regimes changing. This means that the loading source of the considered bearing does in fact have a hydrodynamic nature.

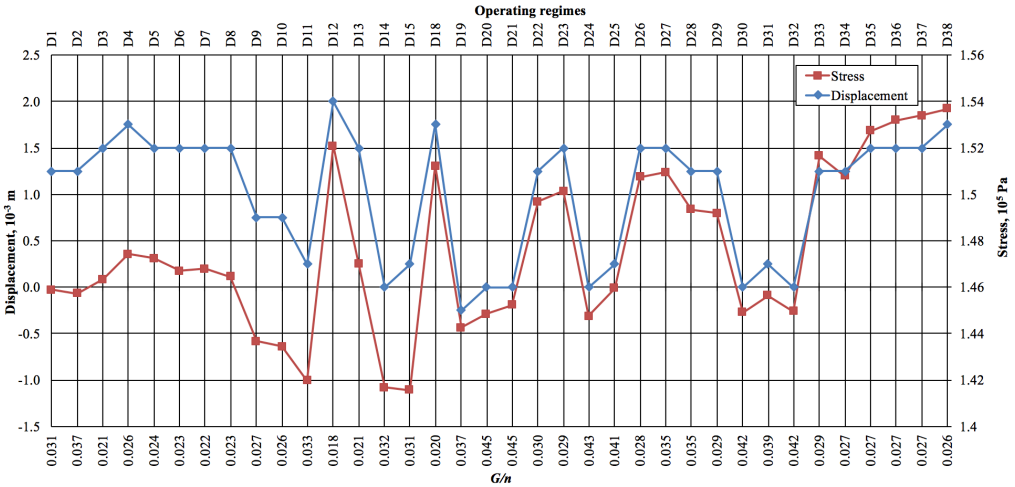

Figure 7.5: Variations of screw-centrifugal stage rotor displacements and stresses on its bearing due to the changing the operating regime parameter

Conducted analysis of pump loading states on different operating regimes has shown that the most unfavorable modes are the modes with a relatively low fuel mass flow rate and high rotational speed. These regimes occur on the flight-idle regime.

Pressure radial distribution at the screw-centrifugal stage inlet was obtained by means of the probe (Figure 7.6). As it can be seen, such pressure distribution leads to non-uniform loading of the screw blades.

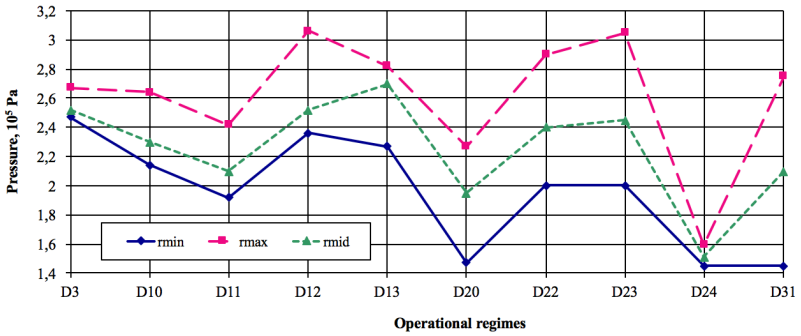

Figure 7.6: Pressure distribution at the screw-centrifugal stage inlet along the radial direction

7.3 Undissolved air influence on pump loading state

Undissolved air influence on the pump loading state was investigated experimentally. The parameters of operating modes for this investigation are shown in the Table 7.2.

Table 7.2: Pump operational regimes

#	N, min^{-1}	Gin, kg/s	P_{in}^{scs}, MPa	P_{out}^{scs}, MPa	P_{out}^{GS} MPa	ΔP_A, MPa
D71	6200	2.687	0.23	1.14	4.1	0
D72	6173	2.582	0.23	1.18	4.05	0.19
D73	6336	4.437	0.23	1.2	5.5	0.4
D74	6500	6.292	0.21	1.2	6.9	0.8
D76	6958	3.750	0.21	1.45	5.2	0.3
D75	6924	3.792	0.21	1.14	5.3	0.47
D77	5027	2.194	0.23	0.865	3.83	0.11
D78	5040	2.194	0.23	0.87	3.9	0.26
D79	5040	2.194	0.23	0.78	3.7	0.44

Air was supplied into the supply pipeline at a distance of 2 m from the inlet to the screw-centrifugal stage. Supply was provided by means of gas pressure reservoir (Figure 7.7).

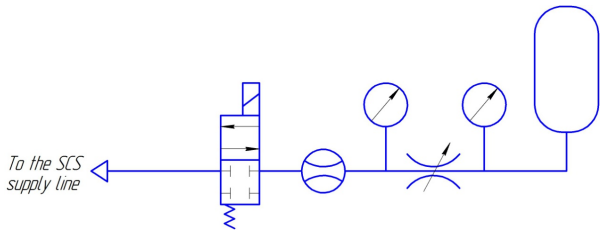

Figure 7.7: Scheme of the air supply

The mean values of stresses on the bearing surface, occurred on different pump operating modes, are shown in Figure 7.8.

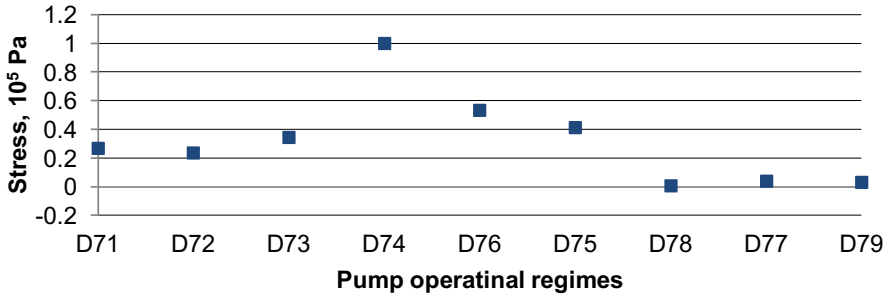

Figure 7.8: Mean values of stresses on the bearing case

The variations of pressure pulsations root-mean-square in different points of pump system are shown in Figure 7.9. Increase of air supply on operating regimes D71 – D73 leads to increasing of stresses on the bearing. Further increasing of air and fuel supply at the same rotational speed leads to decreasing of stresses on the bearing (operating regime D74). Further increasing of air supply only leads to further decreasing of stresses (operating regimes D77 – 79). There is a strong correlation between these obtained results and results which were obtained in papers (Keller, 1983) and (Kurakulin, 1978). Obtained results allow to determine that supply of insignificant amount of air has a stabilazing influence on “pump-pipes”system.

Two sections can be outlained on the graphs of pressure pulsations and vibration variations:

- Initial section. A small amount of air supply leads to sharp increasing of pressure pulsations and vibrations in all sampling points.
- Further increasing of air supply leads to decreasing of pressure pulsations and vibrations in all sampling points. Their RMS values are lower than RMS values obtained during pump operation without air supply.

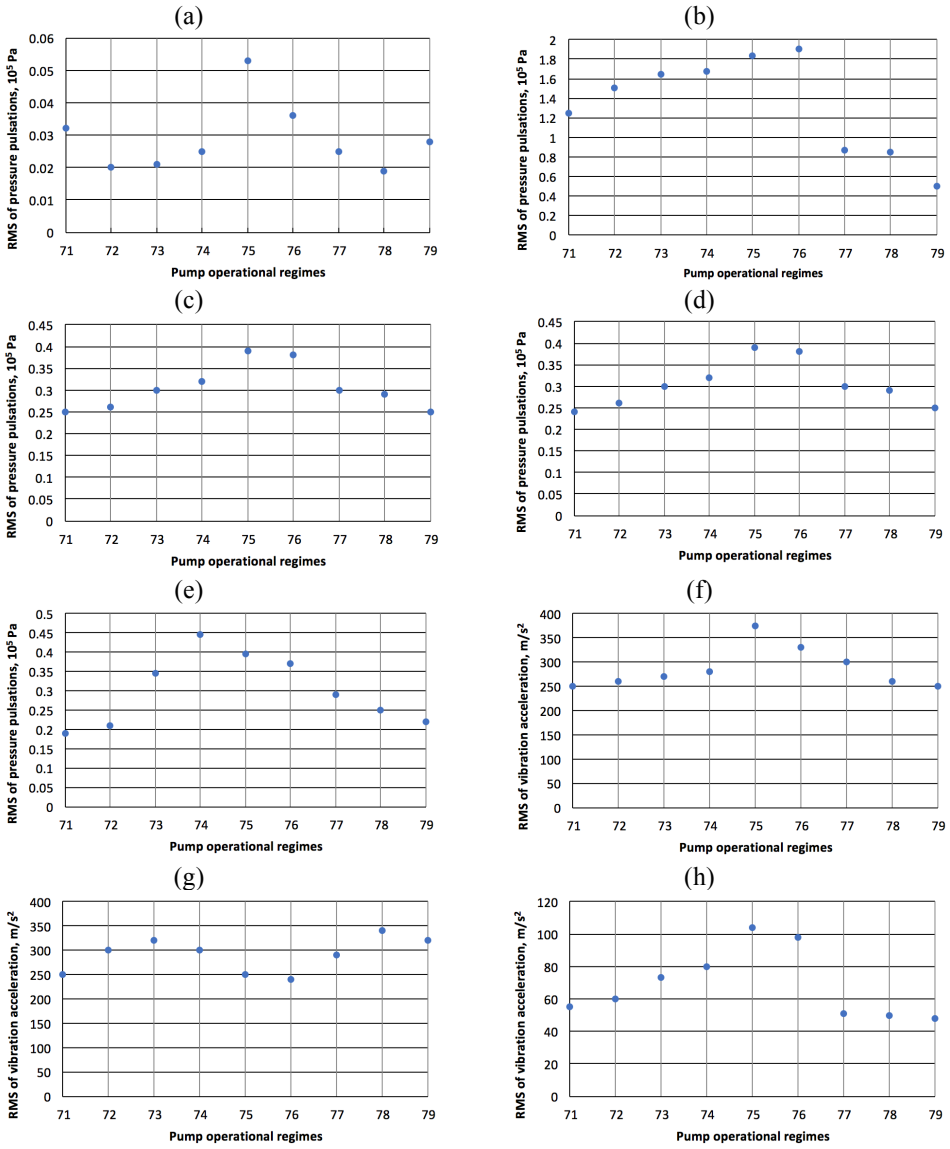

Figure 7.9: Root-mean-square values of pressure pulsations and vibrations at different measurement points

a – pressure pulsations at inlet of the screw-centrifugal stage; b – pressure pulsations at middle of the screw length; c – pressure pulsations at outlet of the screw-centrifugal stage; d – pressure pulsations at cavity between the stages; e – vibration at the flange connecting stages on OX palne; f - vibration at the flange connecting stages on OY palne; g - vibration at the flange connecting stages on OZ palne

Consequently, the increase of the undissolved air volume fraction leads to increases of not only mean values of the axial forces on the bearing, but also to increases of their oscillations. Figure 7.10 - Figure 7.13 show the stress variation on the considered bearing at the same time with the variation of operating regimes (regimes D1 – D38 from

Table 7.1). These figures represent the data obtained by means of stress transducers 1 and 5. They are installed symmetrically relative to the horizontal plane.

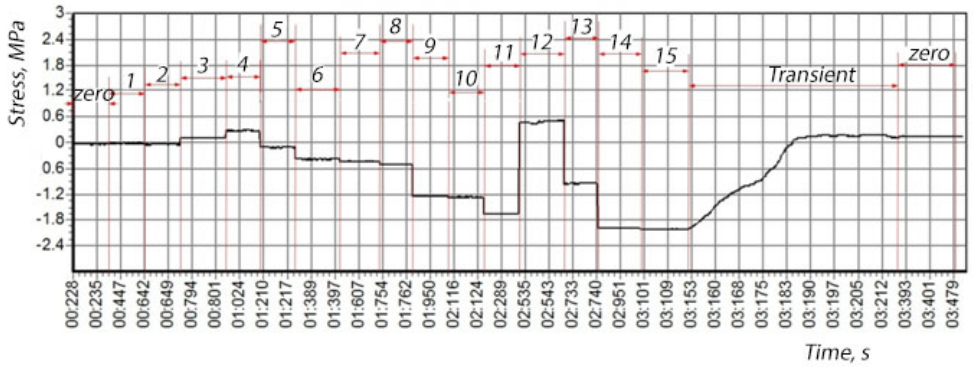

Figure 7.10: Variation of stresses on the bearing. Transducer 1

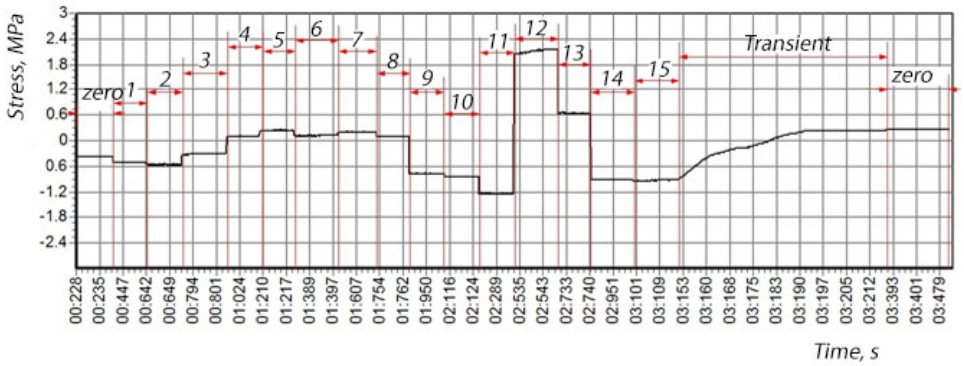

Figure 7.11: Variation of stresses on the bearing. Transducer 5

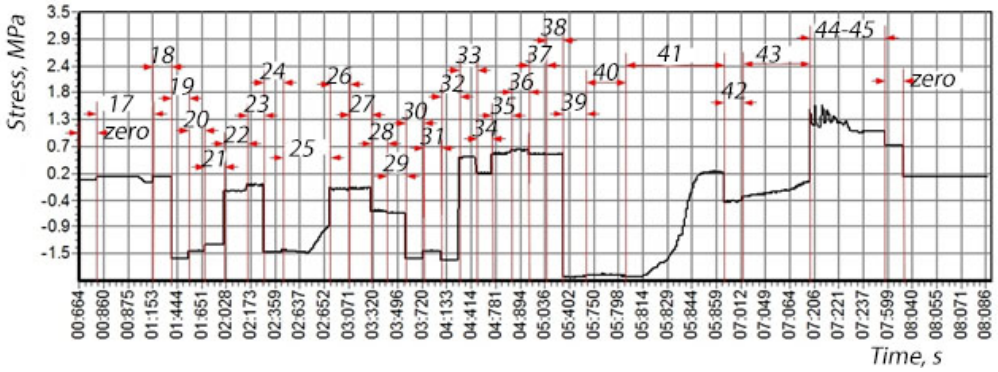

Figure 7.12: Variation of stresses on the bearing. Continuation. Transducer 1

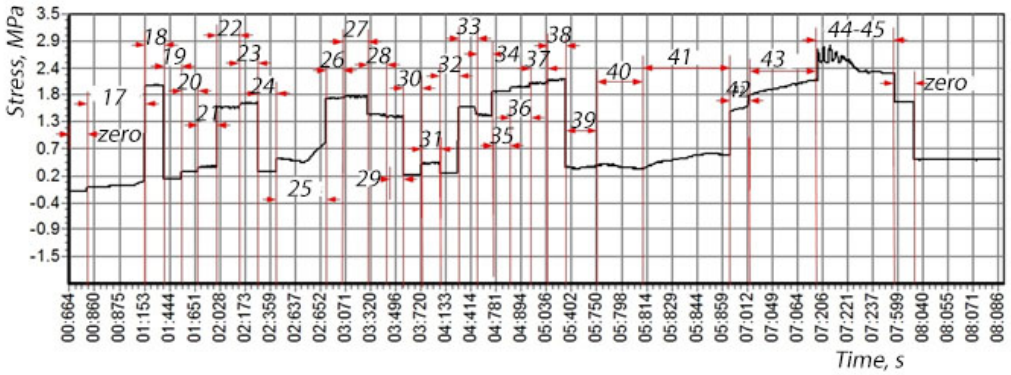

Figure 7.13: Variation of stresses on the bearing. Continuation. Transducer 5

The figures given above allow to conclude that the most loaded operating regimes are steady regimes – D11 – 14, 19, 22, 24, 26, 30, 33 and 39 as well as transient operating regimes – D17, 41, 44-45 (regimes with undissolved air supply). Mean stress values obtained by means of each stress transducer are shown in Table 7.3. These results allow to conclude that bearing loading in cross flow plane is nonuniform. Moreover, in several cases this loading is nonsymmetrical: mean stress values obtained by means of two opposite transducers have different signs. It can lead to flection of the bearing surface. This phenomenon can be explained by fluctuating radial force occurring due to nonsymmetrical pump volute.

Table 7.3: Mean stress values sampling by each transducer

Modes	Stresses, MPa							
	Transducers							
	1	5	2	6	3	7	4	8
11	-1.64	-1.23	-2.31	-0.81	-1.65	-0.28	-0.66	0.02
12	0.49	2.12	0.46	1.73	0.98	1.23	2.27	2.37
13	-0.95	0.65	-0.58	0.47	-0.50	0.42	0.71	1.28
14	-1.99	-0.91	-1.79	-1.22	-1.98	-0.55	-0.85	0.11
17	0.06	0.11	0.13	0.10	0.13	0.10	0.01	0.05
19	-1.60	0.25	-1.20	0.36	-0.97	0.33	-0.25	-0.41
22	-0.21	1.72	-0.04	1.54	0.48	1.87	1.15	0.85
24	-1.47	0.39	-1.12	0.56	-0.97	0.54	-0.11	-0.33
26	-0.17	1.90	0.10	1.58	0.69	2.29	1.52	1.59
30	-1.60	0.33	-1.11	0.45	-1.06	0.71	-0.06	0.18
33	0.47	1.73	0.73	1.39	1.19	2.28	1.78	1.75
39	-1.98	0.48	-1.24	0.65	-1.22	0.90	0.20	0.33
41	-1.26	0.61	-0.57	0.53	-0.32	0.99	0.36	0.69
44-45	1.13	2.56	2.83	1.94	2.48	2.83	2.93	2.75

In such a manner:

- pump acceleration from zero (regime D17) leads to negative stresses on the bearing surface. This illustrates the impact phenomena which takes place inside of the pump;
- all 8 transducers show that there are oscillations of the stresses on the transient operating regime with air supply (D44-45). This may also lead to bearing damage.

More detailed investigations of dissolved air influence on the pump loading state were provided. Parameters of the operating regimes are shown in Table 7.4.

Table 7.4: Boundary conditions

Model	N, min^{-1}	P_{in}^{SCS}, MPa	P_{out}^{SCS}, MPa	G_{in}, kg/s	C_A, %
287	6433	0.19	1.15	4.0711	0
288	6441	0.19	1.15	4.0711	4.0
289	6470	0.19	1.15	4.0711	5.3
290	6420	0.19	1.15	4.7556	6.5

Results obtained showed that supply of dissolved air fraction equal to 4% leads to steep increasing of stresses mean value on the bearing (Figure 7.14). In this case all pump working parameters have not been changed. Increasing of air supply (5.3%) leads to further increasing of stresses on the bearing surface. This figure shows that the character of the loading is changing: lower air fractions lead not only to stress increase but also to their oscillations increase.

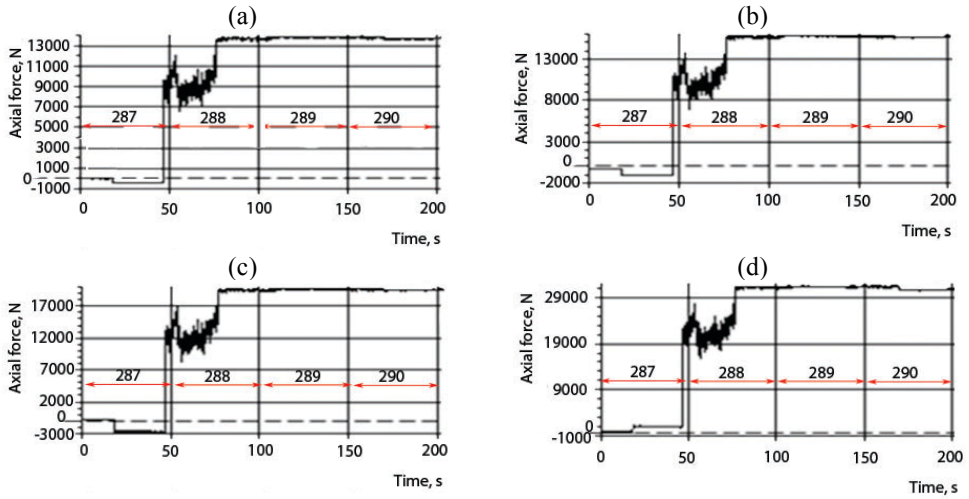

Figure 7.14: Variation of axial force acting on the bearing:
a – mean axial force measured by means of transducers 1-5; b - mean axial force measured by means of transducers 2-6; c - mean axial force measured by means of transducers 3-7; d - mean axial force measured by means of transducers 4-8

Figure 7.15 shows signals from stress transducers while changing the dissolved air supply. It allows to conclude that low air fractions cause step increasing of stresses on the bearing. The same influence of air supply on stresses on the bearing was obtained by means spectrum analysis (Figure 7.16).

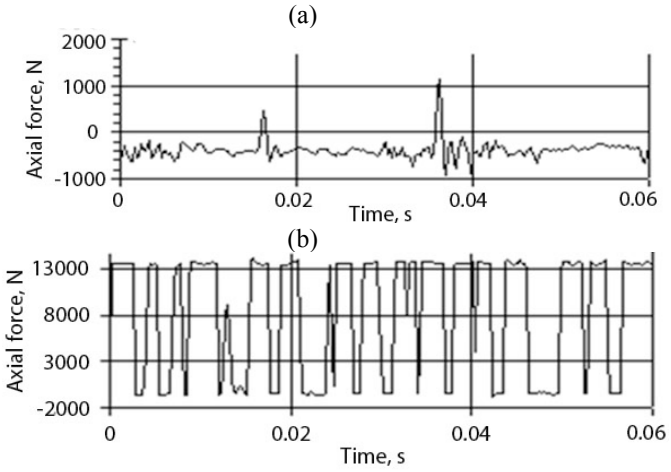

Figure 7.15: Signals of axial force:
a – operating regime 287; b – operating regime 288

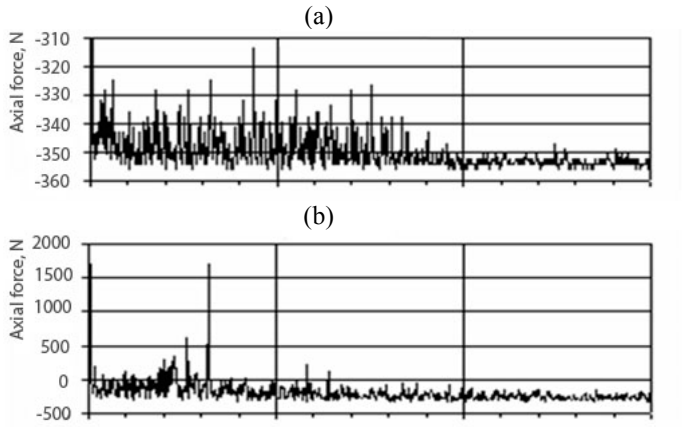

Figure 7.16: Spectrum of axial force acting on the bearing when changing the air supply
a – 287 operating regime; b – 288 operating regime

The pump was disassembled and visually inspected after these experimental investigations. Figure 7.17 a, shows the initial condition of the journal bearing – there were no remarks. The state of the bearing after conducted experiments is shown in Figure 7.17 b and c. The bearing has several damages, the cavitation wear on the inner edge and

circumferential marks on the internal diameter. The results of the journal-and-thrust bearing strain-measurements show that the axial force, occurring on the bearing end face significantly increases due to the air supply. Variable force is the main cause of the considered bearing destructions.

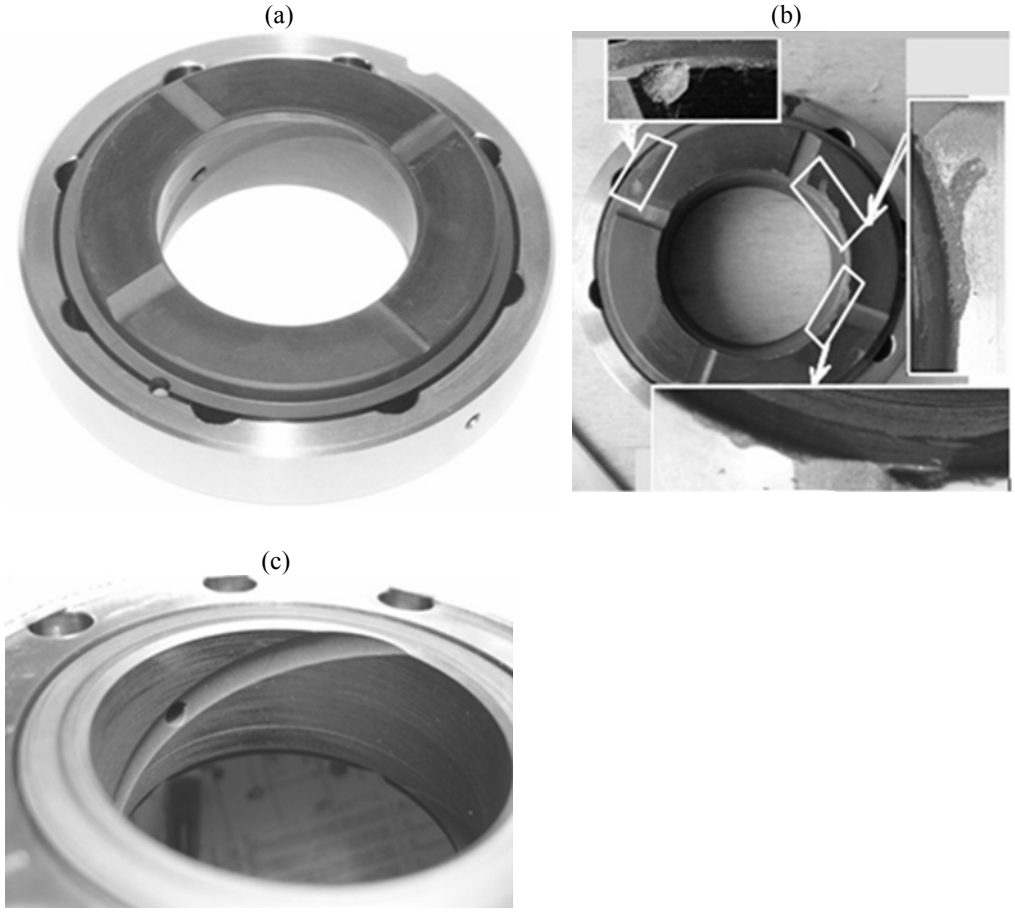

Figure 7.17: Photos of journal bearing state
a – initial condition; b – cavitation wear on the inner edge; c – circumferential marks on the internal diameter

7.4 Acoustic visualization of cavitation in fuel two-stage pump

The acoustic pump field was analyzed for its nominal and cavitation modes in order to evaluate the pump noise dependence on the cavitation processes. The cavitation mode was provided by means of decreasing of mass flow rate through the SCS. The parameters of the operational modes are presented in Table 7.5.

Table 7.5: The studied pump work modes

Operation mode	Nominal mode	Cavitation mode
Gear pump inlet pressure, Pa	$2.0 \cdot 10^5$	$0.18 \cdot 10^5$
N, min^{-1}	500; 1500	
K_{CAV}	9.08	3.46

Operation modes have various cavitation numbers which were estimated as follows:

$$K_{CAV} = \frac{p_{in} - p_{vap}}{\rho \cdot \upsilon^2 / 2}, \tag{7.2}$$

where p_{vap} stand for saturated vapor pressure.

The sound sources were localized by using the beamforming principle. For these purposes, acoustic camera Norsonic (Nor 848) was used (Igolkin, 2012). The plots represent the sound pressure levels for the nominal pump mode (Figure 7.18 and Figure 7.20) and cavitation mode (Figure 7.19 and Figure 7.21). The special attention was given to the 1st fundamental harmonic frequency of the pump unit. Cavitation causes a considerable increase of sound pressure level (Figure 7.18 and Figure 7.19). The same phenomena were observed from Figure 7.20 and Figure 7.21.

There are two sources of cavitation noise: the flow pressure oscillations and the vapour bubble fluctuations (Lyamshev, 1969). Thus, the cavitation leads to the appearance of additional noise sources and it can be estimated by the difference in noise levels. Previously obtained results showed that increasing of the rotational speed at the constant mass flow rate leads to pressure drop at the leading edge of the screw blade. Such pressure drop at low mass flow rate leads to cavitation occurrence. The cavitation noise has the discrete behavior, considerably depending on the cavitation level. The partial cavitation characteristic trait is the considerable increase of the second fundamental harmonic amplitude in relation to the first fundamental harmonic. The fully-developed cavitation is characterized by a considerable amplitude decrease in both fundamental harmonics. In such a manner, acoustic field can be used to develop the diagnostic cavitation properties.

The provided research has shown that the beamforming method is applicable for the acoustic pump cavitation detection. This method requires less working time than the commonly used direct acoustic intensity measurement method (Chudina, 2012). A significant advantage of the beamforming technique is that it can image distant sources as well as moving sources. It is also possible to get quantitative measures of the sound power radiated by the source. However, beamforming has the disadvantage of poor spatial resolution of noise source locations, especially at low frequencies. In this case additional manipulations are required to precisely determine the location of the cavitation zone.

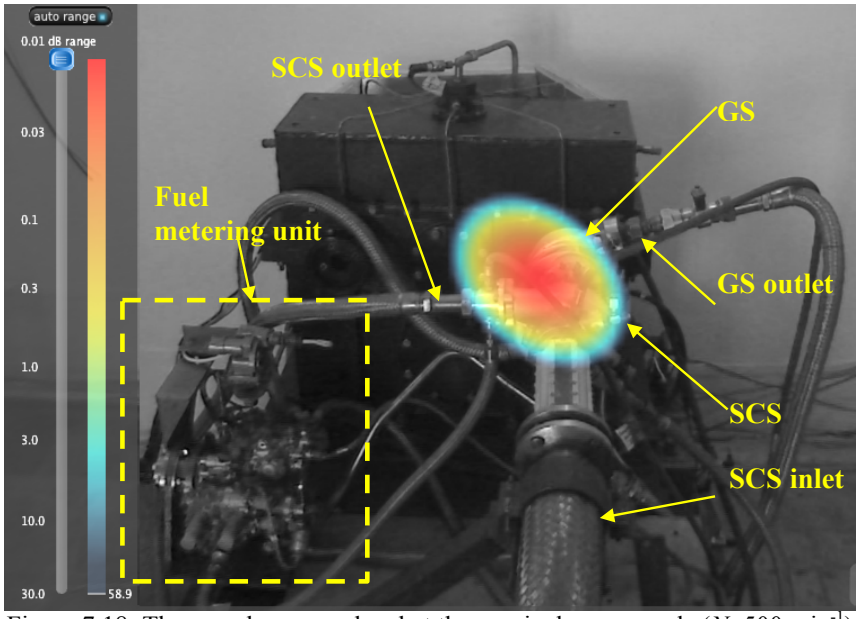

Figure 7.18: The sound pressure level at the nominal pump mode (N=500 min^{-1})

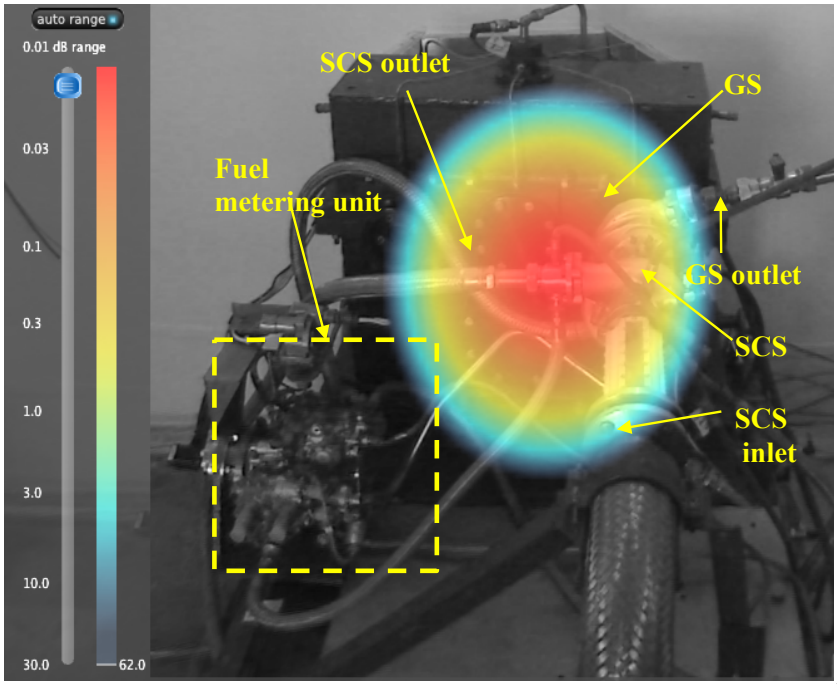

Figure 7.19: The sound pressure level at the cavitation pump mode (N=500 min^{-1})

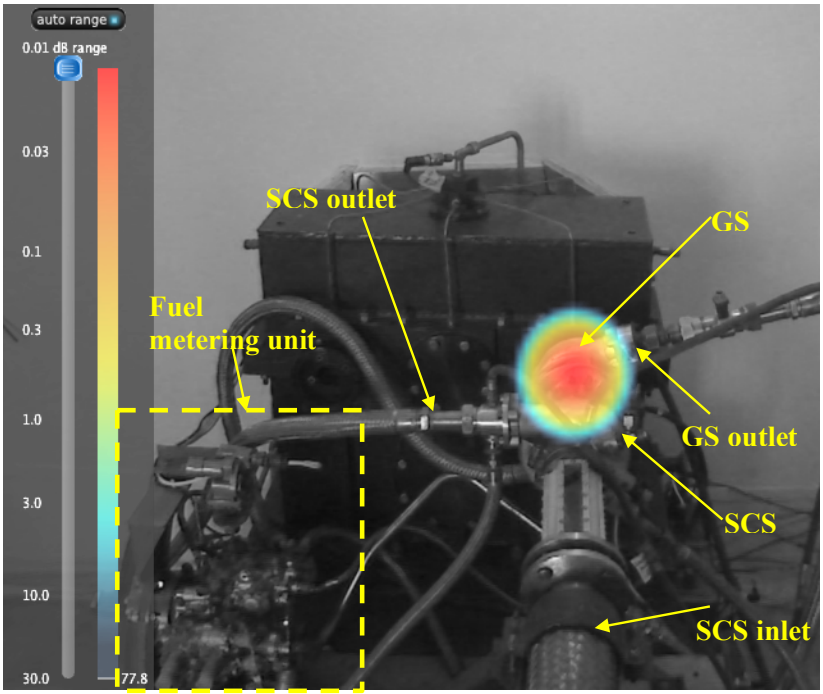

Figure 7.20: The sound pressure level at the nominal pump mode (N=1500 min^{-1})

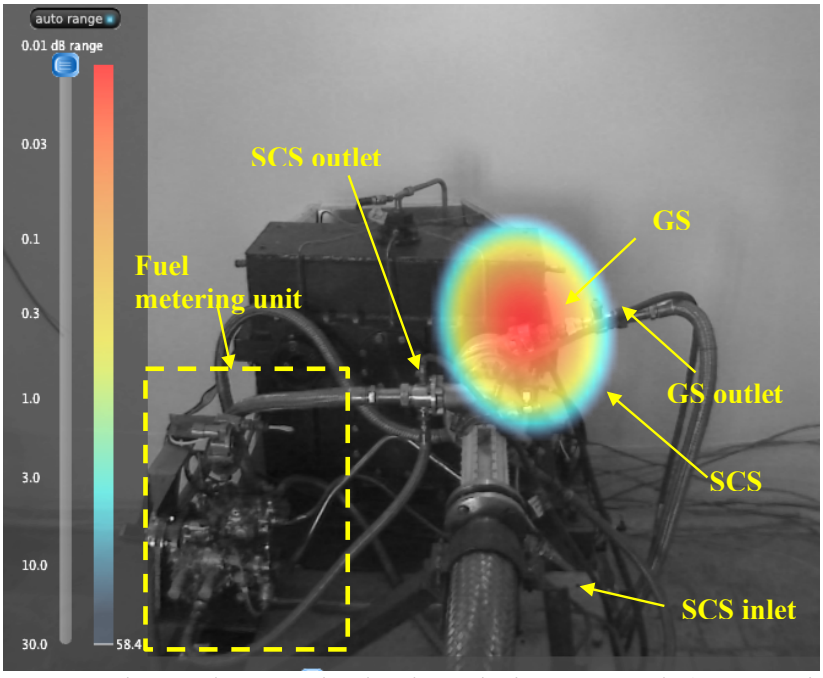

Figure 7.21: The sound pressure level at the cavitation pump mode (N=1500 min^{-1})

8 Design and experimental study of improved two-stage pumps

8.1 Methods and designs for decreasing dynamic loading of aircraft engine fuel pump

High-pressure pumps use compensators of the radial clearances for preventing the leakages. This limits the boundaries of the high pressure zone up to the pump, decreasing space scale. Consequently, it leads to decrease of the static loads on the gear bearings, increase of the pump volume efficiency, and, as a result, increases its operational life. A cone installation before the screw blades helps to reduce the influence of back vortices. A variable screw pith helps to decrease the intensity of cavitation processes. This leads to decrease of angles of attack and as a result to increase the regime parameter, q. Moreover, the following construction methods can be proposed for the screw:

- the implementation of the rational construction form of the screw leading edges;
- drilling the holes at the inlet zones of the screw zones;
- increasing the screw blades surfaces finish;
- increasing the number of screw blades.

All these methods have approved themselves during experimental investigations carried out for prevention of cavitation.

Additional design method for an axial flow pump has been proposed in (Anon., 1993), according to which the chamfers having a circular form should be produced on the pressure side of the screw vanes. Abramov et al. (Abramov, 1993) proposed an interesting form of the screw blades. Screw contains the hub and the spiral blades with profiled edges. These edges have a saw-tooth configuration. The vertices and dedendums of the teeth are placed on coaxial circles. The centres of these circus coincide and located at screw axis. The difference between radii of circus is constant. Such profile of leading edges allows dividing the cavitation cavity on the suction side of a screw into a series of small cavities. This results in increase of system stability in relation to the self-oscillations of the cavitation. The leading edge of the screw can also be profiled as shown in the study of Shcherbatenko (Shcherbatenko, 1980). The leading edge is profiled on the suction side and has a spiral plate fabricated from porous material. When fluid flow meets the screw blade, a low-pressure zone is formed on a suction side of the leading edge. This pressure depends on the distance to the screw centre of rotation: the greater the distance, the greater is the pressure drop. This explains why the cavitation is initially generated on the periphery of the screw. Fluid flows to the wheel inlet through a clearance and then into the blade channels. After that, the pressure is increased by the blades. The produced pressure helps the fluid to penetrate through porous plate into the cavitation zone. It results in pressure increase within this zone. Eventually this allows prevention of the cavitation as its generation conditions are violated. In addition, the fluid penetrating

through the plate acts as a hydrodynamic lubrication, and, as a result, decreases the hydrodynamic losses caused by the drag. Additionally, the design of the leading edge allows increasing the pressure at the screw periphery zone and thereby eliminating the cavitation. Article of Kozlov (Kozlov, 1988) presents a method for increasing the efficiency of the screw-centrifugal pump and decreasing the oscillations of the axial force. Fluid flows though the screw and centrifugal wheel and is then directed to the consumer. Flow around the screw hub induces the back eddies at the pump inlet. The pressure difference between pump outlet and inlet induces the axial force. Fluid flow from channels into the supply line reduces this pressure drop. The cylindrical holes in the hub prevent the negative influence of the fluid head dynamic component. This results in decrease of the axial force oscillations. Uniform spacing of the holes in a circumferential direction allows breaking and prevent the back eddies. The ratio of the holes total width and width of the blade channels should be less than 0.6 to provide efficient influence on reduction of the back eddies. Experimental investigations showed that this design method allows to increase the pump efficiency up to 2 %. Lyashchenko (Lyashchenko, 1981) describes a design method for increasing the anti-cavitation and vibroacoutic performances of the screw-centrifugal pump to increase its efficiency. The pump has an intake pipe with orifices placed over its entire area. These orifices have different sizes and are connected with a high-pressure fluid source. Their flow cross-sections decrease in a direction from inlet blades to outlet proportionally to the pump head. Fluid from the cavity enters to the screw through the channel and orifices. Then it penetrates the clearance and is distributed along the inlet edges where the pressure is low. A supply of the liquid decreases in the direction towards the trailing edges proportional to the pump head. This allows to reduce the cavitation at the pump inlet section.

Several construction measures were already performed to redistribute the static pressure field in the aircraft engine two-stage pump ND-32 aimed to fix the rotor in axial direction. A spring was installed on the shaft from the pump entrance side. It should have clamped down the shaft to the bearing with a strain 50 N. However, this measure did not eliminate the bearing defect. Resonance phenomena are known to occur due to coincidence of gear teeth number and impeller blades number. A number of impeller blades of pumps ND-25 and ND-32 was changed from 11 to 9 during the redesign processes described in paper (OJSC "Scintific and production enterprice "Temp" named after F.Korotkov", 1990). At that, the spring pressing force was increased up to 500 N. The vibroacoutic state of the redesign pump constructions did not differ from their basic constructions. Several operating regimes of the redesign pumps were accompanied by increased vibrations in 2 times in comparison with the basic pump design in area of the two-stage pumps and accessory gear box connection. At that, vibration overload decreasing of supply line flange in 9…62 % at the stage inlet static pressure equal to 0.1 MPa. There were no variations between designs at screw-centrifugal stage inlet pressure 0.3 MPa. The maximum decreasing of pressure pulsation was by 9…14 %. Still, the main component of the oscillation spectrum was gear teeth frequency which amplitude had changed negligible. In such a manner, the hypothesis of pump dynamic loading due to coincidence of the teeth and blade numbers was not confirmed. The similar conclusion was obtained in work (Chebayevskiy, 1973). This paper shows that screw cascade solidity and the

number of its blades does not effect on the flow parameters. Experimental analysis of influence of several factors on the axial loading stage of the two-stage pump bearing was conducted in research (OJSC "Scintific and production enterprice "Temp" named after F.Korotkov", 1990). During these experiments, the mode connection between stages was being changed. These manipulations resulted in changes of the static force distribution. The maximum axial force equal to 1.8 kN was registered in case without the centrifugal wheel, while minimum axial force, 0.45 kN, was obtained in case without the screw. These facts indicate that the screw plays a vital role in axial loading of the bearing.

However, the literature overview conducted did not propose the methods for reducing the back eddies occurring due to the drain and by-pass pipelines influence. In the basic design of the considered pump, the radial blades are installed to prevent the back vortex at the inlet (Figure 8.1).

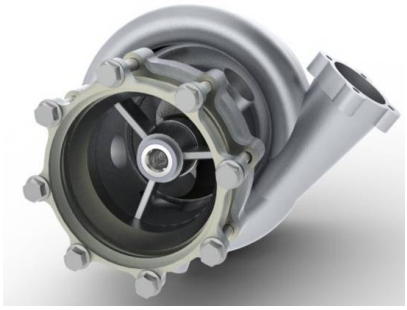

Figure 8.1: Basic construction of the pump ND-32

The following construction redesigns were proposed to decrease the dynamic loading of the whole pump:
1. Transfer of the drain pipelines to 3 m. from the inlet to supply pipeline (Figure 8.2). Whole flow rate from the drain pipelines flows directly to the supply manifold.

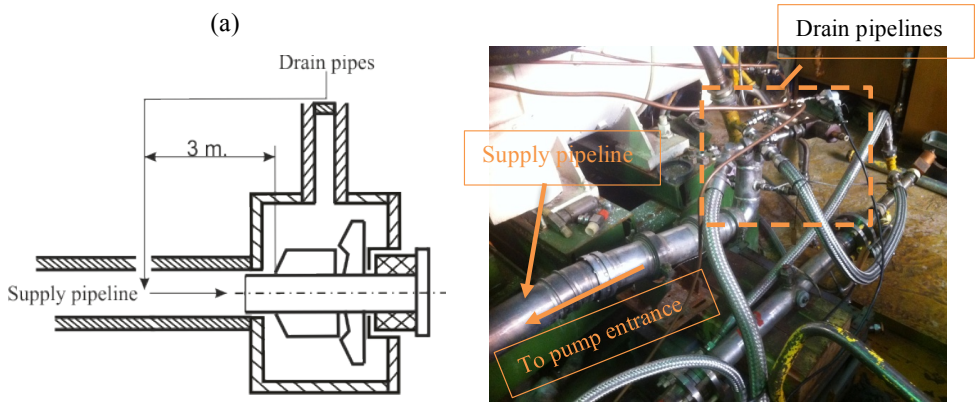

Figure 8.2: Transfer the drain pipelines to supply line

2. Increasing the number of radial blades from 3 to 6 and installing the cylindrical detail with orifices (Figure 8.3). At that, an axial gap is formed between rear end-face of the

detail and volute. The value of the gap is 3 mm. Cylindrical detail is installed instead of the front support. It required changing the inner geometry of the pump inlet, thus the front support was removed. The cylindrical detail has a flange and six radial blades at its inlet section. The detail has also two rows of orifices with diameters of 5 and 4 mm. The total number of orifices is 60. This detail is supposed to prevent the back eddies formation at the inlet of the pump by means of dividing the flow from drain pipelines into a series of small streams. Six blades allow to stabilize the main flow from the supply pipelines. The resistance of the gap equals the resistance of the orifices.

(a) (b)

Figure 8.3: The outward appearance of the cylindrical detail (a) and the modified pump with installed cylindrical detail (b)

3. Adding to the second proposed design the ring-detail for closing the axial gap between the cylindrical detail and the volute. It results in liquid flowing direct from drain pipelines into supply pipelines through orifices in the cylindrical detail.

Figure 8.4: Cylindrical detail with the ring-detail

4. Adding to the third proposed design the cowl. This cowl closes the axial hole in the shaft of the pump rotor. It leads to preventing of pouring out of high-frequency leakages from the gear stage (Figure 8.5). Besides closing the axial hole, the cowl allows to improve the screw flow.

Figure 8.5: The construction of the pump with installed cylindrical detail, ring and cowl

The proposed designs focus on the decrease of the vibration and pulsation loading of the two-stage pump, and, as a result, to decrease the loading of the bearing.

8.2 Experimantal investigations of the proposed pump designs efficiency

Experimental investigations were also carried out to estimate the proposed designs. Operating regimes are shown in

Table 7.1. Figure 8.6 presents the variation of the pump rotational speed and mass flow rate on the investigated operating regimes for all pump designs. It can be seen that pump head insignificantly decreases by 0.05…0.2 MPa with simultaneous increase of pump effectiveness by 0.55 - 1.11 kg/s. These variations remain in tolerance limits of the characteristics. This phenomenon is caused by the increase of the number of radial blades from 3 to 6.

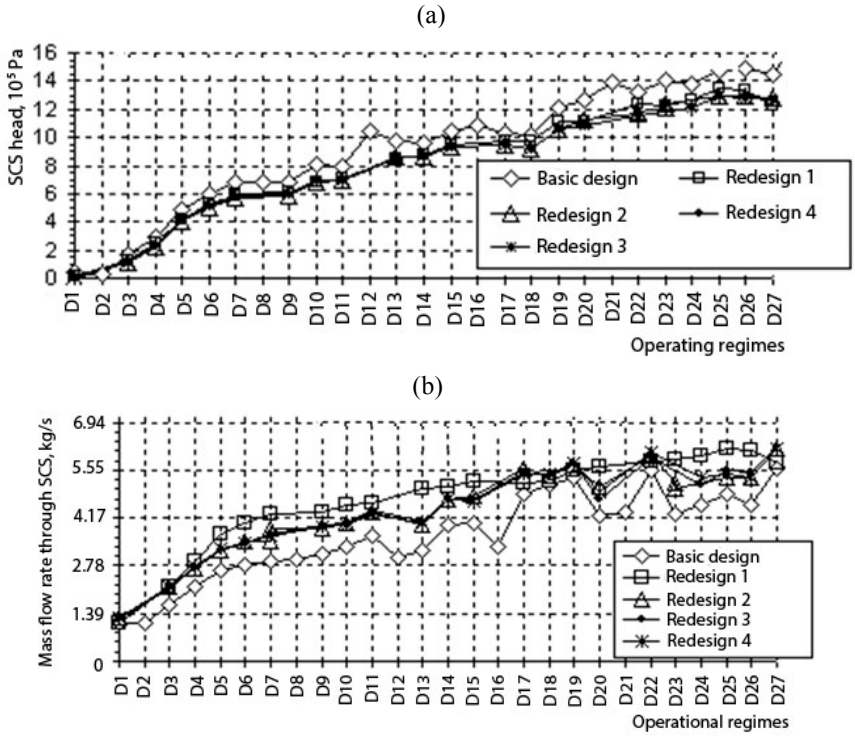

Figure 8.6: Pump performances variation for its different designs

8.2.1 **Static pressure**

Figure 8.7 and Figure 8.8 show the dependence between static pressure, measured at inlet and delivery pipelines, and operating regimes for different pump configurations. These pictures illustrate proposed redesigns that lead to static pressure increase at pump inlet (at lower regimes pressure buildup is 5-10%, at higher regimes – up to 96%). At the same time, both, the negligible drop of static pressure at the pump outlet and the drop at delivery head (about 0.05 – 0.2 MPa) relative to basic pump design were obtained. It is largely due to pump entrance being obscured by enhanced number of guide vanes.

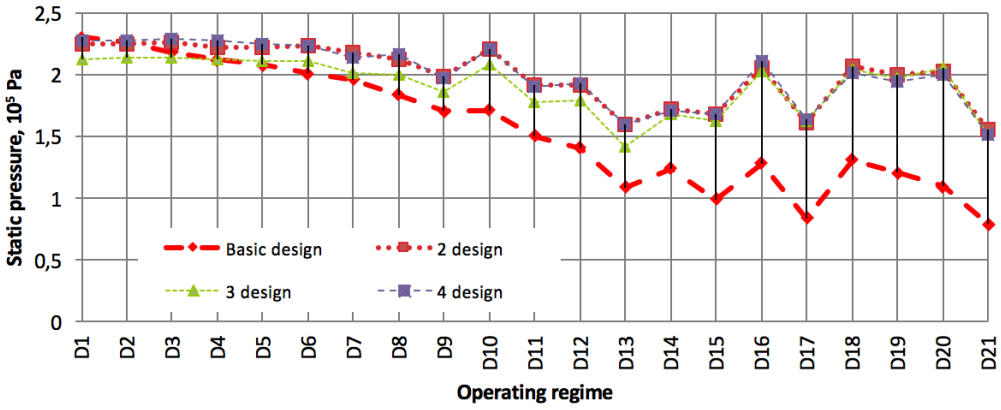

Figure 8.7: Mean values of static pressure at inlet of the designs

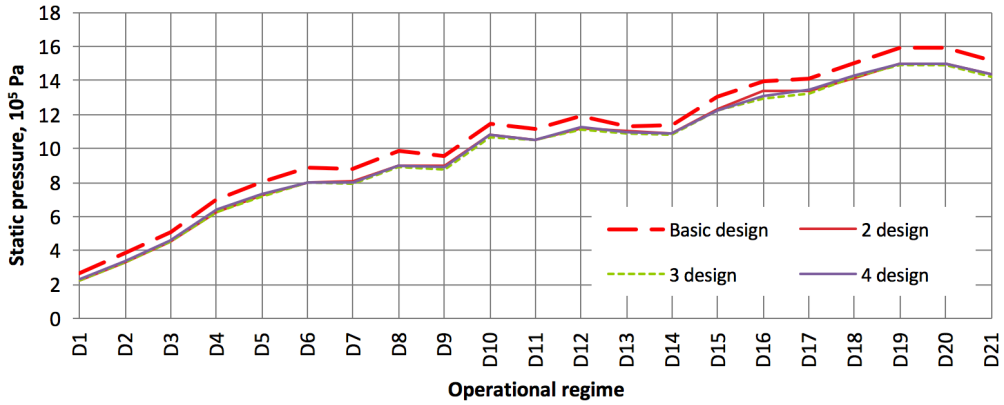

Figure 8.8: Mean values of static pressure at outlet of the designs

Figure 8.9 shows static pressure change at the chamber that situates between pump stages. Leakages from gear stage pour into this chamber. Pressure behavior in it characterizes conditions for bearing lubrication as they are determined by pressure difference between this chamber and the outlet of the centrifugal wheel. In basic design, this pot is connected with entrance of screw centrifugal stage by means of shaft internal diameter and through series of holes in bearing case. At the fourth pump redesign the inlet to shaft internal diameter was closed. The final pump redesign (screen, spinner and without the gap) gave the maximum pressure drop of 1.2 time at regimes increased mass flow.

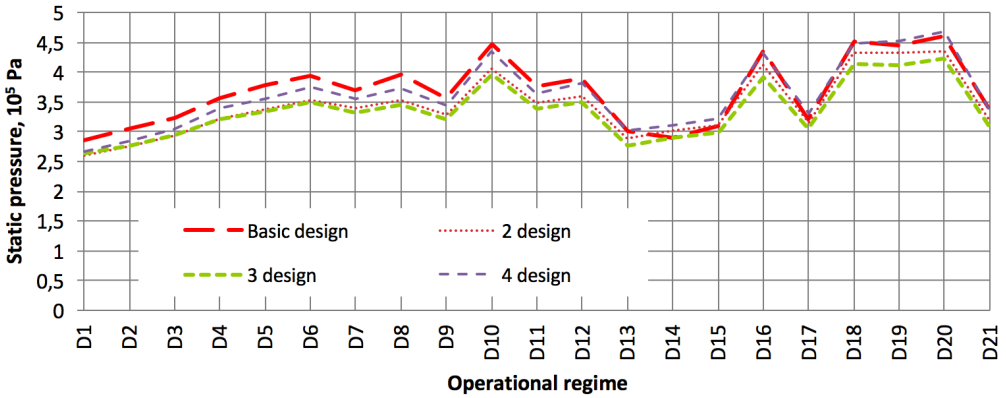

Figure 8.9: Variation of static pressure in the chamber between stages

Figure 9.14 shows the variations of static pressure that was measured by the pressure probe. These variations were measured for all described designs. Operating regimes were equal.

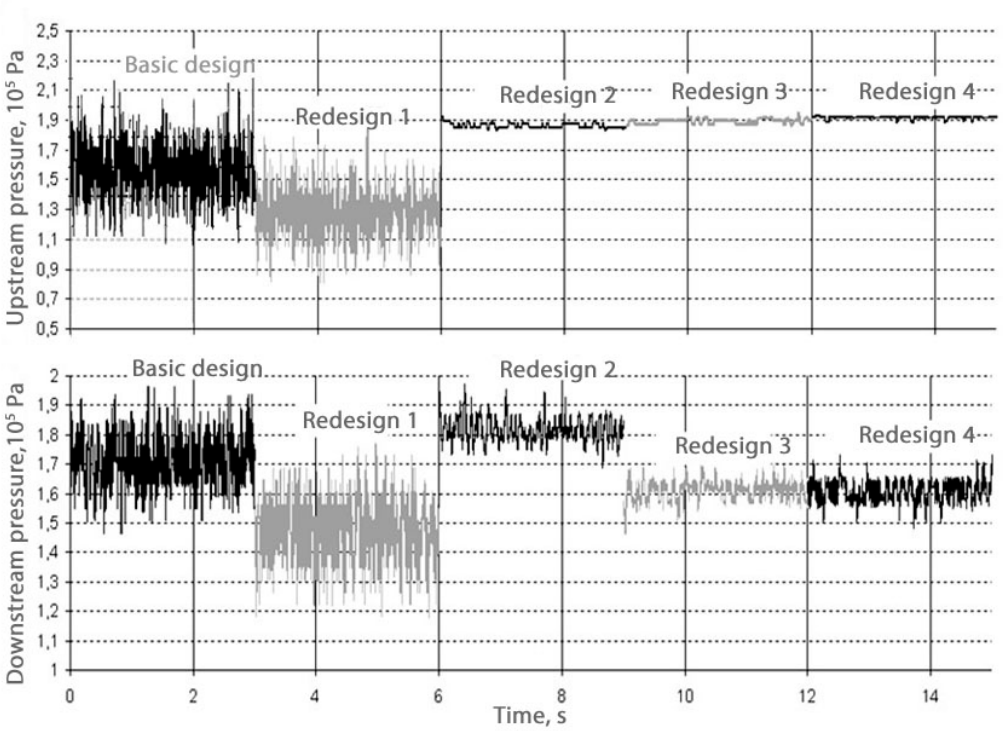

Figure 8.10: Variations of pressure pulsations measured by the probe for the equal operating regimes of proposed pump designs

Cylindrical detail decreases low-frequency pressure pulsations at the pump inlet. The intensity of back eddies measured downstream was also reduced from 0.09 MPa to almost 0. In case of upstream measurement, intensity was reduced from 0.045 MPa to 0.012 MPa. In basic design, the upstream pressure is lower than the downstream pressure. It leads to back eddies formation at the pump inlet. This figure also shows that the relocation of drain pipelines does not result in preventing of back eddies. However, cylindrical detail leads to increase of upstream pressure, and, as a result, to prevention of back eddies. The pressure difference is 0.01…0.025 MPa. The most effective design is the final design with cylindrical detail, ring and cowl. In case of this design, the pressure difference is the highest.

8.2.2 **Pressure pulsations**

Figure 8.11 shows the variation of pressure pulsations at the supply pipeline. Amplitude of pressure pulsations is observed to decrease by 20…45%.

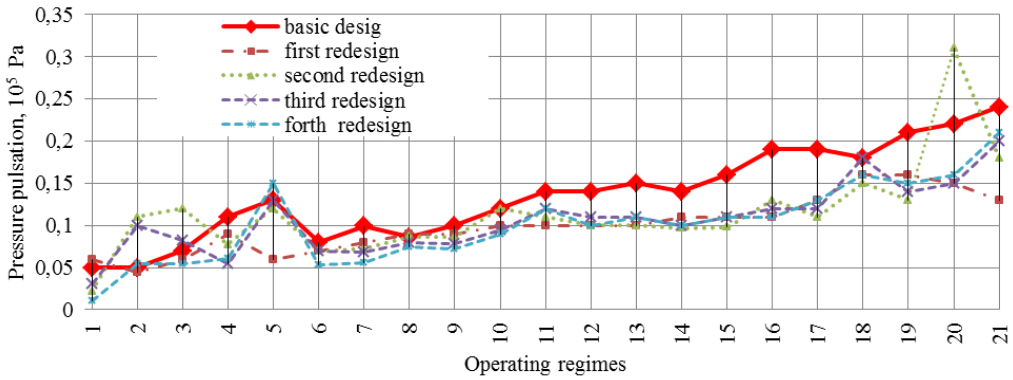

Figure 8.11: Pressure pulsations in the supply pipeline at the distance of 0.6 m from the pump inlet

Changing of the pump designs does not affect significantly the pressure pulsations at the outlet of the screw-centrifugal stage (Figure 8.12). As shown earlier, the pressure oscillations occurred in the pump entrance, in the screw and the centrifugal wheels, in the section behind centrifugal wheel that causes additional pump loading. The results show that the pressure oscillations are almost constant and reach 0.01…0.06 MPa when static pressure is 0.26…0.35 MPa at lower pump regimes. At higher regimes it reaches 0.07…0.11 MPa and 0.36…0.45 MPa, accordingly. Herewith pressure oscillations in chamber between stages are mostly dependant on mass flow rate (Figure 8.14).

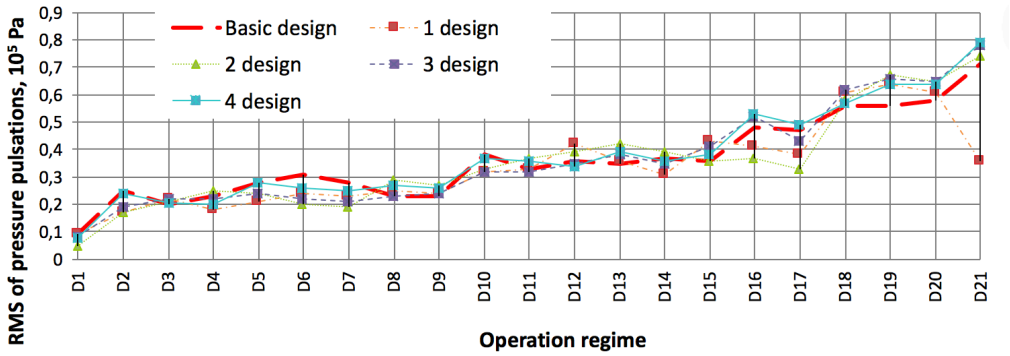

Figure 8.12: Pressure pulsations at the outlet of screw-centrifugal stage

Pressure pulsations in the drain pipeline of the fuel metering unit do not change significantly (Figure 8.13). Their mean value is 0.1 – 0.15 MPa on the whole range of operating modes. Thus, decreasing of flow rate through the fuel metering unit leads to their increasing by 0.01…0.05 MPa. The design of the pump when all of the drain pipelines were transferred to the supply pipeline has the highest level of pressure pulsations in this pipeline. It is higher by 1.3…3 times in comparison to mean values obtained in other pump designs.

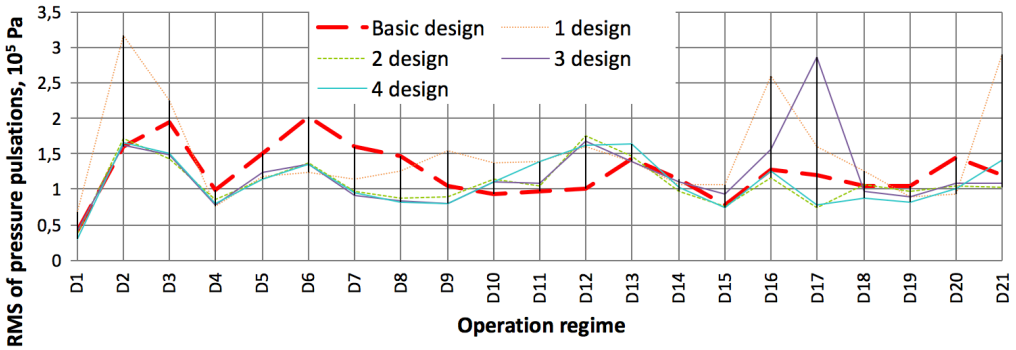

Figure 8.13: Pressure pulsations in the drain pipeline of the fuel metering unit

Influence of pump design variation on level of pressure pulsations at outlet of the gear stage was not detected (Figure 8.14). Only general increase of RMS of pressure pulsations caused by operating modes was observed.

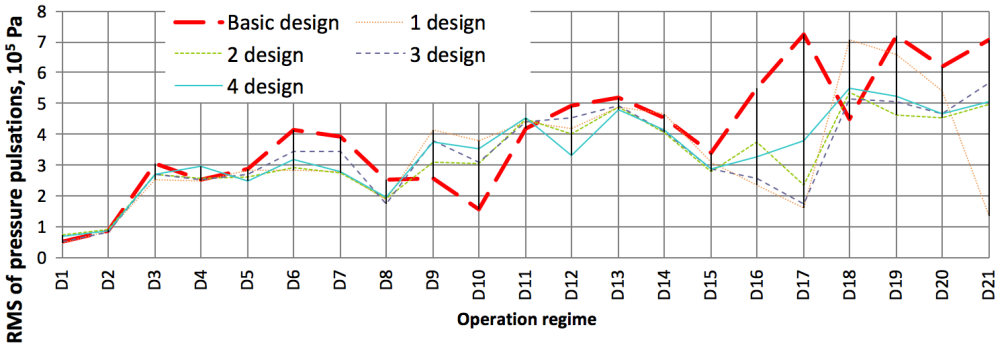

Figure 8.14: Pressure pulsations at the outlet of gear stage

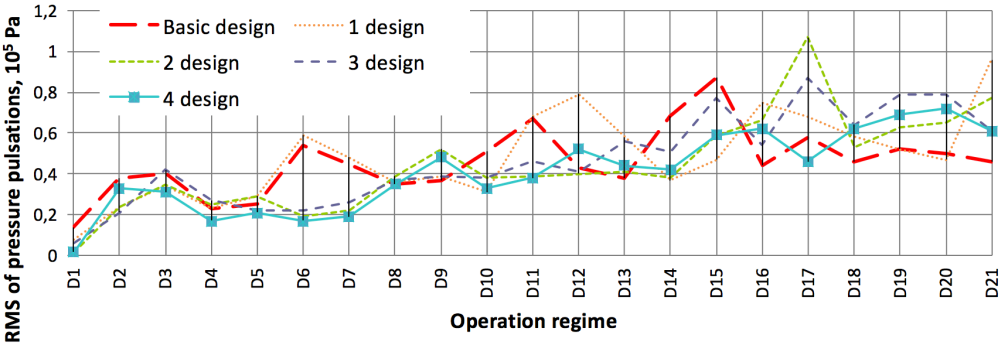

Figure 8.15: Pressure pulsations in the chamber between stages

8.2.3 **Stresses**

The variation of mean values of stresses on the bearing is shown in Figure 8.16. This variation was obtained by means of the 8 stress transducers. Pump redesign has shown to allow to decrease the mean value of stresses on the considered bearing. Herewith, decrease of flow rate leads to increase of stresses on the bearing when rotation speed is constant. Maximum stresses obtained in basic pump design achieved 0.7…1.2 kN.

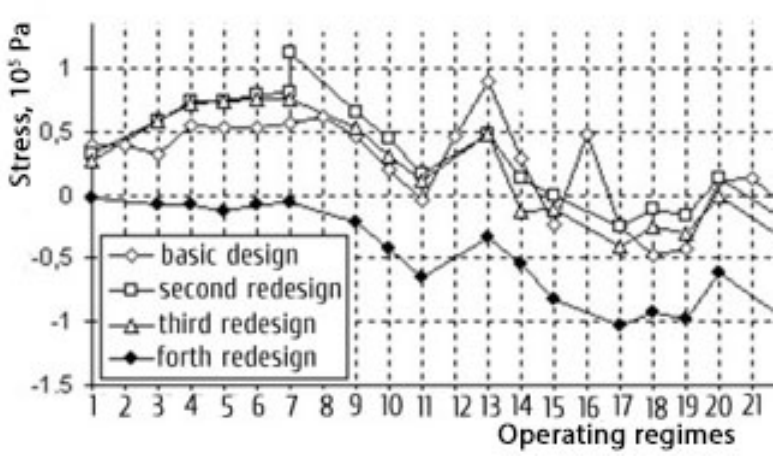

Figure 8.16: Mean values of stresses on the bearing for proposed pump designs

8.2.4 Vibrations

Figure 8.17 - Figure 8.20 show the variation of vibration acceleration on the inlet flange of the pump and on the flange that connects the stages with between each other. Vibration accelerations are seen to be dependent only on rotation speed. Proposed designs were obtained to effect positively on the decrease of vibration acceleration on the XOY plane. For operating regimes 76 – 96, they were reduced in average by 30…40%. For operating regimes 97…102 this influence was opposite. In this case, the vibration accelerations were increased by 20…30% in comparison with basic design. It was caused by the non-optimal flow inside of the centrifugal wheel. For YOZ plane, all designs affect positively on the reduction of vibration accelerations. They allow decreasing the vibration in average by 5…35% on the whole range of operating modes. For XOZ plane, the same effect was obtained, but reduction was detected by 5…7%.

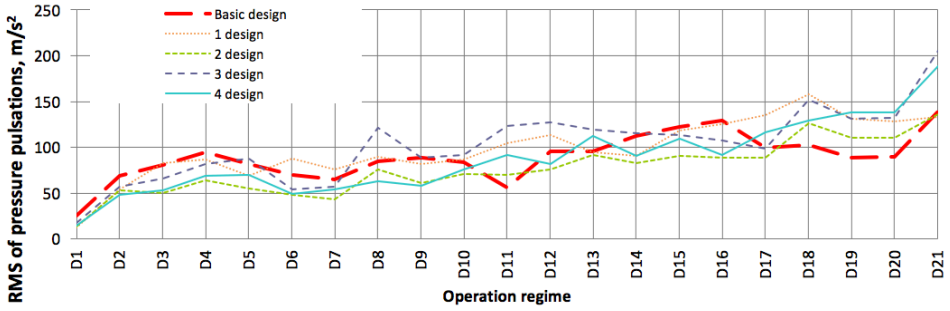

Figure 8.17: Vibration acceleration at the inlet of screw-centrifugal stage along the OX-axis (downstream)

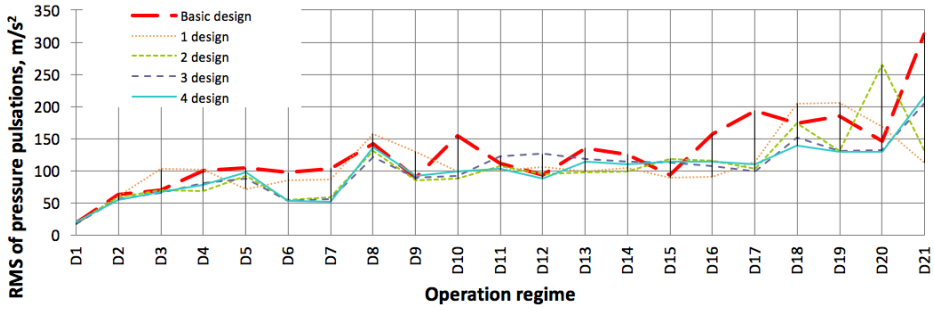

Figure 8.18: Vibration acceleration at the inlet of screw-centrifugal stage along the OY-axis (horizontal plane)

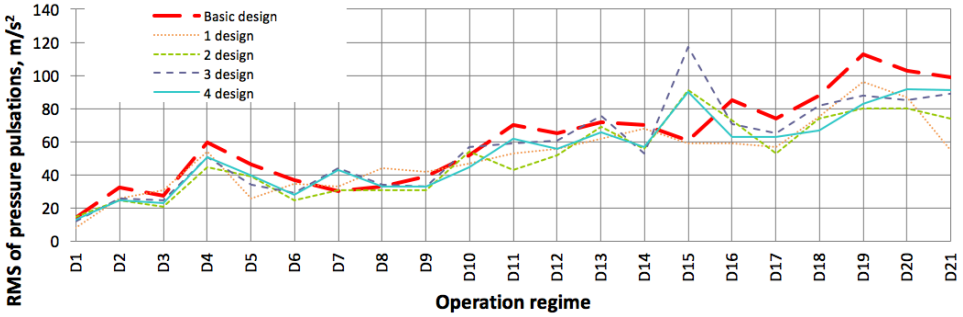

Figure 8.19: Vibration acceleration at the inlet of screw-centrifugal stage along the OZ-axis (vertical plane)

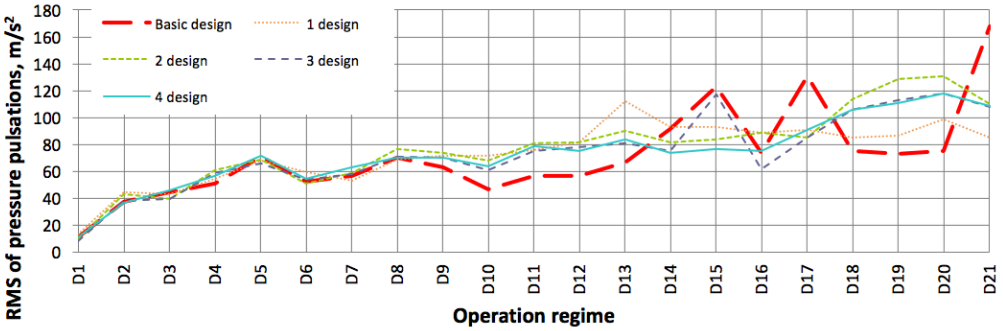

Figure 8.20: Vibration acceleration at the connected flange along the OX-axis (downstream)

Analysis of vibration state of the pump allows to make a conclusion that vibration loading increases with increase in operating mode. The most significant influence of proposed designs on pump vibration state was obtained during increased operating modes. Design with cylindrical detail, ring and cowl was shown to be the most effective.

8.2.5 Visual investigations

The efficiency of proposed designs was investigated experimentally with an undissolved air supply. Parameters of the operating regimes are shown in Table 7.4. Results obtained during visual investigation of the flow inside a pump in case of its basic design are shown in Figure 8.24 - Figure 8.26. Bubble supply allows to understand the flow structure: structure has a significant zone of back vortex, occupying almost all of the cross-section. There are two spirals present at the pump inlet occupying all the considered length of the inlet supply line. The radii of bubbles are equal. Visual investigation also shows that further increase of air supply does not change the structure of the flow. Stagnant air volume is formed in the upper part of the supply pipeline. During operation of the pump, small portions of this volume are separated and entering to the pump inlet. This process has a spontaneous behavior. Experimental investigations show that proposed designs are extremely efficient as they prevent back eddies origin, as well as flow spirals origin (Figure 8.21 - Figure 8.23). Pump design with cylindrical detail, ring and cowl allows to stabilize the flow inside of the pump: air penetrates the pump in the form of small bubbles without a twist. The distribution of bubbles is uniform along the channel cross-section. Such design also allows to prevent a stagnant zone in the upper part of the supply pipeline.

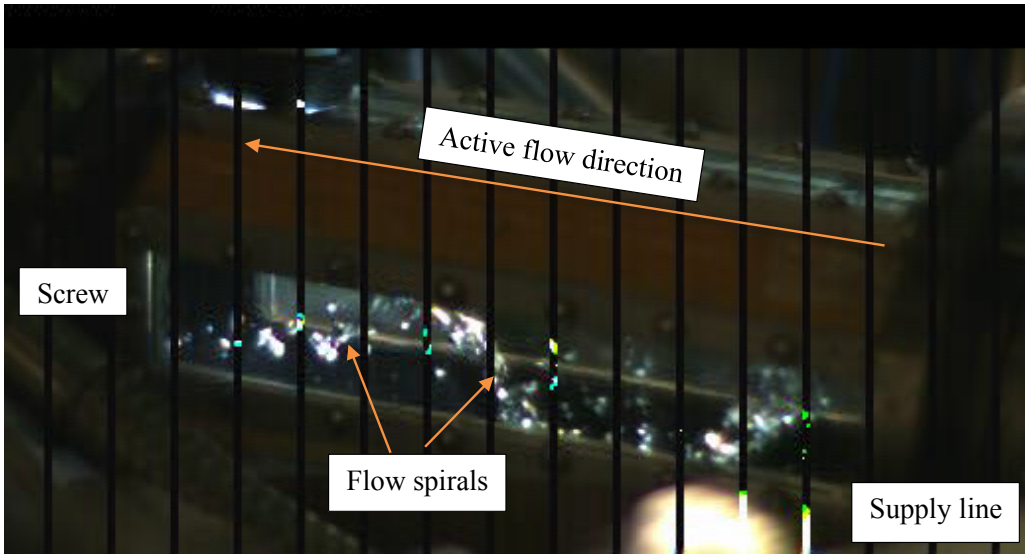

Figure 8.21: Flow before the screw on regime 288. Pump basic design

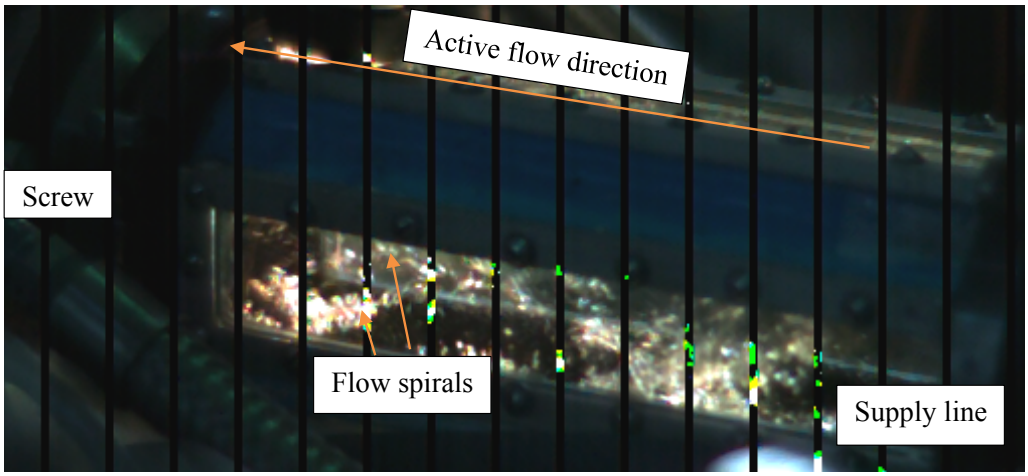

Figure 8.22: Flow before the screw on regime 289. Pump basic design

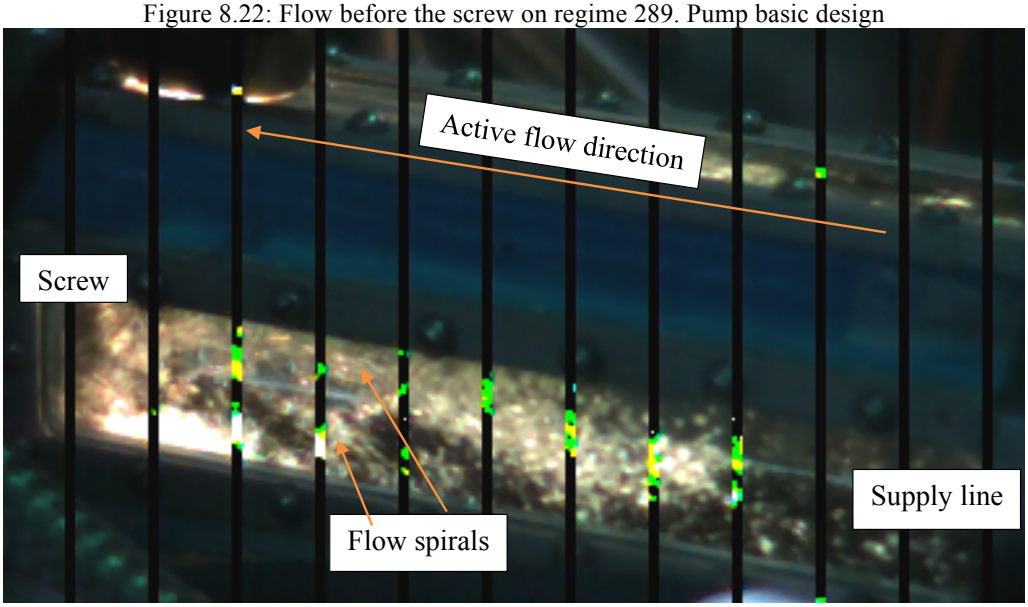

Figure 8.23: Flow before the screw on regime 290. Pump basic design

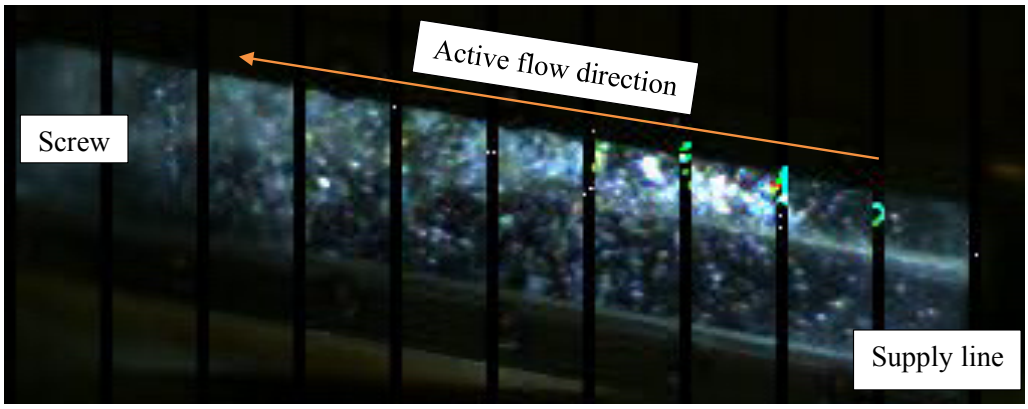

Figure 8.24: Flow before the screw on regime 288. Pump design with 6 blades, orifices for drain flow dividing, ring and cowl

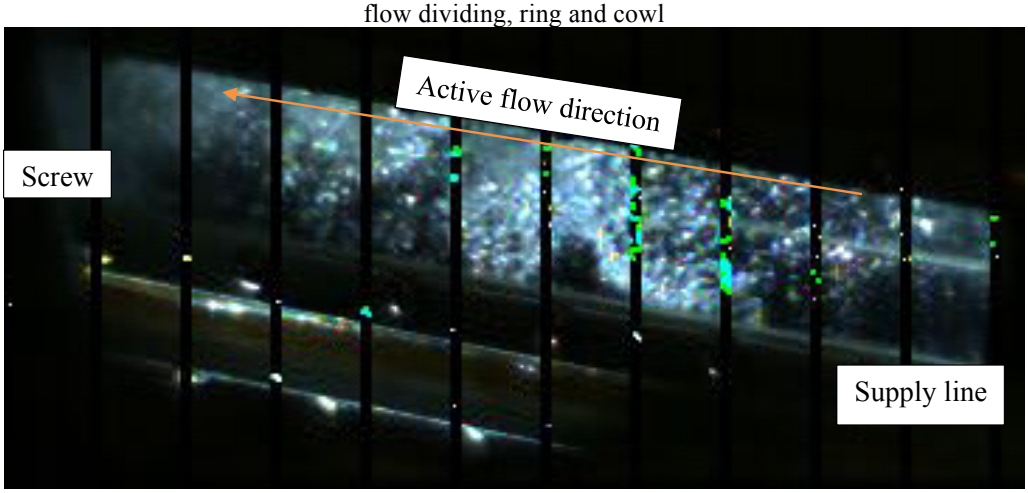

Figure 8.25: Flow before the screw on regime 289. Pump design with 6 blades, orifices for drain flow dividing, ring and cowl

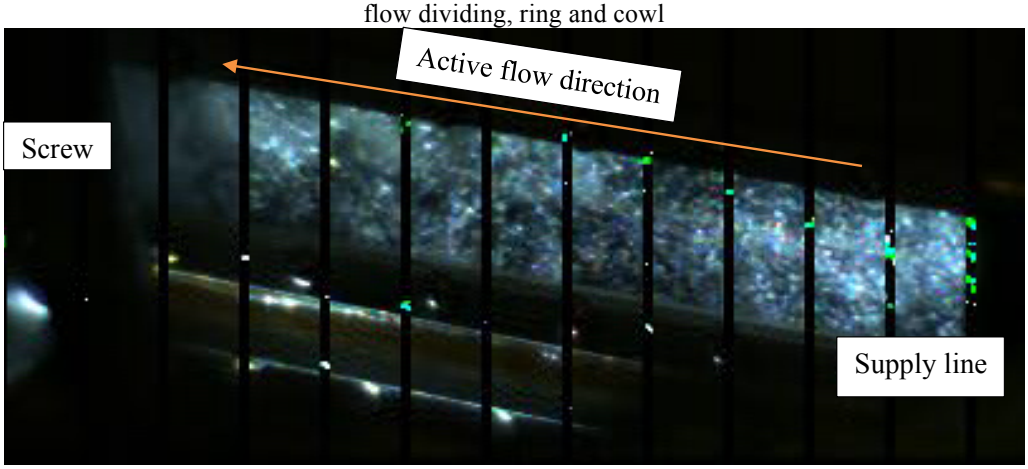

Figure 8.26: Flow before the screw on regime 290. Pump design with 6 blades, orifices for drain flow dividing, ring and cowl

9 Conclusions and Summary

The principal aim of this dissertation is the comprehensive development of the methods for decreasing the dynamic loads in a two-stage pump of aircraft engine. Prospective aviation engines will have to have significantly increased durability, serviceability and efficiency. Realization of these issues depends directly on the fuel systems of the engines, particularly on fuel pumps. Fuel two-stage pumps have demonstrated enormous potential in aviation applications. This potential can be greatly enhanced by the application of the methods and approaches presented within this thesis. Motivated by failures of aircraft engine two-stage pumps ND-25 and ND-32 and by beneficial application of two-stage pumps in aircraft industry, this work aims to answer the questions of reliability of two-stage pumps, the causes of failure and to propose methods for increasing the durability of the pump.

The range of the applications of many existing approaches for evaluating of system reliability is limited. They require an accurate exploitation of the data describing the failures, fault statistics and other parameters. Complexity of aviation fuel systems, numerous hydro-mechanical aggregates, hydrodynamic instability of flow inside pump, such physical phenomena as cavitation and turbulence, as well as presence of undissolved gas make the failure propagation analysis of aircraft fuel pump extremely complex. Each of these factors can be a source of increased pump loading and result in increased wear of the bearing and its destruction. Fuels systems of aircraft afterburner engines have been shown to operate in abnormal conditions. They have to provide a wide range of fluid flow rates at wide range of rotational speeds. These factors lead to high dynamic loading of the fuel system components such as valves and hydraulic pumps in particular. This work provides an analysis of the failure of the two-stage pump ND-32. This pump includes screw-centrifugal booster stage and a gear primary stage. Conducted analysis showed that the journal-and-thrust bearing of the booster stage is the key component of fuel two-stage pumps as it limits the pump durability. This work aims to understand the reasons of its destruction/failure. Provided analysis showed that working processes in a screw-centrifugal stage determine the loading state of a bearing. But pump's stages cannot be considered separately as there is a strong influence of a gear stage on processes in a screw-centrifugal stage. This work developed the simulation model of the screw-centrifugal stage while taking into account the influence of a gear stage. The simulation model and the analysis conducted using the model gives significant insight into the physical processes governing the loading state of screw-centrifugal stages of the fuel pumps. The mathematical fundamentals of simulation model presented here are general and not pump specific, and have application in centrifugal and axial flow pumps design, estimation and optimization. It is applicable to screw-centrifugal pumps with supply, drain and bypassing hydraulic lines, having journal-and-thrust bearing and volute. Simulation model includes the major design elements of fuel screw-centrifugal pumps. Here in the working conditions are very important. Provided simulation model takes into account the influences of the gear stage, mixture flow, cavitation and turbulence. Because this model

is widely applicable rather than pump-specific this work complements the effort in existing hydraulic screw-centrifugal pumps.

This work aims to develop both, the intuitive and technical understanding of aircraft engine fuel pumps, and allowing the application of existing methods of engineering analysis. To do so, a semi-natural test bench was developed. This test bench is complex enough to accurately model the dynamics of an aircraft engine fuel system and a pump as a part of it. It takes into account the real-scale working conditions of the aircraft engine fuel system. Developed semi-natural test bench allows modeling and determining the main characteristics of the engine's system and full-scale fuel aggregates during steady and transient operating modes in closed-loop and open-loop schemes, analyzing the available margin stability of the control systems, performing of the interaction of separate loop and aggregates, investigation of the effect of perturbations and external factors and theperformance of the control system failure. The approach for developing the semi-natural test bench is widely applicable instead of being just engine-specific. As a result, an approach presented in this work can be used for existing hydraulic fuel systems. However, developed test bench has several disadvantages. The first of them is that the mathematical model of the engine does not account of all perturbations in the control system. The second one is the scope of mathematical model and a full-scale aggregates work coordination.

This work aimed to develop the methods for decreasing of dynamic loading of the elements of the pump. Pump structural elements for dynamic loading reduction are presented in this work. The purpose of proposed elements is to improve the streamlining of pump elements and to prevent hydrodynamic losses. New construction elements provide the improvement of pump performances such as head and efficiency, the cavitation performance and allow to reduce the loads acting on pump elements. These structural elements do not change the pump appearance, dimensions and operating regimes. The efficiency of proposed structural elements is most noticeable when the pump operates with undissolved gas.

Chapter 2 analyses the reliability two-stage fuel pump of the of aircraft engine NK-36. Section 2.1 briefly analyses the main approaches for reliability investigation. It also describes the structure of the engine and depicts its node structure. Provided analysis has shown that hydro-mechanical control system is the key system defining the reliability of the whole engine. This conclusion has been made also based on the brief literature review, showing that supply pumps are the most loaded units of the aircraft engines. Section 2.2 developed a reliability analysis of the two-stage fuel pump. It showed that unidentified destruction of the journal-and-thrust bearing of the screw-centrifugal stage is the main cause of the pump failure. Section 2.2 also includes the analysis of the engine fuel system design and develops its node structure. Obtained exploitation data of a two-stage pumps ND-25 and ND-32 allowed to develop their main failure functions and the main failure values. These functions allowed to determine that bearing destruction depends mostly on the operational conditions of considered pumps despite their similar constructions.

Chapter 3 discusses design of the ND-32 two-stage pump, its main features and operational principles. Section 3.1 describes pump design and include the description of pump geometry. Section 3.2 contents the analysis of the pump operation. This analysis has shown that the construction of aircraft fuel system leads to liberation of gas from the liquid fuel. The considered fuel system requires the two-stage pump to supply all the fuel to provide a wide range of operation modes of the aircraft. It means that the pump should provide a wide range of flow rates in the combustion chamber and the afterburner. This fact leads to complication of the pump supply line. Section 3.2 also developed the scheme of mechanical and hydrodynamic interaction of pump stages. This scheme allows to analyze pump operation, main loading source. It shows that hydrodynamic processes in the screw-centrifugal stage and its supply pipeline determine the operation condition of the journal-and-thrust bearing. But stages of the pump cannot be considered separately as there is an interaction between them, and mutual influence. The gear stage, besides vibration influence, affectsthe bearing through the leakages that pour out into the chamber between the stages. Consequently, proved analysis has shown that only screw-centrifugal stage should be thoroughly considered in further investigation. It results in, that Section 3.3 describes geometric notation of screw-centrifugal stage of the pump.

Chapter 4 discusses the simulation model for investigation of flow phenomena and operation processes of the pump screw-centrifugal stage. Hydrodynamic process inside the screw-centrifugal stage have been shown to determine the operative conditions of the considered journal-and-thrust bearing. Section 4.1 shows that only time-dependent, unsteady, dynamic meshing is able to predict the motion of the fluid flow against the very high adverse pressure distribution. Centrifugal and axial flow pumps pose an exceptional challenge due to the fact that there are a number of physical phenomena such as cavitation, turbulence and non-stationary flow, and the rotating components housed within a stationary three-dimensional-casing. Hydraulic pump performances and technical performances are known to be determined experimentally with further evaluation based on the theory of similarity. Empirical equations limit the range of working conditions. Numerical methods are more perspective in case of spatial three-dimensional flow and can take into account such phenomena as cavitation and turbulence in case of multi-component flow. As a result, Section 4.2 described several approaches of three-dimensional analysis of the flow in the kinetic pumps. Literature analysis provided has shown that there is a lack of investigations of flow inside fuel screw-centrifugal stage of aircraft engine pumps, which takes into account the influence of another stage, the cavitation phenomenon and turbulence. Consequently, the simulation model for hydrodynamic and operation processes investigation in the screw-centrifugal stage was developed. Section 4.3 developed a simulation model for tree-dimensional spatial turbulent flow analysis of a screw-centrifugal stage of aircraft engine pump. Provided literature analysis shows that a commercial code ANSYS CFX can be used for numerical solving of the developed model. Section 4.3.1 describes the model of the pump and gives the program structure for the flow inside of the pump numerical simulation. It also describes pump geometry, its features and general data of the screw-centrifugal stage. Calculation domain considers the supply pipeline, elements of screw-centrifugal stage of the fuel pump, its bearing assembly while taking into account the influence of the gear

stage. Typically, the fluid inside engine fuel systems have several components such as kerosene, its vapours and undissolved gas. Consequently, section 4.3.2 showed the Euler-Euler approach for numerical calculation of the multiphase flows. Euler-Euler models working mixture as an interpenetrating continuum. Further sections 4.3.3 – 4.3.6 described the mathematical fundamentals of multicomponent flow simulation. The flow inside the screw-centrifugal stage has been described by means of the non-stationary Navier-Stokes equations in the form of conservation. Fluid motion and transport characteristics are governed by not only three conservation equations, but also by additional equations for describing of turbulence and cavitation. Conservation equations are derived for each phase to obtain a set of equations, which have similar structure for all phases. Section 4.3.5 describes the approaches for turbulent flow simulation. Based on this short overview, the SST turbulence model was used to describe the turbulent stresses forming a significant part of the momentum equation. Section 4.3.6 describes the approaches for cavitation simulation. Cavitation was described byusing the Rayleigh-Plesset equation. The partial gas pressure inside the bubble was assumed to obey the polytropic law and the effective viscosity was taken as a multiple of the liquid dynamic viscosity to account for damping mechanisms in the form of viscous dissipation. Dependencies of kerosene kinematic viscosity and density on its temperature as well as kerosene surface tension were considered. Additionally, the model of bubble collapse was also used to evaluate the wear of the bearing. The coupling of the Rayleigh-Plesset dynamics with the Navier-Stokes equations is achieved by using the Euler-Euler approach. Computational grid is described in Section 4.3.7. Several types of meshes were used for deriving finite element grid models: structured, unstructured, and the combined grids. Block-structured meshes were used for supply channel, radial edges input area as well as for the screw. Unstructured tetra and hexa meshes with prismatic layer were used for designing of drain channels, centrifugal wheel, volute and rear friction bearing area. The computational grids were developed in ANSYS ICEM CFD and AUTOGRID 5 software. The computational finite element grid model was carried out to satisfy the conditions of $y^+ = 1$. For unsteady calculations, the grids were connected by means of a various transient rotor/stator interfaces, i.e., that they change their relative position through the calculation according to the angular velocity. Section 4.3.10 describes the discretization of developed simulation model. The obtained conservation equations were discretized using the finite volume method. ANSYS CFX uses a control volume technique to convert the governing equations into algebraic equations. Section 4.3.11 showed the parameters for unsteady equation solution. The chosen time step is small enough to get the necessary time resolution. Twenty sub-iterations were set up per time for the “flattering” of residuals. Certain underrelaxation factors were increased to values higher than the default values in order to promote residual reduction. Residual RMS values were set to be 10^{-6}. Section 4.4 described verification of the developed simulation model and its accuracy. The testing and verification of the developed numerical model were based on comparison of energy and cavitation characteristics of the screw-centrifugal stage, obtained by calculation and experimental ways. Calculations were carried out with SST and $k-\varepsilon$ turbulence model. SST model has shown to produce the higher accuracy. The comparison of calculated and experimental efficiency

characteristics shows that the computation error is no more than 3%. The evaluation of the cavitation performance has shown that the computation error is no more than 3%. The simulation models are able to predict the energy and cavitation characteristics of the screw-centrifugal stage, as well as the loaded condition of its elements, which is particularly important to determine the cause of increased bearing wearing. The model is also able to evaluate the flow regime, as well as cavity formation. The laser knife method and a high-speed camera were used for visualization of the flow structure at the pump inlet. The comparison of calculated flow structures and obtained experimentally at the same operating regimes has proven the efficiency of SST turbulence model as well as boundary conditions, and also the correctness of the designed grid models. Evaluation by Fisher ratio test showed the adequacy of the model. Calculation error is not more than 4%, taking into account the error gauges. Thus, the numerical model can accurately predict the pump head and cavitation characteristics variations in a wide range of operating regimes.

Chapter 5 implements the developed simulation model of a screw-centrifugal stage operation for investigation of flow phenomena inside it. Section 5.2 describes radial and axial forces, acting on the rotor of screw-centrifugal stage. The contribution of each pump element to the total force was evaluated. The axial force turned out to be caused mostly by the screw. The radial component of the hydrodynamic force emerged in the pump components where there are radial components of flow velocity and lack of symmetry in the pressure distribution in a circumferential direction. Load distribution along front and rear surfaces of considering bearing is nonuniform. It leads to a skew of the bearing. Back vortex flow is discussed in Section 5.3. Developed model has find out a significant influence of the drain pipelines on the back eddies formation. Back eddies results in the flow unsteadiness at the screw-centrifugal stage inlet. The main flow at the pump inlet is divided into two zones. Back eddies lead to additional instability of vortex structure at the pump inlet. The lengths of the specific formations were estimated. During the numerical investigation for determining the main sources of pump dynamic loading, the main focus was made on investigation the process of air intake to the pump inlet. This phenomenon has been discussed in Section 5.4. Volume fractions of undissolved air were chosen based on operating conditions of the fuel system. Section 5.5 describes the numerical results of cavitation simulation inside the stage. Maximum volume of the supplied air was up to 7 % from the whole fluid volume. Numerical results have shown that undissolved air results in increase of both, the average force value, and its amplitude. Rise of the average force value aligned with increased amplitude of pressure fluctuations and the initiation of the pump rotor axial vibration. Flow around an air bubble id similar to the flow around the solid body. As a result, undissolved air hit at the pumps entrance leads to the leap of local velocity, which in turn leads to local pressure breakdown. Significant increase of stresses (more than 18 times) on the bearing in case of air supply was also obtained. In adittion, the numerical studies have shown that cavitation develops at reduced pump operating conditions. Undissolved air supply resulted in occurring of cavitation on the bearing surfaces. Cavitation appears especially on the internal edge of the bearing and on its end faces. Pressure distribution along screw blades have been obtained. Concequently, the numerical analysis conducted confirms the cavitation

character of the bearing end face damages. A model of high-frequency pulsations inside the screw-centrifugal stage induced by pump interaction and operational processes is described in section 5.6. Such pulsations are caused by oscillations spreading from gears as well as from screw and the impeller blades. Obtained results show that there are coincidences of the eddy frequencies separated from the wheels and their natural frequencies on several operating regimes. This section also contents the block diagram of the interaction of vortex disturbances in the screw-centrifugal stage and blades oscillations due to vibrations. Experimentally was obtained that main contribution in total level of vibration makes the high-frequency oscillations above 3 kHz that are occur due to coincidence of vibrations and pressure pulsations. Theoretical and experimental results allow the understanding of the high-frequencies phenomena occurring at the pressure pulsations spectrum.

Hardware-on-the-loop approach is not widespread in aviation engine industry. In spite of a number of studies, there still exsists a lack of investigations devoted to the aviation fuel systems. There is no significant information how to design HIL test bench for the investigation of the characteristics of a turbofan engine fuel system. The question of providing a good accuracy of these tests remains. Chapter 6 contented the analysis of the engineless test benches for experimental investigations of aircraft engine fuel pumps. Section 6.1 showed that the pump operating conditions as a part of the aircraft and as a part of the engineless test bench are different. A semi-naturals test bench was developed for thorough investigation of the pump operation conditions. Section 6.1.1 and 6.1.2 describe the test bench consisting of full-scale hydro-mechanical components and the mathematical model of the engine. The later has been developed and debugged in MATLAB Simulink and NI LabVIEW software. In addition to the fuel two-stage pump, a number of full-scale aggregates such as fuel-metering unit, low-pressure filter, fuel regulator and aggregate of fuel bypassing were also installed. Section 6.2 discussed the measurement techniques and equipment for further experimental investigations of the pump under evaluation. Static pressure was measured in 10 points along two-stage pump, the pressure pulsations were measured in 5 points, vibration accelerations in 4 points. Flow rates through supply and drain pipelines were also measured, as well as the rotor displacements of the screw-centrifugal stage. To understand the stress state of the evaluated bearing, 16 stress transducers were used. Experimental investigations allowed to determine the pressure pulsations, vibrations and loading state of the pump during all of the operation regimes.

Chapter 7 discussed pressure pulsations and vibrations occurring all over the pump operating regimes. Section 7.1 showed the 24 operational regimes which were chosen for pump experimental investigations. These regimes coincide with the operational modes of the real-scale fuel system of NK-36 aircraft engine. Conducted analysis of pump loading states on different operation regimes has shown that the most unfavourable modes are the modes with a relatively low fuel mass flow rate and high rotational speed. Analysis of vibration state of the pump allowed to make a conclusion that vibration loading increases with increasing of operating mode. Experimental investigations were conducted by means of developed test bench, discussed in previously in chapter 6. Section 7.2 represented the

results obtained. It studies the variation of static and dynamic performances of the pump, including pressure pulsations, vibrations and stress distributions. Behavior of the bearing stresses and the rotor displacement variations were shown to coincide over the changing operating regimes. This means that the loading source of the considered bearing has hydrodynamic nature. Non-uniform loading of screw blades has been obtained. Section 7.3 thoroughly observed the influence of dissolved air on the pump loading state. Variations of gas fractions lead to variation of loading state of the pump: small amount of air supply leads to sharp increasing of pressure pulsations and vibrations in all sampling points, further increase of air supply leads to decrease of pressure pulsations and vibrations in all sampling points. Bearing loading was determined to be non-uniform in cross flow plane. The results of the bearing strain measurements showed that the axial force, occurring on the bearing end face, is significantly increased due to the air supply. Increasing of air supply leads to increasing of the stresses on the bearing. Further increasing of air and fuel supply at the same rotational speed lead to decreasing of stresses on the bearing. Moreover, the next step of further increase of air supply only leads to further decrease of stresses. Obtained results allow to determine that supply of insignificant amount of air has stabilazing influence on the "pump-pipes" system. These results allow to conclude that bearing loading in cross flow plane is nonuniform. Moreover, in several cases this loading is nonsymmetrical: mean stress values obtained by means of two opposite strain transducers have different signs. This can lead to flection of the bearing surface. This phenomenon is explained by fluctuating radial force occurring due to nonsymmetrical pump volute. Therefore, the variable force was shown to be one of the main cause of accelerated wear of the bearing under review. After the tests the pump was disassembled and visually inspected. The state of the bearing after conducted experiments exposed several damages of the bearing, the cavitation wears on the inner edge and also the circumferential marks on the internal diameter. Pump cavitation processes was shown in section 7.4 to be detected by the means of the acoustic field analysis. The 1^{st} and 2^{nd} fundamental harmonics are the most "informative" in this context. Obtained acoustic fields were used for developing the diagnostic cavitation properties.

Chapter 8 described the construction methods and designs and proposed the decrease of dynamic loading of the pump. Section 8.1 included a brief analysis of methods and approaches for decreasing of kinetic pumps dynamic loading. This section also described the designs proposed that were aimed at reduction of hydrodynamic instabilities inside the considering pump: transferring of the drain pipelines; increasing of number of radial blades from 3 to 6; orifices for dividing flow through drain pipelines; the ring to direct flows through drain pipelines to the pump input; the cowl for increasing the hydrodynamics of the screw. Proposed improvements are collected into 4 new pump designs. Section 8.2 described experimental investigations of proposed improvements for efficiency. Experimental investigations were conducted on the same 24 regimes of the fuel system operation. The most significant influence of proposed improvements on pump vibration state was obtained on the increased operating modes. Pump design with orifices for drain flows dividing, the increased number of inlet guide vanes, the ring and cowl was shown to be the most effective. It allowed to eliminate back eddies, significantly decrease

pump loading and decrease the influence of undissolved gas at all pump operating regimes.

Appendix A briefly describes the main causes of nonstationary flow inside screw-centrifugal pumps. All described phenomena were investigated to understand their influence on pumps elements loading. All sections of this chapter content a literature review of previous investigations of flow phenomena inside of the centrifugal and axial flow pumps. Section A.1 discussed the back eddies phenomena to understand the flows structure inside pumps and the causes of active currents and back eddies. Section A.2 described the cavitation phenomena inside pumps. The focus of this section was made on understanding of the main principles of cavitation occurring and its influence on pump elements loading. This section also showed dynamics of the gas bubbles occurring due to cavitation. Bubble dynamics include a number of stages. The final stage – collapsing, leads to significant dynamic loading of pump elements and also to cavitation erosion, and results in damage of pump elements. Section A.2 also includes a description of noise and vibration induced by cavitation. Section A.3 is devoted to a description of multicomponent flow inside aircraft fuel pumps. Aviation fuels are known to dissolve a significant amount of gas. A flow swirl and vortex disturbances, originating in attached pipelines, contribute to vaporization of dissolved gas. At that, the violence of dynamical equilibrium in fluid-gas system is possible. This violation is accompanied by the liquid-gas transition and finally results in cavitation. Next Section, A.4, focuses on undissolved gas occurring inside aircraft engine pumps. It includes theoretical and experimental results obtained from literature overview, showing undissolved gas influence on pumps performances and their behavior. The last section of this chapter, section A.5, focuses on vibrations of the centrifugal and axial flow pumps. Vibrations in pumps are mostly induced by rapidly changing mechanical and hydrodynamic forces. This Section shows that combination of increased vibrations and pulsations leads to dynamic loading of the pump rotor, its bearings, sealing and others.

Appendix A. Flow Phenomena and Operational Processes in Screw-centrifugal Pumps

A.1 Backflow vortices

Definition the reasons of the vortex flows origin at blades leading edges is an important issue as physical picture of flow structure at pumps entrance influences on their anti-cavitation performances and stall characteristics.

Works (Chebayevskiy, 1973), (Gulich, 2010) describe a flow scheme in screw-centrifugal pump supply line before a screw. According to these schemes, flow can be divided into 3 zones: back eddies, back current and active current (Figure A.1).

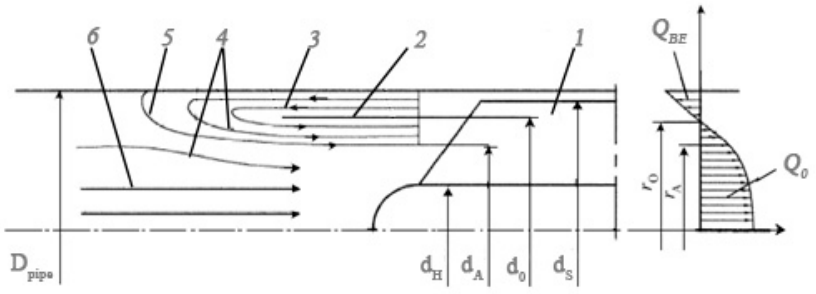

1 - screw; 2 – vortex flow; 3 – back eddies; 4 – forward current; 5 – conditional border between back and active currents; 6 - active current

Figure A.1: Fluid flow scheme in a screw

Zone of active current is constrained by radius r_A and determined by a flow rate through the corresponding section at a reduced power regime. Work (Chebayevskiy, 1973) shows that axial velocity is constant along the active flow. These theoretical results are confirmed by the experimental results obtained by Toyokura et al. (Toyokura, 1961). Back eddies and back currents are divided by a revolution surface with a radius r_0. In this radius axial velocity is zero. The area of a vortex zone decreases in case of increased flow rate and at the same rotational speed and eventually disappear at a certain critical flow rate. Back eddies have a significant circumferential velocity. Propagated upstream along the periphery of the supply pipe, back eddies spin the main flow in direction of rotor rotation.

Papers (Brennen, 2011), (Bakir, 2004), (Stochek, 1978) show backflow vortex presents almost at all centrifugal pumps operating regimes. They constitute additional source of flow instability at pump entrance and as a result increased dynamics loading of pump's elements. Paper (Stochek, 1978) shows that back eddies can represent a source of additional flow instability at a pump entrance as well as a factor of increased vibration

loading of the pumps elements. Back eddies induce the velocity field uneven at a pump inlet, heat fluid, increase a shaft resistance moment, increased noise and vibration, low-frequency pressure pulsations having the character of self-oscillations.

Studies of (Chebayevskiy, 1973) and (Shapiro, 2004) describe the general performances of the velocity field distribution as well as pressure field and drop pressure between inlet and outlet of centrifugal and axial flow pumps. According to these studies, vortex zone occurs stepwise and takes approximately 50 % of the supply pipe cross-section at q=0.5. In this case, stream impingement with an angle of attack equal to half of the blade pitch angle at its top edge. Active flow before a crew has a lower static pressure than static pressure at the inlet. Decreasing of the flow rate leads to increasing of this difference. This phenomenon can be explained by the sharpening of the active flow, its twisting and dissipations due to vortex flows.

Article (Dumov, 1962) depicts that back eddies at the screw inlet are induced by the heavy loads on the blades and a large pressure gradient along the blade channel radius, i.e. depends on the screw output parameters. (Toyokura, 1961) claims that back eddies on the axial wheel inlet origin due to vortex zone near a bush at the outlet of a screw and depend on output parameters of an axial wheel. However, (Chebayevskiy, 1973) shows that flow regime before a blade wheel is defined by the input flow conditions of a wheel and weakly depend on the output parameters.

A.2 Cavitation

High-capacity aircraft and rocket pumps are inescapably prone to the cavitation phenomenon. Cavitation in two-stage aircraft engine pump was detected with the use of the pressure oscillations spectra and visually, using the transparent casing (Gasparov, 2006). Cavitation leads to intensification of noise and vibration. Cavitation is the process of the formation of the vapor bubbles in low pressure regions inside a flow. Vapor bubbles are formed when the pressure in the liquid reaches so-called vapor pressure, p_v, specific for various liquids at the operating temperature. Cavitation can be characterized by means of pressure coefficient, Cp, which can be determined as follows

$$C_p = \frac{p - p_1}{\frac{1}{2}\rho v^2}, \tag{A.1}$$

where p_1 is a reference static pressure required for pump inlet to provide cavitation less flow.

In case of incompressible flow C_p depends on only pump geometry and the Reynolds number, Re. For screw-centrifugal pump Reynolds number can be found from expression

$$Re = \frac{2\omega(R_{T1}^C)^2}{\nu} \tag{A.2}$$

Equation (A.1) allows to determine the minimum permissible pressure

$$p_{min} = p_v - \frac{1}{2}\rho v^2 C_{pmin} \quad \text{(A.3)}$$

Note that total pressure, p^T, of the fluid is known to consist of two components – static and dynamic pressure. Another important parameter of the fluid flow is a volume flow rate, Q. Total pressure can be defined as follows:

$$p^T = p + \frac{1}{2}\rho v^2 \quad \text{(A.4)}$$

The difference between total pressure at pump inlet and outlet, $p_7^T - p_2^T$ defines the fundamental measure of the mechanical energy imparted to the fluid by the pump.

It is worth to mention that minimum pressure in equation (A.3) is a function of the velocity for a given pump, liquid and its temperature. It follows that there is a location where the working pressure is at minimum and where cavitation can occur. Unsteady cavitation processes in a screw-centrifugal pump have been thoroughly investigated in (Eisenberg, 1961). There are 4 cavitation stages in screw-centrifugal pumps:

- cavitation origin. Cavities appear at a periphery of screw leading edges;
- circulating along a screw leading edge cavitation spreading on separate blades;
- transient cavitation. Cavities fluctuate with a certain frequency on all screw blades;
- cavitation stall.

Cavitation inside of a pump is oftentimes invisible (Dovgot'ko, 1976), (Dovgot'ko, 1985). The physics of this phenomena is that cavitation cycle (formation and collapsing of the bubbles) ends until the time moment when flow reaches a screw outlet. Thus, stream velocity at a screw outlet does not change and as a result, pump performances do not vary.

Studies of Chebaevskiy (Chebaevskiy, 1957) and (Chebaevskiy, 1959) show that the first stage of the cavitation within the pump does not immediately lead to pump failures. Moreover, the generation of cavitation does not cause significant variations of pump performances. There can be no damages of the pump parts at a cavitation incipient stage even after continuous use. However, invisible cavitation can induce a significant dynamic loading of the elements of the pump without pump head breakdown (Chebayevskiy, 1973). Pump cavitation breakdown occurs mainly upon engine ignition and its transient operating regimes. They represent a sharp decrease of pump delivery head almost to zero. The depth of this breakdown is defined by the relative volume of the cavitation cavity induced in a pump at inlet pressure decreasing lower critical value. Cavitation cavity is firstly formed in back eddies zone at the periphery of a screw leading edge. Then, it grows while in active and vortex streams. Further, the evolution of the cavitation cavity leads to

both, the decreased intensity of the back eddies until their total disappearance, and, to increase of the cavity size. After that, the full pump delivery head breakdown comes.

Theoretical and experimental results obtained in papers (Grigor'yev, 1985), (Dovgot'ko, 1980) and (Pilipenko, 1977) show that the region of stability of the system screw-centrifugal pump – pipes system relative to cavitation oscillations has an acute-angle form in the parameters of mass ratio $\frac{\overline{Q}}{Q}$ and pump inlet pressure p_{in} plane. This plane shrinks when the current flow rate increases. At that, there is a linear dependence between cavitation oscillations frequency and inlet pressure p_{in}. In such a manner, cavitation self-oscillations frequency depends linearly on the inlet pressure while their amplitudes depend implicitly on the inlet pressure (Chebaevskiy, 1959). Moreover, both frequency and amplitudes of this oscillations depend on the sizes of the cavitation cavities. Generally, increase of the cavitation cavity size leads to decrease of the oscillations frequency and to increased amplitude.

Paper (Grigor'yev, 1985) investigated the influence of the back eddies at a screw-centrifugal pump on stability of the pump systems. This paper considers the origin of the low-frequency pressure and mass flow oscillations on the regimes with intensive back eddies at pump entrance. Such regimes are accompanied by cavitation cavities. These cavities exist not only in screw blade channels but even in back vortex flows. The mathematical model of the cavitation self-oscillations in screw-centrifugal pumps was proposed in this paper. This model takes into account the dynamic properties of the back eddies. Model was obtained for closed-loop systems that usually are used for pumps independent test. Such systems include tank, investigated pump, supply and delivery pipelines. The equations for stability region boundaries were also obtained as follows:

$$O + R_{in}^{SCS} - R_{BE}^{SCS} - Y\left[t_{BE} - \zeta \cdot E_Q - \zeta \cdot E_P \cdot (R_{in}^{SCS} - R_{BE}^{SCS}) + \frac{I_1 - I_T}{R_{out}^{SCS} - \phi} \right] = 0 \qquad \text{(A.5)}$$

$$\omega^2 = \frac{Y}{(I_1 - I_T) + \zeta \cdot E_P \cdot Y + \frac{I_{10}}{I_1 - I_T}} \qquad \text{(A.6)}$$

where I_1 is an inertia resistances of the supply pipeline; I_T is an inertia resistances of the back eddies zone of the supply pipeline; E_P is coefficient taking into account the influence of the dependence between inlet pressure and active stream characteristics on the cavity volume changing in the back eddies zone; E_Q is coefficient taking into account the influence of the dependence between flow rate and active flow characteristics on the cavity volume changing in the back eddies zone; ϕ is slope ratio to the pressure

characteristic of the pump; I_{I0} is an inertia parameter of back eddies zone, which can be found as follows:

$$I_{I0} = -\zeta \cdot E_{I0}^2 \cdot Y, \tag{A.7}$$

where E_{I0} is coefficient characterizing the active flow inertia properties at a screw middle diameter where cavitation cavity exists.

Analysis of the equations (A.5) and (A.6) allows to trace the influence of the back eddies zone dynamic properties on stability of pumps relative to cavitation oscillations (Dovgot'ko, 1980). Paper (Dovgot'ko, 1980) concludes that the main reason of cavitation self-oscillation origin inside the screw-centrifugal pump is an existing of negative cavitation resistance *O* in regimes both, with back eddies and without them. the value *O* characterizes the total volume of cavitation cavities dependence on pressure and flow rate.

The equations for a screw-centrifugal pump dynamic by estimation of the properties Y and *O*, were obtained in paper (Pilipenko, 1977). These equations are appropriate for estimation of these properties in case of invisible cavitation:

$$Y = \frac{1}{\frac{\partial A_k}{\partial P_{in}}} \tag{A.8}$$

$$O = -\frac{\partial A_k}{\partial Q} / \frac{\partial A_k}{\partial P_{in}} \tag{A.9}$$

Experimental methods are often used to study cavitation processes inside of the pumps. The following experimental methods are currently known:

1. The cavitation margin analysis of the pump unit inlet. For the constant mass flow ratio, the pressure drop by 3% and more is unacceptable (ISO 3555, 1977);
2. The visualization of the pump blade internal channel streams with the use of transparent casings and stroboscopes;
3. The cavitation and abrasion allocating method with the use of the stain technique;
4. The static pressure measurement at the flow center or close to its boundary;
5. The ultrasonic measurement method (McNulty, 1982);
6. The pump vibration measurement in the possible vapor separation locations;
7. The acoustic field sound pressure measurement (Chudina, 2003);
8. The acoustic method gives the possibility to localize the cavitation noise source.

The allocation of the sound sources on cavitation pump modes is of a great interest for any noise control engineer. There are four main techniques for the sound source allocation:

- near field acoustic holography (NAH);
- statistically optimized near field acoustic holography (SONAH);
- beam forming (BF);
- direct acoustic intensity measurement.

It is worth noting that none of the methods can distinguish the radiated and reflected sound waves. Thus, a reflecting surface can often be identified as a noise source. Plus, the array of microphones must be non-planar or made up of two parallel planes with more complex signal processing in order to determine whether the sound is coming at the front of the array or from behind it.

One big advantage of the direct measurement of sound intensity adjacent to a noise radiating surface is the relatively large dynamic range (difference in dB between maximum and minimum measurable intensities) that can be achieved. A dynamic range between 30 and 60 dB is common compared to 20 dB for NAH and SONAH using microphones and 40 dB for NAH and SONAH using particle velocity sensors. The dynamic range of beamforming measurements varies from 6 to 15 dB.

Another advantage of the direct intensity measurement method is the wide bandwidth possible (20 Hz to 20 kHz) compared to 250 Hz to 10 kHz for beamforming arrays, but this frequency range is enough to two-stage pump acoustic diagnosis.

However, direct measurement of sound intensity close to a surface does have some problems due the dominance of the reactive sound field in that region. Unlike NAH and SONAH, beamforming operates in the far field of the sound source and it is more accurate at higher frequencies. Frequency ranges and distances between the array and the radiating noise source are depended by array types and numbers of microphones. For a beamforming array of largest dimension D, and distance from the source L, the resolution (or accuracy with which a source can be located) is given by:

$$Res = 1.22\frac{L}{D}\lambda \tag{A.10}$$

For acceptable results, the array should be sufficiently far from the source that it does not subtend an angle greater than 30 deg. in order to cover the entire source. In general, the distance of the array from the sound source should be at least the same as the array diameter, but not greater if possible at all.

The acoustic methods have a number of advantages:

1. Cavitation detection directly during real time of pump working;

2. No need for the specialized test benches, additional transducers and the pump design alterations;
3. Their application is relatively easy and requires no special knowledge.

Cavitation originates at cavitation bubbles having diameters equal to 10^{-7} - 10^{-5} m. These bubbles consist of a mixture of vapor and dissolved gas. When bubbles pass the areas where pressure is lower than saturated vapor pressure, these bubbles begin instantaneously grow. Bubble growth is limited by the diffusion time scale in case of gaseous cavitation. Life time of a cavitation bubble is very short and is in the scale of micro-seconds or nano-seconds. Bubble collapse in areas with increased pressure induces the increased noise, vibration and wear of the details. The collapse of the bubbles happens during very short period of time, about several nanoseconds. The outcome of the collapse of the bubble is a large shockwave. The cavitation bubble collapse is very harmful to the impeller, which suffers violent erosion. On account of bubble collapse alternative highly intensive stress is generated (Zima, 2012). Paper (Shervani-Tabar, 2012) studies experimentally and theoretically the effects of bubble collapse within blades of a centrifugal pump. The overview of hydrodynamic phenomena, scale ratios and methods for erosion and cavitation diagnostics is presented in papers (Karelin, 1970), (Franc, 1997) and (Franc, 2010).

Papers (Bakir, 2004) and (Brennen, 2011) studied experimentally and theoretically the effects of bubble collapse within blades of an inducer. These papers determined that bubble collapsing leads to erosion and results in highly intensive stresses on the pump's elements.

The hydrodynamic cavitation noise is the series of pressure discharges, caused by the cavitation bubble collapses (Hunsaker, 1935). If the wave length is considerably larger than the bubble size, then the fluid compressibility is changed. Consequently, the fluid noise propagation will be suitably different.

The theoretical research on cavitation noise is complicated due to huge quantity of cavitation bubbles interactions (Akulichev, 1965), (Igolkin, 2014). Therefore, the cavitation noise study depends heavily on experimental realizations.

A considerable amount of scientific studies dealing with the issue of cavitation-caused noise and vibration detection have been published over last five decades. The cavitation bubble genesis was studied with the use of a high-speed camera (Akulichev, 1968). The cavitation bubble size was smaller than the wave length. It was shown that the non-stationary cavity bubble genesis period amounts to ten periods of a sound wave. Unique visual investigations of cavitation inside a liquid hydrogen pump were carried out in by Ito et al. (Ito, 2012). The designed test bench presented in this research allowed to study visually the fluid flow in the cryogenic pump for the first time ever. Fanelli (Fanelli, 1996) and Li (Li, 2000) carried out the experimental cavitation noise study and developed the numerical algorithm for prediction of it. Chudina (Chudina, 2003), (Chudina, 2003),

(Chudina, 2012) found out the discrete behavior of cavitation noise, depending on the degree of cavitation. Rus (Rus, 2007) simultaneously measured the noise and vibration levels of the two blade axial-flow turbine. Su Yongsheng (Yongsheng, 2008) determined the centrifugal pump cavitation genesis, comparing the vibration and pulsation ripple signals at nominal operation and cavitation modes. Liu Yuan (Yuan, 2009) proposed the cavitation genesis identification method based on wavelet analysis. Pu Zhongqi (Zhongqi, 2005) also described the cavitation genesis identification method based on wavelet analysis. In article (Yong, 2012) the centrifugal pump cavitation noise and vibration were experimentally studied. The article (Akulichev, 1968) deals with the cavitation noise spectra distinctive features and their dependencies from acoustic cavitation parameters.

The cavitation noise pressure can be described as follows (Akulichev, 1968):

$$F_N(t) = \sum_{k=1}^{N} \sum_{l=-\infty}^{\infty} \varphi(t - lT_0, \varepsilon_k, \nu_l) \tag{A.11}$$

where $T_0 = \frac{2\pi}{\omega_0}$ is the period of oscillations; $\varphi(t, \varepsilon_k, \nu_l)$ stands for the function, defining the elementary signal form for the k^{th} cavitation bubble at the 1st sound wave period; ε_k is the random value, defining the cavity bubble signal parameters at the fixed moment, ν_l is the random value, defining the cavity bubble signal parameter fluctuation.

The equation (A.11) denotes the interaction mechanism of the cavitation bubbles.

The frequency spectrum envelope shape depends on the degree of cavitation. The form of the spectrum envelope depends on the type of cavitation. The vaporous cavitation power spectral density remains constant at low frequency range and decreases at high frequency range proportionally to $\frac{1}{\omega^2}$.

The vaporous cavitation spectrum inherent maximum depicts the gas bubbles resonant frequency and depends on the fluid flow velocity. This frequency can be expressed as follows (Shalnev, 1956):

$$f_0 = \frac{1}{r_B} \tag{A.12}$$

As shown by (Gafurov, 2011), (Gasparov, 2007), (Kryuchkov, 2000), cavitation erosion is a major factor that can lead to increased wear of the angular contact sleeve bearing of aviation pumps. In this process the hydrodynamics processes inside the two-stage pump play a crucial role. Additionally, Kalnin et al. (Kalnin, 1980) shows that cavitation self-oscillations generated in hydraulic pipelines due to attached to a pump aggregates do not lead to it significant dynamic loading of the pump.

A.3 Multicomponent flow

Aviation fuels are known to dissolve a significant amount of gas. This amount is directly proportional to the absolute pressure in aircraft tank and in inverse proportion to a specific weight, surface tension and viscosity of used fuel. A flow swirl and vortex disturbances originating in supply pipelines contribute to dissolved gas vaporization. At that, the violence of dynamical equilibrium in fluid-gas system is possible. This violation is accompanied by the liquid-gas transition and finally results in cavitation. The presence of gas in fuel decreases the anti-cavitation characteristics of blade pumps (Dyro, 1962), (Pilipenko, 1977), (Almazov, 1985).

The dependence represented in Figure A.2 and obtained in work (Chebayevskiy, 1973) is the simplest method to estimate the variation of screw-centrifugal pump cavitation characteristics in case of liberated gas presence.

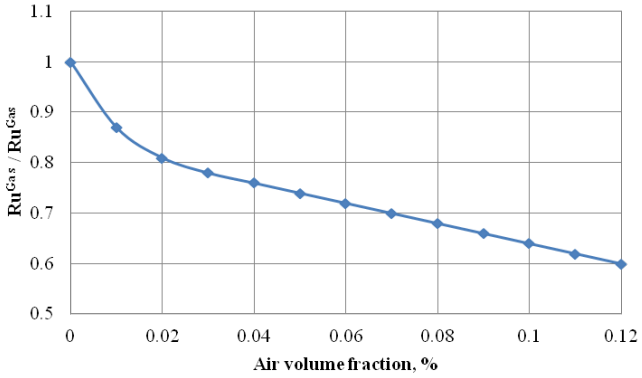

Figure A.2: The liberated gas influence on screw-centrifugal pump anti-cavitation characteristics

Ru is a Rudnev critical coefficient for liquid-gas mixture. This coefficient can be derived from the following equation

$$Ru = \frac{5.62 \cdot \sqrt{Q}}{H_{crit}^{3/4}}, \tag{A.13}$$

Net positive suction head (NPSH) of a pump in case of liquid-gas mixture can be find as follows

$$H_{crit} = \frac{p_{rit} - p_S}{\rho_{fluid} \cdot g} \cdot (1 + C_{gas}) + \frac{Ru_{fluid}}{2g} \cdot (1 + C_{gas})^2 \tag{A.14}$$

The rate of gas liberation from fuel depends on rate of pressure drop in a tank, i.e. on the climb speed of the aircraft. Gas liberation process does not have enough time to archive a dynamical equilibrium state in case of high aircraft climb speeds. It results in fluid

supersaturation by gas which can be liberated at certain conditions. Pressure before a screw is the lowest pressure in a fuel system. It determines the primary occurrence of cavitation at the inlet of s screw blades.

This process is exacerbated by a supply pipeline curvature that lead to stagnant zones formation. In this case, entrapment pockets can occur. They constrict the flow cross-section that, finally, lead to cavitation origin. Entrapment pockets segregated in stagnant zones diffuse extremely slowly. Consequently, cavitation can proceed for a long period of time – 15-20 minutes (Arinushkin, 1967).

A significant role of gas in cavitation processes on operating regimes with reduced flow rates was confirmed during a series of experiments when water with a variety of gas content was used as a working fluid (Chebayevskiy, 1973). Decrease of gas content led to substantial decrease of pressure when cavitation occurs. In case of increased flow rates there were no similar influences of gas content. Therefore, gas content in a working fluid plays a vital role in cavitation origin primary on reduced flow regimes. At that, due to small sizes of gas bubbles they can be invisible. Experimental investigations show that cavitation is generated at a hub between screw and centrifugal wheel on a pump reduced flow operating regimen and on decreased inlet pressure. It can be explained by the partial separation of the invisible gas bubbles. These bubbles are liberating at a screw inlet and then moving along a screw and subsequently merging into large bubbles.

A.4 Undissolved gas

One of the most significant loading sources for pumps is an undissolved gas which can enter the pump (Berti, 2014), (Gafurov, 2014). Experiments (Kalnin, 2002) showed that the behaviour of pump head breakdown in case of undissolved gas penetration to the screw-centrifugal pump inlet is similar to behaviour of pump head breakdown due to the cavitation. This accompanied by the intensive pressure and flow rate self-oscillations inside a fuel system.

In papers (Pilipenko, 1977) and (Vodyanitskiy, 1976) a mathematical model was proposed for determining of the boundaries of stability working zone of hydraulic system with a screw-centrifugal pump in case of free gas presence. This model takes into account capacitance and inertia performances as well as the system hydraulic resistances (Figure A.3).

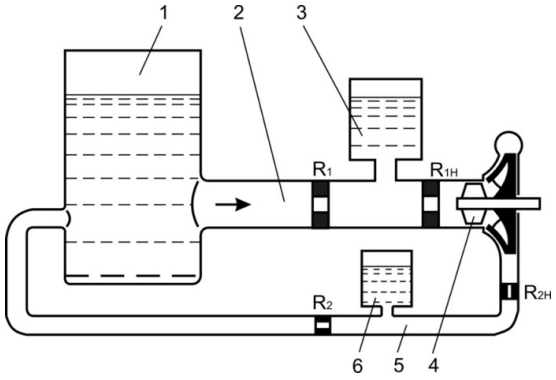

Figure A.3: Structural design of a model for stability working zone determination of a hydraulic system with a screw-centrifugal pump
1 – tank; 2 – supply pipeline; 3 – a lumped elasticity at a pump inlet; 4 – a screw-centrifugal pump; 5 – delivery pipe; 6 – a lumped elasticity after a pump

Undissolved gas was simulated as a lumped elasticity before and after a pump. Cavitation cavities elasticity and cavitation resistance of a pump flow channel can be determined as follows:

$$Y = \frac{f_{stab}^2 \cdot \left[X_{in}^{SCS} \cdot \left(\left(R_{in}^{SCS}\right)^2 + f_{stab}^2 I_1^2\right) - I_1\right] \cdot \left(\left(R_{in}^{SCS}\right)^2 + f_{stab}^2 \cdot I_1^2\right)}{\left(R_{in}^{SCS}\right)^2 + f_{stab}^2 \cdot \left[X_{in}^{SCS} \cdot \left(\left(R_{in}^{SCS}\right)^2 + f_{stab}^2 \cdot I_1^2\right) - I_1\right]^2}; \quad \text{(A.15)}$$

$$O = \frac{R_{in}^{SCS} \cdot \left(\left(R_{in}^{SCS}\right)^2 + f_{stab}^2 \cdot I_1^2\right)}{\left(R_{in}^{SCS}\right)^2 + f_{stab}^2 \cdot \left[X_{in}^{SCS} \cdot \left(\left(R_{in}^{SCS}\right)^2 + f_{stab}^2 \cdot I_1^2\right) - I_1\right]^2}, \quad \text{(A.16)}$$

where f_{stab} is a flow oscillations frequency nearby the stability boundary.

The value of compliance of the lumped elasticity at pump inlet, X_{in}^{SCS} is calculated by taking into account fluid compressibility and wall compliance of the supply pipe.

The resistance of the supply pipe can be neglected. Solution of the equations (A.15) and (A.16) relative to the oscillations frequency gives:

$$f_{stab}^2 = \frac{Y}{I_1 \cdot (1 - C_l \cdot Y)} \quad \text{(A.17)}$$

The analysis of the equation (A.17) shows that the lumped elasticity has an ambiguous influence on the system stability zone at $X_{in}^{SCS} \neq 0$

According to equations (A.15) and (A.16) a stabilizing influence of the coefficient R_1 decreases if

$$\frac{X_{in}^{SCS}\cdot\left(R_{in}^{SCS}\right)^2}{I_1}>\frac{2-X_{in}^{SCS}Y_1}{1-X_{in}^{SCS}Y} \tag{A.18}$$

This condition at low values of R1 executes in a wide range of the lumped elasticity compliance $X_{in}^{SCS}>>\frac{1}{Y}$.

The energy supply to the oscillation system is determined by the negative cavitation resistance *O* and flow rate amplitude at the pump inlet $\delta\overline{Q}_1$. Oscillation energy dissipation is determined by the hydraulic resistance of the supply pipeline R_1 and flow oscillations at the supply pipeline $\delta\overline{Q}_1'$. If flow rate oscillations amplitude before a screw $\delta\overline{Q}_1$ is higher than flow rate oscillations amplitude in supply pipeline $\delta\overline{Q}_1'$, i.e. $\left|\frac{\delta\overline{Q}_1}{\delta\overline{Q}_1'}\right|>1$, then the oscillation energy flux generated by the pump is higher than energy flux dissipated due to hydraulic resistance. This can explain the destabilizing influence of the lumped elasticity compliance at the pump entrance for condition (A.18).

Small values of a lumped elasticity compliance and resistance R_1 lead to fail of condition (A.18). At that, amplitudes ratio $\left|\frac{\delta\overline{Q}_1}{\delta\overline{Q}_1'}\right|<1$ is lower than 1, i.e. flow rate oscillation amplitude in supply pipeline is higher than flow rate oscillation amplitude at pump entrance. In this case generated energy is lower than dissipated energy and lumped elasticity has a stabilizing influence on system stability.

Consequently, compliance increasing of a lumped elasticity at a pump entrance up to value when condition (A.18) is satisfied leads to stabilization influence of the lumped elasticity on system stability. Its further increase leads to destabilizing influence. Hence, obtained results showed the ambiguousness influence of free air influences.

Experimental investigations of a screw pump stability on (Vodyanitskiy, 1978) regimes with undissolved gas confirmed the ambiguous influence of this lumped elasticity. Figure A.4 and Figure A.5 represent screw relative head, $\overline{H}$, and power, $\bar{P}$, versus gas volume fraction, $C=\left(\frac{Q_{gas}}{Q_{fluid}}\right)_{in}$, at pump entrance typical characteristics. Two regions can be subtracted. Region I is a dip at high angles region of $\overline{H}$ and, $\bar{P}$, due to increasing of undissolved gas volume fraction. There is a small correlation between $\overline{H}$ and δ in the characteristic region II. A bubble flow structure in blade channels is observed on region I. At that, there is an increased gas bubbles volume fraction at suction side of screw in direction to a hub. Free gas volume fraction increases due to gas separation to blades suction sides in low-pressure zones. Increased flow-delay angles can also lead to undissolved gas fraction increasing. Flow-delay angles variation can be induced by flow

pushing away to blades pressure sides and by and hydraulic losses. Hydraulic losses occur due to relative fluid flow around gas bubbles. All these factors lead to decreasing of pump head and power. Experimental investigations showed that the mixture flow structure in blade channels varies at a certain undissolved gas fraction. Cavitation cavity originates from suction side of the blade. This cavity mostly consists of gas phase and the isolate itself beyond the screw. For this reason, even at high pump inlet pressure a flow regime with super cavitation can occur in case of two-phase flow. Such flow regime corresponds to the region II.

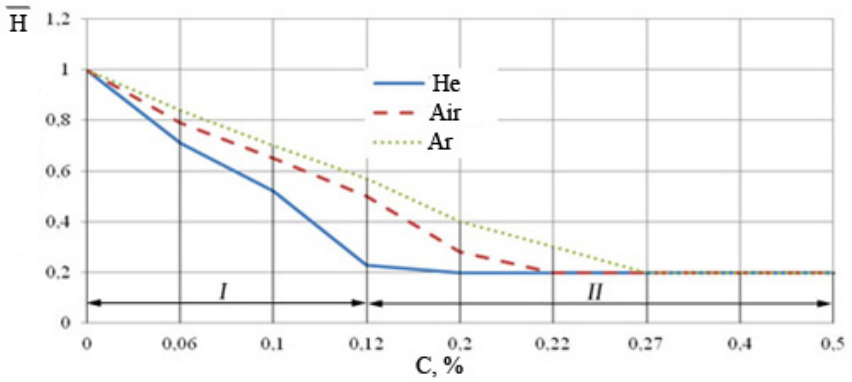

Figure A.4: Pump head versus free gas volume fraction typical characteristics

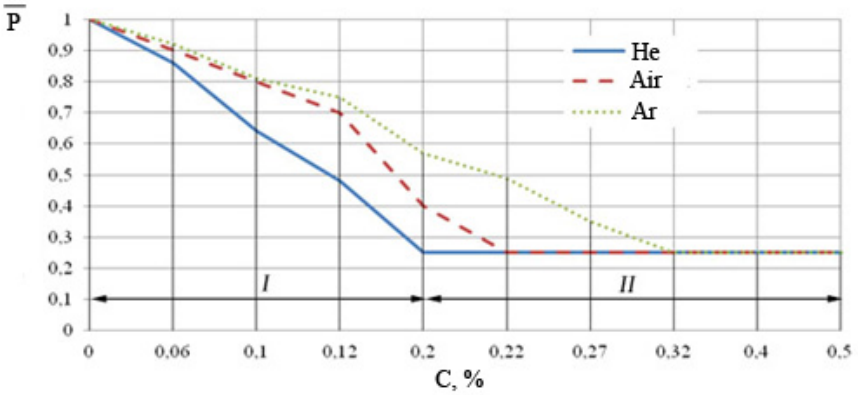

Figure A.5: Pump power versus free gas volume fraction typical characteristics

Papers (Kjeldsen, 2009) and (Keller, 1983) also investigated the influence of undissolved gas on cavitation process inside axial pumps and on their stress states. Obtained results are shown in Figure A.6. They were obtained for six-threaded screw for four different volume flow rates at rotation frequency 900 min^{-1}. Experimental results obtained in paper (Kjeldsen, 2009) showed that cavitation number is a function of the mixture composition. Cavitation number increases due to free gas fraction increasing while tensile stresses on a screw blades does not dependent on the gas volume fraction.

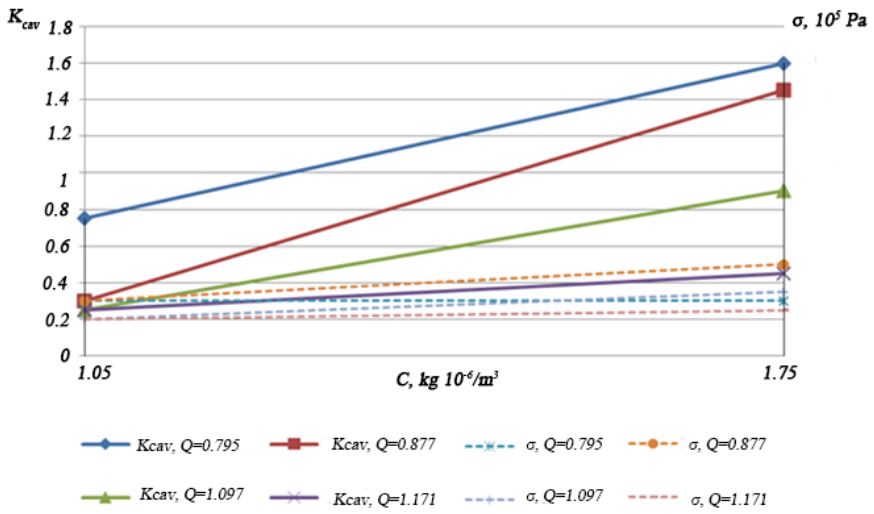

Figure A.6: The dependence of cavitation number and tensile stresses at screw blade on the amount of free gas on the working fluid

Inlet pressure oscillations of a centrifugal pump were investigated in paper (Lecoffre, 1999). Pump rotational speed was constant and equal to N=850 min^{-1}. Volume flow rate was varied from 0.075 to 0.15 m^3/s. Free gas content was also varied. Two regions can be depicted:

- On the first region, a small amount of free gas induces a dramatic increasing of pressure RMS on impeller vanes;
- On the second region, further increasing of free gas content leads to decreasing of pressure RMS. Finally, they become lower than initial value of pressure RMS in case without undissolved gas.

The critical gas content in a stream is known form work (Chebayevskiy, 1973) to be a function of screw-centrifugal pump inlet pressure. The lower inlet pressures the higher the gas content is needed to failure the pump working capacity. The higher shaft rotational speeds the higher gas content is needed to induce a pump breakdown. These phenomena can be explained by a screw breakdown but by a centrifugal wheel breakdown. It occurs at a relative lower free gas content at pump inlet. At that, pump breakdown is defined mostly by the free gas content. It almost does not depend on inlet pressure. Centrifugal wheel breakdown occurs in the moment when cavitation cavities occupy all the length of the blades suction side.

A.5 Vibrations

Nowadays reliability of aviation engines is well known to be depending on vibration and noise levels (Makay, 1978). Rapidly changing mechanical and hydrodynamic forces acting on aviation pumps induce the vibration of its elements. Pressure pulsations in

pumps are the most widespread sources of vibrations and noise. They induce the dynamic loads of pump rotor, its bearings, sealing and others (Alekseev, 1979), (Almazov, 1985), (Brennen, 2011). Kinetic pump generates high intensive pressure pulsations both inside a pump and attached pipelines due to finite number of blades and separated flows. Eventually this leads to occurrence of vibration. Exploitation experience of control and fuel systems shows that fatigue failures are the most significant source of manifolds breakage (Belyy, 1965).

Construction vibration then induces and amplifies pressure pulsations in hydrodynamic canals and leads to changing of their characteristics. Increased vibrations and pulsations in aviation fuel supply lines are well known to lead to undesirable and dangerous effects: instability of control system, cavitation break of the pump, operational instability of gas generator and combustion chamber, decrease in regulatory system accuracy, decrease of fatigue strength of construction elements, changes of the dynamic loads in rotors and its bearings.

In paper (Kalnin, 1980) shows that there is a sharp increase of bearing loading and its vibrations in the range of low fuel flow-to-revolutions ratios of screw-centrifugal pump, $\frac{Q_{in}}{N}$, in comparison on their values on the nominal operating regime (Figure A.7). At that, radial force *Fr* acting on the bearing at $\frac{Q_{in}}{N} = 0.1$ (partial power regime) changes by 5 times. Additionally, the direction of the radial force vector changes. At the nominal operating regime, it directs to the larger cross-sections of the volute while at the low flow-to-revolutions ratio equal to 0.1 it directs to the smaller cross-sections. The direction changing angle is 50 degrees. Vibration overloads and pressure pulsations in the pump at the partial power regime are higher in 3-4 times in comparison with the nominal operating regime. At that, there are no significant changes in axial and radial runouts.

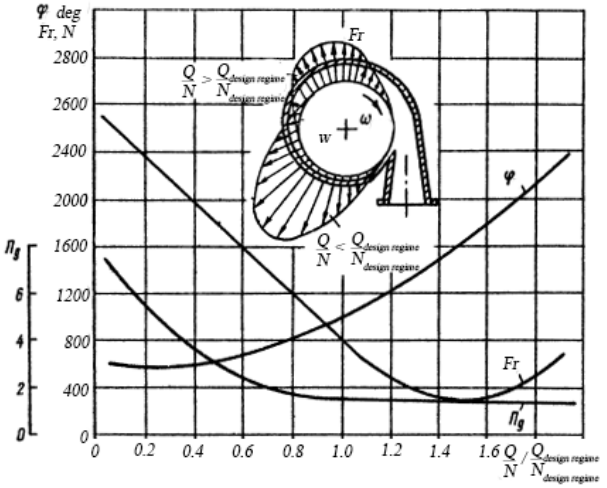

Figure A.7: Changing of radial force on the bearing, its vector and vibration overload

Generally, the most powerful source of induced oscillations inside the two-stage pumps is a gear stage. It generates intensive oscillations with a frequency N^{GS} according to correspond gear tooth mesh frequency (OJSC "Scintific and production enterprice "Temp" named after F.Korotkov", 1990), (Shorin, 1996), (OJSC "Samara construction bureau of engines design", 1993):

$$N^{GS}=f\cdot Num^{GS} \tag{A.19}$$

Another source of induced oscillations is the screw and a centrifugal wheel due to their finite number of blades. Screw-centrifugal stage generates oscillations with a frequency N_{SCS} corresponding to the impeller blade frequency:

$$N^{SCS}=f\cdot Num^{C} \tag{A.20}$$

Experimental results obtained in (Shorin, 1996) indicate that there is a direct influence of pressure pulsations at the entrance to the screw-centrifugal stage and pressure pulsations at the outlet of the gear stage on vibration accelerations. This allows to assume that pressure pulsations have a decisive influence on vibroacoutics characteristics of the pump elements.

Authors of an article (Shorin, 1996) used piezoelectric accelerometers to estimate the vibration state of a two-stage fuel pump ND-25. These transducers were installed in axial directions. The results showed that maximum vibration loads occur o 8.43 and 16.86 Hz. They corresponded to the first and the second tooth harmonics of the gear stage accordingly. Rough estimation of natural vibration frequencies of the manifolds attached to the considered pump showed that they are 52.5 Hz for supply pipeline, 118, 196, 420 and 1050 Hz for manifolds connecting the stages, 715 Hz. These frequencies lie inside a frequency band of the pump. In other words, the resonance phenomena can occur in attached aggregates during the starting operation of the pump.

References

Abramov, S. B. E. G. V. Z. B. S. V. T. Y., 1993. *Rabocheye koleso gidromashiny [Impeller of hydaulic machines]*. USSR.

Akulichev, V., 1968. Experimental study of elementary cavitation zone. *Akusticheskij zhurnal,* 14(3), pp. 337-343.

Akulichev, V. O. V., 1968. Contact the statistical characteristics of acoustic cavitation and cavitation noise. *Akusticheskij zhurnal,* 14(1), pp. 30-36.

Akulichev, V. O. V., 1968. Some statistical characteristics of cavitation. *Akusticheskij zhurnal,* 14(2), pp. 163 - 169.

Akulichev, V. R. L., 1965. Some relations in the cavitation zone. *Akusticheskij zhurnal,* 11(3), p. 287 – 293.

Alekseev, A., 1979. Snizheniye amplitud kolebaniy davleniya pri rezonansnykh rezhimakh raboty [Decrease of amplitudes of pressure oscillations at resonant operating conditions]. *Vestnik mashinostroyeniya,* 8(Decreasing of pressure oscillations amplitudes in case of resonance operating regimes), p. 15 – 17.

Almazov, A., 1985. Kavitatcionoe vibronagruzhenie visokooborotnikh osevikh nasosov [Cavitation load of axial pumps].. *Kavitatsionnyye kolebaniya i dinamika dvukhfaznykh sistem*, p. 41 – 47.

American Psychological Association, 2009. *Publication manual of the American Psychological Association,* Washington, DC: American Psychological Association.

Amone, A. B. P. C. A. S. E. R. C., 2001. *Ariane 5 TPLOX inducer design strategies to enhance cavitating performance.* Pasadena, California, USA, s.n.

Anon., 1993. *Method for decreasing the leakages in gear pumps.* CCCP.

Antonov, A. K. V. K. V., 1990. *Pul'satsii davleniya pri struynykh i otryvnykh techeniyakh [Pressure pulsations at stream and separate flows].* Moscow: Mashinostroyeniye.

Arinushkin, L. S. A. R. P. A. Y. L. L. G. Y. A., 1967. *Авиационные центробежные насосные агрегаты [Aviation centrifugal pumps]*. Moscow: Mashinostroyeniye.

Bagnold, R. A., 1941. *The physics of blown sand and desert dunes.* s.l.:William Morrow & Co..

Bakir, F. R. R. a. G. A., 2004. Numerical and Experimental Investigations of the Cavitating Behavior of an Inducer.. *International Journal of Rotating Machinery,* Volume 10, pp. pp. 15–25.

Balashov, V. K. V. S. R. V. S., 2006. *Tool System for Automatic Scheduling of Data Exchange in Real-Time Distributed Embedded Systems.*. Istanbul, Turkey, s.n., p. pp. 179–184.

Basu, P., 2006. *Combustion and gasification in fluidized beds.* Boca Raton(FL): CRC Press.

Bazovsky, I., 2013. *Reliability theory and practice.* New York: Dover Publications, inc. Mineola.

Belousov, A. K. I., 1974. *Gidrogazodinamicheskoye proyektirovaniye turbonasosnykh agregatov dvigateley letatel'nykh apparatov [Gasdynamics and hydrodynamic design of turbo pump aggregates of aircraft engines]*. Kuybyshev: KuAI.

Belyy, N., 1965. K voprosu o vibratsiyakh i vynoslivosti truboprovodov [To the issue about vibrations and endurance of pipes]. *Vibratsionnaya prochnost' i nadozhnost' aviatsionnykh dvigateley,* pp. 129 - 133.

Berti, S. F. P. M. A. P. V. L. C., 2014. Design and development of a specially modified positive displacement rotary screw pump and relevant hydraulic circuit to enhance "entrained air handling" capability in a closed loop lube oil system. *Journal of Engineering for Gas Turbines and Power*, 136(7).

Blake, W., 1986. *Mechanics of flow-induced sound and vibration.* New York: Academic Pres..

Blokhintsev, D., 1981. *Akustika neodnorodnoy dvizhushcheysya sredy [Acoutics of nonhomogenous moving fluid]*. Moscow: Nauka.

Brennen, C., 2002. Fission of collapsing cavitation bubbles. *J. Fluid Mech,* Volume 153, p. pp. 472.

Brennen, C., 2011. *Cavitation and bubble dynamics.* s.l.:Cambridge University Press.

Brennen, K., 1978. Eksperimental'nyye issledovaniya dinamiki kavitiruyushchikh nasosov [Experimental investigations of cavitating pumps dynamics]. *Transactions of ASME,* 100(2), pp. 136 - 147.

Brentner, K. C. J. R. C. Y. B. B. K., 1996. *Computation of sound generated by flow over a circular cylinder: an acoustic analogy approach.* Tallahassee, Florida, USA, s.n., pp. pp. 289-295.

Brouwer, M., 2000. *Developments in Test and Verification Equipment for Spacecraft.,* Netherlands: s.n.

Bruce, D. W. M. G. S., 1997. *Flow filed analysis of Both the tribal elements and mixing disk zones within a closely intermeshing co-rotating twin-screw extruder.*. Munich, Hanser Publishers, pp. 323-330.

Chebaevskiy, V., 1957. K voprosu o mekhanizme kavitatsii v tsentrobezhnykh nasosakh [To the issue about mechanics of cavitation in centrifugal pumps]. *Teploenergetika*, Volume №9.

Chebaevskiy, V., 1959. Sposob raschota tsentrobezhnykh nasosov na kavitatsiyu [Method of cavitation calculation for centrifugal pumps]. *Vestnik mashinostroeniya*, Volume №8.

Chebayevskiy, V. F. P. V., 1973. *Kavitatsionnyye kharakteristiki vysokooborotnykh shneko-tsentrobezhnykh nasosov [Cavitation performances of high-speed screw-centrifugal pumps]*. Moscow: Mashinostroyeniye.

Chudina, M., 2003. Detection of cavitation phenomenon in a centrifugal pump using audible sound. *Mech. syst. signal process,* 17(6), pp. 1335-1347.

Chudina, M., 2003. Noise as an Indicator of Cavitation in a Centrifugal Pump. *Acoustical Physics,* Volume 49, pp. 463-474.

Chudina, M. P. J. C. J., 2012. *Use of noise and vibration spectra to detection cavitation in kinetic pumps.* s.l., s.n., pp. 456 - 461.

Curle, N., 1955. The influence of solidbound aries upon aerodynamic sound. *Proc. Royal Society A,* Volume 231, pp. pp. 505-514.

Dalpiaz, G. M. E., 2013. *Experimental validation of a model for the dynamic analysis of gear pumps.* Portland, Oregon, USA, s.n.

Demeulenaere, A. L. E. L. D. N. J. L. S., 2002. *Application of the domain scaling approach to the calculation of the unsteady flow in a rocket engine turbopump.* Lausanne, s.n.

Dovgot'ko, I., 1980. About a case of investigation of "screw-centrifugal pump - pipes" system operation stability in relation to cavitation self-oscillations. *Dinamika nasosnykh sistem*, p. 9 – 14.

Dovgot'ko, N., 1976. Analysis of theoretical and experimental results of investigations of influence of screw booster pump design parameters on centrifugal pump-pipes operation sbability. *Kavitatsionnyye avtokolebaniya v nasosnykh sistemakh [Cavitation self-oscillations in pumping systems]*, Volume 1, pp. 53 - 56.

Dovgot'ko, N. I. P. V. V., 1985. Issledovaniye kolebaniy v nasosnoy sisteme s kavitiruyushchimi shnekovym prednasosom i tsentrobezhnym kolesom

[Investigations of oscillations in pump system with cavitating screw booster pump and centrifugal wheel]. *Gidrogazodinamika tekhnicheskikh sistem*, p. 7 – 16.

Dumov, V. P. M. A., 1962. Некоторые результаты исследования работы осевых винтовых колёс [Some investigation results of axial screw wheels operation]. *Energomashinostroenie*, Volume 2.

Dyro, R., 1962. Nekotoryye rezul'taty issledovaniya raboty osevykh vintovykh kolos [Some investigation results of axial screw wheels operation]. *Energomashinostroyeniye*, Volume 2.

Eaton, M. K. P. E. K., 2006. The modelling, prediction, and experimental evaluation of gear pump meshing pressures with particular reference to aero-engine fuel pumps.. *Proceedings of the Institution of Mechanical Engineers. Part I: Journal of Systems and Control Engineering.* , 220(5), pp. Pages 365-379.

Eisenberg, P., 1961. *Cavitation.* Fluid Mechanics ed. s.l.:McGraw Hill.

Ershov, V., 1959. Variatsionnyy printsip maksimuma potoka mekhanicheskoy energii i yego prilozheniye k raschotu osevykh turbomashin [Variation principle of mechanical energy maximum and its implementation for axial turbine machines calculation]. *Izvestiya vuzov. Seriya «Aviatsionnaya tekhnika»*, Volume 1.

Fanelli, M., 1996. *Some Present Trends in Hydraulic Machinery Research, Hydraulic Machinery and Cavitation.* Dordrecht: Kluwer Academic Publishers.

Fatikov, V. P. G. M. I. A. M. K. S. V., 2005. Kompleks informatsionnogo i polunaturnogo modelirovaniya dlya issledovaniya sistem avtomaticheskogo upravleniya i kontrolya mnogodvigatel'nykh silovykh ustanovok pri ikh ekspluatatsii po sostoyaniyu [HIL modeling complex for control systems investigation and many engines power plants control in case]. *Aviatsionno-kosmicheskaya tekhnika i tekhnologiya,* Volume 2, p. pp. 155–160.

Franc, J. P. ,. M. J. M., 1997. Cavitation erosion research in France: the state of the art. *Journal of Marine Science and Technology*, Volume 2, pp. 233 - 244.

Franc, J. P. M. J. M., 2010. *Fundamentals of Cavitation.* s.l.:Kluver Academic Publishers.

Frith, R. S. W., 1996. Comparison of an external gear pump wear model with test data.. *Wear*, August, 196(1-2), pp. 64-71.

Frobenius, M. S. R. F. J. K. G., 2002. Numerical and experimental investigations of the cavitating flow in a centrifugal pump impeller. *ASME,* pp. FEDSM2002-31006.

Frosina, E. ,. S. A. B. D. M. M. O. M., 2013. A tridimensional CFD analysis of the oil pump of a high performance motorbike engine.. *68th Conference of the Italian*

Thermal Machines Engineering Association, ATI 2013, 11 September 2013 through 13 September, Volume 45, pp. Pages 938-948.

Gafurov, S. B. K. G. A., 2014. The semi-natural test bench with virtual gas turbine engine model for fuel supply and control system characteristics investigation.. *Research Journal of Applied Sciences,* 9(11), pp. 806-811.

Gafurov, S. P. A. S. E., 2014. *Reduction of vibroacoustic loads in aviation combined pumps.* St. Petersburg; Russian Federation, s.n.

Gafurov, S. R. L., 2014. *Acoustic visualization of cavitation in fuel combination pump.* Beijing, China, s.n., pp. 3916-3923.

Gafurov, S. R. L. G. A., 2014. *Combined air supply at fuel pump entrance.* Lappeenranta, Finland, s.n.

Gafurov, S. R. L. K. A. M. G. S. E., 2011. Investigation of the causes of the auger-centrifugal pump bearing destruction. *Vestnik Samarskogo gosudarstvennogo aerokosmicheskogo universiteta imeni akademika S.P. Koroleva (nacionalnogo issledovatelskogo universiteta),* 2(33), p. 164 – 171.

Gasparov, M. K. A. R. L. S. E., 2007. *High-frequency axial vibration in a combined pump unit with gear stage..* s.l., s.n., pp. 117-127.

Gasparov, M. K. A. R. L. S. E., 2007. High-frequency axial vibration in a combined pump unit with gear stage.. *Power Transmission and Motion Control,* pp. 117-127.

Gasparov, M. K. A. S. E. a. R. L., 2006. Wavelets in the investigation of the cavitation processes in pump.. *Izvestiya samarskogo naychnogo centra rossiiskoi akademii nauk. ,* 4(8), p. 1131 – 1135.

Gasparov, M. K. A. S. E. S. V., 2006 . *Гидродинамика и виброакустика комбинированных насосных агрегатов [Hydrodynamics and vibroacoutics of combined pumps].* Samara: Samara State Aerospace University.

Gasparov, M. K. A. S. E. S. V., 2006. *Gidrodinamika i vibroakustika kombinirovannykh nasosnykh agregatov [Hydrodynamics and vibroacoustics of two-stage pumps].* Samara: Samara State Aerospace University.

Gerber, A., 2002. *A CFD model for devices operating under extensive cavitation conditions.* New Orleans, Louisiana, USA, s.n., pp. 341- 329.

Geymayr, J. A. B. E. N. F. F., 1995. Fault-tree analysis: a knowledge-engineering approach. *Reliability,* 44(1), p. 37–45.

Ghionea, I. T. C. T. P., 2012. Simulation of the Working Conditions for a Gear Pump Using Finite Element Analysis Method.. *Scientific Bulletin Series C: Fascicle Mechanics, Tribology, Machine Manufacturing Technology.,* 2012(26), pp. 21-27.

Gilchrist, W., 1993. Modelling failure modes and effects analysis. *International Journal of Quality & Reliability Management,* 10(5), p. 16–23.

Gimadiyev, A. G. K. A. S. Y. V. S. V. P., 1998. *Snizheniye vibroakusticheskikh nagruzok v gidromekhanicheskikh sistemakh [Decreasing of vibroacoutic loads in hydro-mechanical systems].* Samara: Samara State Aerospace University.

Godovanyuk, A., 2005. *Elementy kontrolya i upravleniya v imitatsionnykh modelyakh GTD [Elements of control and management in GTE simulation modeling]..* Ufa, UGATU, p. pp. 33–38.

Golberg, F. G. O. P. A., 2010. Onboard Simulation Model as Part of GTE Control System for Improving Fault Tolerance and Control Quality.. In: *Automatic control systems of gas-turbine engines..* s.l.:TORUS PRESS.

Golberg, F. G. O. P. A., 2014. *Improving control reliability and quality of aircraft engines by means the software virtual engine..* St. Petersburg, Russian Federation, s.n.

Goldsteyn, M., 1981. *Aeroakustika [Aeroacoustics].* Moscow: Mashinostroyeniye.

Gonza´lez J., F. E. B. C., 2001. Numerical Simulation of the Dynamic Effects Due to Impeller-Volute Interaction in a Centrifugal Pump.. *ASME J. Fluids Eng.,* Volume 124, p. pp. 348–355.

Gonza´lez, J. S. J. C. B. E. ,. F. J., 2002. Unsteady Flow Structure on a Centrifugal Pump: Experimental and Numerical Approaches. *Proceedings of ASME,* pp. Paper FEDSM2002-31182..

Goto, A. N. S. M. S. Y., 2001. *Hydrodynamic design system for pumps based on 3-D CAD, CFD and inverse design method.* New Orleans, Louisiana, USA, s.n., pp. paper FEDSM2001- 18068.

Goto, A. Z. A., 2002. Hydrodynamic Design of Pump Diffuser Using Inverse Design Method and CFD. *ASME J. Fluids Eng.,* 124(2), p. 319 – 328.

Grigoriev, Y. E. D. N., 1985. *Vliyaniye termodinamicheskogo effekta kavitatsii na nekotoryye parametry kavitatsionnogo techeniya zhidkosti v nasosakh [Influence of the thermodynamic effect of cavitation on some parameters of the cavitation flow in pumps].* Kiev, Naukova Dumka, pp. 31-34.

Grigor'yev, Y. Y. P. V. V., 1985. Vliyaniye dinamicheskikh svoystv obratnykh techeniy na vkhode v nasos na ustoychivost' nasosnykh sistem i chastoty kolebaniy [Influence

of dynamic properties of back eddies at pump entrance on pumps systems stability amd oscillation frequencies]. *Gidrogazodinamika tekhnicheskikh sistem*, p. 3 – 7.

Gulich, J., 2010. *Centrifugal Pumps.* Berlin: Springer.

Guo, A. J. T. W. T. H. Y. Z. D., 2014. Numerical Simulation on the Flow Field of External Gear Pump Based on FLUENT.. *Applied Mechanics & Materials,* Issue 556-562, pp. 1421-1425.

Gurevich, O. B. Y. G. A., 2005. Demonstratsionnaya sistema avtomaticheskogo upravleniya na baze elektroprivoda [Demonstration automatic control system based on motor drive].. In: s.l.:s.n.

Gurevich, Y. S. B. A. S. T. V. I., 2010. Demonstratsionnaya sistema upravleniya i toplivopitaniya gazoturbinnogodvigatelya na baze elektricheskikh privodov [Demonstration automatic control system of aviation gas turbine engines]. In: Moscow: CIAM.

Hagelstein, D. H. K. V. d. B. R. A. E. A. K. R. R. R., 2000. Experimental and Numerical Investigation of the Flow in a Centrifugal Compressor Volute.. *ASME J. Turbomach.,* Volume 122, p. pp. 22 – 31.

Han, H. T. K. K. K. T., 2000. Internal Flow Simulation in Screw-Type Centrifugal Pump. *J. Turbomach.,* 28(3), p. 183–190.

Hardin, J. P. D., 1994. An acoustic/viscous splitting technique for computational aeroacoustics. *Theoretical and Computational Fluid Dynamics,* Volume 6, pp. pp. 323-340..

Heckl, M. M. M., 1980. *Spravochnik po tekhnicheskoy akustike.* Leningrad: Sudostroyeniye.

Hillewaert, K. V. d. B. R. A., 1999. Numerical Simulation of Impeller-Volute Interaction in Centrifugal Compressors. *ASME J. Turbomachinery,* Volume 121, p. 603 – 608.

Hillewaert, K. V. d. B. R. A. E. A. K. ,. R. M., 2000. Experimental and Numerical Investigation of the Flow in a Centrifugal Compressor Volute. *ASME J. Turbomach,* Volume №122, p. 22 – 31.

Hogg, S. L. M. A., 1989. Computation of highly swirling confined flow with a Reynolds stress turbulence model. *AIAA Journal,* Volume 27, pp. 57 - 63.

Holme, P. K. B. J. Y. C. N. H. S. K., 2002. Attack vulnerability of complex networks. *Physical Review E,* 65(5), pp. 56-109.

Hosangadi, A. A. A. V. A. S., 2001. *Generalized Compressible Cavitation Model.* Pasadena, CA, USA, California Institute of Technology, pp. Paper Cav2001-B4-003.

Howe, M., 1979. The role of surface shear stress fluctuations in the generation of boundary layer noise. *Journal of Sound and Vibration,* 65(2), pp. pp. 159-164.

Hunsaker, J. C., 1935. Cavitation research. *Mech. Eng.,* Volume 57, pp. 211 - 216.

Iaccarino, G., 2004. *Numerical Methods in Fluid Dynamics Using Commercial CFD Codes.,* s.l.: s.n.

Ichikawa, T. Y. K., 1971. On pulsation of delivery pressure of gear pump. *Bull JSME,* December, 14(78), pp. 1304-1312.

Iga, Y. O. N. Y. Y. I. T., 2009. *Numerical Investigation of Thermodynamic Effect on Unsteady Cavitation in Cascade.* Ann Arbor, MI, s.n., pp. 16 - 20 .

Igolkin, A., 2014. Vibroacoustic loads reduction in pipe systems of gas distribution stations. *Journal of Dynamics and Vibroacoustics. ,* 1(1).

Igolkin, A. K. A. K. A. S. A. S. E., 2012. *Pressure reducing valve noise reduction.* Vilnius, Lithuania, s.n.

Igolkin, A. K. A. P. A. S. E., 2002. Research of influencing of air delivery in a suction pipe line of the centrifugal pump on its vibroacoustical response. *Vestnik Samarskogo gosudarstvennogo aerokosmicheskogo universiteta im. akademika S.P. Koroleva (nacional'nogo issledovatel'skogo universiteta),* Volume 1, pp. 78-83.

Incorporated, F., 2009. *FIDAP manuals version 8.52,* s.l.: FLUENT Incorporated.

Inozemtsev, A. N. M. S. V., 2008. *Avtomatika i regulirovaniye aviatsionnykh dvigateley i energeticheskikh ustanovok [Automatic and control of aviation engines and power plants].* s.l.:Mashinostroenie.

International, N., 2010. *FINE/Turbo manuals version 4.1,* s.l.: NUMECA International.

ISO 3555, 1977. *Centrifugal, mixed flow and axial pumps - Code for acceptance tests - Class B.* s.l.:s.n.

Ito, Y. T. N. K. Y. K. S. N. T., 2012. *New visualization test facility for liquid nitrogen and water cavitation in rotating inducer.* s.l., s.n., pp. 757-762.

Kai, Z. J.-x. Z. J.-n. C. Y.-w. Z., 2011. Simulation and analysis of flow field inside micro-gear pump with dynamic mesh. *Journal of Lanzhou University of Technology,* Feb, 37(1), pp. 45-49.

Kalnin, V. M. S. V. A., 1980. Nagruzheniye rotora shneko-tsentrobezhnogo nasosa pri avtokolebaniyakh v gidrosisteme [Loading of screw-centrifugal pump rotor in case of self-oscillations in hydraulic system]. *Dinamika nasosnykh sistem,* pp. 22 - 27.

Kalnin, V. S. V., 2002. Dinamika kavitatsii tsentrobezhnykh nasosov ZHRD [Dynamics of cavitation in centrifugal pumps of liquid rocket engines]. *Dvigatel*, 3(21), pp. 38 - 41.

Karelin, V. Y., 1970. *Iznos lopastnykh gidravlicheskikh mashin ot kavitatsii i nanosov [Wear of vane hydraulic machines due to cavitation and alluvium]*. Moscow: Mashinostroyeniye.

Karelin, Y. V., 1975. *Kavitatsionnyye yavleniya v tsentrobezhnykh i osevykh nasosakh [Cavitation phenomena in axial and centrifugal pumps]*. Moscow: Mashinostroyeniye.

Kelecy, F. J., 2003. Numerical Prediction of Cavitation in a Centrifugal Pump. *ONET-CFD Network Newsletter,* Volume 3, pp. 14 - 16.

Keller, A. P. Y. Z., 1983. *Maßstabsgesetze bei der Anfangskavitation,* München: TU München.

Kim, Y. T. T. K. Y. L. M. Y., 2000. Pressure Fluctuation Due to Air Entrainment in Screw-Type Centrifugal Pump. *Trans. JSME,* Volume 644, p. 1126–1131 .

Kinelev, V. G. V. Y. N. K. S., 1976. *Fizicheskaya model' kavitiruyushchego shneko-tsentrobezhnogo nasosa, rabotayushchego v shirokom diapazone rezhimov po raskhodu [Physical model of cavitating screw-centrifugal pump operating in a wide range of mass flow]*. Kiev, Naukova Dumka, pp. 100 - 107.

King, D., 1992. *Fluidized catalytic crackers: an engineering review.* New York, Engineering Foundation, pp. 15-26.

Kjeldsen, M. R. E. A. A., 2009. *Blade load dynamics in cavitating and two phase flows.* Ann Arbor, Michigan, USA, s.n., p. Paper No. 113.

Kojima, E. S. M., 1984. Characteristics of fluidborne noise generated by fluidpower pump. *Bulierin of JSME,* 27(232), pp. P. 2188 - 2195.

Kojima, E. S. M., 1984. Characteristics of fluidborne noise generated by fluid power pump (3rd report, discharge pressure pulsation of external gear pump). *Bulletin of the JSME,* October, 27(232), pp. 2188-2195.

Konami, S. N. T., 2017. *Hydraulic Control Systems – Theory and Practice.*. Singapore: World Scientific Publishing Company.

Kozlov, S. R. V. E., 1988. *Tsentrobezhnyy nasos [Centrifugal pump]*. USSR.

Kruchkov, A. L. V. P. A. S. E., 2000. The investigation of vibroacoustical activity of the combined fuel pump.. *139th Meeting Acoustical Soc. of America,* 5(107), p. 2877.

Kudashev, Y. a. Y. L., 2009. Kharakteristicheskiy funktsional turbulentnykh pul'satsiy davleniya v zadachakh gidroaerodinamicheskogo shumoobrazovaniya [Characteristic functional ot the turbulent pressure pulsations in hydrodynamical noise generation tasks]. *Akusticheskiy zhurnal,* Volume 1, pp. 91-97.

Kunz, R. F. B. A. C. T. S. S. D. R. G. H. J., 1999. *Multi-phase CFD Analysis of Natural and Ventilated Cavitation about Submerged Bodies.* San Francisco, California, USA., s.n.

Kurakulin, Y., 1978. *Влияние вдува воздуха в питающий трубопровод на кавитационные автоколебания в системе «шнеко-центробежный насос - трубопроводы» [Influence of air intake into pump supply pipe on cavitation self-oscillations in "screw-centrifugal pump-pipes" system]*. Kiev, Naukova dumka, p. 82 – 85.

Kurokawa, J. S. S. L. M. J. I. H., 2000. An Innovative Device to Suppression of Performance Curve Instability of Mixed Flow Pump by Use of J-Groove. *Trans. JSME.,* Volume 642, p. 460 – 467.

Kurokawa, J. S. S. L. M. J. I. H., 2000. Suppression of Performance Curve Instability of Mixed Flow Pump by Use of J-Groove. *ASME J. Fluids Eng.,* Volume 122, p. 592 – 597 .

Labbe, O. P. C. R. G. H. M., 2013. A CFD/CAA coupling method applied to jet noise prediction. *Computers & Fluids,* Volume 86, pp. pp. 1-13.

Lecoffre, Y., 1999. *Cavitation – Bubble Trackers.* s.l.:Balkema.

Lighthill, M., 1952. *On sound generated aerodynamically: I. General theory.* s.l., s.n., pp. pp. 564-587.

Li, S., 2000. *Cavitation of Hydraulic Machinery.* London: Imperial College Press..

Liua, X. A. S., 2013. Failure Propagation Analysis of Aircraft Engine Systems. *Procedia Engineering*, Volume 80, pp. 506-521.

Liu, X. A. S., 2014. Failure Propagation Analysis of Aircraft Engine Systems Based on Complex Network.. *3rd International Symposium on Aircraft Airworthiness, ISAA 2013.,* Volume 80, p. 506 – 521.

Li, Y. ,. G. L. ,. T. X., 28 May 2011 through 30 May 2011. *The flow pulsation analysis of an external gear pump.*. Changsha, China, Advanced Materials Research., pp. 2327-2233.

Li, Y. ,. S. F., 2011. Analysis model on trapped oil and backlash calculation in external gear pump.. *Paiguan Jixie Gongcheng Xuebao,* March, 29(2), pp. Pages 118-122]. .

Li, Y. L. K., 2009. Dynamic model of trapped oil and effect of related variables on trapped oil pressure in external spur-gear pump.. *Nongye Jixie Xuebao,* September, 40(9), pp. Pages 214-219.

Li, Y. L. K., 2009. Established formulas for trapped-oil area and relief-load area of external spur-gear pump.. *Nongye Jixie Xuebao,* June, 40(6), pp. Pages 203-207.

Li, Y. S. F., 2012. Simulation and theoretical analysis on trapped oil pressure in external gear pump influenced by vibration.. *Nongye Gongcheng Xuebao,* July, 28(13), pp. Pages 77-81]. .

Longatte, F. K. J. L., 1999. Analysis of Rotor-Stator-Circuit Interactions in a Centrifugal Pump. *Proceedings of ASME,* pp. Paper FEDSM99-6866..

Lyamshev, L., 1969. Theory of hydrodynamic cavitation noise. *Akusticheskij zhurnal,* 15(4), pp. 572-578.

Lyashchenko, V. S. P. V. I. C. V. S. N. S. I., 1981. *Шнековое колесо насоса [Screw wheel of wheel]*. USSR, Patent No. 2430698.

Majidi, K., 2003. *Numerical Calculation of Impeller/Volute Interaction in a Centrifugal Pump.* s.l., s.n., p. 597 – 606..

Majidi, K., 2004. *Unsteady Radial Thrust of a Centrifugal Pump due to the Impeller/Volute Interaction.* s.l., Pacific Center of Thermal-Fluids Engineering, pp. Paper ISROMAC10-2004-032..

Majidi, K. S. H. E., 2000. Numerical Calculation of Secondary Flow in Pump Volute and Circular Casing Using 3D Viscous Flow Techniques [Text]. *Int. J. Rotating Machinery,* 6(4), p. 245 – 252.

Makaryants, G. P. A. S. V. S. E. M. M., 2011. *SELF-Oscillations of the poppet relief pneumatic valve due to instability of the airflow around an inlet port.*. Rio de Janeiro, Brazil, s.n., pp. pp. 2340-2347.

Makaryants, G. S. V. P. A. M. M. S. E., 2012. *The tonal noise reduction of the proportional pilot-operated pneumatic valve.*. Vilnius, Lithuania, s.n., pp. pp. 689-696.

Makay, E. S. O., 1978. *Survey of feed pump outages ,* s.l.: Morrisville.

Manoharan, C. R. C., 2012. Dynamic analysis of hydrodynamic gear pump performance using design of experiment stand operational parameters. *Journal of Mechanical and Civil Engineering,* 1(6), pp. 17-23.

Manring, N. K. S., 2003. The Theoretical Flow Ripple of an External Gear Pump. *Journal of Dynamic Systems, Measurement, and Control,* September, 125(3), pp. 396-404.

Marseguerra, M. Z. E. P. L., 2002. Condition-based maintenance optimization by means of genetic algorithms and monte carlo simulation. *Reliability Engineering & System Safety,* 77(2), p. 151–165.

Marx, Y., 2000. *Numerical simulation of gear-pump flows,* Lausanne: s.n.

McNulty, P. P. I., 1982. Cavitation inception in pumps. *Journal of fluids engineering,* 104(3), pp. 99-104.

Medvitz, R. K. R. B. D., 2002. Performance Analysis of Cavitating Flow in Centrifugal Pumps Using Multiphase CFD.. *Journal of Fluids Engineering,* Volume 124, pp. pp. 377-383.

Meikel, P. S. B. L. K. S. J. R. K., 2013. *Flight and HIL testing of a longitudinal model reference adaptive controller on a high-lag general aviation aircraft..* Boston, MA, United States,, s.n.

Menter, F. G. H., 2000. Application of advanced turbulence models to complex industrial flows. *Advances in Fluid Mechanics: Calculation of Complex Turbulent Flows.*

Menter, R., 1994. Two-Equation Eddy-Viscosity Turbulence Models for Engineering Applications. *AIAA Journal,* 32(8), pp. 1598-1605.

Moore, C. N. M. E., 2000. Epidemics and percolation in small-world networks. *Physical Review E,* 61(5), p. 5678–5682.

Motter, A. L. Y., 2002. Cascade-based at tacks on complex networks. *Physical Review E,* 66(6), pp. pp. 065-102.

Munin, A. K. V. L. Y., 1981. *Aerodinamicheskiye istochniki shuma [Aerodynamic sources of noise].* Moscow: Mashinostroyeniye.

Murthy, J., 2004. *Numerical Methods in Heat, Mass and Momentum Transfer,* West Lafayette, Indiana,: s.n.

Myllyky, H. J., 1999. *Semi-Empirical Model from the Suction Capability of an External Gear Pump.* s.l.:Tampere University of Technology.

Narmada, S. J. M., 1996. Reliability analysis of a complex system with a deteriorating standby unit under common-cause failure and critical human error. *Micro- electronics Reliability,* 36(9), p. pp. 1287–1290..

Nicoud, F. D. F., 1999. Subgrid-Scale Stress Modelling Based on the Square of the Velocity Gradient Tensor. *Flow, Turbulence and Combustion,* pp. pp. 183-200.

OJSC "Samara construction bureau of engines design", 1993. *Opredeleniye sobstvennykh chastot i vibroaktivnosti agregatov [Determination of natural frequencies and vibration activities of aggregates],* Samara: s.n.

OJSC "Samara construction bureau of engines design", 1998. *Stendovaya proverka rabotosposobnosti agregata ND-25 v sostave izdeliya za 100 chasov narabotki v ekspluatatsii [Stand test of the combined pump ND-25 durability as a part of the engine for 100 operating hours of esxploitation],* Samara: s.n.

OJSC "Scintific and production enterprice "Temp" named after F.Korotkov", 1990. *Otsenka vliyaniya ekspluatatsionnykh faktorov na rabotosposobnost' agregata ND-25 [Estimation of exploitation factors influence on combined pump ND-25 durability],* Moscow: s.n.

OJSC "Scintific and production enterprice "Temp" named after F.Korotkov", 1990. *Otsenka vliyaniya ekspluatatsionnykh faktorov na rabotosposobnost' agregata ND-25 [Estimation of exploitation factors influence on combined pump ND-25 durability],* Moscow: s.n.

Olifirov, F. P. F. V. B. V. G. M. G. M. K. D. B. D., 2011. Высокоэффективные лопастные насосные агрегаты для ГТД гражданской авиации [High-efficiency vane pumps for civil aircrafts]. *Dvigatel ,* 5(17), p. 10 – 13.

Ovsyannikov, B. B. B., 1979. *Teoriya i raschet agregatov pitaniya zhidkostnykh raketnykh dvigateley [Theory and calculation of supply aggregates if liquid rocket engines].* Moscow: Mashinostroyeniye.

Ovsyannikov, V. C. V., 1975. *Vysokooborotistyye lopatochnyye nasosy [High-speed vane pumps].* Moscow: Mashinostroenie.

Page, M. G. A., 2001. *Turbulent Flow Computations in Turbine 99 Draft Tube with CFX-TASCflow, FIDAP and FINE/Turbo Turbine 99.* Sweden, s.n.

Panta, M., 2004. *Numerical flow analysis of gear pump,* Youngstown: s.n.

Papazoglou, I., 2000. Semi-markovian reliability mod- els for systems with testable components and general test/outage times. *Reliability Engineering & System Safety,* 68(2), p. pp. 121–133.

Percy, D. F., 2001. Bayesian enhanced strategic decision making for reliability. *European Journal of Operational Research,* 139(1), p. 133–145.

Pilipenko, V. Z. V. N. M., 1977. *Kavitatsionnyye avtokolebaniya i dinamika gidrosistem [Cavitation self-oscillations abd dynamics of hydraulic systems]*. Moscow: Mashinostroyeniye.

Plesset, M., 1949. The Dynamics of cavitation bubbles. *J. Appl. Mechanics,* pp. 277-282.

Pogorelov, G. A. A. G. A., 2013. Tekhnologiya polunaturnogo kompleksnogo modelirovaniya GTD i yego sistem [The technology of GTE and its systems simulation modeling].. *Aviatsionno-kosmicheskaya tekhnika i tekhnologiya,* p. 172 – 180.

Poroseva, S. I. G., 2001. *Simulating separated flows using the k-ε model,* s.l.: s.n.

Powell, A., 1960. Aerodynamic sound and plane boundary. *The Journal of the Acoustical Society of America,* 32(8).

Prokofiev, A. M. G. S. E., 2010. *Modeling of pipeline vibration under the pressure ripples in the working fluid.*. Cairo, Egypt, s.n., pp. 1142-1149.

Rabiner, L. G. B., 1978. *Teoriya i primeneniye tsifrovoy obrabotki signalov [Theory and impementation of signal digital post processing]*. Moscow: Mir.

Raw, M., 1996. Robustness of coupled algebraic multigrid for Navier-Stokes equations. *AIAA,* pp. Paper 96-0297.

Rimskiy-Korsakov, A. B. D. B. L., 1988. *Fizicheskiye osnovy obrazovaniya zvuka v vozdukhoduvnykh mashinakh [Phisical principles of noise formation in blowing machines]*. Moscow: Nauka.

Rivola, A. D. G. M. E., 2014. Modelling dynamic behaviour and noise generation in gear pumps: Procedure and validation. *Applied Acoustics,* Volume 77, pp. 99-111.

Rodionov, L. K. B. K. A. S. E., 2009. Matematicheskoye vektornoye modelirovaniye pul'satsiy podachi zhidkosti shesterennym kachayushchim uzlom [Mathematical vector modelling of mass flow pulsations at gear pump outlet]. *Izvestiya SNC RAN,* 11(3), pp. 257-262.

Rodionov, L. P. F. R. P., 2015. Exploration of acoustic characteristics of gear pumps with polymeric pinion shafts. *Journal Procedia Engineering,* Volume 106, pp. 36-45.

Rodionov, L. R. P. S. J., 2015. A Gear Micropump without Bearings Production. *Applied Mechanics and Materials,* Volume 775, pp. 352-356.

Roe, P., 1992. *Technical Prospects for Computational Aeroacoustics.* Vancouver, British Columbia, Canada, s.n., pp. 206-213.

Rosqvist, T., 2000. Bayesian aggregation of experts' judgements on failure intensity. *Reliability Engineering & System Safety,* 70(3), p. 283–289.

Rundo, M., 2017. Models for Flow Rate Simulation in Gear Pumps: A Review. *Energies,* 10(1261), pp. 1-32.

Rus, T. D. M. H. M., 2007. An Investigation of the Relationship between Acoustic Emission, Vibration. Noise and Cavitation Structures on a Kaplan Turbine. *Journal of Fluids Engineering,* Volume 129, pp. 1112-1122.

Rybkin, Y. U. A. A., 1960. *Shesterennyye nasosy dlya metallorezhushchikh stankov [Gear pumps for metal cutting machines]*. Moscow: Mashinostroenie.

Ryzhikov, Y., 2004. *Imitatsionnoye modelirovaniye. Teoriya i tekhnologii [Simulation modeling. Theory and technology].*. s.l.:Mashinostroenie.

Sakurai, H. K. A. W. S., 2015. The optimal design in external gear pumps and motors. *ASME Transactions on Mechatronics,* 16(5), p. 945 – 952.

Saldanha, P. L. d. S. E. A. F. e. M. P., 2001. An application of nonhomogeneous poisson point processes to the reliability analysis of service water pumps. *Nuclear engineering and design,* 210(1), p. 125– 133.

Sauer, J., 2000. *Instationär kavitierende Strömungen - Ein neues Modell basierend auf Front-Capturing (VoF) und 8 Blasendynamik,* Karlsruhe: Universität Karlsruhe (TU).

Savchenko, V. S. I., 2001. *Proyektirovaniye sistem avtomaticheskogo regulirovaniya gazoturbinnykh dvigateley [Design of automatic regulation systems of gas turbine engines]*. Moscow: Mashinostroyeniye.

Schnerr, I. S. W., 2001. *Physical and numerical modeling of unsteady cavitation dynamics.* New Orleans, USA, s.n.

Senocak, I. S. W., 2002. *Evalution of cavitation models for Navier-Stokes computations.* s.l., s.n., pp. Paper FEDSM2002-31011.

Senocak, I. S. W., 2004. Interfacial Dynamics-Based Modeling of Turbulent Cavitating Flows Part-1: Model development and steady-state computations. *Int. J. for Num. Methods in Fluids,* Volume 44, pp. 975 - 995.

Shakhmatov, E., 1993. *Vibroacoutic characteristic estimation of combined pup ND-25 taking into account dynamic properties of accessory gear box and attached fuel pipelines,* Samara: s.n.

Shakhmatov, E., 2012. *Complex solution of mechanical and aerospace engineering vibroacoustics problems.* s.l., LAP LAMBERT Academic Publishing GmbH&CO.KG, p. 81.

Shakhmatov, E., 2012. *Vibroacustika mashin [Machine vibroacoustics]*. s.l.:LAP LAMBERT Academic Publishing GmbH& CO.KG, Saarbrücken,..

Shakhmatov, E. P. A. K. A. M. G., 2012. *The instability of the pipeline due to transporting fluid's pressure ripples.*. Brisbane, Australia, s.n., pp. pp. 2101-2108.

Shalnev, K., 1956. Kavitatsiya v gidrodinamike [Cavitation in hydrodynamics]. *Izvestiya AN SSSR,* Volume 8, pp. 72-116.

Shapiro, S., 2004. *Struktura real'nogo techeniya v tsentrobezhnykh i osevykh nasosakh [Structure of real-scale flow in cenrifugal and axial flow]*. Moscow: MGIU.

Shapiro, S., 2004. *Struktura real'nogo techeniya v tsentrobezhnykh i osevykh nasosakh [Structure of real-scale flow in cenrifugal and axial flow]*. Moscow: MGIU.

Sharif, M. A. R. W. Y. K. E., 1995. Evaluation of the performance of three turbulence closure models in the prediction of confined swirling flows. *Computers and Fluids,* Volume 2, pp. 81 - 100.

Shcherbatenko, I. S. A. K. V. S. L., 1980. *Nasos [Pump]*. USSR.

Shen, W. S. J., 1993. Comment on the aeroacoustic formulation of hardin and pope. *AIAA Journal,* 37(1), pp. pp. 141-143..

Shervani-Tabar, N. S. R. M. R. S.-T. M. T. B. R. I., 2012. *Experimental and Computational Investigation on the Cavitation Phenomenon in a Centrifugal Pump.*. s.l., s.n., p. pp. 489 – 497.

Sheviakov, A., 1976. *Teoriya avtomaticheskogo upravleniya silovymi ustanovkami letatel'nykh apparatov. Upravleniye VRD [Automatic control theory of flying vehicle power plants]*.. s.l.:Mashinostroenie.

Shorin, V., 1996. *Sovershenstvovaniye akusticheskikh svoystv mashin, oborudovaniya i energeticheskikh ustanovok [Impovement of acoutic properties of machines, facilities and power plants],* Samara: s.n.

Shorin, V., 1996. *Sovershenstvovaniye akusticheskikh svoystv mashin, oborudovaniya i energeticheskikh ustanovok [Impovement of acoutic properties of machines, facilities and power plants],* Samara: s.n.

Shorin, V. G. A. S. E., 1982. Proektirovanie gasitelei kolebanii dlya dempfirovaniya pul'satsii davleniya v sistemakh upravleniya gtd [Design of Vibration Dampers for

Pressure Pulsation Damping in Gas Turbine Engine Control Systems. *Izvestia vyssih ucebnyh zavedenij,* Volume 7, pp. 65-68.

Singhal, A. A. M. L. H. J. Y., 2002. Mathematical Basis and Validation of the Full Cavitation Model.. *Journal of Fluids Engineering,* 124(3), pp. 617 - 624.

Slodczyk, D. S. J., 2011. Designing a pumping system of gear pump s featuring the involute internal gearing.. *Key Engineering Materials,* Volume 490, pp. pp 64-75.

Smol'yakov, A., 2005. *Shum turbulentnykh potokov [Noise of turbulent flows].* s.l.:TSNII im. Akad. A.N. Krylova.

Solutions, F., 2012. *Gear pump Solution, Example X 219,* s.l.: s.n.

Stamatis, D. H., 2003. . *Failure mode and effect analysis: FMEA from theory to execution.* s.l.:Asq Press..

Stepanoff, A. J., 1960. *Tsentrobezhnyye i osevyye nasosy [CENTRIFUGAL AND AXAIL FLOW PUMPS].* New York John Willey & Sons ed. Moscow: Mashgiz.

Stochek, N. S. A., 1978. *Gidravlika zhidkostnykh raketnykh dvigateley [Hydraulics of liquid rocket engines].*. Moscow: Mashinostroyeniye.

Strasser, W., 2007. CFD Investigation of Gear Pump Mixing Using Deforming/Agglomerating Mesh.. *Transactions of the ASME,* Volume 129, pp. 476 - 484.

Stryczek, A., 1991. Pump delivery and its pulsation.. *Przeglad mechaniczny,* Volume 10, pp. 10-14.

Stryczek, J. A. P. J. O. K. D. K. A. B. G. a. R. L., 2015. Visualisation Research of the Flow Processes in the Outlet Chamber–Outlet Bridge–Inlet Chamber Zone of the Gear Pumps. *Archives of Civil and Mechanical Engineering,* 15(1), pp. pp. 95-108.].

Sverbilov, V. S. D. M. G., 2013. *Study on dynamic behavior of a gas pressure relief valve for a big flow rate..* Sarasota, FL, United States, s.n.

Tang, C. W. Y. G. J. G. H., 2014. Fluid-sound coupling simulation and experimental validation for noise characteristics of a variable displacement external gear pump. *Noise Control Engineering Journal,* 62(3), pp. 123-131.

Tatebayashi, Y. T. K., 2002. *Meridian Shape Influence on Screw-Type Centrifugal Pump Performance.* Canada, s.n., pp. Paper FEDSM02-31183.

Tatebayashi, Y. T. K. H. H. ,. K. T., 2001. *A 3-D Simulation of Flow in Screw-Type Centrifugal Pump with Tip Clearance.* China, s.n.

Tatebayashi, Y. T. K. K. T., 2003. Pump Performance Prediction in Screw-Type Centrifugal Pump. *Journal of Turbomachinery,* 31(1), p. 582 – 589.

Technology, A., 2010. *CFX-TASCflow manuals, version 15,* s.l.: AEA Technology .

The Chamber of Commerce and Industry of Ukraine SSR, 1975. *Шум – пути подхода к проблеме со стороны производителей насосов [Noise: approaches for problem solution from pumps producers point of view],* s.l.: s.n.

The Chamber of Commerce and Industry of USSR, 1984. *Исследование характеристик пульсаций нагнетаемого давления в шестеренных насосах [Investigations of characteristics of feed pressure pulsations in gear pumps],* s.l.: s.n.

Toyokura, T., 1961. Studies on the characteristics of Axial-Flow Pumps. *Bulletin of JSME.*, 14(4).

Tsniitastroymash, 1979. *Vliyaniye rabochikh parametrov na pul'satsiyu i uroven' shuma shesterennykh gidronasosov [Influence of working parameters on pressure and noise in gear hydropumps],* Moscow: Tsniitastroymash.

Tsniitestroymash, 1981. *Model' dlya rascheta poter' ot utechek v radial'nom zazore shesterennykh nasosov [Model for loss calculation due to leakages in radial clearance of gear pumps],* s.l.: s.n.

van Wachem, B. S. S., 2008. Derivation, simulation and validation of a cohesive particle flow CFD model. *AIChE Journal,* 54(1), pp. 9-19.

Versteeg, H. M. W., 1995. *An Introduction to Computational Fluid Dynamics. The Finite Volume Method.*. s.l.:Longman.

Vodyanitskiy, V., 1976. Vozniknoveniye avtokolebaniy v gidravlicheskoy sisteme pri podache svobodnogo gaza na vkhod v nasos [Self-oscillations occuring inside hydraulic system due to free air supply at pump inlet]. *Kavitatsionnyye avtokolebaniya v nasosnykh sistemakh*, Volume 1, pp. 86-95.

Vodyanitskiy, V. K. L. Z. L. Y. N. P. V. I. C. V. F., 1978. Vliyaniye nekotorykh fizicheskikh svoystv gazozhidkostnogo rabochego tela na energeticheskiye, kavitatsionnyye i dinamicheskiye kharakteristiki nasosnykh sistem podachi [Influence of several physical properties of luiquid-gas mixture in energetic, cavitation and dynamic]. *Rabochiye protsessy v shneko-tsentrobezhnykh nasosa*, pp. 14 - 22.

VTS, 1978. *Preimushchestva i kharakteristiki shesterennykh nasosov tipa TSR s vnutrennim zatsepleniyem i malym urovnem shuma [Advantages and characteristics of internal gear pumps and low noise],* s.l.: s.n.

Wang, G. H. B. Z. B. Z. M., 2009. *Unsteady Dynamics of Cloud Cavitating Flows around a Hydrofoil.* s.l., s.n., p. Paper №9.

Wang, H. S. D., 2011. External gear pump model and simulation. *Applied Mechanics and Materials,* Volume 127, pp. 228-32.

Wang, M. M. P., 2000. Computation of trailing-edge flow and noise using large-eddy simulation. *AIAA Journal,* Volume 38, pp. 2201-2209.

Wilcox, C., 2006. *Turbulence Modeling for CFD.* third edition ed. s.l.:DCW Industries Inc., La Cañada, -..

Williams, J. H. D. L., 1969. Sound generation by turbulence and surfaces in arbitrary motion. *Proc. Royal Society A,* Volume 264, pp. 321-342.

Yongsheng, S. Y. Z. T. M., 2008. Application of parallel recombination simulated annealing algorithms in recognition of inception cavitation fault. *Journal of Wuhan University of Technology,* Volume 32, pp. 1025-1028.

Yong, W. H. L. S. Y. D. L., 2012. *Experimental measurement on cavitation induced vibration and noise of centrifugal pumps.* s.l., s.n., pp. 498 - 502.

Yong, W. H. L. S. Y. M. T. K. W., 2009. *Prediction Research on Cavitation Performance for Centrifugal Pumps..* s.l., s.n.

Yoon, Y. P. B. H. Y. H. B. S. J., 2014. Numerical simulation of external gear pump using immersed solid method.. *Transactions of the Korean Society of Mechanical Engineers, B. ,* January, 38(1), pp. Pages 95-101.

Yuan, L. Y. H. D. C., 2009. Wavelet entropy based condition test and identification of cavitation. *Journal of Mechanical Strength,* Volume 31, pp. 19-23.

Zaguzov, I. S., 1994. O snizhenii urovney pul'satsiy, vibratsiy i shuma v gidravlicheskikh i toplivnykh sistemakh [About decreasing of levels of pulsations, vibrations and noise in hydraulic and fuel systems]. *Dinamicheskiye protsessy v silovykh i energeticheskikh ustanovkakh letatel'nykh apparatov,* pp. 69 - 74.

Zarubin, B., 2001. *Matematicheskoye modelirovaniye v tekhnike [Mathematical modelling in technics]..* (in Russian) ed. s.l.:MGTU im. N.E. Baumana.

Zazhigayev, L. K. A. R. Y. I., 1978. *Metody planirovaniya i obrabotki rezul'tatov fizicheskogo eksperimenta [Methods of planning and postprocessing of physical experiment results].* Moscow: Atomizdat.

Zhang, M. W. H. T. H., 2002. Numerical Analysis of Unsteady Hydrodynamic forces on a Diffuser Pump Impeller due to Rotor-Stator Interaction. *Proceedings of ASME,* pp. Paper FEDSM2002-31181.

Zhang, X., 2008. Computational fluid dynamic study on cavitation in liquid nitrogen.. *Cryogenics,* Volume 48, pp. pp. 432-438.

Zhongqi, P. W. Z. K. S., 2005. Turbine Cavitation Testing Based on Wavelet Singularity Detection. *Journal of Vibration and Shock,* Volume 24, pp. 71-74.

Zhulinskiy, G. Z. M. Y. V. T. V. B. G. V., 1983. *Шестеренная гидромашина [Gear hydraulic machine]*. USSR, Patent No. № 3428378.

Zima, P. S. M., 2012. *Modeling bubble collapse aggressiveness in traveling bubble cavitation using bubble breakup model.* s.l., s.n., p. 182 – 186.

Zixiang, S. I. M., 2000. *Computational Study on Optimum Inducer Leading Geometry For Stall Suppression in a Centrifugal Blower.* s.l., s.n., pp. FEDSM00-11059.

Zongxiang, L. Z. M. S. Z., 2004. Cascading failure analysis of bulk power system using small-world network model. *Probabilistic Methods Applied to Power Systems,* p. 635–640.

Zwart, P. J. G. A. B. T., 2004. *A two-phase model for predicting cavitation dynamics.* Yokohama, s.n.

ACTA UNIVERSITATIS LAPPEENRANTAENSIS

736. ALMANASRAH, MOHAMMAD. Hot water extraction and membrane filtration processes in fractionation and recovery of value-added compounds from wood and plant residues. 2017. Diss.

737. TOIVANEN, JENNI. Systematic complaint data analysis in a supply chain network context to recognise the quality targets of welding production. 2017. Diss.

738. PATEL, GITESHKUMAR. Computational fluid dynamics analysis of steam condensation in nuclear power plant applications. 2017. Diss.

739. MATTHEWS, SAMI. Novel process development in post-forming of an extruded wood plastic composite sheet. 2017. Diss.

740. KÄHKÖNEN, TOMMI. Understanding and managing enterprise systems integration. 2017. Diss.

741. YLI-HUUMO, JESSE. The role of technical dept in software development. 2017. Diss.

742. LAYUS, PAVEL. Usability of the submerged arc welding (SAW) process for thick high strength steel plates for Arctic shipbuilding applications. 2017. Diss.

743. KHAN, RAKHSHANDA. The contribution of socially driven businesses and innovations to social sustainability. 2017. Diss.

744. BIBOV, ALEKSANDER. Low-memory filtering for large-scale data assimilation. 2017. Diss.

745. ROTICH, NICOLUS KIBET. Development and application of coupled discrete and continuum models in solid particles classification. 2017. Diss.

746. GAST, JOHANNA. The coopetition-innovation nexus: Investigating the role of coopetition for innovation in SMEs. 2017. Diss.

747. KAPOOR, RAHUL. Competition and disputes in the patent life cycle. 2017. Diss.

748. ALI-MARTTILA, MAAREN. Towards successful maintenance service networks – capturing different value creation strategies. 2017. Diss.

749. KASHANI, HAMED TASALLOTI. On dissimilar welding: a new approach for enhanced decision-making. 2017. Diss.

750. MVOLA BELINGA, ERIC MARTIAL. Effects of adaptive GMAW processes: performance and dissimilar weld quality. 2017. Diss.

751. KARTTUNEN, JUSSI. Current harmonic compensation in dual three-phase permanent magnet synchronous machines. 2017. Diss.

752. SHI, SHANSHUANG. Development of the EAST articulated maintenance arm and an algorithm study of deflection prediction and error compensation. 2017. Diss.

753. CHEN, JIE. Institutions, social entrepreneurship, and internationalization. 2017. Diss.

754. HUOTARI, PONTUS. Strategic interaction in platform-based markets: An agent-based simulation approach. 2017. Diss.

755. QU, BIN. Water chemistry and greenhouse gases emissions in the rivers of the "Third Pole" / Water Tower of Asia". 2017. Diss.

756. KARHU, PAIVI. Cognitive ambidexterity: Examination of the cognitive dimension in decision-making dualities. 2017. Diss.

757. AGAFONOVA, OXANA. A numerical study of forest influences on the atmospheric boundary layer and wind turbines. 2017. Diss.

758. AZAM, RAHAMATHUNNISA MUHAMMAD. The study of chromium nitride coating by asymmetric bipolar pulsed DC reactive magnetron sputtering. 2017. Diss.

759. AHI, MOHAMADALI. Foreign market entry mode decision-making: Insights from real options reasoning. 2017. Diss.

760. AL HAMDI, ABDULLAH. Synthesis and comparison of the photocatalytic activities of antimony, iodide and rare earth metals on SnO2 for the photodegradation of phenol and its intermediates under UV, solar and visible light irradiations. 2017. Diss.

761. KAUTTO, JESSE. Evaluation of two pulping-based biorefinery concepts. 2017. Diss.

762. AFZALIFAR, ALI. Modelling nucleating flows of steam. 2017. Diss.

763. VANNINEN, HEINI. Micromultinationals - antecedents, processes and outcomes of the multinationalization of small- and medium-sized firms. 2017. Diss.

764. DEVIATKIN, IVAN. The role of waste pretreatment on the environmental sustainability of waste management. 2017. Diss.

765. TOGHYANI, AMIR. Effect of temperature on the shaping process of an extruded wood-plastic composite (WPC) profile in a novel post-production process. 2017. Diss.

766. LAAKKONEN, JUSSI. An approach for distinct information privacy risk assessment. 2017. Diss.

767. KASURINEN, HELI. Identifying the opportunities to develop holistically sustainable bioenergy business. 2017. Diss.

768. KESKISAARI, ANNA. The impact of recycled raw materials on the properties of wood-plastic composites. 2017. Diss.

769. JUKKA, MINNA. Perceptions of international buyer-supplier relational exchange. 2017. Diss.

770. BAYGILDINA, ELVIRA. Thermal load analysis and monitoring of doubly-fed wind power converters in low wind speed conditions. 2017. Diss.

771. STADE, SAM. Examination of the compaction of ultrafiltration membranes with ultrasonic time-domain reflectometry. 2017. Diss.

772. KOZLOVA, MARIIA. Analyzing the effects of a renewable energy support mechanism on investments under uncertainty: case of Russia. 2017. Diss.

773. KURAMA, ONESFOLE. Similarity based classification methods with different aggregation operators. 2017. Diss.

774. LYYTIKÄINEN, KATJA. Removal of xylan from birch kraft pulps and the effect of its removal on fiber properties, colloidal interactions and retention in papermaking. 2017. Diss.